Supervisory Control of 4WD Vehicle

Master Thesis

M. K. Andersen, R. M. Christensen

Aalborg University
Institute of Electronic Systems
Frederik Bajersvej 7
Telephone 96 35 86 00
www.sict.aau.dk

Title:

Supervisory Control
of 4WD Vehicles

Theme:

Control and Automation

Project period:
Master thesis,
autumn semester 2011
and spring semester 2012

Project group:
11gr935
12gr1035

Participants:
Roald Mikael Christensen
Martin Kolding Andersen

Supervisors:
Hans-Christian Becker Jensen
Torben Nørregaard Matzen

Pages: 179

Copies: 5

Attachments: CD

Finished: 31/5-2012

Synopsis:

In this project a 4WD RC car, driven by four individual electric motors, is constructed. To compensate for missing differential(s) and other hardware, common on vehicles with a thermal combustion engine, a supervisory control controlling the torque and limiting the slip on each wheel individually, is designed.

To estimate the states of the RC car, an extended Kalman filter is developed in three parts. This is updated by eight accelerometers placed on the chassis and a tachometer in each electric motor.

The torque and slip of each wheel, are controlled using feedback linearization combined with PID controllers.

Data from the sensors on the car have been collected, and the Kalman filter and supervisory control have evaluated in a simulated environment. The result shows, that the controller works, but the sensor noise on the car must be reduced.

Preface

This project is a scientific master thesis in Control and Automation at the institute of Electronic Systems at Aalborg University, Denmark. The project is carried out in September 2011 to June 2012, and is funded by EU.

THE EUROPEAN UNION
The European Regional Development Fund
Investing in your future

Structure

The thesis includes a main report in eleven chapters, where documentation, development and design is located. An introduction is given declaring the project problem statement. This is used as basis of the preceding, system requirements, system analysis, system design and development and lastly a system evaluation. The remaining includes an appendix with additional and relevant supplements to the main report.

All sources used are given in [], and listed by the end of the main report along with a nomenclature of variable descriptions, abbreviations and a list of figures. Figures, tables and others are provided with a reference number, and are produced by the project group if no source is stated. Relevant equations are given with a reference number to the left and the unit to the right of the equation.

Illustrations of the 4WD RC vehicle throughout the thesis are given both using CAD drawings and actual pictures.

Acknowledgments

Acknowledgments are given to Daniel Winther Uhrenholt and members of metal workshop at the institute of Electronic Systems, for assistance with constructing the vehicle platform used in the project. Acknowledgments are also given to University Metal College Aalborg for assistance with mechanical CAD drawings of the vehicle drive trains.

Supplements

Various documentation, simulations, graphs, images, scripts, videos etc. and a digital version of the report, are located on the attached DVD and listed in appendix I.

Martin Kolding Andersen

Roald Mikael Christensen

Table of Contents

CHAPTER 1

INTRODUCTION

Vehicles today are made with many different types of engines and mechanical drive systems. The majority is built with an internal combustion engine (ICE), a gearbox and at least one differential. The engines uses fuel (typically petrol or diesel) to produce torque to the gearbox through a clutch. The clutch is used to gradually apply the engine power to the gearbox after a gear change. The gearbox then provides a discrete number of gear ratios, which combined with the ratio of the differential, comprise the total gear ratio between the engine and the wheels. Each gear in the gearbox converts the torque and angular velocity, making it possible for the vehicle to drive in a wide velocity range [2].

The gearbox shaft is connected to each propelling wheel pair through a differential. When a vehicle is turning, the inner and outer wheel spins with different velocities due to the difference in turning radius. This difference in velocity is made possible with the differential, which always distributes the torque to the two wheels in the wheel pair in the same proportion, independently of the velocity difference [11]. Each wheel can thereby rotate with its own velocity. Dependent on the type of differential, the torque distribution can take various values in a ranged interval, and in some differentials it can be changed while driving [3].

In four wheel driven (4WD) vehicles, the gearbox has a central transfer case, which is connected to the differential on each wheel pair with a shaft. The 4WD setup increases the vehicles traction, compared to a vehicle with only one propelling wheel pair. Some 4WD system are designed in a way, that enables the driver to choose whether the rear, front or both wheel pairs should propel the vehicle [10]. All wheel drive (AWD) is another design of 4WD, where a central differential has replaced the central transfer case. With a central differential, torque can be distributed among the wheel pairs, and not only between each wheel in a pair. Some central differentials has the option to function as a central transfer case.

The torque control ability in differentials is also used for ensuring vehicle drive stability. At varying road surface conditions, wheels can spin if more than the required torque is applied to them. Traction control systems (TCS) have been applied using several methods. One of them is to distribute the torque to the wheels with most traction and reduce the torque on the wheels with less traction. In some systems, this is done by changing the differential settings, while other systems reduce the total torque to the drive system or use brakes [11, 4]. During wheel slip, a slip differential connects the wheels together, and the wheel with slip then regains traction. Since traction control increases the road grip, the vehicle drive stability is enhanced and the user is less likely to lose control.

In the group of stability and safety systems is the electronic stability control (ESC). This system depends on electronically operated brakes to control the vehicle direction in a situation, where the vehicle otherwise would be out of control [5]. Like the TCS, the ESC system may influence the torque and rotation of each wheel. ECS is braking the wheels according to calculations done by a computer, trying to act against skidding.

Other vehicles are using electric motors for propulsion instead of the petrol or diesel engines. An electric motor has several advantages compared to an internal combustion engine. It has fewer moving parts, making wear and size smaller and it has a higher efficiency. Typically the electric motor also have a wider dynamic range of angular velocity and torque, which enables smaller or no gearbox [15]. Figure 1.1 illustrates the difference in torque of an internal combustion engine and an electric motor. An electro motor is also capable of providing a breaking force, for which reason the actual breaks might be removed or reduced. Another option, when considering electric propulsion, is to let the wheels be driven by individual motors, also called individual wheel drive (IWD).

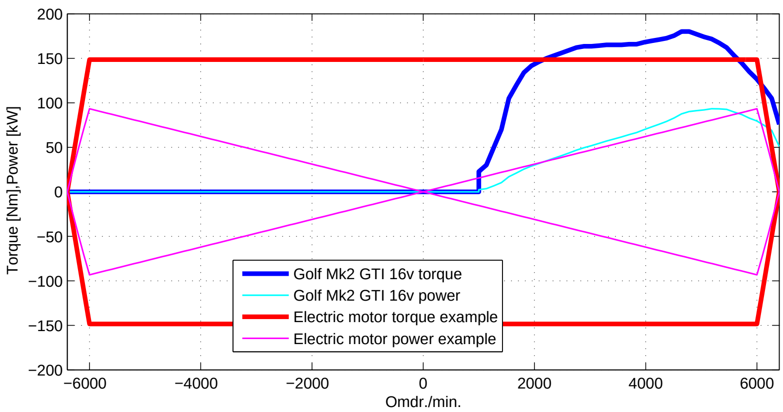

Figure 1.1. Illustrates example of difference in torque of an internal combustion engine and an electric motor.

An IWD setup in a 4WD vehicle provides several control possibilities regarding both drive, stability and safety aspects. Also some drive parts can be removed and the electric motors can be directly fitted to the propelling wheels. Use of differentials can be avoided and removed, by accounting for these with individual drive instead and determine the torque and rotation of each wheel in the controller. The wheel torque and rotation must also be determined in order for the TCS and ESC to function. With IWD implemented, the torque to wheels can not be transfered by use of a slip differential, since this is not part of IWD. Instead the torque to the spinning wheel could be limited by applying the brakes at this wheel.

The objective of this project is to develop a supervisory control for a vehicle with IWD, capable of distributing torque among and maintain traction on the wheels. The system is developed on a 1:5 scale RC car with individual electric motor drive on the wheels.

The project takes place concurrent to a EU funded project, where a similar system on a full sized vehicle, illustrated in figure 1.2, is designed. The project treated here- Supervisory Control of 4WD vehicles, was proposed in connection to the EU project, and all hardware is hereby funded by EU.

Figure 1.2. Full size EU funded vehicle.

CHAPTER 2

SCOPE

The Introduction in chapter 1 presented a brief technical overview of the common modern vehicle. From this basis, the advantages of and possibilities in using electric motors for propulsion, were explained. This lead to several subjects which could be relevant in this project.

This chapter defines the scope for the project in three ways. First in a project outline a number of choices will be made, concerning which of the subjects mentioned in the Introduction chapter 1 on page 1 that will be included in the project. The outline also includes a description of the platform used for the technical development. A specification requirement will then define a list of requirements to be fulfilled by the final product, and finally both demands for subsystems and the system as a unit are are specified together.

2.1 Project Outline

The basis provided by the Introduction proposes a project, where a full scale 4WD vehicle, propelled by a internal combustion engine, is converted to be driven by electric power. However, due to economical and practical reasons, a 1:5 scale remote controlled car, hereafter referred to as the vehicle (see vehicle, appendix E on page 165), is chosen as development platform. The chosen model is from standard implemented with 4WD, thus making it suitable for this project without advanced modifications having to be made to wheels, suspension etc. Also due to its size (1:5 scale), it has a relatively high mass, making it easier to model precisely. E.g. the velocity of a very light vehicle changes very fast, when small forces are applied to it. Hence making it hard to model precisely due to small unknown external forces.

The vehicle shown in figure 2.1, is a gasoline- four wheel driven, 1:5 scale, remote controlled car. The fact that the vehicle is produced with a internal combustion engine induces, that it must undergo the procedure introduced in the Introduction chapter 1. That is, it must be modified to be driven by electro motors propelling wheel each wheel individually.

Figure 2.1. The Titan Monster Truck (See vehicle, appendix E on page 165) [12].

This procedure includes, that the original motor is removed along with the original gearing, transmission, differentials and all unnecessary drive shafts. Four electro motors must then be mounted and each coupled to a wheel through an appropriate gearing, chosen collectively according to the motor characteristics. To be able to fully utilize the four motors at the same time, a sufficiently powerful battery pack must also be mounted.

In relation to the conversion of a vehicle, from a classical drive train to electro motors, a number of technical features must be implemented in order not to loose functionality. First of all, to compensate for the mechanical differentials removed, some other torque distribution system (TDS) must be implemented, allowing the wheels to rotate at distinct velocities, without unintended changes in torque occurring. With an electro motor attached to each propelling wheel, it would be obvious to measure the torque on each wheel and let a controller, distribute the torque in the desired ratio. This technique could be used on 2WD vehicles as well as 4WD vehicles, and must also be integrated in the vehicle.

Four wheel drive increases traction and can be integrated in a vehicle, if high acceleration or extra grip in off road terrain is needed. However 4WD is no guarantee for optimal grip. Once a wheel looses grip, it looses to some degree its ability to produce driving force. Therefor to fully utilize 4WD, all the wheels must stay in grip with the driving surface, allowing all wheels to produce maximum traction force. Hence a traction control system (TCS) is a relevant feature to integrate in the vehicle. However where a traditional TCS uses means, such as reducing engine power and utilizing individual brakes, the individual and electric drive train design, used in the vehicle, enables a simple and precise torque adjustment on the individual wheel. Hence an individual 4WD TCS must be integrated in the vehicle.

This section has revealed that in this project, a 1:5 scale model car must be modified to be propelled by four electro motors, one driving each wheel. To maintain the functionality of the differentials, a torque distribution system (TDS) must be developed and integrated. Also to benefit from 4WD, a traction control system (TCS) must be integrated, which exploits the possibilities in having four independently propelled wheels. From this outline, the next two sections will provide specific requirements and demands for both the vehicle and the TDS and TCS systems.

2.2 Specification Requirements

The previous section provided an outline for the project. To make sure this outline is maintained in the final solution, a series of relevant requirements are specified in this section.

In table 2.1 the slip rate λ is defined as the wheel velocity v_{w} relative to the vehicle velocity v_{v} (see equation 6.34 in section 6.3).

In order to test the TCS on the final product, the vehicle must fulfill some performance requirements given in the first part of table 2.1. In second and third part of table 2.1 requirements to the system, when TCS and TDS active respectively, are stated. Slip is defined as the values of λ that are beyond the limits specified in second part of table 2.1. When TCS is active, a time limit for periods, where slip is present, is define. Also when the TCS acts against slip, the torque must not vary more than a certain limit $T_{\mathrm{w,rip}}$. In third part of table 2.1 a limit for the error between a torque reference and the actual torque is stated.

	Parameter	**Min.**	**Max.**	**Unit**	**Condition**
Performance (TCS and TDS inactive)					
- Drive train					
$v_{\mathrm{w,max}}$	Max. wheel velocity (forward)	13,9		$\frac{\mathrm{m}}{\mathrm{s}}$	
$v_{\mathrm{w,min}}$	Min. wheel velocity (backward)		-6,9	$\frac{\mathrm{m}}{\mathrm{s}}$	
λ_{max}	Max. slip (forward)	50		%	$v_{\mathrm{c}} \leq \frac{v_{\mathrm{w,max}}}{4}$, $\mu \leq 1$
λ_{min}	Min. slip (backward)		-50	%	$v_{\mathrm{c}} \geq \frac{v_{\mathrm{w,min}}}{2}$, $\mu \leq 1$
- Supply battery					
$t_{\mathrm{I_B=I_{B,max}}}$	Battery current duration at max. current consumption	5		s	Battery fully charged
Traction Control System (TCS)					
λ	Slip ratio with TCS active	-10	10	%	
t_{slip}	Time before slip is ended		500	ms	
$T_{\mathrm{w,rip}}$	Torque ripple caused by TCS action	-1	1	Nm	$\lvert\Delta\mu\rvert \leq 0.1$
Torque Distribution System					
$T_{\mathrm{w,err}}$	Torque error rel. reference	-0,5	0,5	Nm	

Table 2.1. Requirements to the final product

Requirements to the final functionality of the vehicle have now been stated. These must be considered in the design procedure, to ensure the performance of the product.

2.3 System Demands

Section 2.1 on page 5 and 2.2 presented first an outline for the project, second a series of testable requirements regarding the functionality of the final product. To ensure that the outline is followed and the requirements are met, this section states a series of demands to each subsystem. These demands also ensures compatibility of the subsystems.

User interface

- Wireless deactivation of the driving power must be possible.
- The user remote controls the vehicle.
- Data can be transmitted wirelessly for logging.

Propelling

- A separate drive train must be connected to each wheel.
- A gearing must convert the torque of the motor sufficiently, to enable the vehicle to make wheel slip under all circumstances.
- The motor must be sufficiently powerful to enable wheel spin at the velocity difference specified by the Specification Requirements section 2.2 under all circumstances.
- A motor driver must convert a low power control signal into a signal suitable for the motor.
- The motor driver must enable the motor to rotate in both directions.
- Each motor must be controlled separately.

Power supply

- All four drive trains must at any time, defined by the Specification Requirements section 2.2, be able to consume power at their maximum.
- All systems besides the power trains must be powered at all times when the power supply is on.

Control system

- All user control goes through the control system.
- The TCS must be integrated.
- The TDS must be integrated.
- The TCS must limit the TDS's control output according to the grip of each wheel respectively.
- The four drive trains must be controlled individually according to the user input, the TCS and the TDS.
- Parameters relevant to the TCS or the TDS must be continuously estimated.

Traction control system (TCS)

- The TCS must depend only on the four drive trains to adjust torque.

Torque distribution system (TDS)

- When TCS is not active, the torque on the wheels is controlled entirely by the TDS and according to the user input.

Demands for six subsystems have now been stated. These should be considered in the design process of every system in order to ensure compatibility. Furthermore the requirements from the Specification Requirements section 2.2 and the Project Outline section 2.1 should be respected throughout this project.

CHAPTER 3

Overall Design

So far, chapter 2 has provided an outline, where choices of the development platform and functionalities, to be implemented, are made. A series of requirements and demands to the final product are stated ensuring it's performance. Bases on these three sections (section 2.1, 2.2 and 2.3), the overall design of the vehicle can now be determined.

Section 2.1 on page 5 stated, that each wheel must be driven by individual electro motors. Furthermore section 2.2 requires, that the vehicle is able to make wheel slip, which requires a relatively high amount of torque. To convert a typical relatively low torque from an electro motor, a drive train gearing is implemented, as illustrated in figure 3.1.

To implement TDS and TCS, knowledge about the velocity and control of torque on the wheels are required. The wheel velocity is obtained by a sensor mounted on the wheel shaft or integrated in the motor. To regulate the wheel torque, and thereby the power to the motor, a motor driver is used. This converts a weak control signal to a high power signal for the motor.

To enhance the TCS eight accelerometers, distributed on four components with two measure axis each, are mounted; one in each corner of the vehicle. These will be used to approximate the normal force on each wheel and the velocity of the vehicle. The vehicle velocity can not allways be measured by the velocity sensors on the wheels, since if torque is applied to a wheel, slip will be present in some degree.

The control system described by section 2.3 is by choice implemented on a DSP, since modern DSPs possess a lot of analogue inputs and outputs and processing power. All the sensors mentioned above, must be read by the DSP which will then, based on these measurements and a drive signal from the user, provide a signal for each of the four motor drivers. The user input is transmitted with a remote control and received by a remote receiver coupled to the DSP. One part of the user input is the steering signal. This is read by the DSP, however directly retransmitted to a servomotor controlling the steering system.

Figure 3.1 below illustrates the position of the hardware on the vehicle. XBEE, supplies and other are located on the circuit board, mounted above the motor drivers.

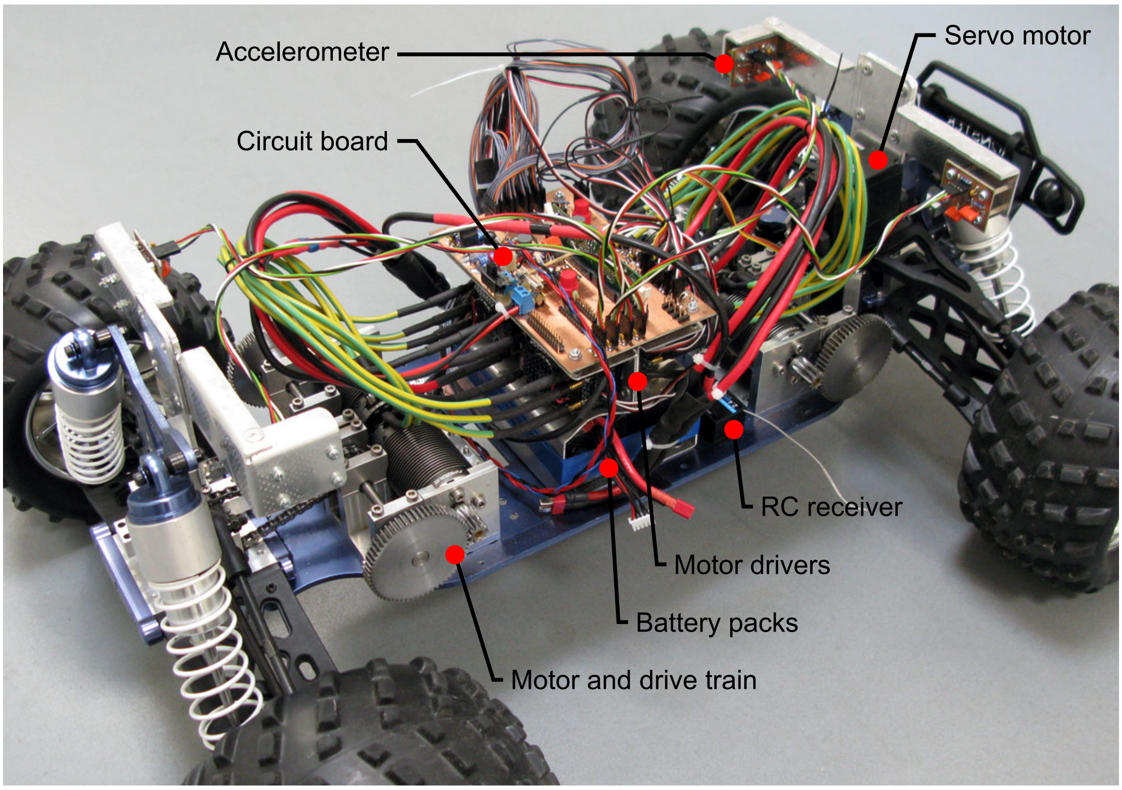

Figure 3.1. Hardware locations on vehicle.

Figure 3.2 shows a block diagram showing the electrical setup of the hardware.

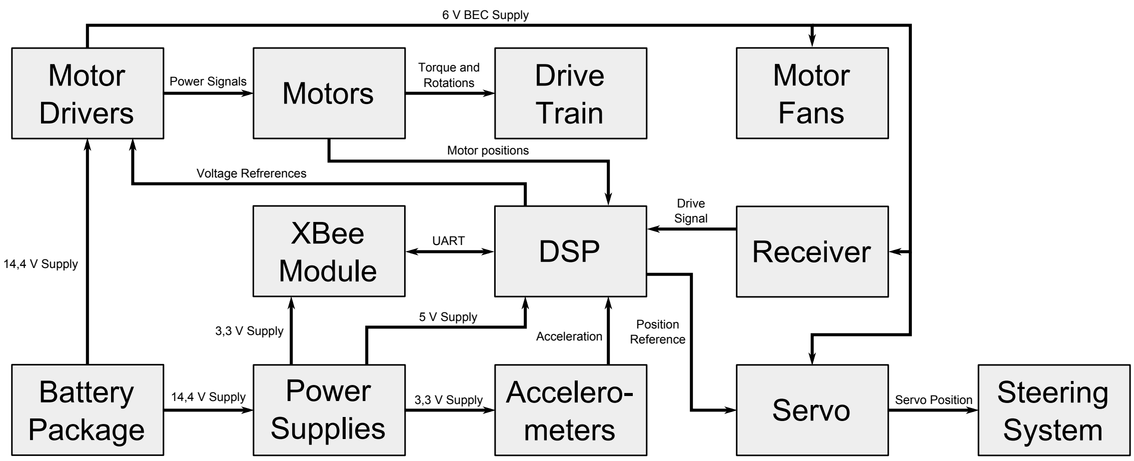

Figure 3.2. Block diagram of vehicle hardware.

An overall design of the vehicle has now been described. This will be used as a guideline in the design process of the individual blocks. In the following an analysis will determine some of the requirements for the design for the systems according to what stated in section 2.

Chapter 4

Technical Analysis

So far, the course of the project have been defined in chapter 2, by describing which modifications must be performed on the vehicle, by stating requirements to the final product and by setting certain demands regarding design choices of the vehicle.

The first step in the design process is to convert the vehicle from being driven by fossil fuel to be driven by electricity. To respect the scope in chapter 2, analysis of relevant design solutions must be performed in order to find specific requirements to the specific components. A part of finding these requirements, is to estimate worst case scenarios regarding the final system. Here the chosen components must perform sufficiently, so the system respects the scope from chapter 2. Along with this, a consideration of how to implement the vehicle control with TDS and TCS is included.

4.1 Motor Choice

As specified, the vehicle must be rebuild to be driven by an electro motor propelling each wheel. In order to choose the type of electro motor to be used in the project, the requirements to torque an angular velocity must be known. Based on these results, the choice of motor can be made.

The only requirement to the motors, before any choice of gearing is made, is how much power it must be able to deliver. This requirement is calculated based on demands to torque and angular velocity.

The torque transferable on each wheel, without slip occurring, is dependent on the road surface and the normal force upon the wheel. The normal force on a wheel changes when weight is transfered to/from other wheels by external driving forces. Based on the initial mass of the vehicle (see appendix E), it is estimated that the mass of the final vehicle will not exceed 20 kg. From this, the normal force $F_{\mathrm{N,w}}$ on each wheel can be calculated as in formula 4.1. In this case, an even weight distribution is assumed.

$$F_{\mathrm{N,w}} = \frac{m_{\mathrm{vhc}} \cdot g}{n_{\mathrm{w}}} \qquad [\mathrm{N}]$$

$$F_{\mathrm{N,w}} = \frac{20 \cdot 9,82}{4} = 49,1 \qquad [\mathrm{N}] \tag{4.1}$$

When considering weight transfer, the worst case scenario occurs when the total force of three wheels is transferred completely to one wheel, meaning that the vehicle is suspended by one wheel. However, it seems reasonable to assume, that at least two wheels will always share the normal force of the vehicle. Hence the worst case scenario of normal force on one wheel $F_{\mathrm{N,w,worst}}$ can be calculated as in equation 4.2.

$$F_{\mathrm{N,w,worst}} = \frac{20 \cdot 9,82}{2} = 98,2 \qquad [\mathrm{N}] \tag{4.2}$$

Given the wheel radius $r_{\mathrm{w}} = 0,095$ m (see appendix E) and the assumption, that the friction coefficient $\mu_{\mathrm{worst}} = 1$, then the wheel torque required in the worst case scenario $T_{\mathrm{w,worst}}$ can be calculated as in equation 4.3.

$$T_{\mathrm{w,worst}} = F_{\mathrm{N,w,worst}} \cdot \mu_{\mathrm{worst}} \times r_{\mathrm{w}} \qquad [\mathrm{Nm}]$$

$$T_{\mathrm{w,worst}} = 98,2 \times 0.095 = 9,33 \qquad [\mathrm{Nm}] \tag{4.3}$$

Hence to respect the demand from section 2.2, the result from equation 4.3 defines a requirement to the minimum amount of torque, that must be available on each wheel shaft. The velocity, at which this torque must be provided, is calculated from the requirement to the slip coefficient and the condition for this (see table 2.2) as in equation 4.4 [15].

$$\lambda = \frac{v_{\mathrm{w}} - v_{\mathrm{v}}}{v_{\mathrm{w}}} \qquad [\%]$$

$$v_{\mathrm{w}} = \frac{v_{\mathrm{v}}}{1-\lambda} \qquad \left[\frac{\mathrm{m}}{\mathrm{s}}\right]$$

$$\text{For } v_{\mathrm{v}} = \left|\frac{v_{\mathrm{w,max}}}{4}\right| = \left|\frac{v_{\mathrm{w,min}}}{2}\right| :$$

$$v_{\mathrm{w}} \geq \frac{\frac{13,9}{4}}{1-0,5} = 6,94 \qquad \left[\frac{\mathrm{m}}{\mathrm{s}}\right] \tag{4.4}$$

Hence the motor must provide a power P_{m} calculated by formula 4.5.

$$P_{\mathrm{m}} \geq F_{\mathrm{N,w,worst}} \cdot \mu_{\mathrm{worst}} \cdot v_{\mathrm{w}} \qquad [\mathrm{W}]$$

$$P_{\mathrm{m}} \geq 98,2 \cdot 6,94 = 681,9 \qquad [\mathrm{W}] \tag{4.5}$$

Several candidates from two companies [13, 14] have been found. The data for the motors are limited, so assumptions on e.g. efficiency, for an estimate of the output power, have to be made. The power and torque of the motors are plotted in figure 4.1 along with requirements to torque and power for distinct gearings and a low estimated efficiency of 80 %.

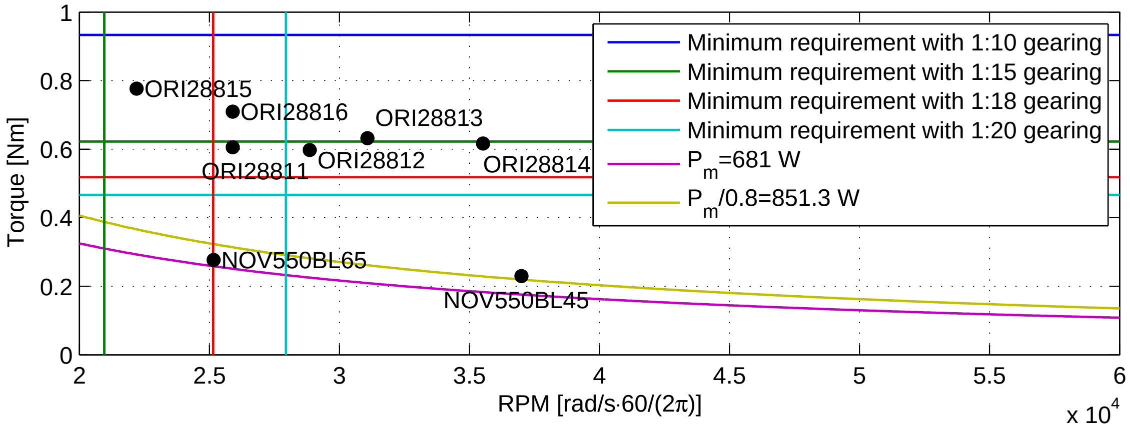

Figure 4.1. Torque and power of various electro motors.

In figure 4.1 it can be seen, that the motor NOV550BL65 from Novac [13] does not fulfill the power requirement, whereas all the motors ORI2881X from Orion [14] and the Novac NOV550BL45 does fulfill it. The figure also shows four torque and velocity requirements corresponding to four different motor to wheel gearings. It is seen, that for a gearing of 1:18 or 1:20 all of the motors from Orion [14] provide sufficient torque to fulfill the requirement. When considering the torque and velocity requirement simultaneously and given the gear ratios shown in figure 4.1, all motors ORI2881X from Orion [14] is applicable in this project. Based on inventory and delivery limitations on some of the motors, the ORI28813 (see appendix E) is chosen.

The chosen motor is a three phase brushless electro motor with position sensor. It thereby depends on a motor driver, which provides a high power three phase signal based on an input signal. For this, the motor driver ORI65107 (see appendix E) is considered. It fulfills the immediate requirements given by the chosen motor. That is, it can handle motors with a kV (revolutions per volt) [14] constant up to 2300, where the chosen motor is a 2100 kV motor. The driver is able to provide 760 A peak current, where the motor can handle 139 A. A further investigation of the motor driver will be performed in section 4.2.

The torque and angular velocity requirement to the electro motors have now been investigated for various choices of gear ratios, and the motor ORI28813 (see appendix E) have been chosen along with a motor driver. In section 5.1 a drive train gear will be developed based on the specifications of the motor.

4.2 Motor Driver

In this section the motor driver ORI65107 (see table E.1 in appendix E) chosen in section 4.1 is investigated. This is done to determine whether the driver is suitable for the use in this project, that is if it contains any revolution, torque etc. controllers. This is not desirable in this project, since a custom made torque controller is developed (see chapter 8), hence e.g. a velocity controller included in the motor driver would have to be neutralized in the DSP software (see chapter 9).

Figure 4.2 shows how the motor driver is connected.

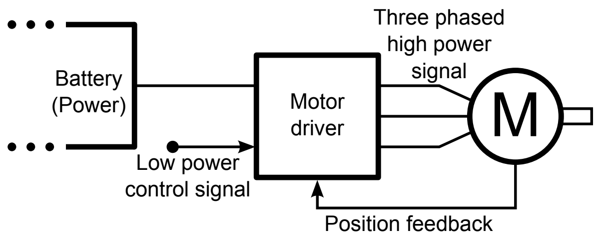

Figure 4.2. Motor driver in connection with motor and battery.

To determine if the motor driver contains any controller, a constant input signal is supplied to the driver. The voltage signal between two phases $V_{\mathrm{m,ph},1}$ is then measured when the motor is running freely, and when a load is applied to the shaft as $V_{\mathrm{m,ph},2}$. The data is seen in figure 4.3. If the angular velocity of the motor is decreased and the amplitude of the voltage between the two phases remain unchanged or is decreased, it is assumed that the driver does not contain any controller, since this would try to act against the decrease of velocity by increasing the motor voltage.

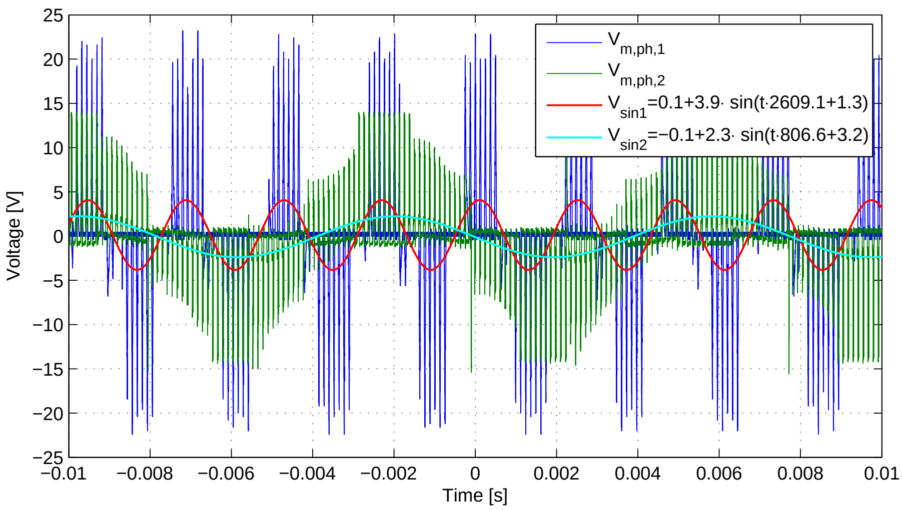

Figure 4.3. Measurements of motor phase voltage.

As the motor driver utilizes PWM to control the motor signal, the corresponding wave form can not be seen directly by looking at the data, but it is assumed, that it follows a sine function. Hence, to extract a precise amplitude and frequency of the two signals in figure 4.3, a sinus function of the form seen in equation 4.6

$$V_{\mathrm{sin}}(n) = X(2) + X(1) \cdot sin\left[t(n) \cdot X(3) + X(4)\right] \quad [\mathrm{V}] \tag{4.6}$$

where

t is a time vector containing a time for each data point in $V_{\mathrm{m,ph}}$

V_{sin} is a vector containing sample points from the fitted sinus function

$X(1)$ is the amplitude of V_{sin}

$X(2)$ a vertical offset of V_{sin}

$X(3)$ is the radian frequency of V_{sin}

$X(4)$ is a horizontal offset in radians of V_{sin}

is fitted to each curve respectively (V_{sin1} and V_{sin2}) by the following MATLAB® code:

```
F = @(X)sinFit(data,X);
X = fminsearch(F,X);

function Err = sinFit(data,X)
   fitData(:,1) = X(2)+X(1)*sin(X(3)*data(:,1)+X(4));
   Err = sum((fitData-data(:,2)).^2);
end
```

where

$\mathtt{data} = \left[t\ V_{\mathrm{m,ph}}\right]$

The results are seen in figure 4.3. To visually validate the result, the measured data are filtered in MATLAB® by an autoregressive filter shown in equation 4.7

$$V_{\mathrm{f}}(n) = V_{\mathrm{f}}(n-1) \cdot c_1 + V_{\mathrm{m,ph}}(n) \cdot c_2 \quad [\mathrm{V}] \tag{4.7}$$

where

V_{f} is the filtered data

$c_1 = 0.9995$ is an adjustable constant

$c_2 = 0.0005$ is an adjustable constant

and c_1 and c_2 are manually tunned. The result is seen in figure 4.4 along with the two fitted sinus functions.

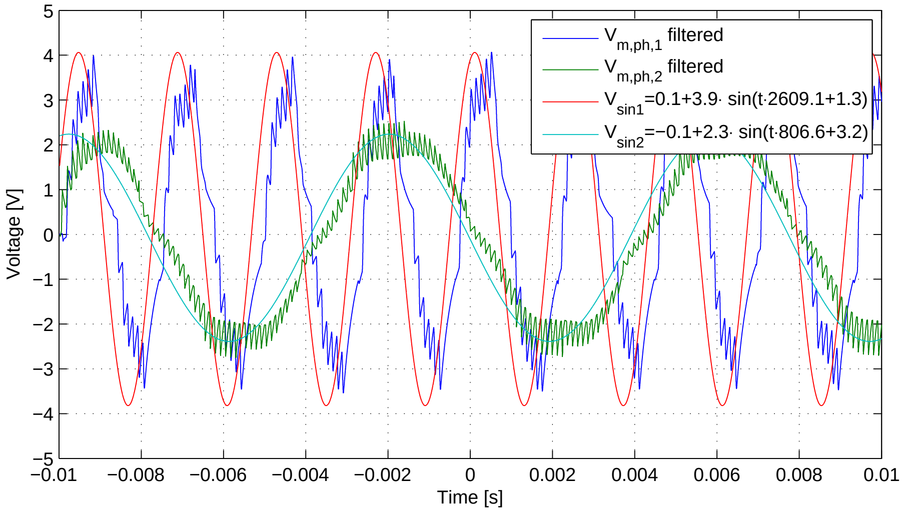

Figure 4.4. Filtered measurements and parameterization of the motor phase voltage

Due to the similarity between the filtered data and the fitted sinus functions, the parameterization of $V_{m,ph,1}$ and $V_{m,ph,2}$ to V_{sin1} and V_{sin1} respectively, is accepted.

The frequency of the voltage between the two phases on the motor is calculated in equation 4.9.

$$f_1 = \frac{X_1(3)}{2 \cdot \pi} = 414,9 \qquad \left[s^{-1}\right] \tag{4.8}$$

$$f_2 = \frac{X_2(3)}{2 \cdot \pi} = 128,6 \qquad \left[s^{-1}\right] \tag{4.9}$$

where

f_1 is the frequency of V_{sin1}

f_2 is the frequency of V_{sin2}

The voltage peak amplitude is directly given by $X(1)$ (see equation 4.11).

$$V_{\text{peak1}} = X_1(1) = 3,04 \qquad [V] \tag{4.10}$$

$$V_{\text{peak2}} = X_2(1) = 2,19 \qquad [V] \tag{4.11}$$

where

V_{peak1} is the peak amplitude of V_{sin1}

V_{peak2} is the peak amplitude of V_{sin2}

By treating the measured data, it can be seen that the amplitude of the voltage between two phases on the motor is decreased as the angular velocity is decreased. Hence it is concluded, that the motor driver does not contain any controller, that could have an impact on the later delevopment in this project. The motor driver ORI65107 (see table E.1 in appendix E) is therefor approved for further use in this project.

The relation between the motor driver signal and the wheel torque and rotational response through the drive train, is modeled in section 6.2. This model is used by the supervisory control developed in chapter 8. The motor provides a measure of the angular velocity, which will be described in the succeeding section.

4.3 Motor Position Feedback

As stated in chapter 3, the velocity of each wheel must be known. The motor provides a position signal, which is used by the motor driver, both chosen in section 4.1, in order to improve the motor control.

The signal consists of the following connections (table 4.1), where the pin connections are as shown in figure 4.5(a) and 4.5(b).

Pin number	Description
1	+5 V
2	+5 V
3	Position 0° (PS0)
4	Position 120° (PS120)
5	Position 240° (PS240)
6	GND

Table 4.1. Connections in motor position signal.

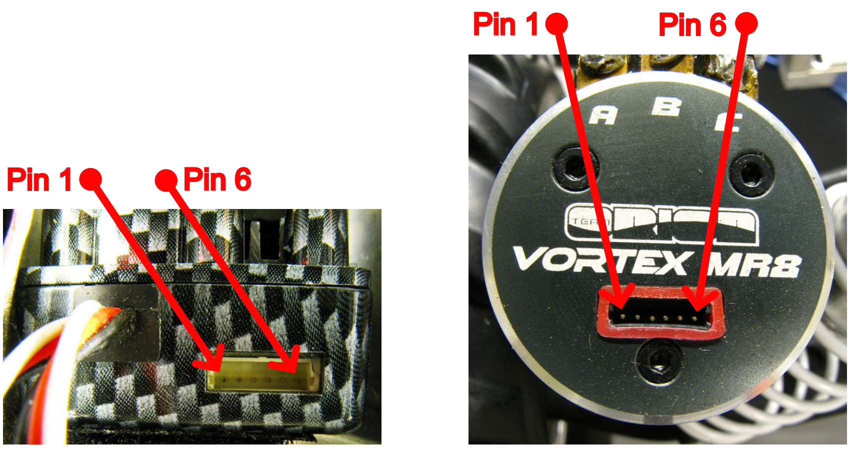

(a) Motor driver pin connections. (b) Motor pin connections.

Figure 4.5. Motor position feedback pin connections.

Connections PS0-240 are pulse trains shifted 0°, 120° and 240° respectively relative to PS0. The signal is sketched in figure 4.6.

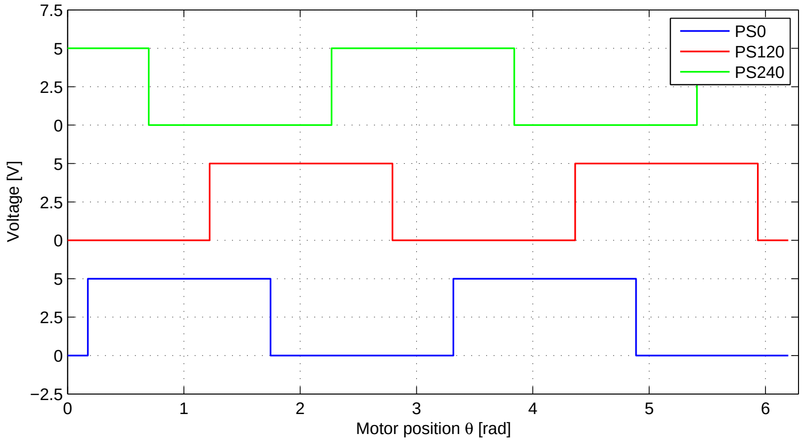

Figure 4.6. Example of motor position signal.

It is estimated, that one of the PS signals will be sufficient to determine the motor velocity with proper precision. If the turning direction is to be determined also, more than one measures is required. The velocity can then be calculated as in equation 4.12.

$$\omega_{\text{m}} = \frac{2\pi}{p_{\text{PSX}}} \qquad \left[\frac{\text{rad}}{\text{s}}\right] \tag{4.12}$$

where p_{PSX} is the period time of one of the signals.

In section 5.2 the information from this section will be used when designing relative hardware.

4.4 Control Considerations

A consideration of how to implement the TDS and TCS control system is given, used for the overall design in section 3 and the development of the supervisory control. According to chapter 2, the controller must for each wheel control the distribution of torque with the TDS and limit slip ratio with the TCS. The controller will determine each motor driver signal, since these are the only available inputs to the vehicle, which will affect the wheel torque and slip ratio. The steering servo is supplied directly with the RC receiver signal κ_{CH1} controlled from the user remote control, and the supervisory control is thereby not to use this.

To supply the controller with a feedback of wheel torque and slip, a vehicle model is derived in chapter 6. The model is to be used in a simulation setup, where the performance of supervisory controller can be verified before implementation on the actual vehicle.

The model is also used to develop an extended Kalman filter (EKF). This will use the model and hardware suppling actual measures ζ of the vehicle corner acceleration and wheel velocities, to derive a feedback of estimated wheel torque and slip ratio for the supervisory control. The

Kalman filter is chosen since this is designed for sensor noise with a normal distribution, which is assumed for the angular motor velocity and accelerometer sensors. The extended Kalman filter is also able to handle nonlinearities in the vehicle model and perform model parameter identification. The development of the extended Kalman filter is described in chapter 7.

The RC receiver signal κ_{CH2} is controlled by the accelerator on the remote control, and used to determine a wheel torque reference. The TDS is then to distribute wheel torque according to this reference, while reference slip ratio is always set at a range of $[-0,1;0,1]$ for the TCS according to chapter 2. The supervisory control, developed in chapter 8, must then with the references and feedback estimates of wheel torque and slip, determine each motor driver signal $V_{\text{m},1\text{-}4}$. An illustration of the considered control system setup is shown in figure 4.7.

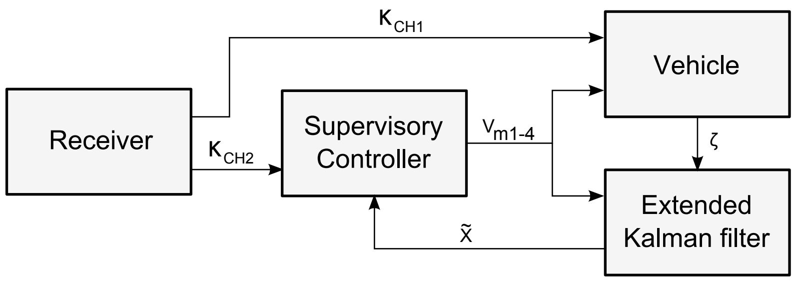

Figure 4.7. Setup considered for supervisory control.

In the succeeding, the hardware from the overall design is designed in chapter 5.2, with use of the considered control setup. Hereafter the vehicle system model will be derived, and hereafter the extended Kalman filter and supervisory controller developed.

CHAPTER 5

HARDWARE DESIGN

In chapter 2 an outline for the project was presented in form of various descriptions, requirements and demands. From this, chapter 3 provided an overall design of the vehicle and various design choices were made. Upon these, a motor and motor driver was found from the analysis in 4. The various design choices consist of both mechanical parts, as e.g. a drive train, and other systems as wireless communication and control of signals for the motor drivers.

As described in section 2.1, a conversion from classical drive train to electro motors is to be performed on the vehicle. Upon mechanical calculations and design, University Metal College Aalborg has supplied a first draft of CAD drawings for the new parts for the electro motor mountings and drive trains. Through the design process, the draft and drawings from University Metal College Aalborg has been altered due to a substitution from belt drive to chain drive. In figure 5.1(a) the original vehicle before modification is shown, and after modification in figure 5.1(b).

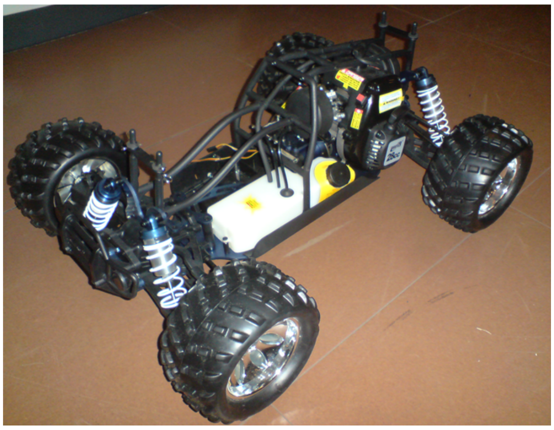

(a) Left front wheel torque response.

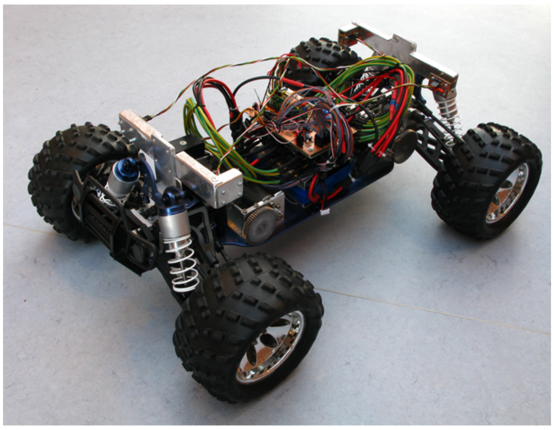

(b) Left rear wheel torque response.

Figure 5.1. Vehicle before and after modification.

The following will describe the design of the mechanical modification and development of other hardware parts.

5.1 Drive Train Gearing

In section 4.1 a motor suitable for the project was found. To convert the specifications of the motor to the specifications required on the wheel, a gear system must be implemented.

The minimum and maximum acceptable gear ratio is found by means of the torque and velocity demand respectively. The minimum requirement to torque on the wheel shaft was in equation 4.3 section 4.1 calculated to $T_{\text{w,worst}} = 9,33$ Nm. Hence the minimum value of the drive train gear ratio N_{dt} can be found as in equation 5.1

$$N_{\text{dt}} \geq \frac{T_{\text{w,worst}}}{T_{\text{m,max}}} = 14,9 \qquad [-] \tag{5.1}$$

where $T_{\text{m,max}} = I_{\text{m,max}} \cdot k_{\text{m}} = 0,63$ Nm is the maximum motor torque and $k_{\text{m}} = \frac{60}{2\pi \cdot kV} = 4,5e-3$ is the motor constant (for $I_{\text{m,max}}$ and kV see [13]). The minimum requirement to the angular velocity $\dot{\theta}_{\text{w}}$ on the wheel shaft can be calculated as in equation 5.2.

$$\dot{\theta}_{\text{w}} = \frac{v_{\text{wr,max}}}{r_{\text{w}}} = 146,3 \qquad \left[\frac{\text{rad}}{\text{s}}\right] \tag{5.2}$$

where $r_{\text{w}} = 0.095$ mm is the wheel radius (see appendix G) and $v_{\text{wr,max}} = 13,9\ \frac{\text{m}}{\text{s}}$ is the requirement to radial wheel velocity from section 2.2. The highest allowable drive train gear ratio can then be calculated as in equation 5.3.

$$N_{\text{dt}} \leq \frac{\dot{\theta}_{\text{m,max}}}{\dot{\theta}_{\text{w}}} = 22,2 \qquad [-] \tag{5.3}$$

where $\dot{\theta}_{\text{m,max}} = \frac{kV \cdot V_{\text{m,in}} \cdot 2\pi}{60} = 3254,7\ \frac{rad}{s}$ is the maximum angular velocity obtainable for the motor [14]. Hence the gear ratio $14,9 \leq N_{\text{dt}} \leq 22,2$. This gear is applied though two different gear ratios, as shown in both a CAD and actual illustration of the drive train in figure 5.2.

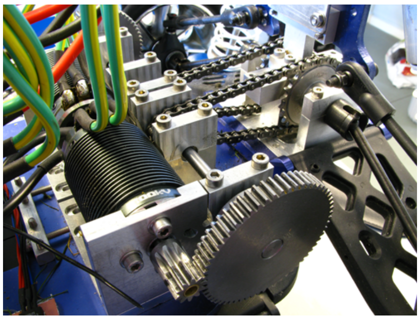

(a) Left rear wheel drive train gearing.

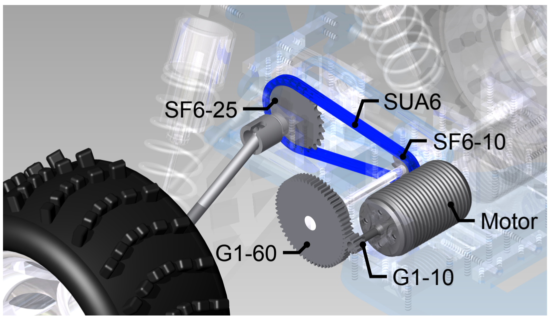

(b) CAD illustration of the right rear wheel drive train gearing.

Figure 5.2. Illustrations of drive train gearing.

To transfer the torque from the motors to the wheel shafts, chains, sprockets and gears from HPC Gears Ltd [6] have been chosen. Due to that the new differential housing (see appendix

G) is a bearing part, the size of the sprockets mounted on the wheel shafts are limited. Therefore the part SF6-25 from [6] has been chosen for this position. To maximize the gear ratio of the chain, the smallest available sprocket SG6-10 from [6] is chosen as a counterpart to the SF6-25.

To connect the sprockets, chains, matching the sprockets, are chosen. All chains are of the type SUA6, where 54 links are used on the front wheel drives and 50 links for those used on the rear wheel drives. In this way, the chain gearing amounts to 1:2,5 which is not within the limits calculated above. Therefore a spur gear of ratio 1:6 is introduced at the motor on the motor housing. This way the total gear ratio will be 1:15. The spur gears chosen are G1-10 and G1-60 from HPC Gears Ltd [6].

Originally belt drives was chosen instead of chains, though these were not able to sustain the motor torque applied through the spur gearing. According to the chain selection process from the supplier HPC [6], the SUA6 chain is just able of handling the motor power and angular velocity of the chain sprockets. The power which the chains are able to sustain, including shocks from the driver and driven applications are found as the chain selection power Psel. For the vehicle the driver and driven applications are the motor and wheel respectively. The types of shocks are found as the application factor $f1$ to the motor power Pm, and then determines Psel.

$$Psel = f1 \cdot Pm \qquad [W] \tag{5.4}$$

$$Psel = 1,5 \cdot 2050 = 3075 \qquad [W] \tag{5.5}$$

The application factor $f1$ is chosen to 1,5 from chart 2 [6], describing moderate shocks from the wheel and slight shocks from the motor. According to HPC, slight chocks are consistent with the motor used. The SUA6 chain is then found from the HPC chain rating chart, with the selection power and maximum angular velocity of the chain sprockets of around 543 $\frac{\text{rad}}{\text{s}}$. The CAD illustration in figure 5.2(b), shows how the motor, wheel, wheel shafts, chains, sprockets and gears are connected together.

To tighten the each chain, the mounting of each motor housing is made so that it can be moved closer to or further away from the differential housing. The five mounting screws of each motor housing are moving inside their own mounting slit of 16 mm in length. The same corresponds for the spur gearing, where the motor and three of its mounting screws can move inside mounting slits of around 2 mm in length, so that the two spur gears can be tightened together. Both types of mounting slits for tightening chains and spur gears are illustrated in figure 5.3.

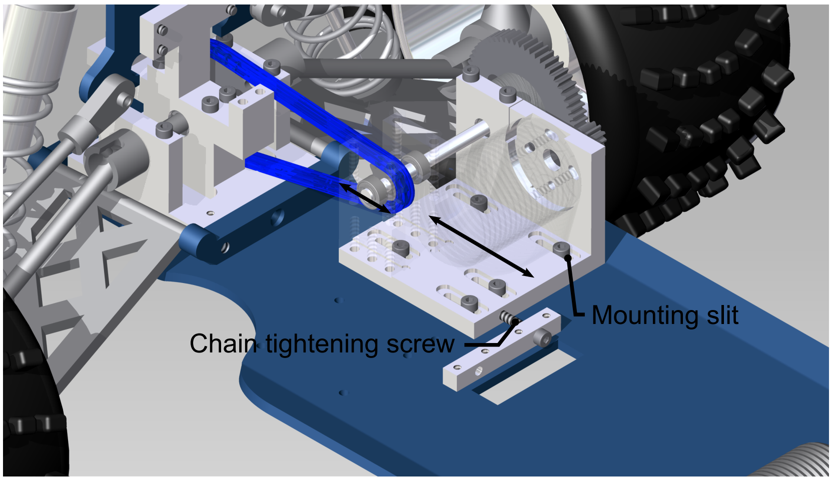

(a) CAD illustration of motor housing mounting slits for chain tightening.

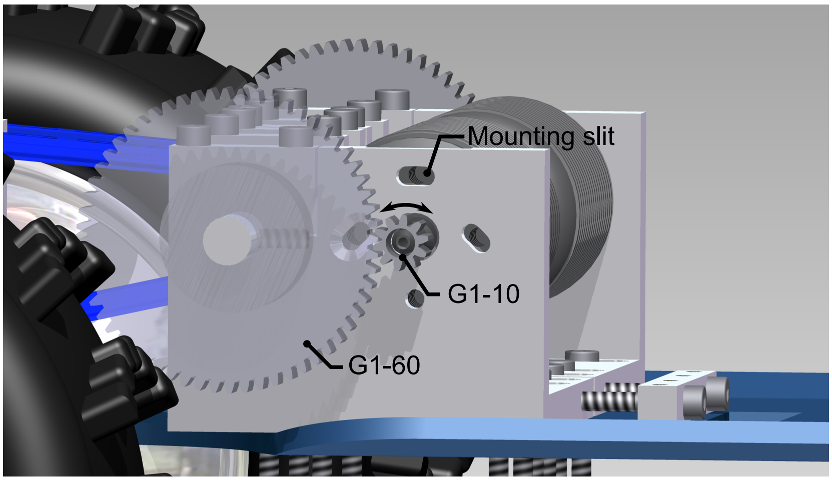

(b) CAD illustration of motor mounting slits for spur gear tightening.

Figure 5.3. Mounting slits for motor housing and motor.

A drive train gearing has been designed, so that the vehicle is now equipped with individual drive. The motors can then supply each wheel with at torque and angular velocity according to what specified in chapter 2. For the supervisory control to control the wheel torque and velocity by the motors as in section 4.4, several circuit boards for the vehicle are designed and described in the succeeding part of of the hardware design.

5.2 Circuit Board Design

One of the choices from the overall design was to implement the supervisory control in a DSP. Hence, in order to connect this DSP to the hardware as described in chapter 5, this section considers the development of two types of circuit boards. A board that contains the DSP, which is hereafter referred to as the main board, and another board containing the accelerometer. The diagrams can be found in appendix F on page 167.

Accelerometer Board

An accelerometer of type ADXL202JE has been found applicable (see [7]) and is used in the project. To be able to place the four accelerometers independently at distinct locations on the chassis of the vehicle as described in chapter 3, a circuit board for these are developed, illustrated in figure 5.4. Each accelerometer measures in two axis, and the measurement is read either as a PWM or a voltage level on two separate pins for each axis. Only one output is needed per axis, but to maintain flexibility regarding future development, both outputs on each axis respectively, can be coupled to the output connector by choice in resistor mounting. Hence the only connections necessary to the board are a supply voltage, a ground and the two lines carrying the measurements (See appendix F).

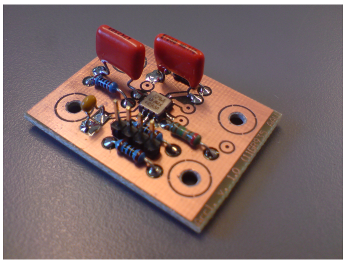

Figure 5.4. The accelerometer board.

Main board

Table 5.2 and 5.1 lists the connections and blocks, which must be integrated on the main board:

Blocks

Name	**Description**
Power supply	3,3 V and 5,0 V. Input power comes from a battery, hence the input voltage may vary.
F28335 control card	-
Manuel driver enable	A button for manually respectively activating and deactivating the drivers.
XBEE module	-
Manuel XBEE reset	A button to reset the XBEE module.

Table 5.1. Blocks to be implemented on the main board.

Connections

Name	**Quantity**	**Number of Pins**	**Reference**
Accelerometers	4	4	Accelerometer 1-4
Motor drivers	4	3	LFW motor 1 RFW motor 2 LRW motor 3 RRW motor 4
Motor position in	4	6	Motor position 1-4 in
Motor position out	4	6	Motor position 1-4 out
Steering servo motor	1	3	Servo
RC receiver channel 1-2	2	3	RC Reciever Ch 1-2
Driver enable	4	2	Driver activition
Battery in	1	2	Battery in
Power switch	1	2	Power switch
Fan power 1-4	4	3	Fan 1- 4

Table 5.2. Connection to be implemented on the main board.

F28335 control card A F28335 control card (see appendix E) is available and hence used in the project. This is a breakout board for the DSP TMS320F28335 (see appendix E and [8]) and it provides the necessary input and output connections from the DSP. Since it eases the physical implementation of the relatively small yet complex DSP, the control card is implemented on the main board rather than the DSP itself. Figure 5.5 shows the physical main board.

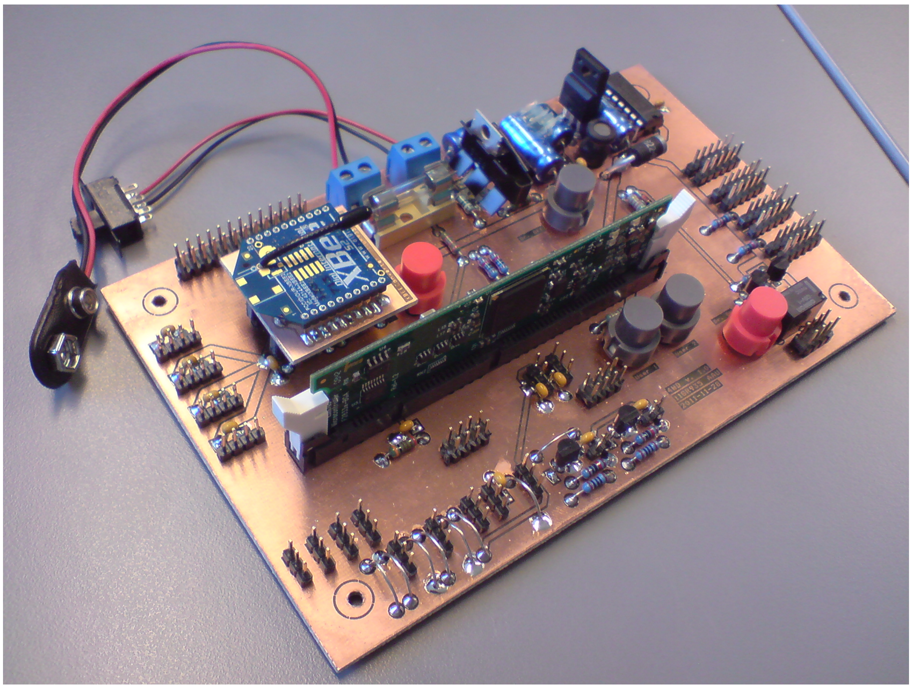

Figure 5.5. The main board.

The DSP operates at 3,3 V, hence all input/output signals must be converted to/from this voltage. However, due to a build in power supply on the F28335 control card, the card requires 5,0 V supply voltage.

XBEE module To implement a wireless data link a XBEE module (see appendix E) has been chosen. A connection is made between one XBEE module on the vehicle and another connected to e.g. a computer for data collection. For connecting one XBEE module to a computer, the XBEE explorer USB board is used (see appendix E). Due to incompatible connector sizes on the XBEE, a break out board has been produced for the vehicle (see figure 5.6), but it can also be bought prefabricated.

The XBEE explorer USB board is also used to set the link between the two XBEE modules before mounting one of them on the vehicle. The XBEE module operates at 3,3 V, hence it is directly compatible with the DSP. Furthermore the seriel interface on the XBEE is compatible with the SCI [8] connection on the DSP.

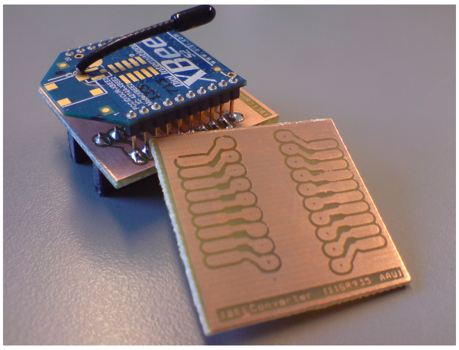

Figure 5.6. The XBEE break out board, with and without XBEE mounted.

Accelerometers A connection for each of the four accelerometers is needed. To read both axis on each of these, eight ADC input ports on the DSP are used (see appendix F). The accelerometers are able to operate at 3,0 V to 5,25 V [7], so by choosing a supply voltage of 3,3 V, no conversion of the signal voltage is needed.

Motor position in and out The motor chosen for the project provides a position feedback to the motor driver (see chapter 4). The signal consists of three pulse trains, shifted by 120° (see section 4.3). To measure the wheel velocity, it is assumed, that one of these signals is sufficient. To capture the position signal, the feedback is lead through the main board by two identical connectors connected pin to pin. One of the three pulse trains from each motor is then measured by a capture input on the DSP [8].

Power supply The main board is powered by the main battery, which is also powering the motor drivers. Therefore some variations in the battery input voltage must be expected and accounted for. The power supply voltages needed are 3,3 V for the XBEE module and 5,0 V for the F28335 control card. By letting the 3,3 V supply power the 5,0 V supply, a battery input voltage of $3,3\ \mathrm{V}+\mathrm{U_d}$ is acceptable, where $\mathrm{U_d}$ is a voltage drop over the power supply. However, if the 5,0 V power supply was driven directly from the battery input, the lowest acceptable battery input voltage would be $5,0\ \mathrm{V}+\mathrm{U_d}$.

RC receiver channel 1-2 To receive user drive signals, a standard RC receiver and transmitter are used. Two channels are needed, one for the propulsion signal and one for steering, hence two connections are implemented. Since all low power RC signals are operating at 6 V, a conversion to 3,3 V of the drive signals is performed in the following simple way. The input clamp current $\mathrm{I_{IK}}$ [8, Absolute Maximum Ratings] for the DSP is ±20 mA, hence a resistor to limit the current from the receiver to the DSP is mounted. The lowest value of the resistor is $(6\ \mathrm{V}-3,3\ \mathrm{V})\,/20e{-}3\ \mathrm{A} = 135\ \Omega$, however to prevent straining the system and to lower the current consumption a value of $10e3\ \Omega$ is chosen. The standard RC signal consists of a PWM with the following characteristics:

Period: 20 ms
Duty cycle, neutral: 7,5 % = 1500 μs
Duty cycle, max.: 10,5 % = 2100 μs
Duty cycle, min.: 4,5 % = 900 μs

The two signals are each measured by a capture input on the DSP. The supply of 6 V to the receiver is provided by one of the motor drivers described in the following.

Motor drivers The motors are controlled through the motor drivers, which takes a standard RC signal as input. However, by trial it has been found, that 3,3 V signal strength is sufficient to be recognized by the motor driver. Hence no conversion has been implemented, and a PWM output from the DSP has been connected to each motor driver. The four motor drivers each provides a standard RC 6 V supply. These supplies are used individually as supply for the blocks listed below.

RC receiver channel 1-2
Fan power 1-4 (see Fan power 1-4 below)
Steering servo motor (see Steering servo motor below)
Multi purpose LED's (see appendix F)

Steering servo motor As well as the motor drivers, the servo motor is controlled by a standard RC signal. Hence the input to the servo motor is directly connected to a PWM output on the DSP. The servo signal is set as the steering signal from the RC receiver. The supply is provided by one of the motor drivers (see motor drivers above).

Fan power 1-4 Four connectors are made for further connecting fans, cooling the propelling motors, and requires a standard RC 6 V supply as the only connection, and they are therefore coupled to one of the supplies from the motor drivers.

Driver enable To prevent unexpected behavior of the vehicle in case of low main battery power, a circuit must be designed, which is able to deactivate the four motor drivers. The type of motor driver used in this project is provided with a switch, which activates/deactivates the motor driver. When the motor driver is activated, the switch short circuits two lines. To replace the switch on the four motor drivers, a relay is implemented on the main board. When active the four control lines on one side are short circuited with the four lines on the other. The relay can only be activated by pressing a button on the main board, but it can be deactivated both by the user, the DSP and the 5,0 V power supply detecting the 3,3 V supply voltage dropping below 1,5 V. This implies, that no matter how the DSP behaves during a low voltage situation, it can not activate the motor drivers.

Three different circuit boards have now been designed. A breakout board for the accelerometers, to make individual positioning possible, a breakout board for the XBEE module to convert incompatible connectors to compatibles, and a third board, called the main board, making the relevant connections to the DSP, and the hardware in between this.

The DSP and the designed circuit boards along with the rest of the vehicle, will serve as development platform for the model developed in the following, and the controller developed in chapter 8.

Chapter 6

Model Development

The main objective of this project is to develop a supervisory controller for the vehicle, which provides TCS and TDS as described in section 4.4. To enable control on states, that are not directly measured, such as wheel torques $T_{w,k}$ and keeping the slip rate λ_k under a specified level (see section 2.2), an observer and thus a model, must be developed. Therefore, in this chapter a dynamic model of the vehicle is designed.

As stated in section 2.3, the system must control the four driving motors individually. This induces the controller to estimate the velocity on each wheel $v_{w,k}$ based on the vehicle velocity v_v and turn radius $r_{t,c\text{-}m}$. From these variables, estimates of the slip ratios λ_k on the wheels can be found.

The velocity on each wheel is dependent on several forces acting between the vehicle and the road. The dynamics of each wheel, the normal force upon these $F_{N,w,k}$ as well as the road condition will determine how much slip will be present on the wheels given a specific amount of torque. Thereby the model must describe weight distribution, transfer of normal forces based on longitudinal and lateral forces, along with spring and damper response of the suspension.

The normal force on a wheel combined with various surface friction coefficients μ result in distinct driving forces F_d to be transfered from the wheels. However, the driving force is also dependent on the difference in ground and wheel velocity (slip ratio) [15], which again is a result of the wheel torque and the dynamics of the wheel. Hence the drive trains, consisting of motors, gearings, shafts and wheels, must be modeled as a dynamic system to know the torque applied to the wheels and the resulting driving force. Summarized the model must describe the following.

- **Wheel steering system**
  Describe the wheel steering angles according to the steering RC signal
- **Suspension**
  Describe the normal force on each wheel by means of the dynamic of the springs and dampers on the vehicle. Describe how the position of the vehicle is affected by the wheels, dependent on the driving forces and wheel torques
- **Drive train**
  Describe the dynamics of the drive trains from motor driver signal to wheel torque and velocity, dependent on the drive forces
- **Surface friction coefficient**
  Describe the friction coefficient for the surface friction coefficient driven on to know how much torque that can be transferred given a certain normal force on the wheels. This is dependent on the slip ratio and thereby wheel and vehicle velocities
- **Horizontal vehicle dynamics**
  Describe the vehicle velocity dependent on the drive forces

The complete vehicle model is illustrated in figure 6.1.

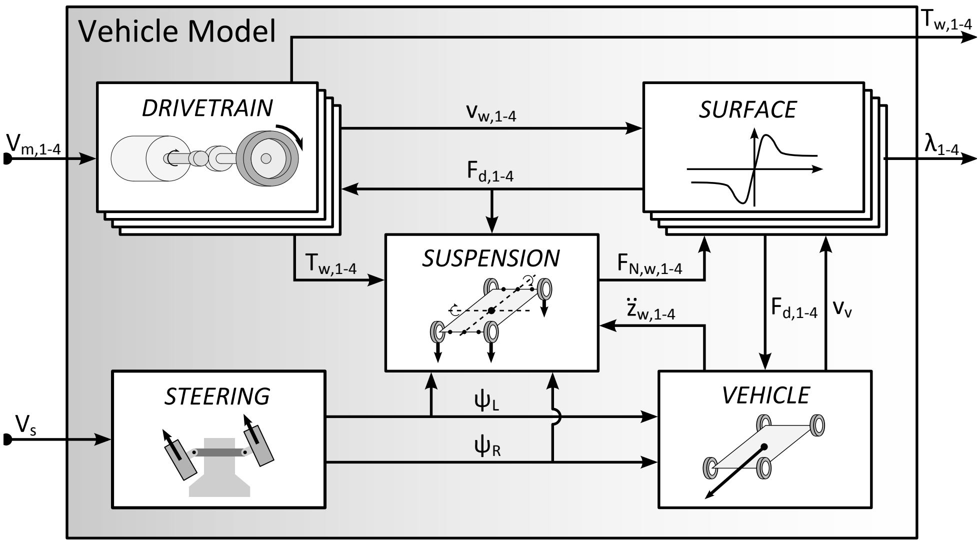

Figure 6.1. Block diagram of the vehicle model

The vehicle model developed in this chapter, from here on written as *VEHICLE MODEL*, has two purposes. Firstly it will replace the actual vehicle in a simulation setup, to test the controller developed in chapter 8 before it is tested on the physical environment. This simulation setup can be seen in figure 6.2 and the corresponding physical setup in figure 6.3.

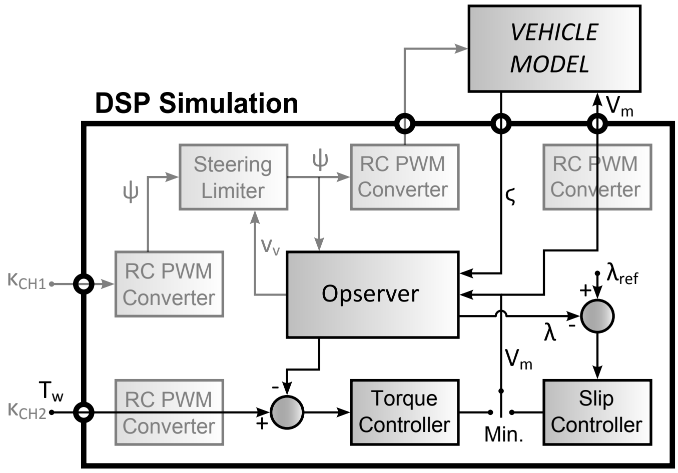

Figure 6.2. Block diagram of simulated DSP in simulated environment

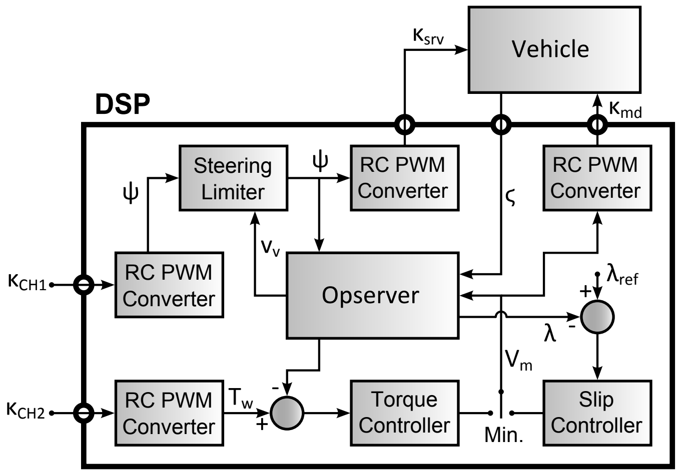

Figure 6.3. Block diagram of DSP setup in physical environment

Secondly the *VEHICLE MODEL* forms the basis for the development of the observer (chapter 7). Since the observer must run in real time on the DSP, the utilization requirement and computational load must be kept in mind. Therefore the observer model will be a simplified version of the *VEHICLE MODEL*, where certain terms are either neglected or substituted with lighter approximations. These modifications will be described in chapter 7 as the observer is developed. The simulation of models are constructed as object oriented programming in MATLAB® , where each model is an object. The first part of the *VEHICLE MODEL* developed is the steering system and wheel base.

6.1 Steering System and Wheel Base

In this project it has been chosen to focus only on straight forward driving. This implies that only longitudinal forces are considered, hence even though sensors to measure lateral accelerations have been implemented in the hardware, these are not used. It also means, that even though developed, the steering system model developed in this chapter will not be used further on. Nor will variations in wheel velocity, caused by turning, be considered in the model. However, even though turning is not considered, the TDS is still to make individual wheel torque and revolutions possible. Different torques and revolution on the wheel would make the vehicle turn, but since the vehicle model of this is simplified and considers straight drive only, the drive forces will result in only longitudinal accelerations and changes in pitch. As part of maintaining an accurate estimate of the normal forces on the wheels, roll is still included in the model, however it may not be affected. The TCS is still to control the wheel slip, thus also wheel angular velocity.

In this chapter the model of the wheel steering angles is derived, and could be considered in future work with expanding the system. The suspension model SUSPENSION and the horizontal vehicle model VEHICLE should use the steering angles, since these affect the normal force on each wheel, and thus the vehicle velocity and orientation.

As described in 2.1, the vehicle differentials are removed and an individual wheel drive is used. The supervisory control will instead distribute torque to each wheel through the drive trains without slip, and thereby include TDS and TCS functions. The wheel traction is dependent on the road friction coefficient and load upon the wheel. The wheel load results from the drive and turning of the vehicle, where forces arise and changes the vehicle weight distribution. The turn radius of the vehicle must therefore be determined for the vehicle weight distribution model in section 6.4. The turn radius depend on forces between the road and wheel, drive train torque, vehicle inertia, wheel base and angle of the steering wheels. The forces between the road and wheel are described by the model in section 6.3. The wheel torque is described by the model in section 6.2. The vehicle inertia and wheel base are included in the model of the weight distribution in section 6.4. Thus a model of the vehicle steering system is to be derived describing the wheel steering angles ψ_{L} and ψ_{R} as illustrated in figure 6.4. The models will then together determine how the vehicle will behave executing a turn.

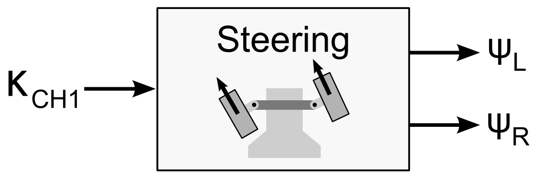

Figure 6.4. Steering system model

The steering system consist of a steering servo motor, which according to a steering servo signal, turns the two steering wheels, through rods in the steering system. First a kinematic model is developed for the steering system, describing the relation from steering servo signal to wheel steering angles. Hereafter a dynamic model is applied to describe the turning response of the steering system and servo combined.

Wheel Steering Angles

The wheel steering angles determines how the force from the wheel torque and surface friction are applied to the vehicle, and thereby how this will drive and turn. A representation of the steering system illustrated in figure 6.5, is made to describe how the rod displacements of the steering system makes the steering wheels turn. The steering system uses a center rack combined with a toe rods to turn the steering wheels, when the steering servo is turned. The representation of the wheel steering system is shown in figure 6.5(a). The representation of the steering system when turning is shown in figure 6.5(b).

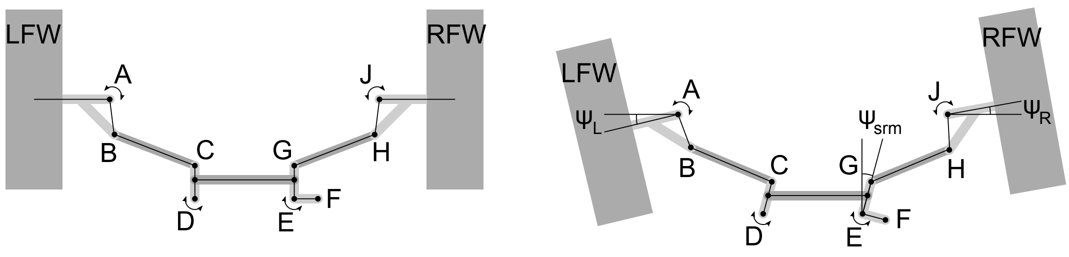

(a) Representation of steering system without turning. (b) Representation of steering system with turning.

Figure 6.5. Representation of steering system

Where AB_{LFW} and JH_{RFW} are the wheel steering arms for each wheel. Joint *A* and *J* are fixed to the suspensions on each side, and the steering wheels will turn around these points when joint *B* and *H* are moved by the toe rods *BC* and *GH*. The toe rods are moved, when the idler arm *CD* and the pitman arm *GEF* are turned around the fixed joints *D* and *E*. The turning is done on both rods though the center rack connection *CG*, when moving the pitman arm *GEF*, and thereby the point *G*. The steering servo is connected to the the pitman arm, and these angles are thereby the same.

$$AC = \sqrt{((Cx - Ax)^2 + (Ay - Cy)^2)} \quad [\mathrm{m}] \tag{6.1}$$

$$\psi_{L|\psi_{srm}=0} = \sin^{-1}\left(\frac{Cx-Ax}{AC}\right) - \cos^{-1}\left(\frac{BC^2-AC^2-AB^2}{-2\cdot AC\cdot AB}\right) \tag{6.2}$$

$$\psi_L = \psi_{L|\psi_{srm}=0} - \sin^{-1}\left(\frac{Cx-Ax}{AC}\right) - \cos^{-1}\left(\frac{BC^2-AC^2-AB^2}{-2\cdot AC\cdot AB}\right) \tag{6.3}$$

$$C(Cx, Cy) = \big(Dx - CD\cdot\sin(\psi_{srm}), Dy + CD\cdot\cos(\psi_{srm})\big) \quad [\mathrm{m}] \tag{6.4}$$

$$JG = \sqrt{((Jx - Gx)^2 + (Jy - Gy)^2)} \quad [\mathrm{m}] \tag{6.5}$$

$$\psi_{R|\psi_{srm}=0} = \sin^{-1}\left(\frac{Jx-Gx}{JG}\right) + \cos^{-1}\left(\frac{GH^2-JG^2-JH^2}{-2\cdot JG\cdot JH}\right) \tag{6.6}$$

$$\psi_R = -\psi_{R|\psi_{srm}=0} + \sin^{-1}\left(\frac{Jx-Gx}{JG}\right) + \cos^{-1}\left(\frac{GH^2-JG^2-JH^2}{-2\cdot JG\cdot JH}\right) \tag{6.7}$$

$$G(Gx, Gy) = \big(Ex - EG\cdot\sin(\psi_{srm}), Ey + EG\cdot\cos(\psi_{srm})\big) \quad [\mathrm{m}] \tag{6.8}$$

Here ψ_L and ψ_R are found from the pitman arm and servo angle angle ψ_{srm} at *EG*. $\psi_{L|\psi_{srm}=0}$ and $\psi_{R|\psi_{srm}=0}$ found by the initial positions of all rods with no turning angle on the steering servo, thus also no turning angles on the steering wheels. In figure 6.6, the connection between ψ_{srm} and the steering wheel angles ψ_{L} and ψ_{R} is shown.

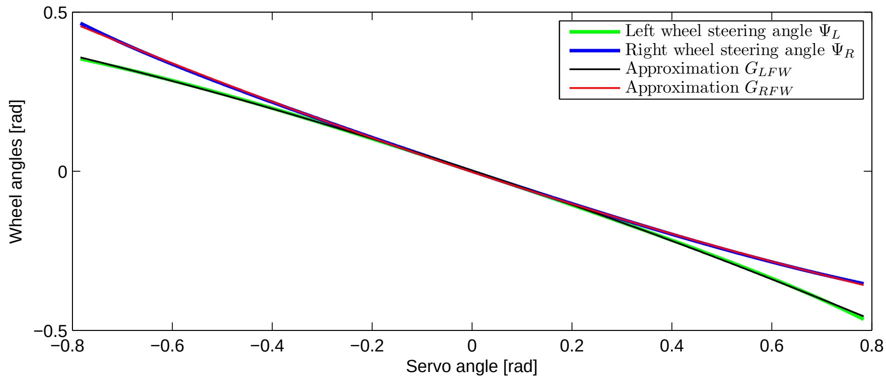

Figure 6.6. Connection form servo angle to steering wheel angles

The functions of ψ_{L} and ψ_{R} are then dependent of the servo position, and are approximated as G_{LFW} and G_{RFW} for each wheel.

(6.9) $$\psi_{\text{L}} = \text{G}_{\text{LFW}}\left(\psi_{\text{srm}}\right) = a_L \cdot \psi_{\text{srm}}^2 + b_L \cdot \psi_{\text{srm}} + c_L \qquad \text{[rad]}$$

(6.10) $$\psi_{\text{R}} = \text{G}_{\text{RFW}}\left(\psi_{\text{srm}}\right) = a_R \cdot \psi_{\text{srm}}^2 + b_R \cdot \psi_{\text{srm}} + c_R \qquad \text{[rad]}$$

The the parameters of G_{LFW} and G_{RFW} are found in a considered range of $\left[-\frac{\pi}{4};\frac{\pi}{4}\right]$, since the servo angle constrained to this.

(6.11)
$$a_L = -0,08362,\ b_L = -0,5191,\ c_L = 0,002195,\ a_R = -0,08362,\ b_R = -0,5191,\ c_R = -0,002195$$

Thus both G_{LFW} and G_{RFW} is used as a gearing from servo position to steering wheel angles. These and are illustrated in figure 6.6 and used for the both vehicle models. The following will find the turning response of the servo combined with the wheel steering system, in relation to the applied servo signal.

Servo Turning Response

The servo consists of a motor and several gears. When a standard RC signal κ_{CH1} is applied, the servo will turn to the angle corresponding to the signal applied. It is expected that this control is controlling the motor voltage proportionally to the angle error between the RC signal reference angle and actual angle position of the servo. A model G_{srm} of the servo turning response, as in figure 6.7, is derived in the following, where the inertia from the steering system and wheels are also included, though without the road condition influence.

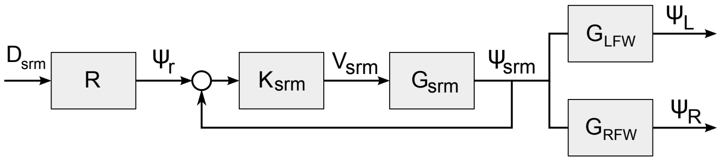

Figure 6.7. Illustration of combined steering system model

Here G_{srm}, G_{LFW} and G_{RFW} together gives the total response from servo signal to wheel steering angles. R describes how the duty cycle D_{srm} of the PWM signal κ_{CH1} is connected to the reference angle ψ_r.

(6.12) $$\psi_{ref} = (D_{srm} - 1{,}5\ m) \cdot a_{srm} \qquad [\text{rad}]$$

The relation a_{srm} between ψ_r and D_{srm} is assumed to be around $\frac{1667 \cdot \pi}{4}$rad. The angle error ψ_e between the reference angle ψ_r and the actual angle ψ_{srm} on the servo, then determines the voltage applied to the motor through the proportional term K_{srm}, such that the motor will turn towards the reference angle. The turning of the motor is determined from the motor parameters.

(6.13) $$\psi_e = \psi_{ref} - \psi_{srm} \qquad [\text{rad}]$$

(6.14) $$V_{srm} = K_{srm} \cdot \psi_e \qquad [\text{V}]$$

(6.15) $$\frac{\mathrm{d}I_{srm}}{\mathrm{d}t} = -\frac{R_{srm}}{L_{srm}} \cdot I_{srm} - \frac{K_{a,srm}}{L_{srm}} \cdot \omega_{srm} + \frac{V_{srm}}{L_{srm}} \qquad \left[\frac{\text{A}}{\text{s}}\right]$$

(6.16) $$\frac{\mathrm{d}\omega_{srm}}{\mathrm{d}t} = \frac{K_{a,srm}}{J_{srm}} \cdot I_{srm} - \frac{b_{srm}}{J_{srm}} \cdot \omega_{srm} \qquad \left[\frac{\text{rad}}{\text{s}^2}\right]$$

These are combined in a motor model of the servo, where ψ_{ref} and ψ_{srm} is used as reference instead of the motor voltage V_{srm} in the estimate χ_{srm}.

(6.17) $$\dot{\chi}_{srm} = \dot{\begin{bmatrix} I_{srm} \\ \psi_{srm} \\ \omega_{srm} \end{bmatrix}} = \begin{bmatrix} -\frac{R_{srm}}{L_{srm}} & -\frac{K_{srm}}{L_{srm}} & -\frac{K_{a,srm}}{L_{srm}} \\ 0 & 0 & 1 \\ \frac{K_{a,srm}}{J_{srm}} & 0 & \frac{b_{srm}}{J_{srm}} \end{bmatrix} \cdot \begin{bmatrix} I_{srm} \\ \psi_{srm} \\ \omega_{srm} \end{bmatrix} + \begin{bmatrix} \frac{K_{a,srm}}{L} \\ 0 \\ 0 \end{bmatrix} \cdot \psi_r \qquad \begin{bmatrix} \frac{\text{A}}{\text{s}} \\ \frac{\text{rad}}{\text{s}} \\ \frac{\text{rad}}{\text{s}^2} \end{bmatrix}$$

(6.18) $$\psi_{srm} = \gamma_{srm} = \begin{bmatrix} 0 & 1 & 0 \end{bmatrix} \cdot \chi_{srm} \qquad [\text{rad}]$$

An illustration of a response according to this model is shown in figure 6.8. Though the servo is not able to supply more than 6 V for the motor voltage V_{srm}, and is thereby not allowed to increase in angular velocity ω_{srm} at some angle error ψ_e, determined by the proportional term K_{srm}. A servo response $\psi_{srm,a}$ is also shown in figure 6.8, where it is turning with a constant rate of its maximum velocity almost all the time.

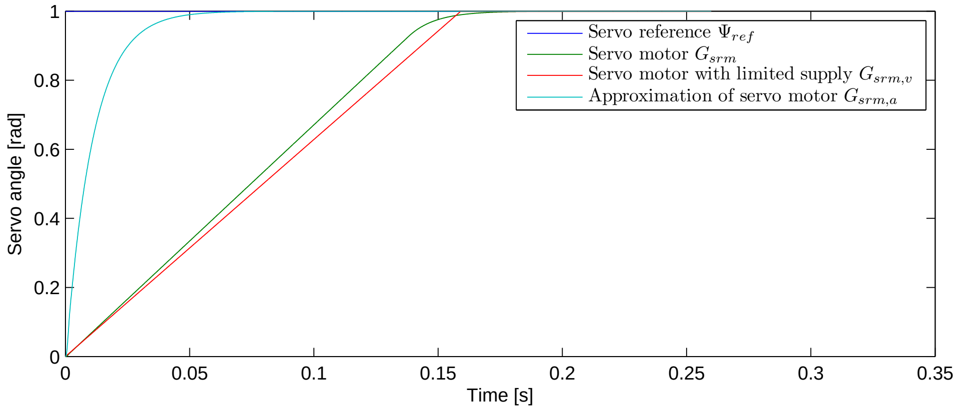

Figure 6.8. Turning responses of servo

Instead of describing the response of ψ_{srm} with the model $\mathrm{G_{srm}}$ including the maximum allowed motor voltage V_{srm} of 6 V, this is instead approximated by $\mathrm{G_{srm,a}}$.

$$\dot{\psi}_{\mathrm{srm}} = \mathrm{G_{srm,a}}\left(\psi_{\mathrm{e}}\right) = \begin{cases} \omega_{\mathrm{turn,srm}} & \psi_{\mathrm{e}} > 0 \\ -\omega_{\mathrm{turn,srm}} & \psi_{\mathrm{e}} < 0 \end{cases} \qquad \left[\frac{\mathrm{rad}}{\mathrm{s}}\right] \tag{6.19}$$

The simplified vehicle model will use $\mathrm{G_{srm,a}}$. $\mathrm{G_{srm,a}}$ uses $\omega_{\mathrm{turn,srm}}$ as the angular velocity of the servo at 6 V supply. This is estimated to be $2\pi\frac{\mathrm{rad}}{\mathrm{s}}$. When there is an angle error between ψ_{r} and ψ_{srm}, the motor will turn with this velocity. According to the specifications, the servo is able of handling a load of 18 kg, and the inertia from the steering system should thereby not affect $\omega_{\mathrm{turn,srm}}$ with the included control. The response using $\mathrm{G_{srm,a}}$ is illustrated in figure 6.8. The actual response of the servo ψ_{srmv} is a combination of the responses of $\mathrm{G_{srm}}$ and $\mathrm{G_{srm,a}}$.

Combining $\mathrm{G_{srm,a}}$, $\mathrm{G_{LFW}}$ and $\mathrm{G_{RFW}}$ gives the modeled relation from RC servo signal κ_{CH1} to each of the wheel steering angles ψ_{L} and ψ_{R}. This is used to determine how the wheel steering angles affect the vehicle weight distribution when turning, thus also the normal load and traction of each wheel.

6.2 Drive Train

The torque on the wheels are to be distributed by the TDS and limited by the TCS to limit wheel slip as specified in 2.2. The torque, which can be applied to the wheel through the drive train without the slip rate exceeding the limit, is determined by the surface friction coefficient and the normal force on the wheel. A model will therefore describe the dynamics of the drive trains, from motor driver signal to wheel torque and velocity. The supervisory control can thereby use the model to apply a signal to each motor driver, to obtain the desired torque on each wheel. It is assumed, that the four drive trains are identical, hence a common model is derived.

Drive train response

Each drive train consist of a motor driver and a motor, chosen in section 4.1, which drives a wheel through a gearing N_{dt}, determined in section 5.1 (see figure 5.2).

The motor driver takes a low power input signal κ_{md} of the RC standard type, described for the RC receiver in section 5.2. The motor driver converts the low power signal to a high power three phase motor voltage signal V_{m} supplied to the motor. These blocks are combined in one model to describe the relation between κ_{md} and the drive train torque and wheel velocity. Gearing backlash or coulomb friction are not included. A representation of the drive train is shown in figure 6.9.

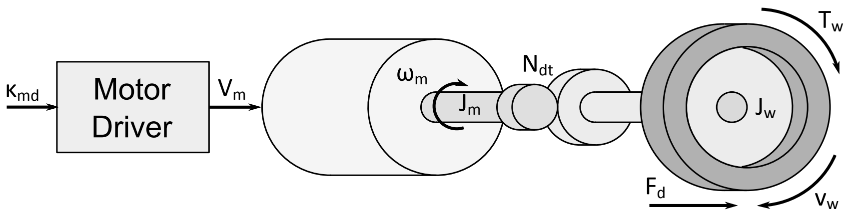

Figure 6.9. Representation of drive train

For the wheel to turn, the drive train must produce a torque T_{w} on the wheel to overcome the torque from the inertia of the wheel and other forces acting upon the wheel, which is combined in the drive force F_{d}. Some of these forces result from the wheel rolling along the road and are thereby dependent on the surface friction coefficient, normal force upon the wheel and both the wheel and vehicle velocity. Thus all torques and wheel velocities affect each other and the vehicle.

The drive force F_{d} is calculated from the normal force $F_{\mathrm{N,w}}$ and the road surface friction coefficient $\mu(\lambda)$ in the horizontal vehicle model *VEHICLE*. The model *DRIVETRAIN* of the drive train will therefore describe the wheel torque T_{w}, wheel velocity v_{w} and sensor output ζ_{m} according to the motor driver control signal κ_{md} and the drive force F_{d} as illustrated in figure 6.10.

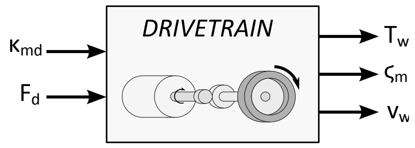

Figure 6.10. Drive train model

κ_{md} is controlled by the supervisory control. It is assumed, that the motor driver can be modeled as shown in figure 6.11, where D_{md} is a duty cycle of the PWM signal κ_{md}, and it relates to the motor voltage as shown in figure 6.11.

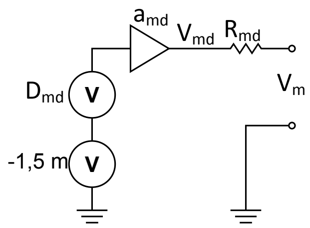

Figure 6.11. Motor driver electrical model

$$V_{\text{md}} = (D_{\text{md}} - 1{,}5\ m) \cdot a_{\text{md}} \qquad [\text{V}] \tag{6.20}$$

where a_{md} is a programmable constant in the motor driver. The motor and motor driver together are modeled with a set of ordinary motor differential equations. Since the internal motor driver resistance R_{md} is serial connected with the internal motor resistance R_{m} it can be included in R_{m}. Hence if equation 6.20 is excluded from the model, the drive train model must describe the relation from V_{m} to T_{w} and v_{w}. The system equations are set up in equation 6.21 and 6.22.

$$\frac{\mathrm{d}I_{\text{m}}}{\mathrm{d}t} = -\frac{R_{\text{m}}}{L_{\text{m}}} \cdot I_{\text{m}} - \frac{K_{\text{a}}}{L_{\text{m}}} \cdot \omega_{\text{m}} + \frac{1}{L_{\text{m}}} \cdot V_{\text{m}} \qquad \left[\frac{\text{A}}{\text{s}}\right] \tag{6.21}$$

$$\left(\frac{J_{\text{w}}}{{N_{\text{dt}}}^2} + J_{\text{m}}\right) \cdot \frac{\mathrm{d}\omega_{\text{m}}}{\mathrm{d}t} = K_{\text{a}} \cdot I_{\text{m}} - b_{\text{m}} \cdot \omega_{\text{m}} - \frac{r_{\text{w}}}{N_{\text{dt}}} \cdot F_{\text{d}} \qquad \left[\frac{\text{rad}}{\text{s}^2}\right]$$

$$\frac{\mathrm{d}\omega_{\text{m}}}{\mathrm{d}t} = \frac{K_{\text{a}}}{\frac{J_{\text{w}}}{N_{\text{dt}}^2} + J_{\text{m}}} \cdot I_{\text{m}} - \frac{b_{\text{m}}}{\frac{J_{\text{w}}}{N_{\text{dt}}^2} + J_{\text{m}}} \cdot \omega_{\text{m}} - \frac{r_{\text{w}}}{\frac{J_{\text{w}}}{N_{\text{dt}}} + N_{\text{dt}} \cdot J_{\text{m}}} \cdot F_{\text{d}} \qquad \left[\frac{\text{rad}}{\text{s}^2}\right]$$

$$\frac{\mathrm{d}\omega_{\text{m}}}{\mathrm{d}t} = \frac{N_{\text{dt}}^2 \cdot K_{\text{a}}}{J_{\text{w}} + N_{\text{dt}}^2 \cdot J_{\text{m}}} \cdot I_{\text{m}} - \frac{N_{\text{dt}}^2 \cdot b_{\text{m}}}{J_{\text{w}} + N_{\text{dt}}^2 \cdot J_{\text{m}}} \cdot \omega_{\text{m}} - \frac{N_{\text{dt}} \cdot r_{\text{w}}}{J_{\text{w}} + N_{\text{dt}}^2 \cdot J_{\text{m}}} \cdot F_{\text{d}} \qquad \left[\frac{\text{rad}}{\text{s}^2}\right] \tag{6.22}$$

The matrix form of 6.21 and 6.22 is seen in 6.23.

$$\dot{\overline{\chi}}_{\mathrm{dt}} = \begin{bmatrix} \frac{\mathrm{d}I_{\mathrm{m}}}{\mathrm{d}t} \\ \frac{\mathrm{d}\omega_{\mathrm{m}}}{\mathrm{d}t} \end{bmatrix}$$

$$\dot{\overline{\chi}}_{\mathrm{dt}} = \begin{bmatrix} -\frac{R_{\mathrm{m}}}{L_{\mathrm{m}}} & -\frac{K_{\mathrm{a}}}{L_{\mathrm{m}}} \\ \frac{N_{\mathrm{dt}}^2 \cdot K_{\mathrm{a}}}{J_{\mathrm{w}}+N_{\mathrm{dt}}^2 \cdot J_{\mathrm{m}}} & -\frac{N_{\mathrm{dt}}^2 \cdot b_{\mathrm{m}}}{J_{\mathrm{w}}+N_{\mathrm{dt}}^2 \cdot J_{\mathrm{m}}} \end{bmatrix} \overline{\chi}_{\mathrm{dt}} + \begin{bmatrix} \frac{1}{L_{\mathrm{m}}} & 0 \\ 0 & -\frac{N_{\mathrm{dt}} \cdot r_{\mathrm{w}}}{J_{\mathrm{w}}+N_{\mathrm{dt}}^2 \cdot J_{\mathrm{m}}} \end{bmatrix} \begin{bmatrix} V_{\mathrm{m}} \\ F_{\mathrm{d}} \end{bmatrix} \tag{6.23}$$

$$\mathbf{A}_{\mathrm{dt}} = \begin{bmatrix} -\frac{R_{\mathrm{m}}}{L_{\mathrm{m}}} & -\frac{K_{\mathrm{a}}}{L_{\mathrm{m}}} \\ \frac{N_{\mathrm{dt}}^2 \cdot K_{\mathrm{a}}}{J_{\mathrm{w}}+N_{\mathrm{dt}}^2 \cdot J_{\mathrm{m}}} & -\frac{N_{\mathrm{dt}}^2 \cdot b_{\mathrm{m}}}{J_{\mathrm{w}}+N_{\mathrm{dt}}^2 \cdot J_{\mathrm{m}}} \end{bmatrix}, \mathbf{B}_{\mathrm{dt}} = \begin{bmatrix} \frac{1}{L_{\mathrm{m}}} & 0 \\ 0 & -\frac{N_{\mathrm{dt}} \cdot r_{\mathrm{w}}}{J_{\mathrm{w}}+N_{\mathrm{dt}}^2 \cdot J_{\mathrm{m}}} \end{bmatrix}$$

χ_{dt} is in 6.24 and 6.26 used to calculate the wheel velocity v_{w} and torque applied to the wheel T_{w}.

$$v_{\mathrm{w}} = \frac{r_{\mathrm{w}}}{N_{\mathrm{dt}}} \cdot \omega_{\mathrm{m}} \tag{6.24}$$

$$T_{\mathrm{w}} = \frac{\dot{\omega}_{\mathrm{m}}}{N_{\mathrm{dt}}} \cdot J_{\mathrm{w}} + r_{\mathrm{w}} \cdot F_{\mathrm{d}} \qquad [\mathrm{Nm}] \tag{6.25}$$

$$T_{\mathrm{w}} = \frac{J_{\mathrm{w}}}{N_{\mathrm{dt}}} \cdot \left(\frac{N_{\mathrm{dt}}^2 \cdot K_{\mathrm{a}}}{J_{\mathrm{w}}+N_{\mathrm{dt}}^2 \cdot J_{\mathrm{m}}} \cdot I_{\mathrm{m}} - \frac{N_{\mathrm{dt}}^2 \cdot b_{\mathrm{m}}}{J_{\mathrm{w}}+N_{\mathrm{dt}}^2 \cdot J_{\mathrm{m}}} \cdot \omega_{\mathrm{m}} - \frac{N_{\mathrm{dt}} \cdot r_{\mathrm{w}}}{J_{\mathrm{w}}+N_{\mathrm{dt}}^2 \cdot J_{\mathrm{m}}} \cdot F_{\mathrm{d}} \right) + r_{\mathrm{w}} \cdot F_{\mathrm{d}} \qquad [\mathrm{Nm}]$$

$$T_{\mathrm{w}} = \frac{J_{\mathrm{w}} \cdot N_{\mathrm{dt}} \cdot K_{\mathrm{a}}}{J_{\mathrm{w}} + N_{\mathrm{dt}}^2 \cdot J_{\mathrm{m}}} \cdot I_{\mathrm{m}} - \frac{J_{\mathrm{w}} \cdot N_{\mathrm{dt}} \cdot b_{\mathrm{m}}}{J_{\mathrm{w}} + N_{\mathrm{dt}}^2 \cdot J_{\mathrm{m}}} \cdot \omega_{\mathrm{m}} - \frac{J_{\mathrm{w}} \cdot r_{\mathrm{w}}}{J_{\mathrm{w}} + N_{\mathrm{dt}}^2 \cdot J_{\mathrm{m}}} \cdot F_{\mathrm{d}} + r_{\mathrm{w}} \cdot F_{\mathrm{d}} \qquad [\mathrm{Nm}]$$

$$T_{\mathrm{w}} = \underbrace{\frac{J_{\mathrm{w}} \cdot N_{\mathrm{dt}} \cdot K_{\mathrm{a}}}{J_{\mathrm{w}} + N_{\mathrm{dt}}^2 \cdot J_{\mathrm{m}}}}_{\text{Current term}} \cdot I_{\mathrm{m}} - \underbrace{\frac{J_{\mathrm{w}} \cdot N_{\mathrm{dt}} \cdot b_{\mathrm{m}}}{J_{\mathrm{w}} + N_{\mathrm{dt}}^2 \cdot J_{\mathrm{m}}}}_{\text{Viscous damping term}} \cdot \omega_{\mathrm{m}} + \underbrace{\left(r_{\mathrm{w}} - \frac{J_{\mathrm{w}} \cdot r_{\mathrm{w}}}{J_{\mathrm{w}} + N_{\mathrm{dt}}^2 \cdot J_{\mathrm{m}}} \right)}_{\text{Drive force term}} \cdot F_{\mathrm{d}} \qquad [\mathrm{Nm}] \tag{6.26}$$

6.24 and 6.26 are seen in matrix form in 6.27. Notice that the wheel inertia J_{w} and motor inertia J_{m} are combined when calculating the motor angular acceleration $\dot{\omega}_{\mathrm{w}}$, whereas the wheel torque T_{w} is only dependent on the wheel inertia J_{w}, change of motor angular velocity $\dot{\omega}_{\mathrm{m}}$ and the drive force F_{d} (see 6.26).

$$\overline{\gamma}_{\mathrm{dt}} = \begin{bmatrix} T_{\mathrm{dt}} \\ v_{\mathrm{w}} \end{bmatrix}$$

$$\overline{\gamma}_{\mathrm{dt}} = \begin{bmatrix} \frac{J_{\mathrm{w}} \cdot N_{\mathrm{dt}} \cdot K_{\mathrm{a}}}{J_{\mathrm{w}}+N_{\mathrm{dt}}^2 \cdot J_{\mathrm{m}}} & -\frac{J_{\mathrm{w}} \cdot N_{\mathrm{dt}} \cdot b_{\mathrm{m}}}{J_{\mathrm{w}}+N_{\mathrm{dt}}^2 \cdot J_{\mathrm{m}}} \\ 0 & \frac{r_{\mathrm{w}}}{N_{\mathrm{dt}}} \end{bmatrix} \overline{\chi}_{\mathrm{dt}} + \begin{bmatrix} 0 & r_{\mathrm{w}} - \frac{J_{\mathrm{w}} \cdot r_{\mathrm{w}}}{J_{\mathrm{w}}+N_{\mathrm{dt}}^2 \cdot J_{\mathrm{m}}} \\ 0 & 0 \end{bmatrix} \begin{bmatrix} V_{\mathrm{m}} \\ F_{\mathrm{d}} \end{bmatrix} \tag{6.27}$$

$$\mathbf{C}_{\mathrm{dt}} = \begin{bmatrix} \frac{J_{\mathrm{w}} \cdot N_{\mathrm{dt}} \cdot K_{\mathrm{a}}}{J_{\mathrm{w}}+N_{\mathrm{dt}}^2 \cdot J_{\mathrm{m}}} & -\frac{J_{\mathrm{w}} \cdot N_{\mathrm{dt}} \cdot b_{\mathrm{m}}}{J_{\mathrm{w}}+N_{\mathrm{dt}}^2 \cdot J_{\mathrm{m}}} \\ 0 & \frac{r_{\mathrm{w}}}{N_{\mathrm{dt}}} \end{bmatrix}, \mathbf{D}_{\mathrm{dt}} = \begin{bmatrix} 0 & r_{\mathrm{w}} - \frac{J_{\mathrm{w}} \cdot r_{\mathrm{w}}}{J_{\mathrm{w}}+N_{\mathrm{dt}}^2 \cdot J_{\mathrm{m}}} \\ 0 & 0 \end{bmatrix}$$

Where b_{m} is identified in section A.3. The identification of the drive train b_{m} indicates that the coulomb friction is not as negligible as first assumed. This result in two choices of designing the drive train model. One is to add the coulomb friction to the model and achieve higher estimation performance of the extended Kalman filter. When adding the friction the drive train model becomes hybrid, consisting of a model for coulomb friction at low wheel velocity and one for high. The other option is to only use viscous friction, and decrease the Kalman filter estimation performance. It is chosen to neglect the coulomb friction and hybrid model, and estimate the viscous friction b_{m} as close to the combined of the two frictions as possible.

The model, consisting of $\mathbf{A}_{\mathrm{dt}}$, $\mathbf{B}_{\mathrm{dt}}$, $\mathbf{C}_{\mathrm{dt}}$ and $\mathbf{D}_{\mathrm{dt}}$, is discretized using the MATLAB® functions *ss()* and *c2d()*.

When modeling the sensor output from the motor, it is assumed, that every transition in the pulse from the real sensor (see figure 4.6 in section 4.3) happens according to a normal distribution centered around the motor positions $\theta_{\mathrm{m},k}$, which are the nominal positions of the shifts. Formula 6.28 and 6.29 shows how the angular motor velocity sensor output is calculated.

$$\begin{aligned}
(6.28)\qquad \zeta_{\mathrm{m},n} &= \frac{\mathcal{N}\left(\theta_{\mathrm{m},n}, {\sigma_{\mathrm{m}}}^2\right) - \mathcal{N}\left(\theta_{\mathrm{m},n-1}, {\sigma_{\mathrm{m}}}^2\right)}{\Delta t} && \left[\frac{\mathrm{rad}}{\mathrm{s}}\right] \\
&= \frac{\theta_{\mathrm{m},n} - \theta_{\mathrm{m},n-1}}{\Delta t} + \frac{\mathcal{N}\left(0, {\sigma_{\mathrm{m}}}^2\right) - \mathcal{N}\left(0, {\sigma_{\mathrm{m}}}^2\right)}{\Delta t} && \left[\frac{\mathrm{rad}}{\mathrm{s}}\right] \\
&= \omega_{\mathrm{m}} + \frac{\mathcal{N}\left(0, {\sigma_{\mathrm{m}}}^2\right) - \mathcal{N}\left(0, {\sigma_{\mathrm{m}}}^2\right)}{\frac{c}{\omega_{\mathrm{m}}}}, \quad c = \theta_{\mathrm{m},n} - \theta_{\mathrm{m},n-1} && \left[\frac{\mathrm{rad}}{\mathrm{s}}\right] \\
&= \omega_{\mathrm{m}} + \omega_{\mathrm{m}} \cdot \mathcal{N}\left(0, \left(\frac{\sqrt{2} \cdot \sigma_{\mathrm{m}}}{c}\right)^2\right) && \left[\frac{\mathrm{rad}}{\mathrm{s}}\right] \\
(6.29)\qquad &= \omega_{\mathrm{m}} + \omega_{\mathrm{m}} \cdot \frac{\sqrt{2} \cdot \sigma_{\mathrm{m}}}{c} \cdot \mathcal{N}(0,1) && \left[\frac{\mathrm{rad}}{\mathrm{s}}\right]
\end{aligned}$$

These are then used, when estimates within both χ_{dt} and γ_{dt} are to be found for the drive train.

6.3 Vehicle Horizontal Dynamics

To provide the drive force F_{d} to the rest of the model and the *VEHICLE* itself, both the wheel velocity, the normal force on the wheels $F_{\mathrm{N,w}}$ and the vehicle velocity v_{v} must be known. The wheel velocity is determined by the drive train model *DRIVETRAIN* in section 6.2 and the normal force by the suspension model *SUSPENSION* in section 6.4. In this section a model of the horizontal movement of the vehicle, here called *VEHICLE*, is developed. This will provide the velocity of the vehicle, so the drive force can be determined. Figure 6.12 shows the indputs and outputs of the *VEHICLE* block.

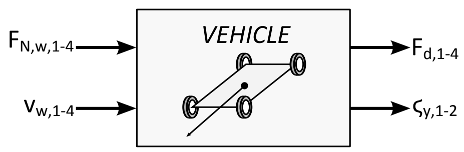

Figure 6.12. Vehicle horizontal dynamics model.

where

- $F_{\mathrm{N,w}}$ is the wheel ground force, also called the normal force
- v_{w} is the wheel velocity
- F_{d} is the drive force from a wheel
- ζ_{y} is the acceleration sensor output of the vehicle

The vehicle velocity is affected by the drive forces $F_{\mathrm{d},1-4}$ as described by equation 6.30.

$$\frac{\mathrm{d}v_{\mathrm{v}}}{\mathrm{d}t} = \frac{\sum \overline{F}_{\mathrm{d}}}{m_{\mathrm{v}}} \qquad \left[\frac{\mathrm{m}}{\mathrm{s}^2}\right] \tag{6.30}$$

Since the vehicle velocity is the only dynamic state in this part of the model, the model state vector is given as in equation 6.31. The system equation is given in equation 6.32.

$$\chi_{\mathrm{v}} = v_{\mathrm{v}} \tag{6.31}$$

$$\dot{\chi}_{\mathrm{v}} = \dot{v}_{\mathrm{v}} = \frac{\sum \overline{F}_{\mathrm{d}}}{m_{\mathrm{v}}}$$

$$\dot{\chi}_{\mathrm{v}} = 0 \cdot \chi_{\mathrm{v}} + \begin{bmatrix} \frac{1}{m_{\mathrm{v}}} & \frac{1}{m_{\mathrm{v}}} & \frac{1}{m_{\mathrm{v}}} & \frac{1}{m_{\mathrm{v}}} \end{bmatrix} \cdot \overline{F}_{\mathrm{d}} \tag{6.32}$$

Hence the system matrices are:

$$\mathbf{A}_{\mathrm{v}} = \begin{bmatrix} 0 \end{bmatrix}, \mathbf{B}_{\mathrm{v}} = \begin{bmatrix} \frac{1}{m_{\mathrm{v}}} & \frac{1}{m_{\mathrm{v}}} & \frac{1}{m_{\mathrm{v}}} & \frac{1}{m_{\mathrm{v}}} \end{bmatrix} \tag{6.33}$$

In order to calculate the drive force, the slip ratio λ and friction coefficient μ can now be found for each wheel using the wheel velocities and the vehicle velocity. For practical reasons a separate block, containing these calculations, have been created as a part of *VEHICLE*. The inputs and outputs to the block is shown in figure 6.13.

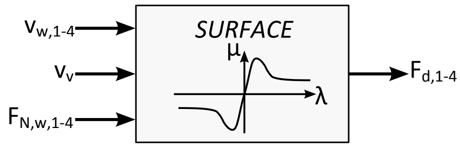

Figure 6.13. Surface friction coefficient model.

The slip ratio is found in equation 6.34 taken from [15, p. 3].

$$\lambda_k = \frac{v_{\mathrm{w},k} - v_{\mathrm{v}}}{\sqrt{{v_{\mathrm{w},k}}^2 + {\epsilon_\lambda}^2}} \tag{6.34}$$

where ϵ_λ is a minimum denominator for λ and is not included in [15].

The surface friction coefficient μ is a function of the wheel slip λ from equation 6.34. The formula varies with the type of road surface and its conditions. Examples of μ curves for different road surfaces are shown in figure 6.14.

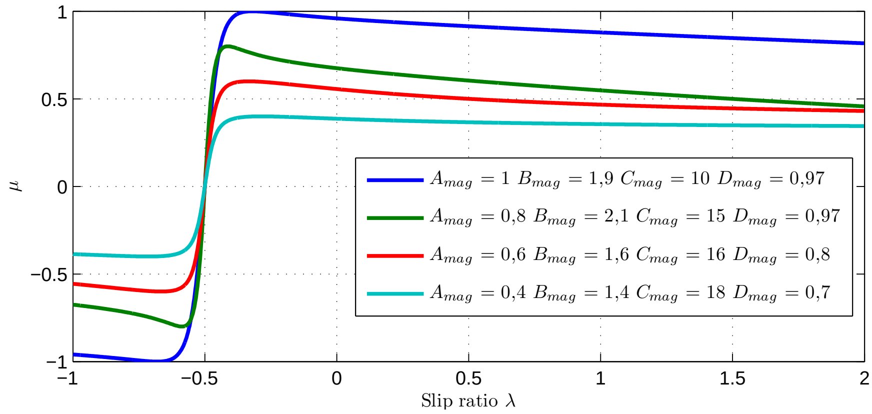

Figure 6.14. Surface friction coefficient curves for different surfaces and conditions.

The formula used to calculate the surface friction coefficient in this project, is called the Magic Formula [1, p. 239] and is shown in equation 6.35. For further information on the Magic Formula see [1].

$$\mu_k = A_{\text{mag}} \cdot \sin\left(B_{\text{mag}} \cdot \tan^{-1}\left[\left(1 - D_{\text{mag}}\right) \cdot C_{\text{mag}} \cdot \lambda_k + D_{\text{mag}} \cdot \tan^{-1}\left(C_{\text{mag}} \cdot \lambda_k\right)\right]\right) \tag{6.35}$$

In this model, inspired by the Simulink *Tire-Road Interaction (Magic Formula)* block from MATLAB®, the constants have been chosen to:

$$A_{\text{mag}} = 1,\ B_{\text{mag}} = 1.9,\ C_{\text{mag}} = 10,\ D_{\text{mag}} = 0.97 \tag{6.36}$$

which approximates the curve for dry asphalt. The constants are dependent on the deformation of the tire and are thereby a function of the vertical force $F_{\text{N,w},k}$ on the wheel. Though it has been chosen to use this simplified model. Now the drive force F_{d} can be found as in equation 6.37.

$$F_{\text{d},k} = F_{\text{N,w},k} \cdot \mu_k \tag{6.37}$$

Finally two longitudinal acceleration sensor outputs must be modeled. For this the following output equations are stated.

$$\bar{\zeta}_{\mathrm{y}} = \mathrm{sense}\begin{pmatrix} a_{\mathrm{v}} \\ a_{\mathrm{v}} \end{pmatrix}$$

(6.38)
$$\bar{\zeta}_{\mathrm{y}} = \begin{bmatrix} 0 \\ 0 \end{bmatrix} \chi_{\mathrm{v}} + \begin{bmatrix} \frac{1}{m_{\mathrm{v}}} & \frac{1}{m_{\mathrm{v}}} & \frac{1}{m_{\mathrm{v}}} & \frac{1}{m_{\mathrm{v}}} \\ \frac{1}{m_{\mathrm{v}}} & \frac{1}{m_{\mathrm{v}}} & \frac{1}{m_{\mathrm{v}}} & \frac{1}{m_{\mathrm{v}}} \end{bmatrix} \cdot \bar{F}_{\mathrm{d}} + \mathcal{N}_{1-2}\left(0, \sigma_{\mathrm{y}}^{2}\right)$$

$$\mathbf{C}_{\mathrm{v}} = \begin{bmatrix} 0 \\ 0 \end{bmatrix}, \mathbf{D}_{\mathrm{v}} = \begin{bmatrix} \frac{1}{m_{\mathrm{v}}} & \frac{1}{m_{\mathrm{v}}} & \frac{1}{m_{\mathrm{v}}} & \frac{1}{m_{\mathrm{v}}} \\ \frac{1}{m_{\mathrm{v}}} & \frac{1}{m_{\mathrm{v}}} & \frac{1}{m_{\mathrm{v}}} & \frac{1}{m_{\mathrm{v}}} \end{bmatrix}$$

where $\mathcal{N}\left(0, \sigma_{\mathrm{v}}{}^{2}\right)$ is a normal distribution with zero mean and σ_{v} standard deviation. The horizontal vehicle model *VEHICLE*, consisting of $\mathbf{A}_{\mathrm{v}}$, $\mathbf{B}_{\mathrm{v}}$, $\mathbf{C}_{\mathrm{v}}$ and $\mathbf{D}_{\mathrm{v}}$, is discretized using the MATLAB® functions *ss()* and *c2d()*.

6.4 Wheel Load and Suspension

For the *VEHICLE* model to calculate the drive force F_{d}, the normal force on each wheel $\bar{F}_{\mathrm{N,w}}$ must be known. Hence in this section the suspension, the movement of the chassis and the wheels is modeled to provide this value. This part of the vehicle model is called *SUSPENSION*. The inputs and outputs of *SUSPENSION* block are shown in figure 6.15

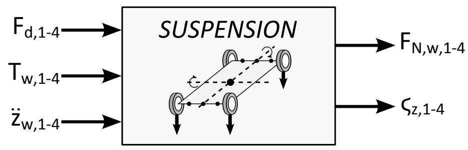

Figure 6.15. Inputs and outputs to/from *SUSPENSION*.

where

- $F_{\mathrm{d,1\text{-}4}}$ is the drive force produced by wheel 1-4 $w_{1\text{-}4}$.
- $T_{\mathrm{w,1\text{-}4}}$ is the wheel torque, that is affecting wheel 1-4 $w_{1\text{-}4}$.
- $\ddot{z}_{\mathrm{w,1\text{-}4}}$ is the the vertical acceleration of wheel 1-4 $w_{1\text{-}4}$ due to the surface.
- $F_{\mathrm{N,1\text{-}4}}$ is the vertical force, transfered from the ground to wheel 1-4 $w_{1\text{-}4}$.
- $\zeta_{\mathrm{o,1\text{-}4}}$ is the acceleration measured along the z-axis at chassis corner 1-4 $o_{1\text{-}4}$.

The vertical force of the wheels $\bar{F}_{\mathrm{N,w}}$, here called the normal force, is a combination of two things: The vertical acceleration of the wheel mass, which includes the gravitational acceleration, and the vertical force from the suspension F_{s}. The normal force can be calculated as in equation 6.39.

(6.39)
$$\bar{F}_{\mathrm{N,w}} = \bar{m}_{\mathrm{w}} \cdot \left(\ddot{\bar{z}}_{\mathrm{w}} + g\right) + \bar{F}_{\mathrm{s}} \qquad [N]$$

(6.40)
$$\bar{F}_{\mathrm{s}} = \bar{F}_{0,\mathrm{s}} + \bar{K}_{\mathrm{s}} \cdot \left(\bar{z}_{\mathrm{o}} - \bar{z}_{\mathrm{w}}\right) + \bar{b}_{\mathrm{s}} \cdot \left(\dot{\bar{z}}_{\mathrm{o}} - \dot{\bar{z}}_{\mathrm{w}}\right) \qquad [N]$$

where $F_{0,\mathrm{s},1-4}$, $K_{\mathrm{s},1-4}$, $b_{\mathrm{s},1-4}$ are the spring and damper constants found in appendix A.1. Notice that the spring constants are the combined constants of the suspension itself and those of the tire. A vertical tire deformation is also present dependent on the vertical force $F_{\mathrm{N,w},k}$ on the wheel, affecting the wheel slip ratio. Wheel torque will also deform the tire, where the wheel velocity will be different around the surface of the tire. At some velocity the wheel will instead expand in size changing the drive train gearing. The deformations of the tire from wheel torque, vertical force and wheel velocity are not considered and neglected in the vehicle model. The front and rear suspension also have a certain range, where the springs and dampers can be compressed and expanded within. Though suspension constrains from these are as the tire deformation not considered.

g is the gravitational constant of the Earth and $\overline{z}_{\mathrm{o}}$ is the z-coordinates of the corners of the chassis. $\overline{z}_{\mathrm{o}}$ can be calculated from the height (z-coordinate) of the chassis mass z_{c} and the orientation of the chassis. Also the distances from the chassis mass center to the corners are needed. In this model three distances are assumed always to have the same sizes, that is the distances from the chassis mass center to the wheels, to the chassis corners and to the accelerometers for each corner of the vehicle respectively. Figure 6.16 shows these common coordinates $\overline{d}_{\mathrm{x}}$ and $\overline{d}_{\mathrm{y}}$ relative to the chassis mass center. Also the orientation of the chassis, roll ϕ and pitch θ, is shown.

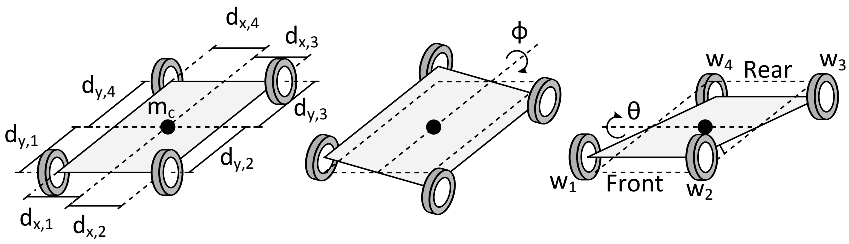

Figure 6.16. Positions of wheels.

It is assumed that $d_{\mathrm{x},1} - d_{\mathrm{x},2} = d_{\mathrm{x},4} - d_{\mathrm{x},3} = \Delta_{\mathrm{x,w}}$ and $d_{\mathrm{y},1} - d_{\mathrm{y},4} = d_{\mathrm{y},2} - d_{\mathrm{y},3} = \Delta_{\mathrm{y,w}}$. This lead to the following equations, that is used to initialize $\overline{d}_{\mathrm{x}}$ and $\overline{d}_{\mathrm{y}}$.

$$\overline{d}_{\mathrm{x}} = \left(\begin{bmatrix} d_{\mathrm{xp}} \\ d_{\mathrm{xp}} - 1 \\ d_{\mathrm{xp}} - 1 \\ d_{\mathrm{xp}} \end{bmatrix} + \mathscr{U}\left(-\delta_{\mathrm{max,dx}}, \delta_{\mathrm{max,dx}}\right) \right) \cdot \Delta_{\mathrm{x,w}} \qquad [m] \tag{6.41}$$

$$\overline{d}_{\mathrm{y}} = \left(\begin{bmatrix} d_{\mathrm{yp}} \\ d_{\mathrm{yp}} \\ d_{\mathrm{yp}} - 1 \\ d_{\mathrm{yp}} - 1 \end{bmatrix} + \mathscr{U}\left(-\delta_{\mathrm{max,dy}}, \delta_{\mathrm{max,dy}}\right) \right) \cdot \Delta_{\mathrm{y,w}} \qquad [m] \tag{6.42}$$

Here $d_{\mathrm{xp}} = [0;1]$ and $d_{\mathrm{yp}} = [0;1]$ shifts the chassis mass m_{c} in the x and y direction respectively, $\mathscr{U}\left(-\delta_{\mathrm{max,dx}}, \delta_{\mathrm{max,dx}}\right)$ and $\mathscr{U}\left(-\delta_{\mathrm{max,dy}}, \delta_{\mathrm{max,dy}}\right)$ models uncertainties in the chassis mass position and $\delta_{\text{max,dx}}$ and $\delta_{\text{max,dy}}$ provides limits for the deviation. The height of the corners $\overline{z}_{\text{o}}$ can now be calculated as in equation 6.43

$$\overline{z}_{\text{o}} = z_{\text{c}} + \overline{d}_{\text{x}} \cdot \sin(\phi) \cdot \cos(\theta) + \overline{d}_{\text{y}} \cdot \sin(\theta) \qquad [\text{m}] \tag{6.43}$$

To simplify the latter calculations, 6.43 is approximated by the expression in equation 6.44.

$$\overline{z}_{\text{o}} = z_{\text{c}} + \overline{d}_{\text{x}} \cdot \sin(\phi) + \overline{d}_{\text{y}} \cdot \sin(\theta) \qquad [\text{m}] \tag{6.44}$$

The error of this approximation with ϕ and θ within $\pm\frac{pi}{8}$ rad $= \pm 22,5°$ is shown in figure 6.17.

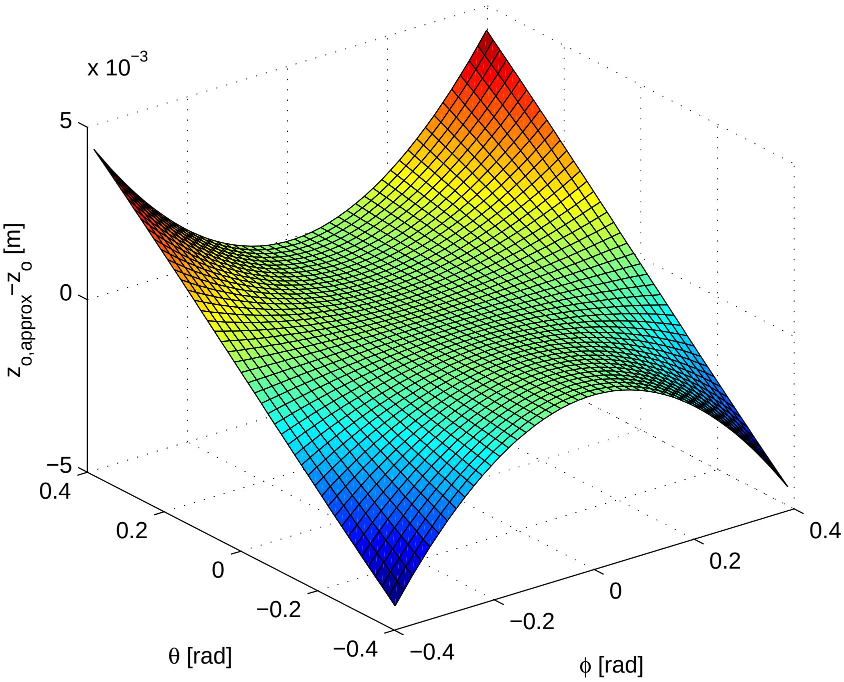

Figure 6.17. Error of chassis corner height approximation.

The boundaries of ϕ and θ are chosen from what is considered a realistic maximum for these variables. It can be seen i figure 6.17, that the error does not exceed ± 5 mm which is found acceptable. $\dot{\overline{z}}_o$ in equation 6.45, is to be used in equation 6.39, is the time derivative of equation 6.44

$$\dot{\overline{z}}_{\text{o}} = \dot{z}_{\text{c}} + \overline{d}_{\text{x}} \cdot \dot{\phi} \cdot \cos(\phi) + \overline{d}_{\text{y}} \cdot \dot{\theta} \cdot \cos(\theta) \qquad \left[\frac{\text{m}}{\text{s}}\right] \tag{6.45}$$

Since 6.45 is the derivative of 6.44, which is an approximation, the error of 6.45 has been investigated and plotted in figure 6.18. Also here ϕ and θ within $\pm\frac{pi}{8}$ rad $= \pm 22,5°$ and $\dot{\phi} = \dot{\theta} = 1$ and $\dot{z}_{\text{c}} = 0$.

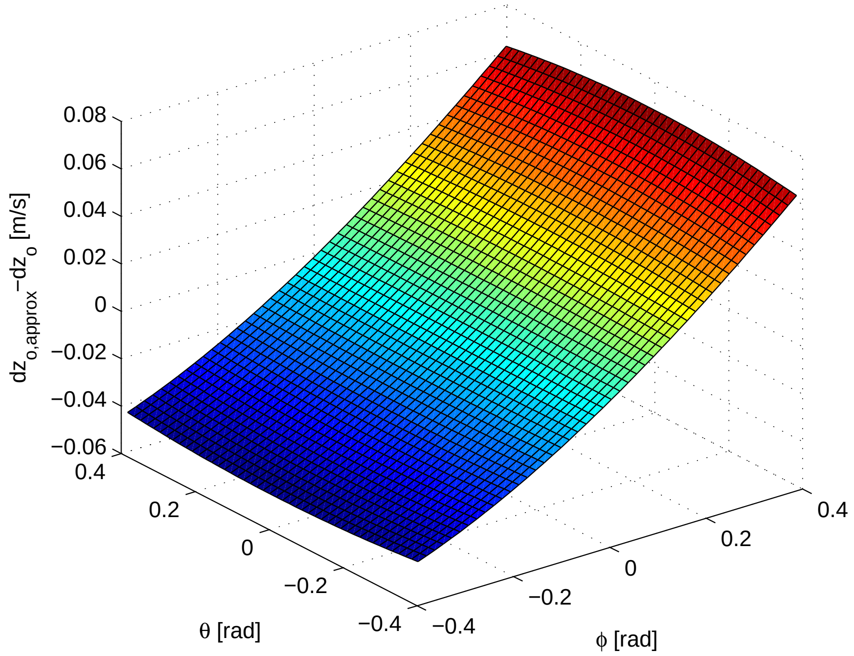

Figure 6.18. Error of vertical chassis corner velocity approximation.

It can be seen, that here the error does not exceed $\pm 0.07\ \frac{\text{m}}{\text{s}}$ which is also accepted. To simplify the latter equations, z_{o} and $\dot{z}_{\text{o}}$ are gathered in an intermediate result vector γ_{o} as in equation 6.46.

$$\overline{\gamma}_{\text{o}} = \begin{bmatrix} z_{\text{o}1} & z_{\text{o}2} & z_{\text{o}3} & z_{\text{o}4} & \frac{\mathrm{d}z_{\text{o}1}}{\mathrm{d}t} & \frac{\mathrm{d}z_{\text{o}2}}{\mathrm{d}t} & \frac{\mathrm{d}z_{\text{o}3}}{\mathrm{d}t} & \frac{\mathrm{d}z_{\text{o}4}}{\mathrm{d}t} \end{bmatrix}^{\text{T}} \tag{6.46}$$

$$\overline{\gamma}_{\text{o}} = \begin{bmatrix} z_{\text{c}} - d_{\text{z,c}} + \overline{d}_{\text{x,w}} \cdot sin\left(\phi\right) + \overline{d}_{\text{y,w}} \cdot sin\left(\theta\right) \\ \dot{z}_{\text{c}} + \overline{d}_{\text{x,w}} \cdot \dot{\phi} \cdot cos\left(\phi\right) + \overline{d}_{\text{y,w}} \cdot \dot{\theta} \cdot cos\left(\theta\right) \end{bmatrix} \tag{6.47}$$

The chassis height z_{c} and orientation θ and ϕ are given by the dynamics of, and the forces and torques acting on the chassis. The chassis height is the double integral of the vertical chassis acceleration, as stated in equation 6.48 and 6.49. The vertical acceleration consists of the gravity and the force from the suspension, combined with the mass of the chassis.

$$\begin{aligned} \chi_{\text{c}}(1) &= z_{\text{c}} \\ \chi_{\text{c}}(2) &= \dot{z}_{\text{c}} \\ \dot{\chi}_{\text{c}}(1) &= \chi_{\text{c}}(2) \\ \dot{\chi}_{\text{c}}(2) &= \ddot{z}_{\text{c}} = -g + \frac{\sum \overline{F}_{\text{s}}}{m_{\text{c}}} \end{aligned} \tag{6.48}$$

$$\ddot{z}_{\text{c}} = -g + \frac{\sum \overline{F}_{0,\text{s}}}{m_{\text{c}}} + \frac{\overline{K_{\text{s}}}^{\text{T}} \cdot \left(\overline{\gamma}_{\text{o}}(1:4) - \overline{z}_{\text{w}}\right)}{m_{\text{c}}} + \frac{\overline{b_{\text{s}}}^{\text{T}} \cdot \left(\overline{\gamma}_{\text{o}}(5:8) - \dot{\overline{z}}_{\text{w}}\right)}{m_{\text{c}}} \qquad \left[\frac{\text{m}}{\text{s}^2}\right] \tag{6.49}$$

For simplicity K_{s} and b_{s} is gathered in a vector ξ as in 6.50.

$$\overline{\xi} = \begin{bmatrix} K_{\mathrm{s1}} \\ \cdots \\ K_{\mathrm{s4}} \\ b_{\mathrm{s1}} \\ \cdots \\ b_{\mathrm{s4}} \end{bmatrix} \tag{6.50}$$

Now 6.49 can be rewritten to 6.51

$$\ddot{z}_{\mathrm{c}} = -g + \frac{\sum \overline{F}_{0,\mathrm{s}}}{m_{\mathrm{c}}} + \frac{\overline{\xi}^{\mathrm{T}} \cdot \overline{\gamma}_{\mathrm{o}}}{m_{\mathrm{c}}} - \frac{\overline{\xi}\,(1:4)^{\mathrm{T}} \cdot \overline{z}_{\mathrm{w}}}{m_{\mathrm{c}}} - \frac{\overline{\xi}\,(5:8)^{\mathrm{T}} \cdot \dot{\overline{z}}_{\mathrm{w}}}{m_{\mathrm{c}}} \qquad \left[\frac{\mathrm{m}}{\mathrm{s}^2}\right] \tag{6.51}$$

Dynamic equations for the roll ϕ is derived in a similar way. As described in the beginning of this chapter, lateral forces are not included in this model. Hence the only forces affecting the roll is the forces from the suspension F_{s}. As for the chassis height, the two chassis orientation angles are double integrals of the respective angular accelerations. For the roll, the equations are given in 6.52 and 6.53.

$$\chi_{\mathrm{c}}\,(3) = \phi$$
$$\chi_{\mathrm{c}}\,(4) = \dot{\phi}$$
$$\dot{\chi}_{\mathrm{c}}\,(3) = \chi_{\mathrm{c}}\,(4) \tag{6.52}$$
$$\dot{\chi}_{\mathrm{c}}\,(4) = \ddot{\phi}_{\mathrm{c}} = \frac{T_{\mathrm{c},\phi}}{J_{\mathrm{c},\phi}} \qquad \left[\frac{\mathrm{rad}}{\mathrm{s}^2}\right] \tag{6.53}$$

Torque that affects rotation of the chassis appears, when the suspension forces weighted by the distance to the chassis mass center are not equal on both sides of the chassis mass center. This applies to both axis. Figure 6.19(a) illustrates an example.

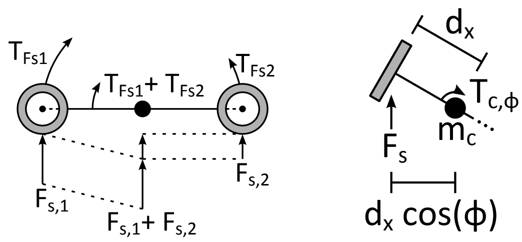

(a) Chassis torque pricipal.

(b) Torque affecting chassis in ϕ direction.

Figure 6.19. Torques affecting chassis.

The torque affecting the chassis in the ϕ direction $T_{\mathrm{c},\phi}$ is illustrated in figure 6.19(b) and the formula is given in equation 6.54.

(6.54) $$T_{c,\phi} = cos\left(\chi_c(3)\right) \cdot \overline{d}_{x,w}{}^{T} \overline{F}_{0,s} + cos\left(\chi_c(3)\right) \cdot \begin{bmatrix} \overline{d}_x \\ \overline{d}_x \end{bmatrix}^{T} \xi \left(\overline{\gamma}_o - \begin{bmatrix} z_w \\ \dot{z}_w \end{bmatrix} \right) \qquad [\mathrm{Nm}]$$

To simplify the equations, two new vectors are created ξ_x and ξ_y:

(6.55) $$\overline{\xi}_x = \begin{bmatrix} K_{s1} \\ \cdots \\ K_{s4} \\ b_{s1} \\ \cdots \\ b_{s4} \end{bmatrix}_i \cdot \begin{bmatrix} d_{x,w1} \\ \cdots \\ d_{x,w4} \\ d_{x,w1} \\ \cdots \\ d_{x,w4} \end{bmatrix}_i \qquad \overline{\xi}_y = \begin{bmatrix} K_{s1} \\ \cdots \\ K_{s4} \\ b_{s1} \\ \cdots \\ b_{s4} \end{bmatrix}_i \cdot \begin{bmatrix} d_{y,w1} \\ \cdots \\ d_{y,w4} \\ d_{y,w1} \\ \cdots \\ d_{y,w4} \end{bmatrix}_i$$

These vectors are simply the spring constants weighted with the distances from the chassis mass center, to the wheel positions in the x and y direction respectively. The vectors allow easy calculation of the chassis torque. Equation 6.54 can now be inserted in 6.53 to obtain 6.56 below:

(6.56) $$\ddot{\phi}_c = \frac{cos\left(\chi_c(3)\right) \cdot \overline{d}_{x,w}{}^{T} \overline{F}_{0,s}}{J_{c,\phi}} + \frac{cos\left(\chi_c(3)\right) \cdot \overline{\xi}_x{}^{T} \cdot \overline{\gamma}_o}{J_{c,\phi}} - \frac{cos\left(\chi_c(3)\right) \cdot \overline{\xi}_x{}^{T} \cdot \begin{bmatrix} \overline{z}_w \\ \dot{\overline{z}}_w \end{bmatrix}}{J_{c,\phi}} \qquad \left[\frac{\mathrm{rad}}{\mathrm{s}^2}\right]$$

The same procedure is used for deriving the dynamic equations for the pitch θ. The pitch however is not only affected by the suspension forces F_s, but also the wheel torques T_w and the drive forces F_d.

$$\chi_c(5) = \theta$$
$$\chi_c(6) = \dot{\theta}$$
(6.57) $$\dot{\chi}_c(5) = \chi_c(6)$$
(6.58) $$\dot{\chi}_c(6) = \ddot{\theta}_c = \frac{T_{c,\theta}}{J_{c,\theta}} \qquad \left[\frac{\mathrm{rad}}{\mathrm{s}^2}\right]$$

The torque affecting the chassis in the θ direction $T_{c,\theta}$ is illustrated in figure 6.20 and the formula is given in equation 6.59.

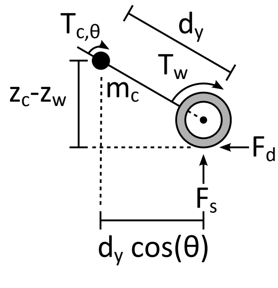

Figure 6.20. Torque affecting chassis in θ direction.

$$(6.59)\quad T_{c,\theta} = cos\left(\chi_c(5)\right)\cdot \overline{d}_{y,w}{}^{T}\overline{F}_{0,s} + cos\left(\chi_c(5)\right)\cdot \overline{\xi}_y{}^{T}\cdot\overline{\gamma}_o - cos\left(\chi_c(5)\right)\cdot\overline{\xi}_y{}^{T}\cdot\begin{bmatrix}\overline{z}_w\\ \dot{\overline{z}}_w\end{bmatrix} + \cdots$$

$$cos\left(\chi_c(5)\right)\cdot\sum\overline{F}_d\cdot\chi_c(1) - cos\left(\chi_c(5)\right)\cdot\overline{F}_d{}^{T}\cdot\overline{z}_w + \sum\overline{T}_w \qquad [\mathrm{Nm}]$$

With 6.59 inserted in 6.58, 6.58 becomes:

$$(6.60)\quad \ddot{\theta}_c = \frac{cos\left(\chi_c(5)\right)\cdot\overline{d}_{y,w}{}^{T}\overline{F}_{0,s}}{J_{c,\theta}} + \frac{cos\left(\chi_c(5)\right)\cdot\overline{\xi}_y{}^{T}\cdot\overline{\gamma}_o}{J_{c,\theta}} - \frac{cos\left(\chi_c(5)\right)\cdot\overline{\xi}_y{}^{T}\cdot\begin{bmatrix}\overline{z}_w\\ \dot{\overline{z}}_w\end{bmatrix}}{J_{c,\theta}} + \cdots$$

$$\frac{cos\left(\chi_c(5)\right)\cdot\sum\overline{F}_d\cdot\chi_c(1)}{J_{c,\theta}} - \frac{cos\left(\chi_c(5)\right)\cdot\overline{F}_d{}^{T}\cdot\overline{z}_w}{J_{c,\theta}} + \frac{\sum\overline{T}_w}{J_{c,\theta}} \qquad \left[\frac{\mathrm{rad}}{\mathrm{s}^2}\right]$$

Also the position of the wheels are given by a double integration of the acceleration of these. The accelerations are given as inputs (see figure 6.15), which means that the equations are straight forward (see equation 6.61 and 6.62)

$$\overline{\chi}_c(7:10) = \overline{z}_w$$

$$\overline{\chi}_c(11:14) = \dot{\overline{z}}_w$$

$$(6.61)\quad \dot{\overline{\chi}}_c(7:10) = \overline{\chi}_c(11:14)$$

$$(6.62)\quad \dot{\overline{\chi}}_c(11:14) = \ddot{\overline{z}}_w$$

With the wheel dynamics included in the state vector, equation 6.51, 6.56 and 6.60 can be rewritten to equation 6.63 to 6.65.

$$(6.63)\quad \ddot{z}_c = -g + \frac{\sum\overline{F}_{0,s}}{m_c} + \frac{\overline{\xi}^{T}\cdot\overline{\gamma}_o}{m_c} - \frac{\overline{\xi}^{T}\cdot\overline{\chi}_c(7:14)}{m_c}$$

$$(6.64)\quad \ddot{\phi}_c = \frac{cos\left(\chi_c(3)\right)\cdot\overline{d}_{x,w}{}^{T}\overline{F}_{0,s}}{J_{c,\phi}} + \frac{cos\left(\chi_c(3)\right)\cdot\overline{\xi}_x{}^{T}\cdot\overline{\gamma}_o}{J_{c,\phi}} - \frac{cos\left(\chi_c(3)\right)\cdot\overline{\xi}_x{}^{T}\cdot\overline{\chi}_c(7:14)}{J_{c,\phi}}$$

$$(6.65)\quad \ddot{\theta}_c = \frac{cos\left(\chi_c(5)\right)\cdot\overline{d}_{y,w}{}^{T}\overline{F}_{0,s}}{J_{c,\theta}} + \frac{cos\left(\chi_c(5)\right)\cdot\overline{\xi}_y{}^{T}\cdot\overline{\gamma}_o}{J_{c,\theta}} - \frac{cos\left(\chi_c(5)\right)\cdot\overline{\xi}_y{}^{T}\cdot\overline{\chi}_c(7:14)}{J_{c,\theta}} + \cdots$$

$$\cdots + \frac{cos\left(\chi_c(5)\right)\cdot\sum\overline{F}_d\cdot\chi_c(1)}{J_{c,\theta}} - \frac{cos\left(\chi_c(5)\right)\cdot\overline{F}_d{}^{T}\cdot\overline{\chi}_c(7:10)}{J_{c,\theta}} + \frac{\sum\overline{T}_w}{J_{c,\theta}}$$

The complete *SUSPENSION* state vector can now be written as seen in equation 6.67 below.

$$(6.66)\quad \dot{\overline{\chi}}_c = \begin{bmatrix} \frac{dz_c}{dt} & \frac{d^2z_c}{dt^2} & \frac{d\phi_c}{dt} & \frac{d^2\phi_c}{dt^2} & \frac{d\theta_c}{dt} & \frac{d^2\theta_c}{dt^2}\cdots & & & \\ \cdots & \frac{dz_{w1}}{dt} & \frac{dz_{w2}}{dt} & \frac{dz_{w3}}{dt} & \frac{dz_{w4}}{dt} & \frac{d^2z_{w1}}{dt^2} & \frac{d^2z_{w2}}{dt^2} & \frac{d^2z_{w3}}{dt^2} & \frac{d^2z_{w4}}{dt^2} \end{bmatrix}^{T}$$

$$(6.67)\quad \dot{\overline{\chi}}_c = \begin{bmatrix} \chi_c(2) & \ddot{z}_c & \chi_c(4) & \ddot{\phi}_c & \chi_c(6) & \ddot{\theta}_c & \cdots & & \\ \cdots & \chi_c(11) & \chi_c(12) & \chi_c(13) & \chi_c(14) & \ddot{z}_{w1} & \ddot{z}_{w2} & \ddot{z}_{w3} & \ddot{z}_{w4} \end{bmatrix}$$

A zero order hold discretization on this state vector (equation 6.67) has been performed and the result is shown in equation 6.68 through 6.75.

$$\chi_{\mathrm{c},n}(1) = \chi_{\mathrm{c},n-1}(1) + t_{\mathrm{s}} \cdot \chi_{\mathrm{c},n-1}(2) + \frac{{t_{\mathrm{s}}}^2}{2} \cdot \ddot{z}_{\mathrm{c},n} \tag{6.68}$$

$$\chi_{\mathrm{c},n}(2) = \chi_{\mathrm{c},n-1}(2) + t_{\mathrm{s}} \cdot \ddot{z}_{\mathrm{c},n} \tag{6.69}$$

$$\chi_{\mathrm{c},n}(3) = \chi_{\mathrm{c},n-1}(3) + t_{\mathrm{s}} \cdot \chi_{\mathrm{c},n-1}(4) + \frac{{t_{\mathrm{s}}}^2}{2} \cdot \ddot{\phi}_{\mathrm{c},n} \tag{6.70}$$

$$\chi_{\mathrm{c},n}(4) = \chi_{\mathrm{c},n-1}(4) + t_{\mathrm{s}} \cdot \ddot{\phi}_{\mathrm{c},n} \tag{6.71}$$

$$\chi_{\mathrm{c},n}(5) = \chi_{\mathrm{c},n-1}(5) + t_{\mathrm{s}} \cdot \chi_{\mathrm{c},n-1}(6) + \frac{{t_{\mathrm{s}}}^2}{2} \cdot \ddot{\theta}_{\mathrm{c},n} \tag{6.72}$$

$$\chi_{\mathrm{c},n}(6) = \chi_{\mathrm{c},n-1}(6) + t_{\mathrm{s}} \cdot \ddot{\theta}_{\mathrm{c},n} \tag{6.73}$$

$$\chi_{\mathrm{c},n}(7:10) = \chi_{\mathrm{c},n-1}(7:10) + t_{\mathrm{s}} \cdot \chi_{\mathrm{c},n-1}(11:14) + \frac{{t_{\mathrm{s}}}^2}{2} \cdot \ddot{\overline{z}}_{\mathrm{w},n} \tag{6.74}$$

$$\chi_{\mathrm{c},n}(11:14) = \chi_{\mathrm{c},n-1}(11:14) + t_{\mathrm{s}} \cdot \ddot{\overline{z}}_{\mathrm{w},n} \tag{6.75}$$

where $\ddot{z}_{\mathrm{c},n}$, $\ddot{\phi}_{\mathrm{c},n}$ and $\ddot{\theta}_{\mathrm{c},n}$, given in equation 6.76 to 6.78, are the discrete form of $\ddot{z}_{\mathrm{c}}$, $\ddot{\phi}_{\mathrm{c}}$ and $\ddot{\theta}_{\mathrm{c}}$ from equation 6.63 to 6.65.

$$\ddot{z}_{\mathrm{c},n} = -g + \frac{\sum \overline{F}_{0,\mathrm{s}}}{m_{\mathrm{c}}} + \frac{\overline{\xi}^{\mathrm{T}} \cdot \overline{\gamma}_{\mathrm{o},n-1}}{m_{\mathrm{c}}} - \frac{\overline{\xi}^{\mathrm{T}} \cdot \overline{\chi}_{\mathrm{c},n-1}(7:14)}{m_{\mathrm{c}}} \tag{6.76}$$

$$\ddot{\phi}_{\mathrm{c},n} = \frac{cos(\chi_{\mathrm{c},n-1}(3)) \cdot {\overline{d}_{\mathrm{x,w}}}^{\mathrm{T}} \overline{F}_{0,\mathrm{s}}}{J_{\mathrm{c},\phi}} + \frac{cos(\chi_{\mathrm{c},n-1}(3)) \cdot {\overline{\xi}_{\mathrm{x}}}^{\mathrm{T}} \cdot \overline{\gamma}_{\mathrm{o},n-1}}{J_{\mathrm{c},\phi}} - \frac{cos(\chi_{\mathrm{c},n-1}(3)) \cdot {\overline{\xi}_{\mathrm{x}}}^{\mathrm{T}} \cdot \overline{\chi}_{\mathrm{c},n-1}(7:14)}{J_{\mathrm{c},\phi}} \tag{6.77}$$

$$\begin{aligned} \ddot{\theta}_{\mathrm{c},n} = & \frac{cos(\chi_{\mathrm{c},n-1}(5)) \cdot {\overline{d}_{\mathrm{y,w}}}^{\mathrm{T}} \overline{F}_{0,\mathrm{s}}}{J_{\mathrm{c},\theta}} + \frac{cos(\chi_{\mathrm{c},n-1}(5)) \cdot {\overline{\xi}_{\mathrm{y}}}^{\mathrm{T}} \cdot \overline{\gamma}_{\mathrm{o},n-1}}{J_{\mathrm{c},\theta}} - \frac{cos(\chi_{\mathrm{c},n-1}(5)) \cdot {\overline{\xi}_{\mathrm{y}}}^{\mathrm{T}} \cdot \overline{\chi}_{\mathrm{c},n-1}(7:14)}{J_{\mathrm{c},\theta}} + \cdots \\ & \cdots + \frac{cos(\chi_{\mathrm{c},n-1}(5)) \cdot \sum \overline{F}_{\mathrm{d},n} \cdot \chi_{\mathrm{c},n-1}(1)}{J_{\mathrm{c},\theta}} - \frac{cos(\chi_{\mathrm{c},n-1}(5)) \cdot {\overline{F}_{\mathrm{d},n}}^{\mathrm{T}} \cdot \overline{\chi}_{\mathrm{c},n-1}(7:10)}{J_{\mathrm{c},\theta}} + \frac{\sum \overline{T}_{\mathrm{w},n}}{J_{\mathrm{c},\theta}} \end{aligned} \tag{6.78}$$

The modeling of the acceleration measurement from the vertical accelerometers $\overline{\zeta}_{\mathrm{z}}$ is a sum of the vertical acceleration of the chassis at the position of the accelerometers, the gravity of the earth and some sensor noise. The expression for $\overline{\zeta}_{\mathrm{z}}$ is derived by double differentiating the vertical sensor position with respect to time and adding the gravity and sensor noise. The result is shown in equation 6.79.

$$
\begin{aligned}
\overline{\zeta}_{z,n} =& g + \mathcal{N}_{1-4}\left(0, {\sigma_o}^2\right) + \cdots \\
& \cdots + \frac{d^2}{dt^2}\left[\chi_{c,n}(1) + \overline{d}_{x,zs} \cdot \sin\left(\chi_{c,n}(3)\right) + \overline{d}_{y,zs} \cdot \sin\left(\chi_{c,n}(5)\right)\right] \\
\overline{\zeta}_{z,n} =& g + \mathcal{N}_{1-4}\left(0, {\sigma_o}^2\right) + \cdots \\
& \cdots + \frac{d}{dt}\left[\chi_{c,n}(2) + \overline{d}_{x,zs} \cdot \chi_{c,n}(4) \cdot \cos\left(\chi_{c,n}(3)\right) + \overline{d}_{y,zs} \cdot \chi_{c,n}(6) \cdot \cos\left(\chi_{c,n}(5)\right)\right] \\
\overline{\zeta}_{z,n} =& g + \mathcal{N}_{1-4}\left(0, {\sigma_o}^2\right) + \dot{\chi}_{c,n}(2) + \cdots \\
& \cdots + \overline{d}_{x,zs} \cdot \dot{\chi}_{c,n}(4) \cdot \cos\left(\chi_{c,n}(3)\right) - \overline{d}_{x,zs} \cdot \chi_{c,n}(4)^2 \cdot \sin\left(\chi_{c,n}(3)\right) + \cdots \\
& \cdots + \overline{d}_{y,zs} \cdot \dot{\chi}_{c,n}(6) \cdot \cos\left(\chi_{c,n}(5)\right) - \overline{d}_{y,zs} \cdot \chi_{c,n}(6)^2 \cdot \sin\left(\chi_{c,n}(5)\right) \\
\overline{\zeta}_{z,n} =& g + \mathcal{N}_{1-4}\left(0, {\sigma_o}^2\right) + \ddot{z}_{c,n} + \cdots \\
& \cdots + \overline{d}_{x,zs} \cdot \ddot{\phi}_{c,n} \cdot \cos\left(\chi_{c,n}(3)\right) - \cdots \\
& \cdots - \overline{d}_{x,zs} \cdot \chi_{c,n}(4)^2 \cdot \sin\left(\chi_{c,n}(3)\right) + \cdots \\
& \cdots + \overline{d}_{y,zs} \cdot \ddot{\theta}_{c,n} \cdot \cos\left(\chi_{c,n}(5)\right) - \cdots \\
& \cdots - \overline{d}_{y,zs} \cdot \chi_{c,n}(6)^2 \cdot \sin\left(\chi_{c,n}(5)\right)
\end{aligned}
\tag{6.79}
$$

Here $\mathcal{N}\left(0, {\sigma_o}^2\right)$ is a normal distribution with zero mean and σ_o standard deviation. Since equation 6.79 is simplified after the same principals as equation 6.47 it is not accurate. The error of equation 6.79 however has not been investigated here, since the accurate formula would be quite large.

A detailed model of the vehicle have now been developed. It consists of three blocks: *DRIVETRAIN*, *VEHICLE* and *SUSPENSION* which models the drive train, the horizontal vehicle movement and the suspension respectively. These blocks are connected via. input output relations, and they each model relevant sensors that are present on the vehicle. The model can be supplied with a sample rate and iterated with the desired input, to simulate a scenario on the vehicle. This model called the *SYSTEM MODEL* will be used to test the setup, before tested in real life.

Chapter 7

Observer Development

In the beginning of chapter 6 it is described how the controller, the observer and the vehicle or the vehicle model *VEHICLE MODEL* will interact and block diagrams of the setups are shown in figure 6.2 and 6.3. It is also described how the supervisor control needs an observer to estimate the states that must be controlled. In section 4.4 it was decided to apply an extended Kalman filter (EKF) as observer. This decision was based on the fact, that the system is nonlinear and the assumption, that the sensor noise is white. Furthermore, parameter estimation can easily be implemented in an EKF. The Kalman filter is developed with basis in the *VEHICLE MODEL* developed in chapter 6. Like the *VEHICLE MODEL* the Kalman filter will be separated in three blocks. These are the horizontal vehicle dynamics Kalman filter *VEHICLE*^{Kf}, the drive train Kalman filter *DRIVETRAIN*^{Kf} and the vehicle load and suspension Kalman filter *SUSPENSION*. The blocks are connected as shown in figure 7.1 below, and combined they form the *VEHICLE KALMAN FILTER*.

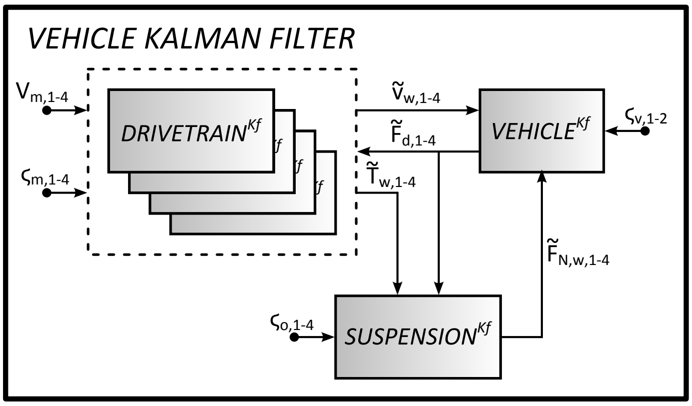

Figure 7.1. Block diagram of the *VEHICLE KALMAN FILTER*.

The decision to create the Kalman filter in three blocks is based on the intension of reducing the computational load. It must be recognized, that this way of creating the Kalman filter will degrade its performance, as not all states can be updated by all sensor inputs. Only states associated with the same block as the sensor can be updated by the sensor. The difference in performance will not be investigated in this treatise, since this would be quite extensive. The performance of the Kalman filter will, however, be evaluated in chapter 10.

The list below will clarify or refresh some notations.

$\tilde{\star}$ Constant or variable belong to the *VEHICLE KALMAN FILTER*

$\overline{\star}$ Vector form

$\bigstar$ Matrix form

$\star^-$ Apriori value

$\star^+$ Aposteriori value

$\star_n$ Discrete time index

The first block developed is the *DRIVETRAIN*^{Kf}.

7.1 Drive Train

The purpose of this part of the *VEHICLE KALMAN FILTER*, is to estimate the torque generated on the wheel shafts and the velocity of the wheels, given an angular velocity measurements from the motors. The inputs to and outputs from this block is seen in figure 7.2 below.

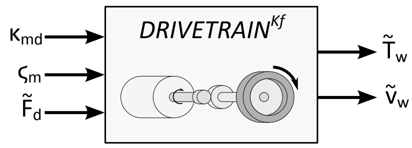

Figure 7.2. Input to and outputs from the *DRIVETRAIN*^{Kf} block.

The wheel torque $\widetilde{T}_\mathrm{w}$ is used in the wheel load and suspension Kalman filter block *SUSPENSION*^{Kf}, developed in section 7.2, to estimate the change in pitch. The wheel velocity $\tilde{v}_\mathrm{w}$ is used by the horizontal vehicle movement Kalman filter block *VEHICLE*^{Kf}, developed in section 7.3, to estimate the driveforce $\widetilde{F}_\mathrm{d}$.

In section 6.2 a model for the drive train was developed. This model consist of the four matrices $\mathbf{A}_\mathrm{dt}$, $\mathbf{B}_\mathrm{dt}$, $\mathbf{C}_\mathrm{dt}$ and $\mathbf{D}_\mathrm{dt}$. Since the model is already in matrix form, the development of this part of the Kalman filter is straight forward.

The Kalman filter consists of a prediction step and an update step. The prediction step consists of calculating a state a priori estimate $\tilde{\overline{\chi}}_\mathrm{dt}^-$ which is based on the knowledge of the system, a sensor estimate $\tilde{\overline{\zeta}}_\mathrm{dt}$ based on the state a priori estimate and lastly an iteration on the covariance propagation matrix $\widetilde{\mathbf{P}}_\mathrm{dt}^-$ to get the covariance of the a priori state estimate. The update step consists of calculating the Kalman filter gain $\widetilde{\mathbf{K}}_\mathrm{dt}$, correcting the a priori state vector to get the a posteriori state estimate $\tilde{\overline{\chi}}_\mathrm{dt}^+$ and lastly an iteration on the covariance propagation matrix to get the covariance $\widetilde{\mathbf{P}}_\mathrm{dt}^+$ of the a posteriori state estimate.

The a priori state estimate is calculated in equation 7.1.

$$\tilde{\overline{\chi}}_{\mathrm{dt},n}^- = \widetilde{\mathbf{A}}_{\mathrm{dt},n} \cdot \tilde{\overline{\chi}}_{\mathrm{dt},n-1}^+ + \widetilde{\mathbf{B}}_{\mathrm{dt},n} \cdot \begin{bmatrix} V_{\mathrm{m},n} \\ \widetilde{F}_{\mathrm{d},n} \end{bmatrix} \tag{7.1}$$

where $\widetilde{\mathbf{A}}_{\text{dt},n}$ and $\widetilde{\mathbf{B}}_{\text{dt},n}$ is the discretized system and input matrix from section 6.2. Since the motor angular velocity is a state in $\tilde{\tilde{\chi}}_{\text{dt}}$ (see section 6.2), the estimate of the angular velocity measurement from the motor, can be estimated with the matrix $\widetilde{\mathbf{H}}_{\text{dt}}$ as in equation 7.2.

$$\tilde{\zeta}_{\text{dt},n} = \widetilde{\mathbf{H}}_{\text{dt},n} \cdot \tilde{\tilde{\chi}}^{-}_{\text{dt},n} \tag{7.2}$$

$$\widetilde{\mathbf{H}}_{\text{dt},n} = \begin{bmatrix} 0 & 1 \end{bmatrix} \tag{7.3}$$

The covariance propagation matrix $\widetilde{\mathbf{P}}^{-}_{\text{dt}}$ is given in equation 7.4.

$$\widetilde{\mathbf{P}}^{-}_{\text{dt},n} = \widetilde{\mathbf{A}}_{\text{dt},n} \cdot \widetilde{\mathbf{P}}^{+}_{\text{dt},n-1} \cdot \widetilde{\mathbf{A}}^{\text{T}}_{\text{dt},n} + \widetilde{\mathbf{Q}}_{\text{dt},n} \tag{7.4}$$

where $\widetilde{\mathbf{Q}}_{\text{dt},n}$ is the process noise covariance matrix. The values of $\widetilde{\mathbf{Q}}_{\text{dt}}$ have been set according to intuition and knowledge about the system, knowing that:

$$\widetilde{\mathbf{Q}}_{\text{dt},n,k,i} = \text{cov}\left(\tilde{\tilde{w}}_{\text{dt},n,k}, \tilde{\tilde{w}}_{\text{dt},n,i}\right) \tag{7.5}$$

and assuming that:

$$0 = \text{cov}\left(\tilde{\tilde{w}}_{\text{dt},n,k}, \tilde{\tilde{w}}_{\text{dt},n,i}\right),\ k \neq i$$

$$\widetilde{\mathbf{Q}}_{\text{dt},n} = \begin{bmatrix} \tilde{\tilde{w}}^{2}_{\text{dt},n,1} & 0 & \cdots & 0 \\ 0 & \tilde{\tilde{w}}^{2}_{\text{dt},n,2} & \cdots & \cdots \\ \cdots & \cdots & \cdots & \cdots \\ 0 & \cdots & \cdots & \tilde{\tilde{w}}^{2}_{\text{dt},n,k} \end{bmatrix}$$

where $\tilde{\tilde{w}}_{\text{dt},n,k}$ is the process noise on state $\tilde{\chi}_{\text{dt},n,k}$. $\widetilde{\mathbf{Q}}_{\text{dt},n}$ has been manually tuned to:

$$\widetilde{\mathbf{Q}}_{\text{dt},n} = \begin{bmatrix} 0 & 0 \\ 0 & 0.1^2 \end{bmatrix} \tag{7.6}$$

This value means that the angular velocity of the motor varies with a standard deviation of $\pm 0.1 \frac{rad}{s}$ due to noise. The Kalman filter gain is given in equation 7.7.

$$\widetilde{\mathbf{K}}_{\text{dt},n} = \widetilde{\mathbf{P}}^{-}_{\text{dt},n} \cdot \widetilde{\mathbf{H}}^{\text{T}}_{\text{dt},n} \cdot \left(\widetilde{\mathbf{H}}_{\text{dt},n} \cdot \widetilde{\mathbf{P}}^{-}_{\text{dt},n} \cdot \widetilde{\mathbf{H}}^{\text{T}}_{\text{dt},n} + \widetilde{\mathbf{R}}_{\text{dt},n}\right) \tag{7.7}$$

where $\widetilde{\mathbf{R}}_{\text{dt},n}$ is the sensor noise covariance matrix given by equation 7.8.

$$\widetilde{\mathbf{R}}_{\text{dt},n,k,i} = \text{cov}\left(\tilde{\tilde{k}}_{\text{dt},n,k}, \tilde{\tilde{k}}_{\text{dt},n,i}\right) \tag{7.8}$$

where, as for $\tilde{\mathbf{Q}}_{\mathrm{dt},n}$, the following is assumed:

$$
\begin{aligned}
0 =& \operatorname{cov}\left(\tilde{\tilde{k}}_{\mathrm{dt},n,k}, \tilde{\tilde{k}}_{\mathrm{dt},n,i}\right), \; k \neq i \\
\tilde{\mathbf{R}}_{\mathrm{dt},n} =& \begin{bmatrix} \tilde{\tilde{k}}^2_{\mathrm{dt},n,1} & 0 & \cdots & 0 \\ 0 & \tilde{\tilde{k}}^2_{\mathrm{dt},n,2} & \cdots & \cdots \\ \cdots & \cdots & \cdots & \cdots \\ 0 & \cdots & \cdots & \tilde{\tilde{k}}^2_{\mathrm{dt},n,k} \end{bmatrix}
\end{aligned}
$$

and $\tilde{\tilde{k}}_{\mathrm{dt},n}$ is the sensor noise. Since there is only one sensor present from each drive train, $\tilde{\mathbf{R}}_{\mathrm{dt},n}$ is a one dimensional value for each n. However it varies according to equation 6.29 in section 6.2. Hence $\tilde{\mathbf{R}}_{\mathrm{dt},n}$ is given as in equation 7.9

$$
\tilde{\mathbf{R}}_{\mathrm{dt},n} = \left(\omega_{\mathrm{m},n} \cdot \frac{\sqrt{2} \cdot \sigma_{\mathrm{m}}}{c}\right)^2 \tag{7.9}
$$

where the value of σ_{m} is found in appendix A.4. Now the a posteriori state can be calculated from the sensor noise and Kalman gain as in equation 7.10.

$$
\tilde{\tilde{\chi}}^{+}_{\mathrm{dt},n} = \tilde{\tilde{\chi}}^{-}_{\mathrm{dt},n} + \tilde{\mathbf{K}}_{\mathrm{dt},n} \cdot \left(\zeta_{\mathrm{dt},n} - \tilde{\zeta}_{\mathrm{dt},n}\right) \tag{7.10}
$$

and the covariance propagation matrix for the a posteriori state is given by equation 7.11

$$
\tilde{\mathbf{P}}^{+}_{\mathrm{dt},n} = \left(\mathbf{I} - \tilde{\mathbf{K}}_{\mathrm{dt},n} \cdot \tilde{\mathbf{H}}_{\mathrm{dt},n}\right) \cdot \tilde{\mathbf{P}}^{-}_{\mathrm{dt},n} \tag{7.11}
$$

To sum up, the *DRIVETRAIN*^{Kf} consists of the following calculations. First the prediction step:

$$
\begin{aligned}
\tilde{\tilde{\chi}}^{-}_{\mathrm{dt},n} =& \tilde{\mathbf{A}}_{\mathrm{dt},n} \cdot \tilde{\tilde{\chi}}^{+}_{\mathrm{dt},n-1} + \tilde{\mathbf{B}}_{\mathrm{dt},n} \cdot \begin{bmatrix} V_{\mathrm{m},n} \\ \tilde{F}_{\mathrm{d},n} \end{bmatrix} \\
\tilde{\zeta}_{\mathrm{dt},n} =& \tilde{\mathbf{H}}_{\mathrm{dt},n} \cdot \tilde{\tilde{\chi}}^{-}_{\mathrm{dt},n} \\
\tilde{\mathbf{P}}^{-}_{\mathrm{dt},n} =& \tilde{\mathbf{A}}_{\mathrm{dt},n} \cdot \tilde{\mathbf{P}}^{+}_{\mathrm{dt},n-1} \cdot \tilde{\mathbf{A}}^{\mathrm{T}}_{\mathrm{dt},n} + \tilde{\mathbf{Q}}_{\mathrm{dt},n}
\end{aligned}
$$

Then $\tilde{\mathbf{R}}_{\mathrm{dt},n}$ must be updated, before the update step is performed.

$$
\tilde{\mathbf{R}}_{\mathrm{dt},n} = \left(\omega_{\mathrm{m},n} \cdot \frac{\sqrt{2} \cdot \sigma_{\mathrm{m}}}{c}\right)^2
$$

Lastly the update step is performed:

$$
\begin{aligned}
\widetilde{\mathbf{K}}_{\mathrm{dt},n} &= \widetilde{\mathbf{P}}^{-}_{\mathrm{dt},n} \cdot \widetilde{\mathbf{H}}^{\mathrm{T}}_{\mathrm{dt},n} \cdot \left(\widetilde{\mathbf{H}}_{\mathrm{dt},n} \cdot \widetilde{\mathbf{P}}^{-}_{\mathrm{dt},n} \cdot \widetilde{\mathbf{H}}^{\mathrm{T}}_{\mathrm{dt},n} + \widetilde{\mathbf{R}}_{\mathrm{dt},n} \right) \\
\widetilde{\overline{\chi}}^{+}_{\mathrm{dt},n} &= \widetilde{\overline{\chi}}^{-}_{\mathrm{dt},n} + \widetilde{\mathbf{K}}_{\mathrm{dt},n} \cdot \left(\zeta_{\mathrm{dt},n} - \widetilde{\zeta}_{\mathrm{dt},n} \right) \\
\widetilde{\mathbf{P}}^{+}_{\mathrm{dt},n} &= \left(\mathbf{I} - \widetilde{\mathbf{K}}_{\mathrm{dt},n} \cdot \widetilde{\mathbf{H}}_{\mathrm{dt},n} \right) \cdot \widetilde{\mathbf{P}}^{-}_{\mathrm{dt},n}
\end{aligned}
$$

7.2 Wheel Load and Suspension

The purpose of this block, called *SUSPENSION*^{Kf} is to estimate the normal force on the wheels, based on how the vehicle accelerates, the suspension and more. The inputs and outputs of *SUSPENSION*^{Kf} are shown in figure 7.3.

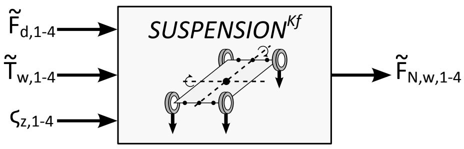

Figure 7.3. Inputs and outputs to/from *SUSPENSION*^{Kf}.

The normal force of the wheels $\widetilde{F}_{\mathrm{N,w}}$ is used by the horizontal vehicle movement Kalman filter block *VEHICLE*^{Kf} to estimate the drive force $\widetilde{F}_{\mathrm{d}}$. The procedure used to develop the *SUSPENSION*^{Kf} is the same, as the one used to develop the drive train Kalman filter block *DRIVETRAIN*^{Kf}, for which reason some of the steps in this section are not explained in details. For details see section 7.1.

In section 6.4 the wheel load and suspension model *SUSPENSION* is developed. This part of the model will form the basis for the development of this part of the Kalman filter. It can be seen in the system equations $\dot{\overline{\chi}}_{\mathrm{c}}$ equation 6.67 that the system is nonlinear. For this reason an EKF must be developed. To reduce the complexity of the model, it is assumed, that all vertical wheel velocities and positions are zero and thus all terms containing these, can be removed. Furthermore all trigonometric expressions are replaced with first order Taylor polynomials as in equation 7.12 and 7.12.

$$sin(x) \rightarrow x \tag{7.12}$$

$$cos(x) \rightarrow 1 \tag{7.13}$$

To investigate the error on the output $\overline{F}_{\mathrm{N,w}}$ two versions of the *VEHICLE MODEL* have been simulated simultaneously under the same conditions. The only difference between the two models is, that all trigonometric expressions in *SUSPENSION* in one of the models have been approximated by the expressions from equation 7.12 and 7.13. In the simulation, both models have been asserted the motor voltage V_{m} signal shown in figure 7.4.

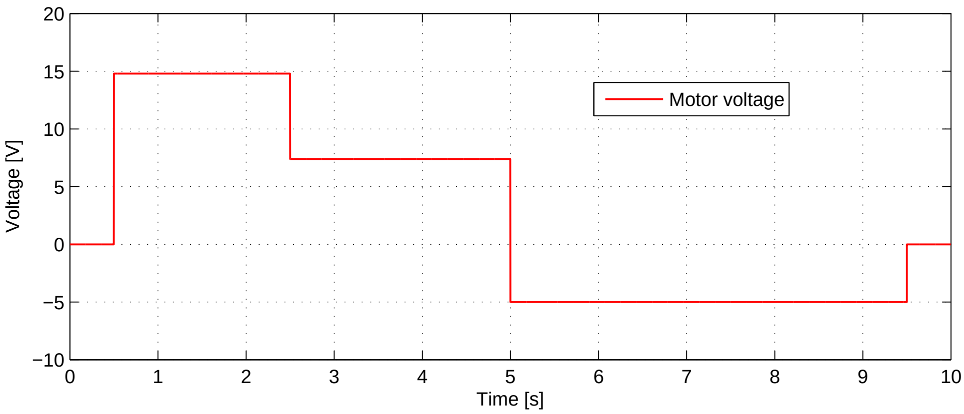

Figure 7.4. Motor voltage V_{m} signal used in Taylor approximation error investigation.

Since the motor signal is brought to its max from zero, it is assumed, that this signal will cause an error which is representative for what can be expected at most for all motor signals. The normal force on the right front wheel $F_{\mathrm{N,w,1}}$ using the two models is shown in figure 7.5 and the normal force on the right rear wheel $F_{\mathrm{N,w,4}}$ in figure 7.6.

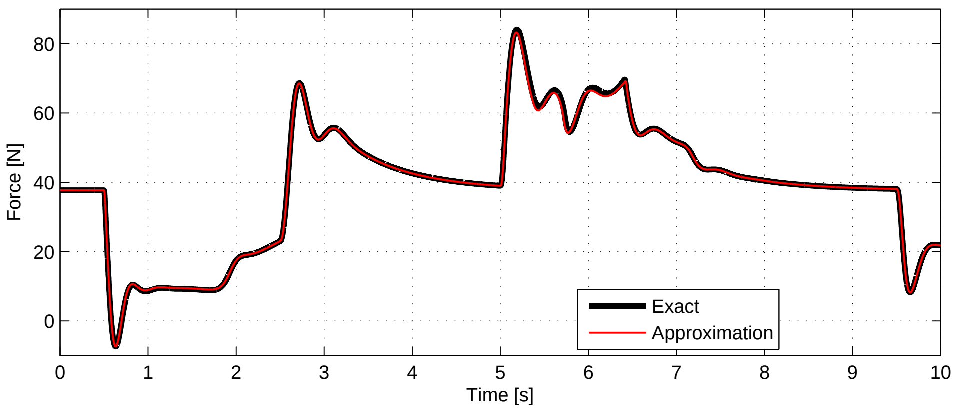

Figure 7.5. Normal force on the right front wheel $F_{\mathrm{N,w,1}}$ in Taylor approximation error investigation.

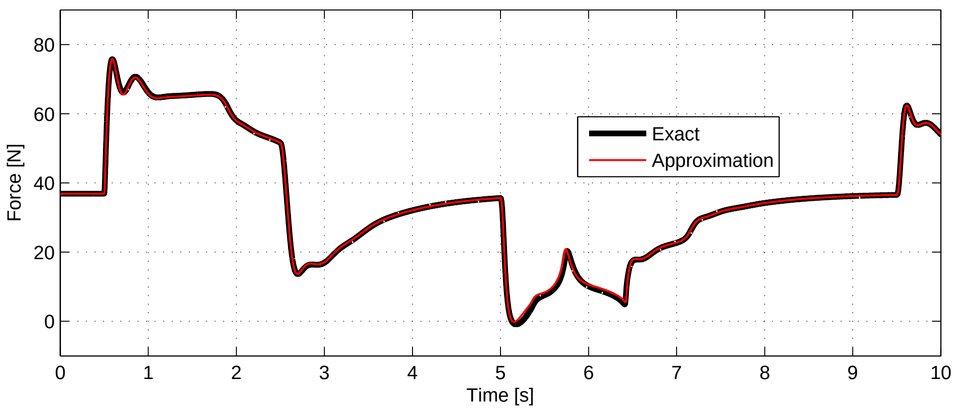

Figure 7.6. Normal force on the right rear wheel $F_{\mathrm{N,w,4}}$ in Taylor approximation error investigation.

The result seen in figure 7.5 and 7.6 is considered acceptable.

By performing simplifications according to equation 7.12 and 7.13 on equation 6.47, the intermediate result vector in *SUSPENSION*^{Kf} $\tilde{\bar{\gamma}}_o^{\pm}$ is given as in equation 7.14 and 7.15.

$$\tilde{\bar{\gamma}}_o = \begin{bmatrix} z_{o1} & z_{o2} & z_{o3} & z_{o4} & \frac{dz_{o1}}{dt} & \frac{dz_{o2}}{dt} & \frac{dz_{o3}}{dt} & \frac{dz_{o4}}{dt} \end{bmatrix}^T$$

(7.14)
$$\tilde{\bar{\gamma}}_o^{-} = \begin{bmatrix} \tilde{\chi}_c^{-}(1) - d_{z,c} + \bar{d}_{x,w} \cdot \tilde{\chi}_c^{-}(3) + \bar{d}_{y,w} \cdot \tilde{\chi}_c^{-}(5) \\ \tilde{\chi}_c^{-}(2) + \bar{d}_{x,w} \cdot \tilde{\chi}_c^{-}(4) + \bar{d}_{y,w} \cdot \tilde{\chi}_c^{-}(6) \end{bmatrix}$$

(7.15)
$$\tilde{\bar{\gamma}}_o^{+} = \begin{bmatrix} \tilde{\chi}_c^{+}(1) - d_{z,c} + \bar{d}_{x,w} \cdot \tilde{\chi}_c^{+}(3) + \bar{d}_{y,w} \cdot \tilde{\chi}_c^{+}(5) \\ \tilde{\chi}_c^{+}(2) + \bar{d}_{x,w} \cdot \tilde{\chi}_c^{+}(4) + \bar{d}_{y,w} \cdot \tilde{\chi}_c^{+}(6) \end{bmatrix}$$

Simplifying equation 6.63 to 6.65 yields equation 7.16 to 7.18.

(7.16)
$$\ddot{\tilde{z}}_{c,n}^{-} = -g + \frac{\sum \bar{F}_{0,s}}{m_c} + \frac{\bar{\xi}^T \cdot \tilde{\bar{\gamma}}_{o,n-1}^{+}}{m_c}$$

(7.17)
$$\ddot{\tilde{\phi}}_{c,n}^{-} = \frac{\bar{d}_{x,w}^{\;T} \bar{F}_{0,s}}{J_{c,\phi}} + \frac{\bar{\xi}_x^{\;T} \cdot \tilde{\bar{\gamma}}_{o,n-1}^{+}}{J_{c,\phi}}$$

(7.18)
$$\ddot{\tilde{\theta}}_{c,n}^{-} = \frac{\bar{d}_{y,w}^{\;T} \bar{F}_{0,s}}{J_{c,\theta}} + \frac{\bar{\xi}_y^{\;T} \cdot \tilde{\bar{\gamma}}_{o,n-1}^{+}}{J_{c,\theta}} + \frac{\sum \tilde{\bar{F}}_{d,n} \cdot \tilde{\chi}_{c,n-1}^{+}(1)}{J_{c,\theta}} + \frac{\sum \tilde{\bar{T}}_{w,n}}{J_{c,\theta}}$$

The a priori state vector $\tilde{\bar{\chi}}_{c,n}^{-}$, shown in equation 7.19 to 7.24, is then simply a copy of 6.68 to 6.73 with variable substitution from model to Kalman filter.

(7.19)
$$\tilde{\chi}_{c,n}^{-}(1) = \tilde{\chi}_{c,n-1}^{+}(1) + t_s \cdot \tilde{\chi}_{c,n-1}^{+}(2) + \frac{t_s^{\,2}}{2} \cdot \ddot{\tilde{z}}_{c,n}^{-}$$

(7.20)
$$\tilde{\chi}_{c,n}^{-}(2) = \tilde{\chi}_{c,n-1}^{+}(2) + t_s \cdot \ddot{\tilde{z}}_{c,n}^{-}$$

(7.21)
$$\tilde{\chi}_{c,n}^{-}(3) = \tilde{\chi}_{c,n-1}^{+}(3) + t_s \cdot \tilde{\chi}_{c,n-1}^{+}(4) + \frac{t_s^{\,2}}{2} \cdot \ddot{\tilde{\phi}}_{c,n}^{-}$$

(7.22)
$$\tilde{\chi}_{c,n}^{-}(4) = \tilde{\chi}_{c,n-1}^{+}(4) + t_s \cdot \ddot{\tilde{\phi}}_{c,n}^{-}$$

(7.23)
$$\tilde{\chi}_{c,n}^{-}(5) = \tilde{\chi}_{c,n-1}^{+}(5) + t_s \cdot \tilde{\chi}_{c,n-1}^{+}(6) + \frac{t_s^{\,2}}{2} \cdot \ddot{\tilde{\theta}}_{c,n}^{-}$$

(7.24)
$$\tilde{\chi}_{c,n}^{-}(6) = \tilde{\chi}_{c,n-1}^{+}(6) + t_s \cdot \ddot{\tilde{\theta}}_{c,n}^{-}$$

Even though equation 7.14 and 7.15 have been simplified, equation 7.23 and 7.24 are still nonlinear since they contain the term $\sum \tilde{\bar{F}}_{d,n} \cdot \tilde{\chi}_{c,n-1}^{+}(1)$ and where inputs are multiplied with states. Therefore in order to calculate the a priori state covariance matrix $\tilde{\mathbf{P}}_{c,n}^{-}$, a Jacobian of the system equations around $\tilde{\bar{\chi}}_{c,n}^{-}$ and the given inputs must be calculated. The result $\tilde{\mathbf{A}}_{c,n}$ is shown in equation 7.25 to 7.30.

$$\text{(7.25)}\quad \widetilde{\mathbf{A}}_{\mathrm{c},n}(1,:) = \begin{bmatrix} 1 & t_\mathrm{s} & 0 & 0 & 0 & 0 \end{bmatrix} + \frac{{t_\mathrm{s}}^2}{2} \cdot \begin{bmatrix} \frac{\sum \bar{\xi}(1{:}4)}{m_\mathrm{c}} & \frac{\sum \bar{\xi}(5{:}8)}{m_\mathrm{c}} & \frac{\bar{\xi}(1{:}4)^\mathrm{T} \cdot \bar{d}_{\mathrm{x,w}}}{m_\mathrm{c}} & \frac{\bar{\xi}(5{:}8)^\mathrm{T} \cdot \bar{d}_{\mathrm{x,w}}}{m_\mathrm{c}} & \frac{\bar{\xi}(1{:}4)^\mathrm{T} \cdot \bar{d}_{\mathrm{y,w}}}{m_\mathrm{c}} & \frac{\bar{\xi}(5{:}8)^\mathrm{T} \cdot \bar{d}_{\mathrm{y,w}}}{m_\mathrm{c}} \end{bmatrix}$$

$$\text{(7.26)}\quad \widetilde{\mathbf{A}}_{\mathrm{c},n}(2,:) = \begin{bmatrix} 0 & 1 & 0 & 0 & 0 & 0 \end{bmatrix} + t_\mathrm{s} \cdot \begin{bmatrix} \frac{\sum \bar{\xi}(1{:}4)}{m_\mathrm{c}} & \frac{\sum \bar{\xi}(5{:}8)}{m_\mathrm{c}} & \frac{\bar{\xi}(1{:}4)^\mathrm{T} \cdot \bar{d}_{\mathrm{x,w}}}{m_\mathrm{c}} & \frac{\bar{\xi}(5{:}8)^\mathrm{T} \cdot \bar{d}_{\mathrm{x,w}}}{m_\mathrm{c}} & \frac{\bar{\xi}(1{:}4)^\mathrm{T} \cdot \bar{d}_{\mathrm{y,w}}}{m_\mathrm{c}} & \frac{\bar{\xi}(5{:}8)^\mathrm{T} \cdot \bar{d}_{\mathrm{y,w}}}{m_\mathrm{c}} \end{bmatrix}$$

$$\text{(7.27)}\quad \widetilde{\mathbf{A}}_{\mathrm{c},n}(3,:) = \begin{bmatrix} 0 & 0 & 1 & t_\mathrm{s} & 0 & 0 \end{bmatrix} + \frac{{t_\mathrm{s}}^2}{2} \cdot \begin{bmatrix} \frac{\sum \bar{\xi}_\mathrm{x}(1{:}4)}{J_{\mathrm{c},\phi}} & \frac{\sum \bar{\xi}_\mathrm{x}(5{:}8)}{J_{\mathrm{c},\phi}} & \frac{\bar{\xi}_\mathrm{x}(1{:}4)^\mathrm{T} \cdot \bar{d}_{\mathrm{x,w}}}{J_{\mathrm{c},\phi}} & \frac{\bar{\xi}_\mathrm{x}(5{:}8)^\mathrm{T} \cdot \bar{d}_{\mathrm{x,w}}}{J_{\mathrm{c},\phi}} & \frac{\bar{\xi}_\mathrm{x}(1{:}4)^\mathrm{T} \cdot \bar{d}_{\mathrm{y,w}}}{J_{\mathrm{c},\phi}} & \frac{\bar{\xi}_\mathrm{x}(5{:}8)^\mathrm{T} \cdot \bar{d}_{\mathrm{y,w}}}{J_{\mathrm{c},\phi}} \end{bmatrix}$$

$$\text{(7.28)}\quad \widetilde{\mathbf{A}}_{\mathrm{c},n}(4,:) = \begin{bmatrix} 0 & 0 & 0 & 1 & 0 & 0 \end{bmatrix} + t_\mathrm{s} \cdot \begin{bmatrix} \frac{\sum \bar{\xi}_\mathrm{x}(1{:}4)}{J_{\mathrm{c},\phi}} & \frac{\sum \bar{\xi}_\mathrm{x}(5{:}8)}{J_{\mathrm{c},\phi}} & \frac{\bar{\xi}_\mathrm{x}(1{:}4)^\mathrm{T} \cdot \bar{d}_{\mathrm{x,w}}}{J_{\mathrm{c},\phi}} & \frac{\bar{\xi}_\mathrm{x}(5{:}8)^\mathrm{T} \cdot \bar{d}_{\mathrm{x,w}}}{J_{\mathrm{c},\phi}} & \frac{\bar{\xi}_\mathrm{x}(1{:}4)^\mathrm{T} \cdot \bar{d}_{\mathrm{y,w}}}{J_{\mathrm{c},\phi}} & \frac{\bar{\xi}_\mathrm{x}(5{:}8)^\mathrm{T} \cdot \bar{d}_{\mathrm{y,w}}}{J_{\mathrm{c},\phi}} \end{bmatrix}$$

$$\text{(7.29)}\quad \widetilde{\mathbf{A}}_{\mathrm{c},n}(5,:) = \begin{bmatrix} 0 & 0 & 0 & 0 & 1 & t_\mathrm{s} \end{bmatrix} + \frac{{t_\mathrm{s}}^2}{2} \cdot \begin{bmatrix} \frac{\sum \bar{\xi}_\mathrm{y}(1{:}4)}{J_{\mathrm{c},\theta}} + \frac{\sum \tilde{\bar{F}}_{\mathrm{d},n}}{J_{\mathrm{c},\theta}} & \frac{\sum \bar{\xi}_\mathrm{y}(5{:}8)}{J_{\mathrm{c},\theta}} & \frac{\bar{\xi}_\mathrm{y}(1{:}4)^\mathrm{T} \cdot \bar{d}_{\mathrm{x,w}}}{J_{\mathrm{c},\theta}} & \frac{\bar{\xi}_\mathrm{y}(5{:}8)^\mathrm{T} \cdot \bar{d}_{\mathrm{x,w}}}{J_{\mathrm{c},\theta}} & \frac{\bar{\xi}_\mathrm{y}(1{:}4)^\mathrm{T} \cdot \bar{d}_{\mathrm{y,w}}}{J_{\mathrm{c},\theta}} & \frac{\bar{\xi}_\mathrm{y}(5{:}8)^\mathrm{T} \cdot \bar{d}_{\mathrm{y,w}}}{J_{\mathrm{c},\theta}} \end{bmatrix}$$

$$\text{(7.30)}\quad \widetilde{\mathbf{A}}_{\mathrm{c},n}(6,:) = \begin{bmatrix} 0 & 0 & 0 & 0 & 0 & 1 \end{bmatrix} + t_\mathrm{s} \cdot \begin{bmatrix} \frac{\sum \bar{\xi}_\mathrm{y}(1{:}4)}{J_{\mathrm{c},\theta}} + \frac{\sum \tilde{\bar{F}}_{\mathrm{d}}}{J_{\mathrm{c},\theta}} & \frac{\sum \bar{\xi}_\mathrm{y}(5{:}8)}{J_{\mathrm{c},\theta}} & \frac{\bar{\xi}_\mathrm{y}(1{:}4)^\mathrm{T} \cdot \bar{d}_{\mathrm{x,w}}}{J_{\mathrm{c},\theta}} & \frac{\bar{\xi}_\mathrm{y}(5{:}8)^\mathrm{T} \cdot \bar{d}_{\mathrm{x,w}}}{J_{\mathrm{c},\theta}} & \frac{\bar{\xi}_\mathrm{y}(1{:}4)^\mathrm{T} \cdot \bar{d}_{\mathrm{y,w}}}{J_{\mathrm{c},\theta}} & \frac{\bar{\xi}_\mathrm{y}(5{:}8)^\mathrm{T} \cdot \bar{d}_{\mathrm{y,w}}}{J_{\mathrm{c},\theta}} \end{bmatrix}$$

It can be seen, that the only entrances in $\widetilde{\mathbf{A}}_{\mathrm{c},n}$ that changes, and therefore needs to be updated, are $\widetilde{\mathbf{A}}_{\mathrm{c},n}(5,1)$ and $\widetilde{\mathbf{A}}_{\mathrm{c},n}(6,1)$.

The estimation of the acceleration measurement from the vertical accelerometers $\tilde{\bar{\zeta}}_\mathrm{z}$ is a sum of the vertical acceleration of the chassis at the position of the accelerometers and the gravity of the earth. The expression for $\tilde{\bar{\zeta}}_\mathrm{z}$ is derived by double differentiating the vertical sensor position with respect to time, adding the gravity and simplifying by applying the Taylor approximations from equation 7.12 and 7.13. The result is shown in equation 7.33.

$$\begin{aligned}
\tilde{\bar{\zeta}}_{\mathrm{z},n} &= g + \frac{\mathrm{d}^2}{dt^2}\left[\tilde{\chi}^-_{\mathrm{c},n}(1) + \bar{d}_{\mathrm{x,zs}} \cdot \sin\left(\tilde{\chi}^-_{\mathrm{c},n}(3)\right) + \bar{d}_{\mathrm{y,zs}} \cdot \sin\left(\tilde{\chi}^-_{\mathrm{c},n}(5)\right)\right] \\
\tilde{\bar{\zeta}}_{\mathrm{z},n} &= g + \frac{\mathrm{d}}{dt}\left[\tilde{\chi}^-_{\mathrm{c},n}(2) + \bar{d}_{\mathrm{x,zs}} \cdot \tilde{\chi}^-_{\mathrm{c},n}(4) \cdot \cos\left(\tilde{\chi}^-_{\mathrm{c},n}(3)\right) + \bar{d}_{\mathrm{y,zs}} \cdot \tilde{\chi}^-_{\mathrm{c},n}(6) \cdot \cos\left(\tilde{\chi}^-_{\mathrm{c},n}(5)\right)\right] \\
\text{(7.31)}\quad \tilde{\bar{\zeta}}_{\mathrm{z},n} &= g + \dot{\tilde{\chi}}^-_{\mathrm{c},n}(2) + \cdots \\
&\cdots + \bar{d}_{\mathrm{x,zs}} \cdot \dot{\tilde{\chi}}^-_{\mathrm{c},n}(4) \cdot \cos\left(\tilde{\chi}^-_{\mathrm{c},n}(3)\right) - \bar{d}_{\mathrm{x,zs}} \cdot \tilde{\chi}^-_{\mathrm{c},n}(4)^2 \cdot \sin\left(\tilde{\chi}^-_{\mathrm{c},n}(3)\right) + \cdots \\
&\cdots + \bar{d}_{\mathrm{y,zs}} \cdot \dot{\tilde{\chi}}^-_{\mathrm{c},n}(6) \cdot \cos\left(\tilde{\chi}^-_{\mathrm{c},n}(5)\right) - \bar{d}_{\mathrm{y,zs}} \cdot \tilde{\chi}^-_{\mathrm{c},n}(6)^2 \cdot \sin\left(\tilde{\chi}^-_{\mathrm{c},n}(5)\right)
\end{aligned}$$

Applying the Taylor approximation on 7.31 yields equation 7.32.

$$\text{(7.32)}\quad \begin{aligned}
\tilde{\bar{\zeta}}_{\mathrm{z},n} = g &+ \dot{\tilde{\chi}}^-_{\mathrm{c},n}(2) + \bar{d}_{\mathrm{x,zs}} \cdot \dot{\tilde{\chi}}^-_{\mathrm{c},n}(4) - \bar{d}_{\mathrm{x,zs}} \cdot \tilde{\chi}^-_{\mathrm{c},n}(4)^2 \cdot \tilde{\chi}^-_{\mathrm{c},n}(3) + \cdots \\
&+ \bar{d}_{\mathrm{y,zs}} \cdot \dot{\tilde{\chi}}^-_{\mathrm{c},n}(6) - \bar{d}_{\mathrm{y,zs}} \cdot \tilde{\chi}^-_{\mathrm{c},n}(6)^2 \cdot \tilde{\chi}^-_{\mathrm{c},n}(5)
\end{aligned}$$

Finally equation 7.33 can be obtained by inserting $\ddot{\tilde{z}}^{-}_{\mathrm{c},n}$, $\ddot{\tilde{\phi}}^{-}_{\mathrm{c},n}$ and $\ddot{\tilde{\theta}}^{-}_{\mathrm{c},n}$.

$$
\begin{aligned}
\tilde{\bar{\zeta}}_{\mathrm{z},n} = & g + \ddot{\tilde{z}}_{\mathrm{c},n} + \cdots \\
& \cdots + \bar{d}_{\mathrm{x,zs}} \cdot \ddot{\tilde{\phi}}_{\mathrm{c},n} - \cdots \\
& \cdots - \bar{d}_{\mathrm{x,zs}} \cdot \tilde{\chi}^{-}_{\mathrm{c},n}(4)^2 \cdot \tilde{\chi}^{-}_{\mathrm{c},n}(3) + \cdots \\
& \cdots + \bar{d}_{\mathrm{y,zs}} \cdot \ddot{\tilde{\theta}}_{\mathrm{c},n} - \cdots \\
& \cdots - \bar{d}_{\mathrm{y,zs}} \cdot \tilde{\chi}^{-}_{\mathrm{c},n}(6)^2 \cdot \tilde{\chi}^{-}_{\mathrm{c},n}(5)
\end{aligned}
\tag{7.33}
$$

Since the sensor estimate function in equation 7.33 is nonlinear, the Jacobian matrix $\widetilde{\mathbf{H}}_{\mathrm{c},n}$ must be derived around the state $\tilde{\bar{\chi}}^{-}_{\mathrm{c},n}$ and the inputs $\tilde{\bar{F}}_{\mathrm{d},n}$ and $\tilde{\bar{T}}_{\mathrm{w},n}$ for latter use in equation 7.37. This has been done in equation 7.34.

$$
\widetilde{\mathbf{H}}_{\mathrm{c},n}(i,:) = \begin{bmatrix}
\frac{\sum\bar{\xi}(1:4)}{m_\mathrm{c}} + d_{\mathrm{x,zs}}(i) \cdot \frac{\sum\bar{\xi}_\mathrm{x}(1:4)}{J_{\mathrm{c},\phi}} + d_{\mathrm{y,zs}}(i) \cdot \frac{\sum\bar{\xi}_\mathrm{y}(1:4)}{J_{\mathrm{c},\theta}} + \frac{\sum\tilde{\bar{F}}_{\mathrm{d},n}}{J_{\mathrm{c},\theta}} \\
\frac{\sum\bar{\xi}(5:8)}{m_\mathrm{c}} + d_{\mathrm{x,zs}}(i) \cdot \frac{\sum\bar{\xi}_\mathrm{x}(5:8)}{J_{\mathrm{c},\phi}} + d_{\mathrm{y,zs}}(i) \cdot \frac{\sum\bar{\xi}_\mathrm{y}(5:8)}{J_{\mathrm{c},\theta}} \\
\frac{\bar{\xi}(1:4)^\mathrm{T} \cdot \bar{d}_{\mathrm{x,zs}}}{m_\mathrm{c}} + d_{\mathrm{x,zs}}(i) \cdot \frac{\bar{\xi}_\mathrm{x}(1:4)^\mathrm{T} \cdot \bar{d}_{\mathrm{x,zs}}}{J_{\mathrm{c},\phi}} - d_{\mathrm{x,zs}}(i) \cdot \tilde{\chi}^{-}_\mathrm{c}(4)^2 + d_{\mathrm{y,zs}}(i) \cdot \frac{\bar{\xi}_\mathrm{y}(1:4)^\mathrm{T} \cdot \bar{d}_{\mathrm{x,zs}}}{J_{\mathrm{c},\theta}} \\
\frac{\bar{\xi}(5:8)^\mathrm{T} \cdot \bar{d}_{\mathrm{x,zs}}}{m_\mathrm{c}} + d_{\mathrm{x,zs}}(i) \cdot \frac{\bar{\xi}_\mathrm{x}(5:8)^\mathrm{T} \cdot \bar{d}_{\mathrm{x,zs}}}{J_{\mathrm{c},\phi}} - d_{\mathrm{x,zs}}(i) \cdot 2 \cdot \tilde{\chi}^{-}_\mathrm{c}(4) \cdot \tilde{\chi}^{-}_\mathrm{c}(3) + d_{\mathrm{y,zs}}(i) \cdot \frac{\bar{\xi}_\mathrm{y}(5:8)^\mathrm{T} \cdot \bar{d}_{\mathrm{x,zs}}}{J_{\mathrm{c},\theta}} \\
\frac{\bar{\xi}(1:4)^\mathrm{T} \cdot \bar{d}_{\mathrm{y,zs}}}{m_\mathrm{c}} + d_{\mathrm{x,zs}}(i) \cdot \frac{\bar{\xi}_\mathrm{x}(1:4)^\mathrm{T} \cdot \bar{d}_{\mathrm{y,zs}}}{J_{\mathrm{c},\phi}} + d_{\mathrm{y,zs}}(i) \cdot \frac{\bar{\xi}_\mathrm{y}(1:4)^\mathrm{T} \cdot \bar{d}_{\mathrm{y,zs}}}{J_{\mathrm{c},\theta}} - d_{\mathrm{y,zs}}(i) \cdot \tilde{\chi}^{-}_\mathrm{c}(6)^2 \\
\frac{\bar{\xi}(5:8)^\mathrm{T} \cdot \bar{d}_{\mathrm{y,zs}}}{m_\mathrm{c}} + d_{\mathrm{x,zs}}(i) \cdot \frac{\bar{\xi}_\mathrm{x}(5:8)^\mathrm{T} \cdot \bar{d}_{\mathrm{y,zs}}}{J_{\mathrm{c},\phi}} + d_{\mathrm{y,zs}}(i) \cdot \frac{\bar{\xi}_\mathrm{y}(5:8)^\mathrm{T} \cdot \bar{d}_{\mathrm{y,zs}}}{J_{\mathrm{c},\theta}} - d_{\mathrm{y,zs}}(i) \cdot 2 \cdot \tilde{\chi}^{-}_\mathrm{c}(6) \cdot \tilde{\chi}^{-}_\mathrm{c}(5)
\end{bmatrix}^\mathrm{T}
\tag{7.34}
$$

It can be seen, that only column 1, 3, 4, 5, 6, 7, 8, 9 and 10 in $\widetilde{\mathbf{H}}_\mathrm{c}$ need to be updated.

As part of the covariance propagation matrix for the a priori states $\widetilde{\mathbf{P}}^{-}_\mathrm{c}$ is the process noise $\widetilde{\mathbf{Q}}_\mathrm{c}$ seen in formula 7.35. As for the *DRIVETRAIN*^{Kf} $\widetilde{\mathbf{Q}}_\mathrm{c}$ have been set according to intuition and knowledge about the system and keeping formula 7.5 in mind.

$$
\widetilde{\mathbf{Q}}_\mathrm{c} = \begin{bmatrix}
0 & 0 & 0 & 0 & 0 & 0 \\
0 & 0{,}05^2 & 0 & 0 & 0 & 0 \\
0 & 0 & 0 & 0 & 0 & 0 \\
0 & 0 & 0 & (0{,}0175 \cdot 5)^2 & 0 & 0 \\
0 & 0 & 0 & 0 & 0 & 0 \\
0 & 0 & 0 & 0 & 0 & (0{,}0175 \cdot 5)^2
\end{bmatrix}
\tag{7.35}
$$

The number in the $\widetilde{\mathbf{Q}}_\mathrm{c}$ matrix means, that the vertical velocity of the chassis mass center is assumed to be affected by zero mean white noise with a standard deviation of 5 $\frac{\mathrm{cm}}{\mathrm{s}}$, that the roll is assumed to be affected by zero mean white noise with a standard deviation of 5 $\frac{\mathrm{deg}}{\mathrm{s}}$ and that the pitch is assumed to be affected by zero mean white noise also with a standard deviation of 5 $\frac{\mathrm{deg}}{\mathrm{s}}$.

The covariance propagation matrix $\tilde{\mathbf{P}}^{-}_{\mathrm{c},n}$ for the a priori states can now be calculated as in equation 7.36.

$$\tilde{\mathbf{P}}^{-}_{\mathrm{c},n} = \tilde{\mathbf{A}}_{\mathrm{c},n}\tilde{\mathbf{P}}^{+}_{\mathrm{c},n-1}\tilde{\mathbf{A}}^{\mathrm{T}}_{\mathrm{c},n} + \tilde{\mathbf{Q}}_{\mathrm{c}} \tag{7.36}$$

The Kalman gain is given in equation 7.37.

$$\tilde{\mathbf{K}}_{\mathrm{c},n} = \tilde{\mathbf{P}}^{-}_{\mathrm{c},n}\tilde{\mathbf{H}}^{\mathrm{T}}_{\mathrm{c},n}\left(\tilde{\mathbf{H}}_{\mathrm{c},n}\tilde{\mathbf{P}}^{-}_{\mathrm{c},n}\tilde{\mathbf{H}}^{\mathrm{T}}_{\mathrm{c},n} + \tilde{\mathbf{R}}_{\mathrm{c},n}\right)^{-1} \tag{7.37}$$

where $\tilde{\mathbf{R}}_{\mathrm{c},n}$ is given in 7.38. For detail, see section 7.1.

$$\tilde{\mathbf{R}}_{\mathrm{c},n} = \begin{bmatrix} \sigma_{\mathrm{z}}{}^2 & 0 & \cdots & 0 \\ 0 & \sigma_{\mathrm{z}}{}^2 & \cdots & \cdots \\ \cdots & \cdots & \cdots & \cdots \\ 0 & \cdots & \cdots & \sigma_{\mathrm{z}}{}^2 \end{bmatrix} \tag{7.38}$$

where the value of σ_{z} is found in appendix A.4. Lastly the a posteriori states $\tilde{\bar{\chi}}^{+}_{\mathrm{c},n}$ and the covariance propagation matrix for this $\tilde{\mathbf{P}}^{+}_{\mathrm{c},n}$ can be found.

$$\tilde{\bar{\chi}}^{+}_{\mathrm{c},n} = \tilde{\bar{\chi}}^{-}_{\mathrm{c},n} + \tilde{\mathbf{K}}_{\mathrm{c},n}\left(\bar{\zeta}_{\mathrm{z},n} - \tilde{\bar{\zeta}}_{\mathrm{z},n}\right) \tag{7.39}$$

$$\tilde{\mathbf{P}}^{+}_{\mathrm{c},n} = \left(\mathbf{I} - \tilde{\mathbf{K}}_{\mathrm{c},n}\tilde{\mathbf{H}}_{\mathrm{c},n}\right)\tilde{\mathbf{P}}^{-}_{\mathrm{c},n} \tag{7.40}$$

7.3 Horizontal Vehicle Movement

The purpose of this part of the *VEHICLE KALMAN FILTER*, called *VEHICLE*^{Kf}, is to estimate the drive force $\overline{F}_{\mathrm{d}}$. The drive force is used by both the drive train and the suspension block. Two independent sensors provide measurements of the vehicle acceleration in the y direction. The inputs and outputs to and from the *VEHICLE*^{Kf} is shown in figure 7.7.

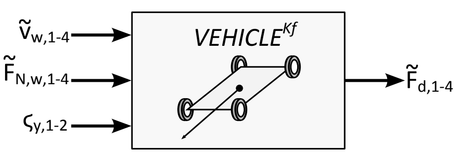

Figure 7.7. Vehicle horizontal dynamics Kalman filter.

As described in section 6.3 the surface model is part of the vehicle model, since these are closely related. For the Kalman filter the same applies, the surface friction coefficient is a part of *VEHICLE*^{Kf}. The inputs and output to and from this block is shown in figure 7.8.

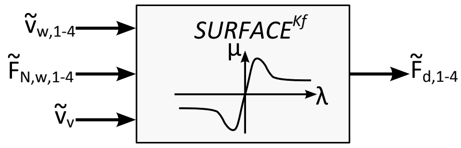

Figure 7.8. Surface friction coefficient for Kalman filter

The surface part of *VEHICLE*^{Kf} is identical to its counterpart in the *VEHICLE*, and will therefore not be described further. For details on the surface part of *VEHICLE*^{Kf} see section 6.3.

The development of the *VEHICLE*^{Kf} takes basis in the *VEHICLE* part of the *VEHICLE MODEL* developed in section 6.3. However, since the *VEHICLE*^{Kf} is updated by accelerometer measurements, and these must be estimated by the state vector $\tilde{\tilde{\chi}}_{\mathrm{v},n}$, the previous state is saved as an extra state, and the a priori state estimate is then given as in equation 7.41.

$$\tilde{\tilde{\chi}}^{-}_{\mathrm{v},n} = \begin{bmatrix} \tilde{v}_{\mathrm{v},n-1} \\ \tilde{v}_{\mathrm{v},n} \end{bmatrix}$$

$$\tilde{\tilde{\chi}}^{-}_{\mathrm{v},n}(1) = \tilde{\tilde{\chi}}^{+}_{\mathrm{v},n-1}(2)$$

$$\tilde{\tilde{\chi}}^{-}_{\mathrm{v},n}(2) = \tilde{\tilde{\chi}}^{+}_{\mathrm{v},n-1}(2) + t_{\mathrm{s}} \cdot \frac{\sum \tilde{\tilde{F}}_{\mathrm{d},n}}{m_{\mathrm{v}}}$$

$$\tilde{\tilde{\chi}}^{-}_{\mathrm{v},n} = \begin{bmatrix} 0 & 1 \\ 0 & 1 \end{bmatrix} \cdot \tilde{\tilde{\chi}}^{+}_{\mathrm{v},n-1} + \begin{bmatrix} 0 & 0 & 0 & 0 \\ \frac{t_{\mathrm{s}}}{m_{\mathrm{v}}} & \frac{t_{\mathrm{s}}}{m_{\mathrm{v}}} & \frac{t_{\mathrm{s}}}{m_{\mathrm{v}}} & \frac{t_{\mathrm{s}}}{m_{\mathrm{v}}} \end{bmatrix} \cdot \tilde{\tilde{F}}_{\mathrm{d},n} \tag{7.41}$$

$$\tilde{\mathbf{A}}_{\mathrm{v}} = \begin{bmatrix} 0 & 1 \\ 0 & 1 \end{bmatrix} \tag{7.42}$$

Equation 7.43 will then provide the sensor estimate.

$$\tilde{\tilde{\zeta}}_{\mathrm{y},n} = \tilde{H}_{\mathrm{v}} \cdot \tilde{\tilde{\chi}}^{-}_{\mathrm{v},n} \tag{7.43}$$

$$\tilde{H}_{\mathrm{v}} = \begin{bmatrix} -\frac{1}{t_{\mathrm{s}}} & \frac{1}{t_{\mathrm{s}}} \\ -\frac{1}{t_{\mathrm{s}}} & \frac{1}{t_{\mathrm{s}}} \end{bmatrix}$$

Since the first state in $\tilde{\tilde{\chi}}^{-}_{\mathrm{v},n}(1)$ is the velocity from last sample and therefore already updated by sensor error, it is assumed, that only the current velocity $\tilde{\tilde{\chi}}^{-}_{\mathrm{v},n}(2)$ contains noise. Hence the process noise covariance matrix $\tilde{Q}_{\mathrm{v}}$ is given as in equation 7.44.

$$\tilde{Q}_{\mathrm{v}} = \begin{bmatrix} 0 & 0 \\ 0 & 0{,}01^2 \end{bmatrix} \tag{7.44}$$

where 0,01 assumes, that noise with a standard deviation of 10 $\frac{\mathrm{cm}}{\mathrm{s}}$ is present on the velocity a priori estimate (For detail see equation 7.5 in section 7.1). The covariance propagation matrix $\tilde{\mathbf{P}}^{-}_{\mathrm{v},n}$ for the a priori states is given as in equation 7.45.

$$\widetilde{\mathbf{P}}^{-}_{\text{v},n} = \widetilde{\mathbf{A}}_{\text{v}} \cdot \widetilde{\mathbf{P}}^{+}_{\text{v},n-1} \cdot \widetilde{\mathbf{A}}^{\text{T}}_{\text{v}} + \widetilde{\mathbf{Q}}_{\text{v},n} \tag{7.45}$$

The Kalman filter gain is given in equation 7.46.

$$\widetilde{\mathbf{K}}_{\text{v},n} = \widetilde{\mathbf{P}}^{-}_{\text{v},n} \cdot \widetilde{\mathbf{H}}^{\text{T}}_{\text{v}} \cdot \left(\widetilde{\mathbf{H}}_{\text{v}} \cdot \widetilde{\mathbf{P}}^{-}_{\text{v},n} \cdot \widetilde{\mathbf{H}}^{\text{T}}_{\text{v}} + \widetilde{\mathbf{R}}_{\text{v}}\right) \tag{7.46}$$

where $\widetilde{\mathbf{R}}_{\text{v}}$ is the sensor noise covariance matrix given by equation 7.47.

$$\widetilde{\mathbf{R}}_{\text{v}} = \begin{bmatrix} \sigma_{\text{y}}{}^2 & 0 \\ 0 & \sigma_{\text{y}}{}^2 \end{bmatrix} \tag{7.47}$$

where the value of σ_{y} is found in appendix A.4. The state a posteriori estimates are found in equation 7.48 and the covariance propagation matrix for the a posteriori state estimate in equation 7.45. For details see section 7.1.

$$\widetilde{\widetilde{\chi}}^{+}_{\text{v},n} = \widetilde{\widetilde{\chi}}^{-}_{\text{v},n} + \widetilde{\mathbf{K}}_{\text{v},n} \cdot \left(\zeta_{\text{v},n} - \widetilde{\zeta}_{\text{v},n}\right) \tag{7.48}$$

$$\widetilde{\mathbf{P}}^{+}_{\text{v},n} = \left(\mathbf{I} - \widetilde{\mathbf{K}}_{\text{v},n} \cdot \widetilde{\mathbf{H}}_{\text{v},n}\right) \cdot \widetilde{\mathbf{P}}^{-}_{\text{v},n} \tag{7.49}$$

7.4 Summary and Evaluation

A Kalman filter estimating the relevant states of the vehicle has been developed. For simplicity, it has been created in three blocks. This way of creating the Kalman filter is not the conventional way, and it might reduce the performance of the Kalman filter. As described in the introduction to this chapter, the difference in performance between a conventional, that is a Kalman filter which is not split into blocks, and the developed Kalman filter will not be explored in this treatise. The performance of the developed Kalman filter will however be evaluated here, by exerting the *VEHICLE MODEL* and the *VEHICLE KALMAN FILTER* with a motor voltage signal, and examining how well the Kalman filter follows the vehicle model. Relevant plots are found in appendix C.

An overall evaluation of the outputs of the simulation, plotted in appendix C, has been performed. It is concluded, that the Kalman filter *VEHICLE KALMAN FILTER* designed in this chapter performs sufficiently, to be used by the supervisor control developed in chapter 8.

CHAPTER 8

CONTROLLER DEVELOPMENT

As described in section 4.4, the supervisory control is to distribute torque between the wheels and limit the slip ratio according to chapter 2. The control will consist of the TDS and TCS described in section 2.3. The TDS will handle the distribution of torque between the wheels instead of the removed differentials. The TCS will be activated when wheel slip is present, and limit this to a range of $[-0,1;0,1]$. Thus the purpose of the supervisory control is to limit slip, not to be confused with maximum utilization of the traction. The highest traction would be at the slip ratio λ, where $\mu(\lambda)$ is at its maximum A_{mag}.

The slip ratio reference λ_{ref} is either -0,1 or 0,1 depending on the sign of the slip. A reference of zero would result in zero drive force F_{d}, and the vehicle would then not be able to accelerate. The TCS will only act when the wheel slip is outside $[-0,1;0,1]$.

With the reference of the slip ratio i place, the wheel torque reference $T_{\text{w,ref}}$ must be determined. The duty cycle D_{CH2} of the PWM signal κ_{CH2}, is based on the accelerator on the remote control. The wheel torque reference is determined in equation 8.1 by combining D_{CH2} and the vehicle velocity v_{v}.

$$T_{\text{w,ref}} = \underbrace{(D_{\text{CH2}} - 1,5\ m) \cdot a_{\text{T,ref}}}_{\text{Remote control term}} - \underbrace{v_{\text{v}} \cdot |v_{\text{v}}| \cdot b_{\text{T,ref}}}_{\text{Velocity term}} \qquad \text{[Nm]} \tag{8.1}$$

The velocity term is included having an quadratic effect opposite to the vehicle direction on $T_{\text{w,ref}}$. Without this, releasing the accelerator, would not deaccelerate the vehicle as expected, since zero torque T_{w} will result in no change to the vehicle velocity. With $a_{\text{T,ref}} = 15000$ and $b_{\text{T,ref}} = 0,0459$ a wheel torque reference of 9 Nm is the maximum obtainable torque and a velocity of 14 $\frac{\text{m}}{\text{s}}$ is the maximum vehicle velocity.

A center differential can be simulated, by scaling the torque references $T_{\text{w,ref}}$ between the front and rear wheels, such that the distribution is altered. For the controller development, even distribution is chosen.

The supervisory control is to determine each motor driver signal $V_{\text{m},1-4}$. The TDS and TCS produces the motor driver signal $V_{\text{m,T},1-4}$ and $V_{\text{m},\lambda,1-4}$ respectively. A selector chooses between

$V_{\mathrm{m,T}}$ and $V_{\mathrm{m},\lambda}$ the one with the numerically lowest value to the motor driver signal V_{m}. The TDS, TCS selector, illustrated in figure 8.1, is applied on each wheel.

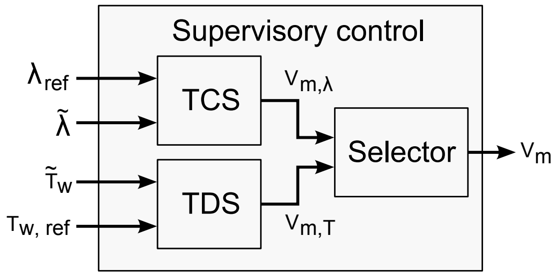

Figure 8.1. TDS and TCS functions within supervisory control.

The extended Kalman filter will supply the estimates of wheel torque $\tilde{T}_{\mathrm{w}}$ and wheel slip $\tilde{\lambda}$, and the controller is to determine $V_{\mathrm{m,T}}$ and $V_{\mathrm{m},\lambda}$, such that these will turn towards their respective reference.

TDS

The TDS is developed by using the linear relation from motor driver signal V_{m} to wheel torque T_{w}, described in section 6.2. This relation will indicate if the wheel torque is controllable from the motor driver signal V_{m} by a output controllability matrix $\mathscr{C}_{\mathrm{T}}$.

(8.2)
$$\mathscr{C}_{\mathrm{T}} = \begin{bmatrix} \mathbf{C}_{\mathrm{dt}} \cdot \mathbf{B}_{\mathrm{dt}} & \mathbf{C}_{\mathrm{dt}} \cdot \mathbf{A}_{\mathrm{dt}} \cdot \mathbf{B}_{\mathrm{dt}} & \mathbf{D}_{\mathrm{dt}} \end{bmatrix}$$

This has full rank $rank(\mathscr{C}_{\mathrm{T}}) = 2$ and the wheel torque are thereby controllable by the motor driver signal. When $\mathbf{C}_{\mathrm{dt}}$ and $\mathbf{D}_{\mathrm{dt}}$ also describe the wheel velocity v_w, this is also controllable. Since F_{d} is used as an input, this is not included when determining if the wheel torque is controllable or not. Though it is assumed controllable, when F_{d} depend on surface friction coefficient μ, the wheel slip λ and normal force $F_{\mathrm{N,w}}$, which all again depend on the wheel torque. It could be proven by using Lie brackets and including F_{d} in the differential equations, which then becomes nonlinear.

The stability of the wheel torque is analyzed by using Lyapunov [9]. If χ_{dt} is found stable by the Lyapunov function $V_{\mathrm{Lyap,T}}$ in equation 8.4, then so is also the wheel torque T_{w}. q_i are the entries of $\mathbf{A}_{\mathrm{dt}}$, $\mathbf{B}_{\mathrm{dt}}$, $\mathbf{C}_{\mathrm{dt}}$ and $\mathbf{D}_{\mathrm{dt}}$, e.g. $q_{10} = \frac{r_{\mathrm{w}}}{N_{\mathrm{dt}}}$.

$$\mathbf{A}_{\text{dt}} = \begin{bmatrix} q_1 & q_2 \\ q_4 & q_5 \end{bmatrix}, \mathbf{B}_{\text{dt}} = \begin{bmatrix} q_3 & 0 \\ 0 & q_6 \end{bmatrix}, \mathbf{C}_{\text{dt}} = \begin{bmatrix} q_7 & q_8 \\ 0 & q_{10} \end{bmatrix}, \mathbf{D}_{\text{dt}} = \begin{bmatrix} 0 & q_9 \\ 0 & 0 \end{bmatrix} \tag{8.3}$$

$$V_{\text{Lyap,T}} = \tfrac{1}{2} \cdot q_4 \cdot I_{\text{m}}^2 - \tfrac{1}{2} \cdot q_2 \cdot \omega_{\text{m}}^2 \tag{8.4}$$

$$V_{\text{Lyap,T}} = \tfrac{1}{2} \cdot \frac{N_{\text{dt}}^2 \cdot K_{\text{a}}}{J_{\text{w}} + N_{\text{dt}}^2 \cdot J_{\text{m}}} \cdot I_{\text{m}}^2 + \tfrac{1}{2} \cdot \frac{K_{\text{a}}}{L_{\text{m}}} \cdot \omega_{\text{m}}^2 \tag{8.5}$$

$$\dot{V}_{\text{Lyap,T}} = q_4 \cdot I_{\text{m}} \cdot \left(q_1 \cdot I_{\text{m}} + q_2 \cdot \omega_{\text{m}} + q_3 \cdot V_{\text{m}}\right) - q_2 \cdot \omega_{\text{m}} \cdot \left(q_4 \cdot I_{\text{m}} + q_5 \cdot \omega_{\text{m}} + q_6 \cdot F_{\text{d}}\right) \tag{8.6}$$

$$\dot{V}_{\text{Lyap,T}} = q_1 \cdot q_4 \cdot I_{\text{m}}^2 - q_2 \cdot q_5 \cdot \omega_{\text{m}}^2 \tag{8.7}$$

$$\dot{V}_{\text{Lyap,T}} = -\frac{R_{\text{m}}}{L_{\text{m}}} \cdot \frac{N_{\text{dt}}^2 \cdot K_{\text{a}}}{J_{\text{w}} + N_{\text{dt}}^2 \cdot J_{\text{m}}} \cdot I_{\text{m}}^2 - \frac{K_{\text{a}}}{L_{\text{m}}} \cdot \frac{N_{\text{dt}}^2 \cdot b_{\text{m}}}{J_{\text{w}} + N_{\text{dt}}^2 \cdot J_{\text{m}}} \cdot \omega_{\text{m}}^2 \tag{8.8}$$

With $V_{\text{Lyap,T}} \geq 0$ and $\dot{V}_{\text{Lyap,T}} \leq 0$, the wheel torque is stable before applying any control. The TDS would then not have to stabilize the torque, but instead only turn it towards its reference $T_{\text{w,ref}}$. Notice that F_{d} is again not included, and considered zero. The TDS controller is developed by using feedback linearization from V_{m} to T_{w}, and in equation 8.9 the relative degree of this is found [9].

$$\begin{aligned} T_{\text{w}} &= q_7 \cdot I_{\text{m}} + q_8 \cdot \omega_{\text{m}} + q_9 \cdot F_{\text{d}} \\ \dot{T}_{\text{w}} &= q_7 \cdot \underbrace{\left(q_1 \cdot I_{\text{m}} + q_2 \cdot \omega_{\text{m}} + q_3 \cdot V_{\text{m}}\right)}_{\dot{I}_{\text{m}}} + q_8 \cdot \underbrace{\left(q_4 \cdot I_{\text{m}} + q_5 \cdot \omega_{\text{m}} + q_6 \cdot F_{\text{d}}\right)}_{\dot{\omega}_{\text{m}}} + q_9 \cdot \dot{F}_{\text{d}} \end{aligned} \tag{8.9}$$

The linearization is found to have relative degree one, since $V_{\text{m,T}}$ appears in $\dot{T}_{\text{w}}$. $V_{\text{m,T}}$ must then be developed in a way, that neutralizes all terms in $\dot{T}_{\text{w}}$ by means of $\alpha_{\text{Tw}}(\chi)$ and $\beta_{\text{Tw}}(\chi)$, while a new control term U_{Tw} is included instead.

$$\begin{aligned} \dot{T}_{\text{w}}|_{V_{\text{m}}=V_{\text{m,T}}} &= U_{\text{Tw}} \\ V_{\text{m,T}} &= \alpha_{\text{Tw}}(\chi) + \beta_{\text{Tw}}(\chi) \cdot U_{\text{Tw}} \end{aligned} \tag{8.10}$$

$$\begin{aligned} \dot{T}_{\text{w}} =& q_7 \cdot \left(q_1 \cdot I_{\text{m}} + q_2 \cdot \omega_{\text{m}} + q_3 \cdot \underbrace{\left(\alpha_{\text{Tw}} + \beta_{\text{Tw}} \cdot U_{\text{Tw}}\right)}_{V_{\text{m}}=V_{\text{m,T}}} \right) - \cdots \\ & \cdots - q_8 \cdot \left(q_4 \cdot I_{\text{m}} + q_5 \cdot \omega_{\text{m}} + q_6 \cdot F_{\text{d}}\right) + q_9 \cdot \dot{F}_{\text{d}} \end{aligned} \tag{8.11}$$

$$\begin{aligned} \dot{T}_{\text{w}} =& q_7 \cdot q_1 \cdot I_{\text{m}} + q_7 \cdot q_2 \cdot \omega_{\text{m}} + q_7 \cdot q_3 \cdot \alpha_{\text{Tw}} + q_7 \cdot q_3 \cdot \beta_{\text{Tw}} \cdot U_{\text{Tw}} + \cdots \\ & \cdots + q_8 \cdot q_4 \cdot I_{\text{m}} + q_8 \cdot q_5 \cdot \omega_{\text{m}} + q_8 \cdot q_6 \cdot F_{\text{d}} + q_9 \cdot \dot{F}_{\text{d}} \\ \alpha_{\text{Tw}} =& -\frac{q_7 \cdot q_1 \cdot I_{\text{m}} + q_7 \cdot q_2 \cdot \omega_{\text{m}} + q_8 \cdot q_4 \cdot I_{\text{m}} + q_8 \cdot q_5 \cdot \omega_{\text{m}} + q_8 \cdot q_6 \cdot F_{\text{d}} + q_9 \cdot \dot{F}_{\text{d}}}{q_7 \cdot q_3} \end{aligned}$$

$$\alpha_{\text{Tw}} = -\frac{\left(q_7 \cdot q_1 + q_8 \cdot q_4\right) \cdot I_{\text{m}} + \left(q_7 \cdot q_2 + q_8 \cdot q_5\right) \cdot \omega_{\text{m}} + q_8 \cdot q_6 \cdot F_{\text{d}} + q_9 \cdot \dot{F}_{\text{d}}}{q_7 \cdot q_3} \tag{8.12}$$

$$\beta_{\text{Tw}} = \frac{1}{q_7 \cdot q_3} \tag{8.13}$$

Now the extended Kalman filter, is not only to supply the estimates $\tilde{T}_{\text{w}}$ and $\tilde{\lambda}$, but also $\tilde{\chi}_{\text{dt}}$ and $\tilde{F}_{\text{d}}$. $\dot{F}_{\text{d}}$ is derived by using a previous sample of F_{d}. With the selector choosing $V_{\text{m}} = V_{\text{m,T}}$

the TDS is able to control the wheel torque by using the new control term U_{Tw} affecting $\dot{T}_{\mathrm{w}}$ directly. When the control $V_{\mathrm{m,T}}$ is applied as V_{m}, the ordinary motor differential equations χ_{dt} are altered.

$$\frac{\mathrm{d}I_{\mathrm{m}}}{\mathrm{d}t} = \frac{1}{q_7} \cdot \left(q_8 \cdot I_{\mathrm{m}} + q_9 \cdot \dot{F}_{\mathrm{d}} + U_{\mathrm{Tw}}\right) \qquad \left[\frac{\mathrm{A}}{\mathrm{s}}\right] \tag{8.14}$$

$$\frac{\mathrm{d}\omega_{\mathrm{m}}}{\mathrm{d}t} = q_4 \cdot I_{\mathrm{m}} + q_5 \cdot \omega_{\mathrm{m}} + q_6 \cdot F_{\mathrm{d}} \qquad \left[\frac{\mathrm{rad}}{\mathrm{s}^2}\right] \tag{8.15}$$

The TDS will with U_{Tw}, act on the error T_{e} between the wheel torque reference $T_{\mathrm{w,ref}}$ and the estimate of wheel torque $\tilde{T}_{\mathrm{w}}$ on the vehicle, as in equation 8.16.

$$T_{\mathrm{e}} = T_{\mathrm{w,ref}} - T_{\mathrm{w}} \qquad [\mathrm{Nm}] \tag{8.16}$$

With the control U_{Tw} having a proportional control term on the torque error $P_{\mathrm{c,T}} \cdot T_{\mathrm{e}}$, the wheel torque will turn towards the reference wheel torque $T_{\mathrm{w,ref}}$. When using feedback linearization, U_{Tw} does no require any integral term, when effects increasing and decreasing the wheel torque are neutralized.

There are several other methods which could be used, when implementing the objectives of the wheel torque controller $V_{\mathrm{c,T}}$. The surface friction coefficient will change with the road conditions, and thereby also the vehicle model parameters, which will then affect F_{d}. The same is present for the slip controller TCS. If the system is made able to identify these parameters changes while driving, an adaptive control could be used to change the controller according to the parameters, and thereby supply sufficient performance at any road condition. Another method is to use several individual robust controllers, each designed to act within a certain range of road parameters A_{mag}, B_{mag}, C_{mag} and D_{mag}, without identifying them. Then either the system or user could choose between these controllers for each of the road conditions and parameter ranges of these.

The differences between the two control methods are their performance and stability. The adaptive control gives performance at any road condition, though the stability is dependent on the performance of the vehicle model parameter identification. An implementation of this identification in the extended Kalman filter from section 7 will not guarantee either stability or convergence of the parameters. The individual robust controllers will supply stability within the parameter range of the their uncertainty models, though these affect the performance. When the range of uncertainty is increased, the performance will decrease.

There is also a possibility to combine both methods, and let the system identify the vehicle model parameters, and also have a different uncertainty model upon the parameters. Instead of using the uncertainty models to describe the parameters to be within several ranges, the system will identify the parameters and use one uncertainty model to describe the uncertainty of the parameters identification. The adaptive controller must thereby only be changed so that it is still stable within this parameter identification uncertainty range. With the new uncertainty models a different performance would be present. Though the identification must be stable itself for the controller to be robust, and identify the parameters inside the ranges of the described uncertainty.

Other types of control are also possible as e.g. sliding mode, which is able to handle the parameter uncertainties. Though it has been chosen to use the wheel torque controller $V_{\mathrm{c,T}}$ without any adaptive terms or parameter identification of the road conditions.

$$U_{\mathrm{Tw}} = P_{\mathrm{c,T}} \cdot T_{\mathrm{e}} \tag{8.17}$$

Where U_{Tw} is then use in the feedback linearization $V_{\mathrm{m,T}}$, and the TDS will then distribute torque to each wheel. The TCS is then to limit slip ratio to within the reference range.

TCS

The TCS is developed, so that this will limit the slip ratio to within the range of $[-0,1;0,1]$. The wheel slip ratio is assumed controllable and stable, as the torque and velocity is. The same approach as for the TDS is used, deriving a feedback linearization $V_{\mathrm{m},\lambda}$ of the nonlinear relation from motor driver signal V_{m} to the slip ratio λ. First the relative degree of feedback linearization is found. Again q_i are the entries of $\mathbf{A}_{\mathrm{dt}}$, $\mathbf{B}_{\mathrm{dt}}$, $\mathbf{C}_{\mathrm{dt}}$ and $\mathbf{D}_{\mathrm{dt}}$. A simplified version of λ is used, without the minimum denominator ϵ_λ and neutralizing the wheel direction with $\sqrt{v_{\mathrm{w},k}{}^2 + \epsilon_\lambda{}^2}$. The TCS is only able to act on forward drive and positive wheel and vehicle velocities.

$$\lambda = \frac{v_{\mathrm{w}} - v_{\mathrm{v}}}{v_{\mathrm{w}}} \tag{8.18}$$

$$\dot{\lambda} = \frac{\dot{v}_{\mathrm{w}} \cdot (v_{\mathrm{v}} - v_{\mathrm{w}})}{v_{\mathrm{w}}^2} - \frac{\dot{v}_{\mathrm{v}} - \dot{v}_{\mathrm{w}}}{v_{\mathrm{w}}} \tag{8.19}$$

$$\ddot{\lambda} = \frac{2 \cdot \dot{v}_{\mathrm{w}} \cdot (\dot{v}_{\mathrm{v}} - \dot{v}_{\mathrm{w}})}{v_{\mathrm{w}}^2} - \frac{\ddot{v}_{\mathrm{v}} - \ddot{v}_{\mathrm{w}}}{v_{\mathrm{w}}} - \frac{2 \cdot \dot{v}_{\mathrm{w}}^2 \cdot (v_{\mathrm{v}} - v_{\mathrm{w}})}{v_{\mathrm{w}}^3} + \frac{\ddot{v}_{\mathrm{w}} \cdot (v_{\mathrm{v}} - v_{\mathrm{w}})}{v_{\mathrm{w}}^2} \tag{8.20}$$

$$\ddot{\lambda} = \frac{2 \cdot \dot{v}_{\mathrm{w}} \cdot (v_{\mathrm{w}} \cdot \dot{v}_{\mathrm{v}} - \dot{v}_{\mathrm{w}} \cdot v_{\mathrm{v}}) + \ddot{v}_{\mathrm{w}} \cdot v_{\mathrm{w}} \cdot ((v_{\mathrm{v}} - v_{\mathrm{w}}) + v_{\mathrm{w}}) - v_{\mathrm{w}}^2 \cdot \ddot{v}_{\mathrm{v}}}{v_{\mathrm{w}}^3} \tag{8.21}$$

$$v_{\mathrm{w}} = q_{10} \cdot \omega_{\mathrm{m}} \tag{8.22}$$

$$\dot{v}_{\mathrm{w}} = q_{10} \cdot \dot{\omega}_{\mathrm{m}} = q_{10} \cdot \left(q_4 \cdot I_{\mathrm{m}} + q_5 \cdot \omega_{\mathrm{m}} + q_6 \cdot F_{\mathrm{d}}\right) \tag{8.23}$$

$$\ddot{v}_{\mathrm{w}} = q_{10} \cdot \left(q_4 \cdot \left(q_1 \cdot I_{\mathrm{m}} + q_2 \cdot \omega_{\mathrm{m}} + q_3 \cdot V_{\mathrm{m}}\right) + q_5 \cdot \dot{\omega}_{\mathrm{m}} + q_6 \cdot \dot{F}_{\mathrm{d}}\right) \tag{8.24}$$

The motor driver signal V_{m} appears within $\ddot{v}_{\mathrm{w}}$, thus a relative degree two is found between this and the slip ratio λ.

The motor driver signal $V_{\mathrm{m},\lambda}$ is derived in equation 8.26, so that neutralizes all terms within $\ddot{\lambda}$ by means of $\alpha_\lambda(\chi)$ and $\beta_\lambda(\chi)$, while a new control signal U_λ is included instead.

$$\ddot{\lambda}|_{V_m=V_{m,\lambda}} = U_\lambda \tag{8.25}$$

$$V_{m,\lambda} = \alpha_\lambda(\chi) + \beta_\lambda(\chi)\cdot U_\lambda \tag{8.26}$$

$$\ddot{\lambda} = \frac{2\cdot\dot{v}_w\cdot(v_w\cdot\dot{v}_v - \dot{v}_w\cdot v_v) - v_w^2\cdot\ddot{v}_v}{v_w^3} + \cdots \tag{8.27}$$

$$\cdots + \frac{q_{10}\cdot q_4\cdot v_w\cdot v_v\cdot\left(q_1\cdot I_m + q_2\cdot\omega_m + q_3\cdot\underbrace{\left(\alpha_{m,\lambda}(\chi)+\beta_{m,\lambda}(\chi)\cdot U_\lambda\right)}_{V_m=V_{m,\lambda}}\right)}{v_w^3} + \cdots$$

$$\cdots + \frac{q_{10}\cdot v_w\cdot v\cdot\left(q_5\cdot\dot{\omega}_m + q_6\cdot\dot{F}_d\right)}{v_w^3}$$

$$\alpha_\lambda(\chi) = -\frac{q_1\cdot I_m + q_2\cdot\omega_m + \frac{2\cdot\dot{v}_w\cdot(v_w\cdot\dot{v}_v-\dot{v}_w\cdot v_v)-v_w^2\cdot\ddot{v}_v+q_{10}\cdot v_w\cdot v_v\cdot(q_5\cdot\dot{\omega}_m+q_6\cdot\dot{F}_d)}{q_{10}\cdot q_4\cdot v_w\cdot v_v}}{q_3} \tag{8.28}$$

$$\beta_\lambda(\chi) = \frac{v_w^3}{q_3\cdot q_{10}\cdot q_4\cdot v_w\cdot v_v} \tag{8.29}$$

Again the extended Kalman filter is already supplying the estimates $\tilde{\chi}_{dt}$ and $\tilde{F}_d$, but is now also to supply the estimate of vehicle velocity $\tilde{v}_v$. U_λ will affect $\ddot{\lambda}$ directly, when $V_{m,\lambda}$ is applied as V_m. The zero dynamics of the feedback linearization are assumed to be stable. $\dot{F}_d$, $\dot{v}_v$ and $\ddot{v}_v$ are found using previous samples of F_d and v_v. Again the ordinary motor differential equations within χ_{dt} are altered, when the control $V_{m,\lambda}$ is applied.

$$\frac{dI_m}{dt} = -\frac{2\cdot\dot{v}_w\cdot(v_w\cdot\dot{v} - \dot{v}_w\cdot v) - v_w^2\cdot\ddot{v} + q_{10}\cdot v_w\cdot v\cdot\left(q_5\cdot\dot{\omega}_m + q_6\cdot\dot{F}_d\right) + \frac{v_w^3\cdot U_\lambda}{q_3}}{q_{10}\cdot q_4\cdot v_w\cdot v} \quad \left[\frac{A}{s}\right] \tag{8.30}$$

$$\frac{d\omega_m}{dt} = q_4\cdot I_m - q_5\cdot\omega_m - q_6\cdot F_d \quad \left[\frac{rad}{s^2}\right] \tag{8.31}$$

The TCS is designed, such that U_λ will act on the error λ_e between the slip ratio reference range of $[-0,1;0,1]$ and the estimate $\tilde{\lambda}$ of actual wheel slip ratio on the vehicle.

$$\lambda_e = \begin{cases} -0,1-\lambda & \lambda < -0.1 \\ 0,1-\lambda & \lambda > 0.1 \end{cases} \tag{8.32}$$

Adding a double derivative control term $DD_{c,\lambda}$ and derivative control term $D_{c,\lambda}$ to λ_e as in equation 8.33, will result in the controlling the wheel slip towards the reference with both proportional and integral effect, since the relation has relative degree two.

$$U_\lambda = D_{c,\lambda}\cdot\dot{\lambda}_e + DD_{c,\lambda}\cdot\ddot{\lambda}_e \quad [V] \tag{8.33}$$

The wheel slip ratio will turn towards the reference range of $[-0,1;0,1]$. The TCS is only to act when wheel slip is outside the reference slip ratio range. If not, the vehicle would always accelerate or deaccelerate, when the wheel slip would always turn towards 0,1 or -0,1.

Another possibility of limiting the wheel slip, is to implement the parameter identification of the road conditions in the extended Kalman filter. Upon these the TCS could act on the difference in accelerattion of vehicle and wheel acc_{dif} [15]. When these accelerations becomes closer, the wheel slip will decrease. Choosing a limit for acc_{dif}, makes it possible to find a maximum torque, that can be applied to each wheel, as in equation 8.35.

$$acc_{\text{dif}} = \frac{\dot{v}_{\text{W}}}{\dot{v}_{\text{V}}} \tag{8.34}$$

$$\dot{v}_{\text{W}} = acc_{\text{dif}} \cdot \dot{v}_{\text{V}} \tag{8.35}$$

The maximum torque is the torque is found such that the wheel acceleration $\dot{v}_{\text{W}}$ will not exceed the scaled vehicle acceleration $acc_{\text{dif}} \cdot \dot{v}_{\text{V}}$. This maximum torque reference could be chosen to limit the user reference torque $T_{\text{w,ref}}$, and still have a double derivative and derivative control to overcome model and identification errors. Though performance would still be affected by the model parameter identification errors and estimation performance of χ_{dt} and all others estimates. With no estimation of the parameters, the TCS is thus chosen to only use the feedback linearization and derivative control, together with the selector to be designed in the following.

TCS and TDS selector

The selector is developed, so that the TDS $V_{\text{m,T}}$ is applied when the slip ratio is within the range of $[-0,1;0,1]$.

$$V_{\text{m}} = V_{\text{m,T}} \mid -0.1 < \lambda < 0,1 \qquad [\text{V}] \tag{8.36}$$

When slip is $\lambda \leq -0.1$ the highest of $V_{\text{m,T}}$ and $V_{\text{m},\lambda}$ is chosen, and when slip is $\lambda \geq 0.1$ the lowest of the two is chosen as V_{m} instead.

$$V_{\text{m}} = \begin{cases} V_{\text{m},\lambda} & V_{\text{m,T}} \leq V_{\text{m},\lambda} \ , \ \lambda < -0.1 \\ V_{\text{m,T}} & V_{\text{m,T}} > V_{\text{m},\lambda} \ , \ \lambda < -0.1 \\ V_{\text{m,T}} & V_{\text{m,T}} < V_{\text{m},\lambda} \ , \ \lambda > 0.1 \\ V_{\text{m},\lambda} & V_{\text{m,T}} \geq V_{\text{m},\lambda} \ , \ \lambda > 0.1 \end{cases} \tag{8.37}$$

With the TDS, TCS ans selector, the user is able to control the vehicle by applying torque with the remote control accelerator, until wheel slip is so severe that the TCS will limit it. The TDS, TCS and selector are to be implemented on the vehicle in the following, and evaluated in in section 10.3.

CHAPTER 9

SOFTWARE IMPLEMENTATION

In chapter 3 it was chosen to use a DSP for the supervisory control, and in section 5.2 a circuit board, connecting the DSP to the relevant hardware, was described. The circuit board also implements an XBEE module to enable wireless communication. In this section the software for the DSP is developed, along with software for handling the XBEE communication and data logging. In the design process, the scope from chapter 2 must be respected.

9.1 Real Time System

As described in section 2.2, the system must be able to control the wheel torques and TDS and TCS must be implemented. These functions and systems require a precise scheduling. Also the system must handle other tasks, e.g. communication. To meet these requirements, it is chosen to implement a real time system.

Each task in the system has its own objective, e.g. to handle a transmission over the wireless communication or update the velocity on each motor. The real time system will schedule and execute the tasks through several steps as given in the following.

- Update the time register of each task
- Perform a prioritized queuing of the tasks, that have reached their scheduling time
- Execute the first task from the queue. This is also the task with the highest priority
- Update the order of all scheduled tasks in the queue

Combining all steps composes the real time system as illustrated in figure 9.1.

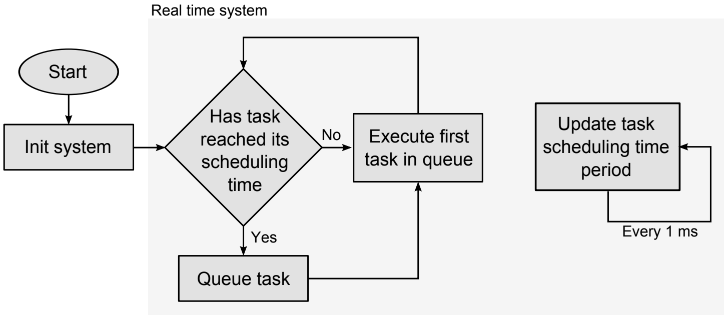

Figure 9.1. Real time system queue and execution structure.

Every task has its own time register, containing the time left for the task to be executed and rescheduled. The time register for each task is updated with 1 ms interval. Each time a task has been executed, the time delay, until the next scheduled execution of this task, is added to the time register of the task. This means, that if the task is executed later than scheduled, the time register will not be set to the full period time of the task. The time register is instead loaded with the value it would assume, if the task had been executed at the scheduled time. Using this method prevents, that tasks that are executed to late will be permanently shifted in time.

A task can be executed later, than it is scheduled for, due to e.g. execution of another task with higher priority. An illustration of this scenario is given in figure 9.2, where two tasks are scheduled and executed at the same time.

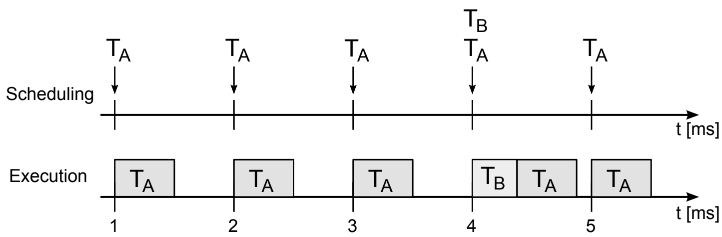

Figure 9.2. Scheduling and execution of two tasks in real time system.

At 4 ms task T_A is delayed due to the execution of task T_B, which has a higher priority than task T_A. Task T_A is scheduled to run at a period time of 1 ms and it has a completion time of 0,5 ms, while task T_B is scheduled to run at a period time of more than 4 ms and has a completion time less than 0,5 ms. Notice that task T_A is delayed only where the execution of the tasks are in conflict with each other.

If a queued task exceeds its deadline, the system dismisses the task, since the job performed by the task is no longer relevant.

Scheduling queue

To provide the option of scheduling several task at the same time, a prioritized FIFO queue is used. When a task is scheduled to run, it is inserted into the queue at the first available place according to the task priority. The task will be placed at the location, where only tasks with higher priority are in front.

When one task execution ends, the next one must begin and the task placed first in the queue is retrieved and executed. The task is removed from the queue, and the tasks still in queue are shifted. If the queue does not contain any tasks, the system will simply idle.

With the prioritization of tasks implemented, tasks which are critical to be performed in a specific time period, will sustain this as much as possible. Tasks which higher priority than others, could e.g. be the ones handling transmissions over the wireless communications. If a task is inserted into the queue, when another task with the same priority is already present, the task will be placed after the one already present.

The queue is able to contain 20 tasks in total. If a task is scheduled at a time where 20 tasks is already in the queue, the task will not be executed. If 20 tasks are in queue the system is either utilized more than possible or the length of the queue must be increased. However it is estimated, that a length of 20 tasks is sufficient for this system. Hence the queue should never or only in short periods reach full capacity.

System utilization

A high system utilization may influence the precision of the task executions compared to the scheduling. If the system utilization is near a critical point, tasks will be executed later than scheduled. It is even possible with prioritization, that some tasks will never be executed with a critical utilization. An illustration of such a utilization is given in figure 9.3.

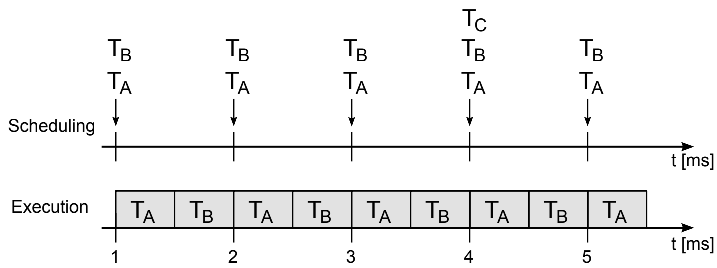

Figure 9.3. Real time system where task C will never be executed due to utilization and prioritization.

Here task T_A and T_B are prioritized higher than task T_C. Hence if the real time system is fully utilized by the other two tasks, T_C will not be executed. If the execution time of task T_A and/or T_B is reduced, the utilization is also reduced and task T_C is able to run. However if the three tasks require more than 1 ms to execute in total, all tasks executed after the scheduling point of task T_C at 4 ms is delayed.

To prevent utilizing the system more than possible, the utilization U from each task must be lees than 1.

(9.1) $$U = \frac{t_{\mathrm{e}}}{t_{\mathrm{stp}}} < 1 \qquad [-]$$

Where t_{e} is the completion time and t_{stp} the scheduling time period of a task. This states that a task can not be scheduled with a time less than is takes to carry out and complete the task. All tasks must together also have a total utilization U_{total} less than 1.

(9.2) $$U_{\mathrm{total}} = \sum_{i=1}^{N_{\mathrm{tasks}}} \frac{t_{\mathrm{e}}(i)}{t_{\mathrm{stp}}(i)} < 1 \qquad [-]$$

Where N_{tasks} is the total amount of tasks.

Beside the option to let tasks be scheduled and executed periodically, the real time system also enables tasks to be executed sporadically bases on events, or they can be executed as interrupts. A sporadic task could be a task associated with a button press performed by a user. Since a user is relatively "slow" compared to the response of the DSP, the execution time of the associated task is not critical, and the task can be queued with a low priority. An example of an interrupt based task could be the task that handles data received on a UART. Since important data might be lost if the associated task is delayed, an interrupt based execution would be preferred.

With the real time system developed in this section, one task is fully completed before handling the next task, only interrupted by interrupt based tasks. If the system is to handle several very large tasks at once, the system could be altered to implement multi threading. Multi threading could be implemented as proposed in section H.

System Tasks

The tasks are the ones being scheduled and retrieved from the queue with their specific scheduling cycle time period. The objectives of each task will be described in the following.

- `scia_receive()` - sporadic execution
  Receives data from the universal data interface when this is transmitted to the DSP.

- `scia_transmit()` - 10 ms scheduling time period
  Transmit data from the DSP to the universal data interface. The data transmitted contain reading of all accelerometers, motor velocities and voltages.

- `motor_rst()` - 25 ms scheduling time period
  If κ_{CH12} is not responding on the RC receiver, the driver signals are set to neutral.

- `servo_rst()` - 25 ms scheduling time period
  If κ_{CH1} is not responding on the RC receiver, the servo motor signal and position is set to straight forward.

- `EKF_TDS_TCS()` - 10 ms scheduling time period
  Derives the next estimate prediction with the extended Kalman filter, uses these to determine the four motor driver signals with the supervisory control.

- `key_update()` - 100 ms scheduling time period
  Updates the user keys on the vehicle. If key1 is pressed the scia_transmit() task is executed. If key2 is pressed all EKF estimates are initialized again.

- `safety_update()` - 10 ms scheduling time period
  This task checks if the real time system is running, if the motor driver signals are updated and if the vehicle RC receiver is receiving κ_{CH1} and κ_{CH2}. If one of these system is not responding, the motor drivers are disabled.

EKF and Supervisory Control Implementation

The extended Kalman filter and supervisory controller, developed in section 7 and 8, are as described as running in a object oriented simulation setup. The DSP has no ability to perform the matrix computations used here, since these functions does not exist. Instead the matrices are made by using double pointers instead as e.g. the *DRIVETRAIN*^{Kf} matrix $\mathbf{A}_{\mathrm{dt}}$, which is noted as `susp_Ak[2][2]`. The pointers then represent a matrix, where the first index denotes row, and the second the column entry of the matrix.

Functions are then made, which can perform the matrix multiplications in the Kalman filter prediction and update steps. An example of one of these functions `mult_ABA2()`, is given in the following.

```
void mult_ABA2(float R[][2], float A[][2], int m1, int n1,
  float B[][2], int m2, int n2,
    float C[][2], int m3, int n3){

  int k1, k2, k3;
  float R1[2][2], R2[2][2];

  // Transpose of C
  for(k1=0; k1<n3; k1++){
    R1[k1][k2] = 0;
    for(k2=0; k2<m3; k2++){
      R1[k1][k2] = (float)C[k2][k1];
    }
  }

  // Multiply A and B
  for(k1=0; k1<m1; k1++){
    for(k2=0; k2<n2; k2++){
      R2[k1][k2] = 0;
      for(k3=0; k3<m1; k3++){
```

```
        R2[k1][k2] = R2[k1][k2]+(float)A[k1][k3]*(float)B[k3][k2];
      }
    }
  }

  // Multiply AB and C
  for(k1=0; k1<m1; k1++){
    for(k2=0; k2<n2; k2++){
      R[k1][k2] = 0;
      for(k3=0; k3<m1; k3++){
        R[k1][k2] = (float)R[k1][k2]+(float)R2[k1][k3]*(float)R1[k3][k2];
      }
    }
  }
}
```

`mult_ABA2()` is able to take three matrices and multiply them into the result `R[][2]`, as long as their column size does no exceed two. An example where the extended Kalman filter is to update the covariance propagation matrix $\widetilde{\mathbf{P}}^{-}_{\mathrm{dt}}$ in the prediction step of the *DRIVETRAIN*^{Kf} of right front wheel, is given in the following. The covariance propagation matrix is denoted as `dt1_Pk`, the system matrix as `dt1_Ak` and the process noise covariance matrix as `dt1_Qk`.

```
// Drive train covariance propagation matrix update
mult_ABA2(dt1_Pk,dt1_Ak,2,2,dt1_Pk,2,2,dt1_Ak,2,2);

// Add process noise to covariance propagation matrix
dt1_Pk[1][1] = dt1_Pk[1][1]+dt1_Qk[1][1];
dt1_Pk[3][3] = dt1_Pk[3][3]+dt1_Qk[3][3];
dt1_Pk[5][5] = dt1_Pk[5][5]+dt1_Qk[5][5];
```

This procedure is valid for all prediction and update steps of the complete Kalman filter. Hereafter the supervisory control is to derive all motor driver signal V_{m} and apply these with the Kalman filter estimates. An example for the the right front wheel is given in the following where the estimate $\tilde{T}_{\mathrm{w}}$ is derived as `Tw[0]`, along with a feedback linearization control term U_{Tw} as `U_tw[0]` and motor voltage V_{m} as `Vm[0]`.

```
// Update right front wheel torque
Tw[0] = q7*dt1_x[0]+q8*dt1_x[1]+q9*Fd[0];

// Derive control term U_tw
U_tw[0] = P_cT*T_e[0];

// Derive motor driver signal Vm
Vm[0] = alpha_Tw[0]+beta_Tw[0]*U_tw[0];
```

Where `dt1_x[0]` and `dt1_x[1]` are the estimates $\tilde{\chi}_{\mathrm{dt}}$, `T_e[0]` the wheel torque error T_{e}, and `alpha_Tw[0]` and `beta_Tw[0]` the feedback linearization terms $\alpha_{\mathrm{Tw}}(\chi)$ and $\beta_{\mathrm{Tw}}(\chi)$, all found previously in the Kalman filter and supervisory control.

With these tasks, functions and the real time system and the DSP would be able to control the vehicle drive and update some of the drive parameters through the user interface. The system is not finally implemented Kalman filter on the vehicle, when the parameter identification of this is not final. The real time system file is included on the attached DVD as `4WD.c`. In the following the universal data interface is described, which will be used to store and display several vehicle parameters, along with enable and disable features.

9.2 Universal Data Interface

A graphical interface is used to administer the data logging feature and the vehicle driving power deactivation function (see section 2.3). Also control parameters of the vehicle can be altered on the fly from here. The interface is created using Java and will be running on a computer. The program utilizes objects including several classes when connecting between each other and hardware, as illustrated in figure 9.4, which all have unique jobs. The universal data interface consist of three objects in total, which are described in the following.

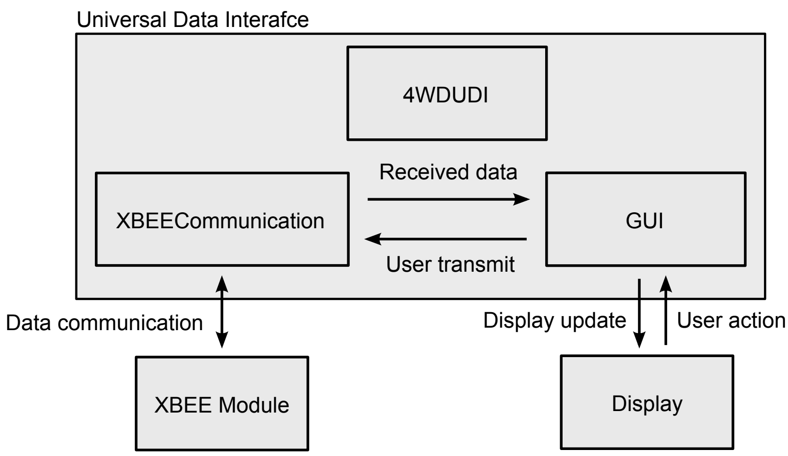

Figure 9.4. Object oriented universal data interface. Connection between objects and hardware.

Objects

- 4WDUDI
  This object only initializes and creates GUI and XBEECommunication objects and combines them.
- XBEECommunication
  This object handles the seriel communication between between the two XBEE modules. This implements several other classes, such that it can handle communication receive exceptions, when the vehicle transmits to the universal data interface. The data received contains the estimations of vehicle velocity, along with each wheel velocity and slip. These are used by the GUI object, which displays these on the graphical interface on

the computer.

To handle the communication, the object searches for all seriel connection available on the device or computer, where the application is running on. The user is then able to choose the XBEE module between the found connections which are displayed in a list. When the communication is established, the universal data interface will, besides receiving the vehicle estimates and display them, also transmit data to the vehicle every 100 ms, allowing its drive to be either enabled or disabled.

Through the graphical interface, the user is able to choose not to only receive and display the vehicle estimates, but also log and store them into a file. The GUI object will determine when the log is enabled or disabled, and which file to store to. Thus the logging feature is implemented.

- GUI
  This object creates the graphical interface, as shown in figure 9.5. This contains several buttons, where one initiates a new search for seriel connections and displays them. If a search is initiated and done, the user is hereafter allowed to connect to one of the found connections by pressing a connect button. This button is only enabled for use, if a connection is found. If this button is pressed more than once, the connection already established is closed and a new is made to the connection chosen.

  When the connection is established, the user can press a button to enable or disable the vehicle drive. If the drive is disabled, the vehicle will not respond to the remote control. Another button creates the log file for the vehicle estimation store. Each time a new log is created, the GUI names this according to the date and time. By this, a file will be present for each log initiated. The user is able to typed in a different file name than the date through the graphical interface.

  Next to the buttons, an illustration of the vehicle is given. At each wheel the received estimates of wheel velocity, torque and slip is displayed, and above these the vehicle velocity. Above the buttons, an list area is created where the found connections are written to, along with system errors if these occurs. A system error could e.g. be if the user tries to connect to a port, which is already in use.

An illustration of the universal data interface is given in figure 9.5.

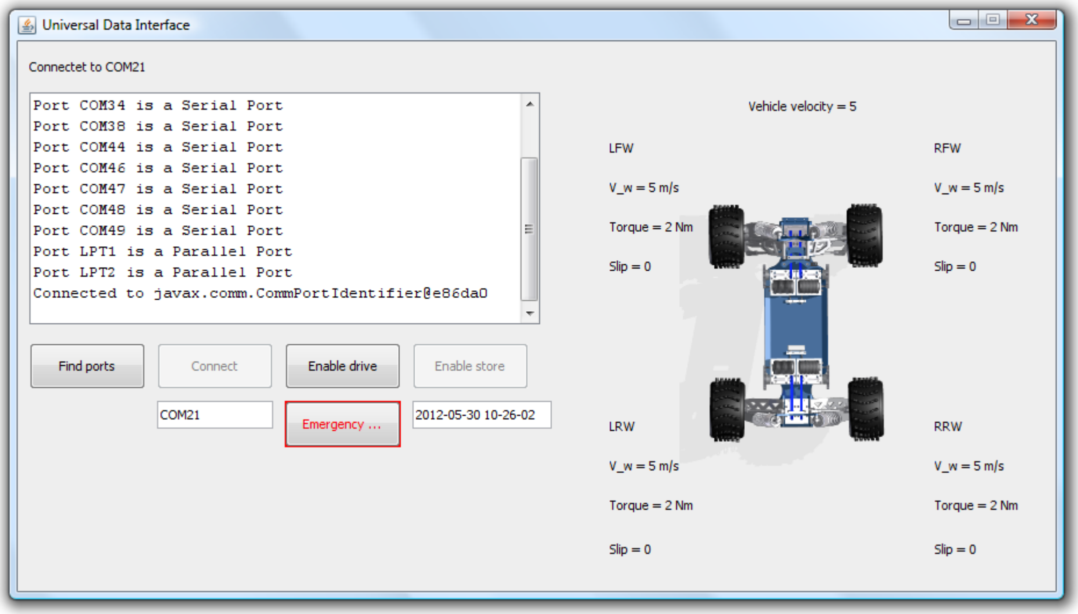

Figure 9.5. Universal data interface application.

The application files is included on the attached DVD. With the universal data interface and the real time system, the user is able to control the vehicle. The system is as for the real time system not used or finally implemented, when the parameter identification of the Kalman filter is not final.

CHAPTER 10

Evaluation

So far, the dynamics of the vehicle in two dimensions have been modeled in chapter 6. The model, referred to as the *VEHICLE MODEL*, forms the basis for the development of the observer in chapter 7 called the *VEHICLE KALMAN FILTER*. The supervisory control have been developed in chapter 8. It consists of a torque controller and a slip controller, which uses the Kalman estimates as feedback. The evaluation of these blocks in this chapter takes basis in data recorded from the vehicle while driven by a user. The data was recorded using a wireless connection between the vehicle and a computer for data logging.

10.1 Evaluating the Model

To evaluate the *VEHICLE MODEL*, simulated sensor outputs from the model must be compared to sensor outputs recorded from the vehicle while identical initial states and input signals are given to the model and the vehicle. For this reason a data sample have been recorded from the vehicle, while being driven by a user at the users will. The data sample contains the input signals and the sensor outputs. Plots showing all data can be found in appendix B while representative plots will be shown here. The input signal for motor #1 is shown in figure 10.1.

Since not all parameters in the model have been estimated, identical sensor output data from the model and vehicle can not be expected. However, if the model is principally correct, common tendencies in the data will be expected. The sensor outputs for the model and the vehicle is plotted in figure 10.2 to 10.4. The sensor output from the vehicle is filtered by MATLAB® *sgolayfilt* with order 1 and window length 11 (*sgolayfilt*(data,1,11)). The original data can be seen in appendix B along with the data for motor #2-4 and vertical vertical accelerometer #2-4.

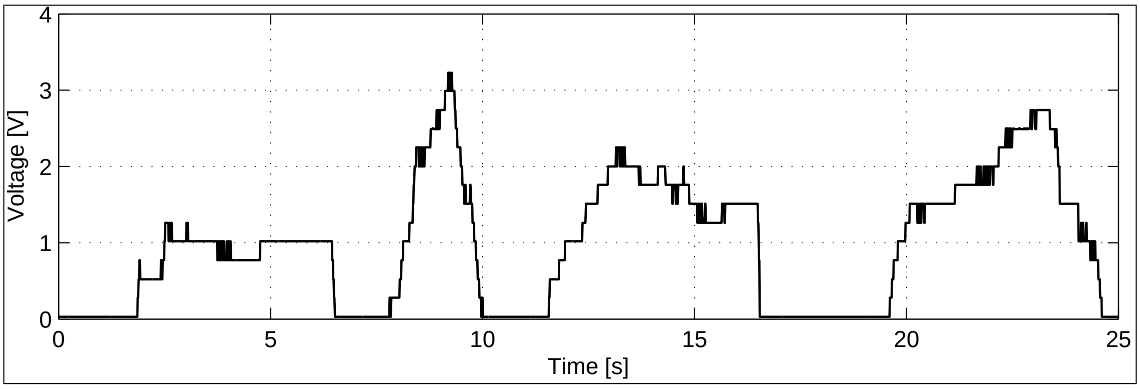

Figure 10.1. Motor input voltage signal #1.

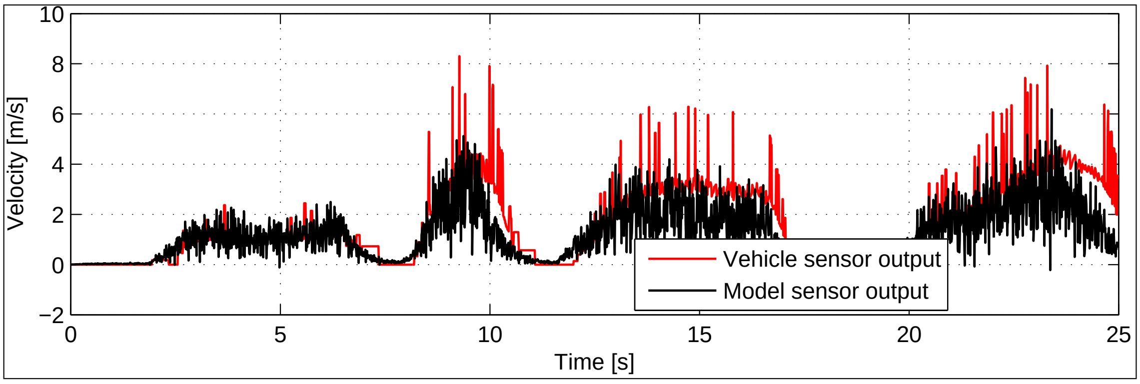

Figure 10.2. Motor 1 sensor output signal.

Figure 10.2 show, that both outputs consist of four periods around 5, 10, 15 and 22,5 seconds. The curves are in phase and are clearly correlated. Specifically is the amplitude in the first period around 5 seconds remarkably similar for the two outputs.

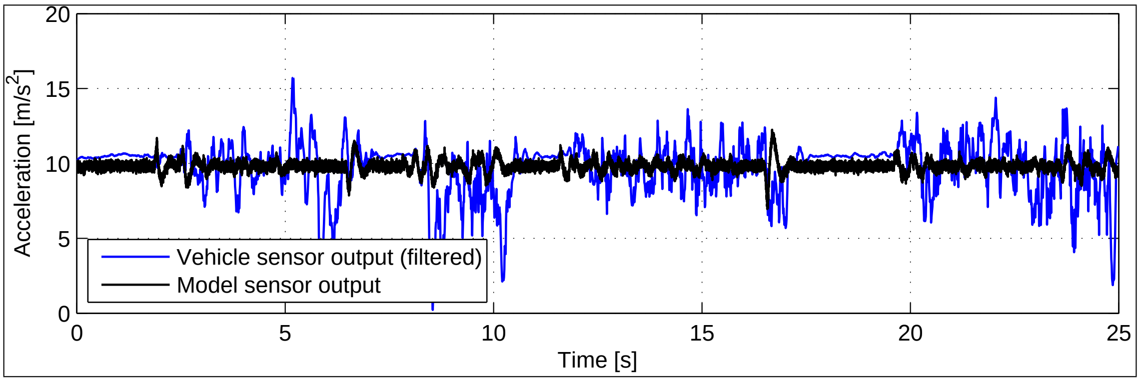

Figure 10.3. Vertical acceleration sensor #1 filtered.

Figure 10.3 shows no obvious correlation between the two signal except from, what can be considered noise, in the same periods around 5, 10, 15 and 22,5 seconds.

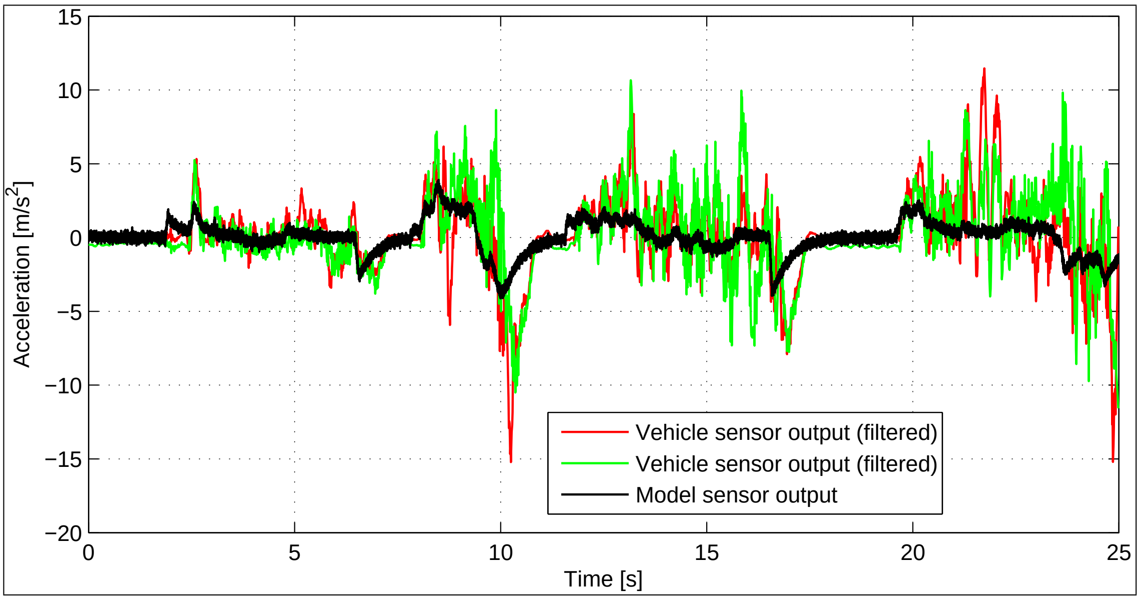

Figure 10.4. Horizontal acceleration sensors filtered.

The signals in figure 10.4 show common tendencies. E.g. at 7 seconds, where both signals rise from approximately -2,5 $\frac{\text{m}}{\text{s}^2}$ to 0 $\frac{\text{m}}{\text{s}^2}$, at 10 seconds, where both signals peaks to a low value and then rise to 0 $\frac{\text{m}}{\text{s}^2}$.

10.2 Evaluating the Kalman Filter

To evaluate the Kalman filter, two capabilities are considered: The ability to estimate the states based on sensor inputs, and the ability to reduce sensor noise. The first ability to be considered, is the ability to estimate states. Since the states to be estimated must be known in order to evaluate the result, the model has been used to simulate sensor outputs. The simulation is based on the motor inputs shown in appendix C. Furthermore, the surface parameters A_{mag}, B_{mag}, C_{mag} and D_{mag} in the model are changed, from the values chosen in section 6.3, to $A_{\text{mag}} = 0,8$, $B_{\text{mag}} = 1.6$, $C_{\text{mag}} = 2$ and $D_{\text{mag}} = 0.7$. This introduces a difference in the vehicle model compared to the model used in the Kalman filter, since if the models were identical, sensor inputs to the observer would be unnecessary.

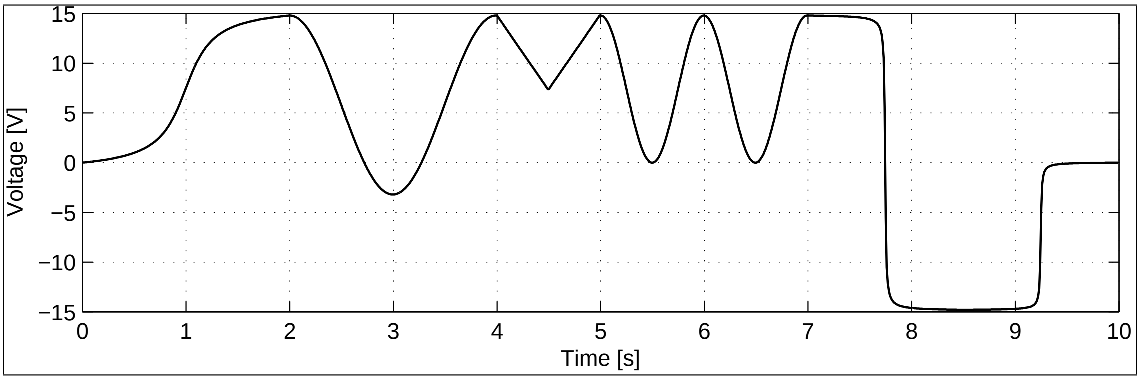

Figure 10.5. Motor input voltage #1.

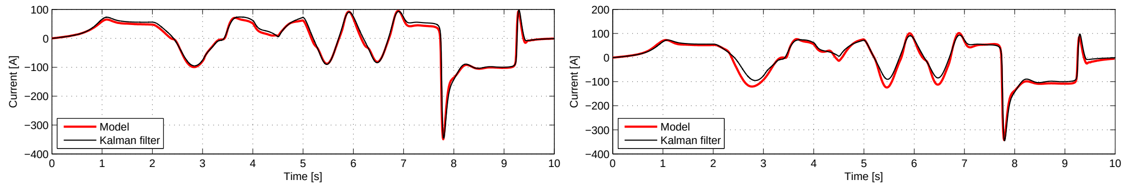

(a) With sensor update. (b) With sensor update disabled.

Figure 10.6. Current in Motor #1.

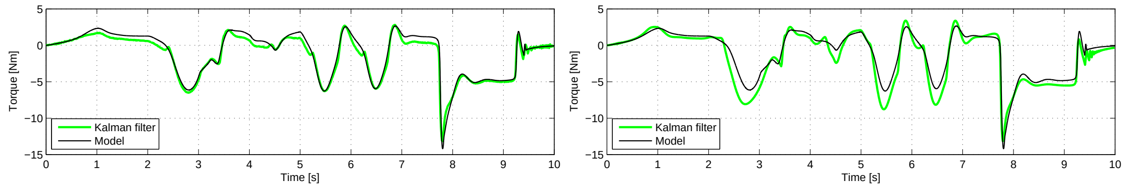

(a) With sensor update. (b) With sensor update disabled.

Figure 10.7. Torque transfered to wheel #1.

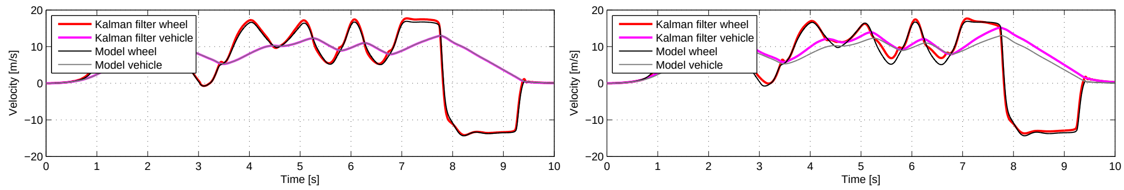

(a) With sensor update. (b) With sensor update disabled.

Figure 10.8. Velocity on wheel #1 and vehicle.

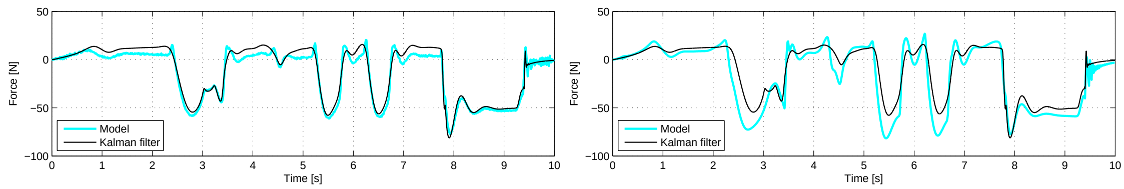

(a) With sensor update. (b) With sensor update disabled.

Figure 10.9. Drive force from wheel #1.

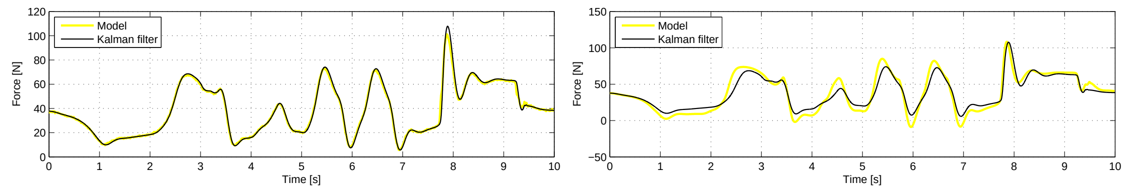

(a) With sensor update. (b) With sensor update disabled.

Figure 10.10. Normal force on wheel #1.

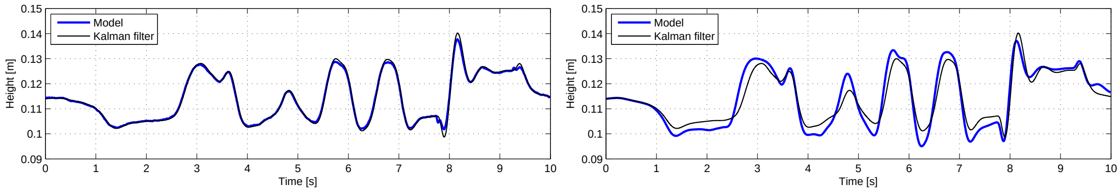

(a) With sensor update.   (b) With sensor update disabled.

Figure 10.11. Height of chassis mass center.

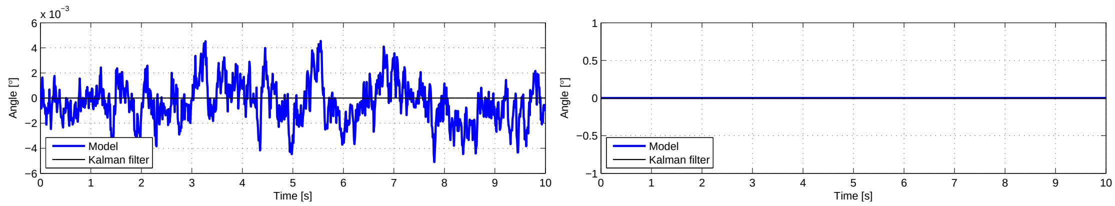

(a) With sensor update.   (b) With sensor update disabled.

Figure 10.12. Chassis roll.

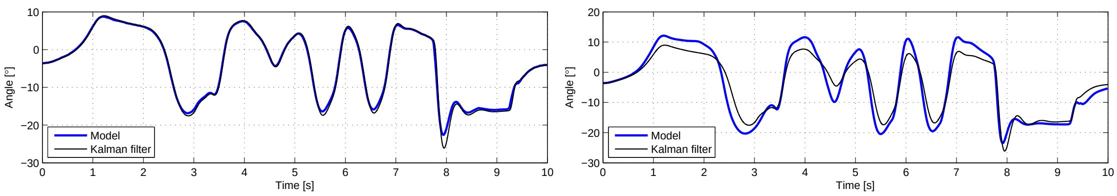

(a) With sensor update.   (b) With sensor update disabled.

Figure 10.13. Chassis pitch.

It can be seen from figure 10.6 to 10.13, that the Kalman filter is able to estimate the states of the model even though the model is not as expected. The figures *a* above generally shows less error on the state estimate than the figures *b*. The complete set of data can be seen in appendix C.

The ability of the Kalman filter to suppress noise is tested, by suppling the vehicle sensor measurements to the Kalman filter. The result is seen in figure 10.14 to 10.21.

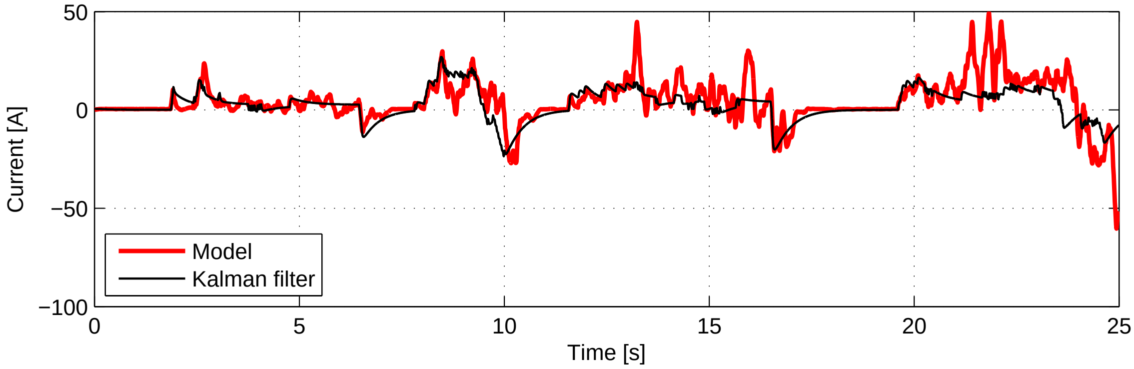

Figure 10.14. Current in Motor #1.

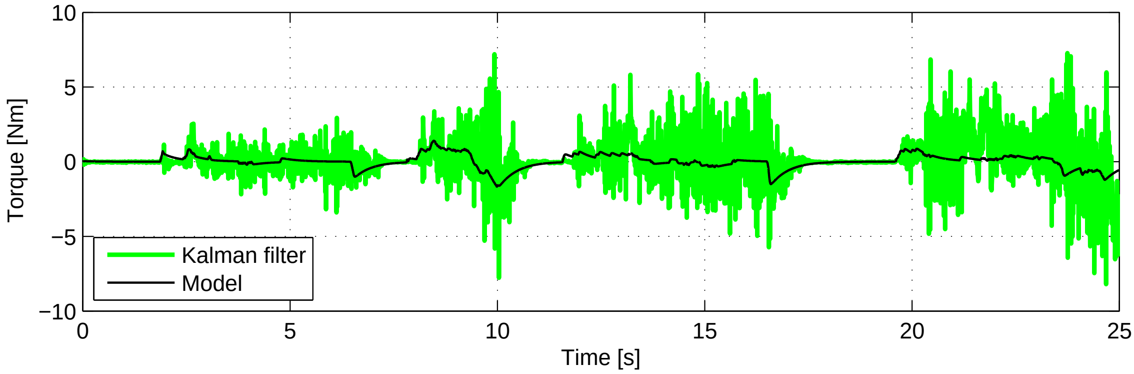

Figure 10.15. Torque transfered to wheel #1.

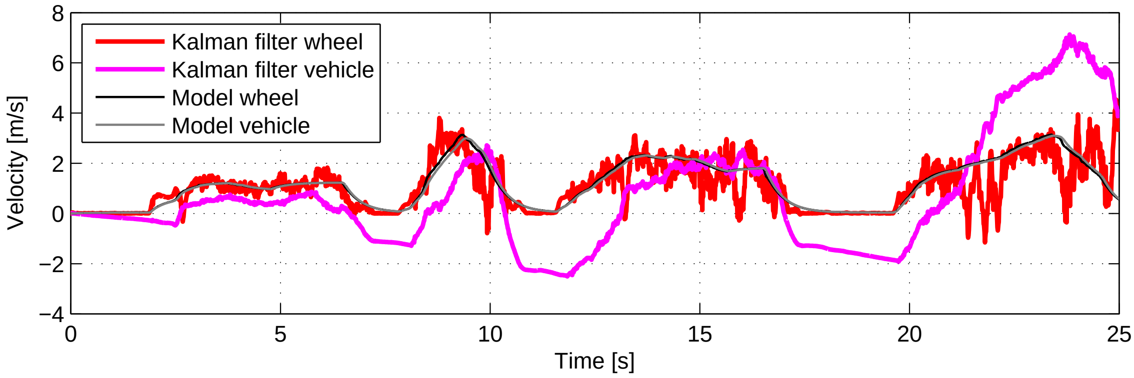

Figure 10.16. Velocity on wheel #1 and vehicle velocity.

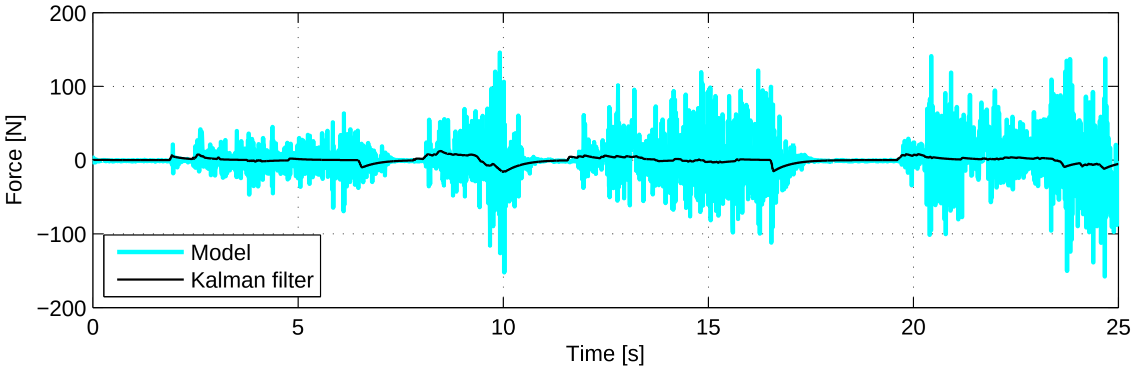

Figure 10.17. Drive force from wheel #1.

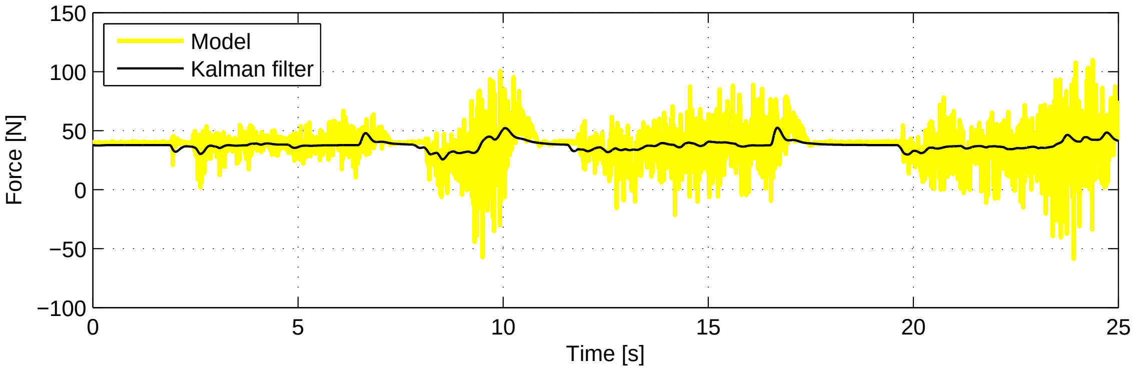

Figure 10.18. Normal force on wheel #1.

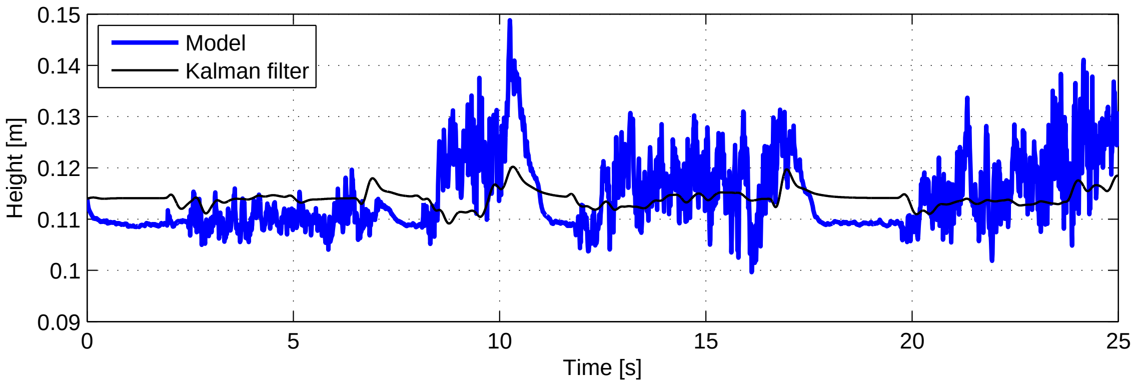

Figure 10.19. Height of chassis mass center.

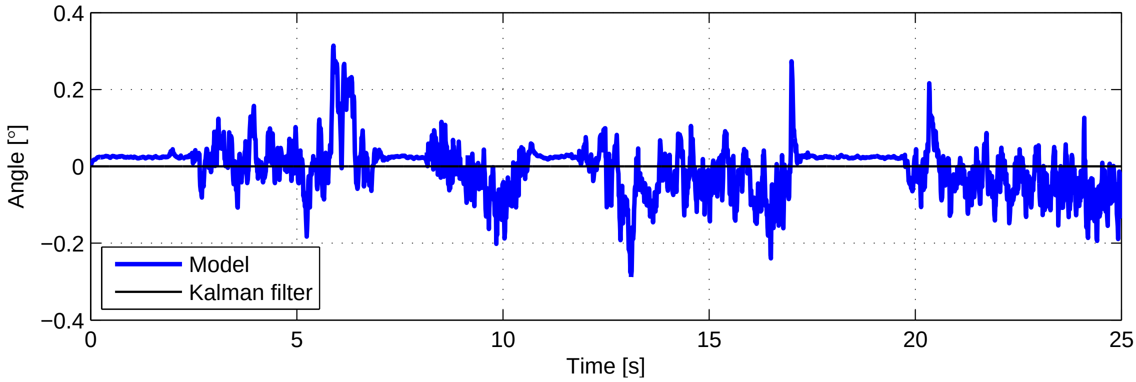

Figure 10.20. Chassis roll.

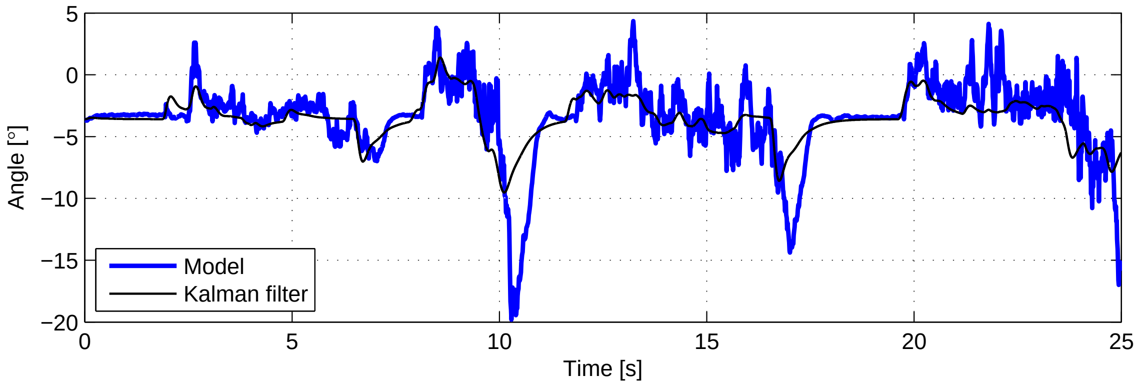

Figure 10.21. Chassis pitch.

Figure 10.17 shows that the Kalman filter estimates a drive force greater than the vehicle is able to provide on one wheel. From this and a general impression of the noise on figure 10.14 to 10.21, it is concluded, that the Kalman filter needs further tuning to reduce the noise, unless the sensor noise from the vehicle can be reduced directly.

10.3 Evaluating the Supervisory Control

The extended Kalman filter has been evaluated, and the supervisory control is now to be evaluated using the simulation setup of the Kalman filter. The estimated states are supplied to the controller, which will then determine the motor driver signal V_{m}, which are then used as feedback to the simulated Kalman filter and vehicle model.

The approval of the controller is based on the performance of the TDS and TCS, and how these are able to control the estimate wheel torque $\tilde{T}_{\mathrm{w}}$ and wheel slip ratio $\tilde{\lambda}$. During the evaluation, the road conditions are the same for the Kalman filter and vehicle model. The evaluation is based on specific wheel responses of the vehicle. All wheel responses of the TDS and TCS are located in chapter D.

Examples are given for specific wheels in the following.

TDS

The TDS was designed using feedback linearization, and the performance of this is evaluated separately before adding the proportional control term $P_{\text{c,T}}$, since the estimation performance of the Kalman filter is crucial to the feedback linearization. If the estimation $\tilde{\chi}_{\text{dt}}$ is not strictly close to χ_{dt}, $V_{\text{m,T}}$ will not completely neutralize the terms of $\dot{T}_{\text{w}}$. An illustration of a wheel torque response $\tilde{T}_{\text{w}}$ where a sine function is asserted at U_{Tw} is shown in figure 10.22.

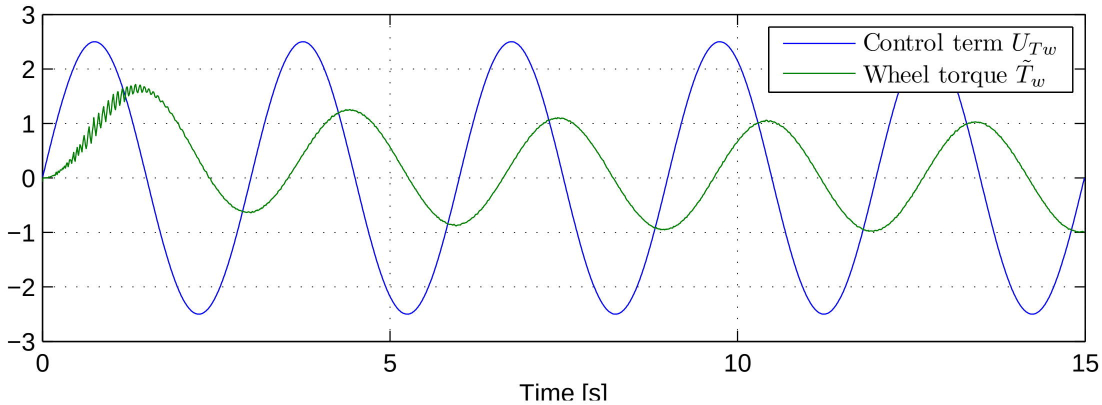

Figure 10.22. Responses of wheel torque feedback linearization.

As noticed, $\tilde{T}_{\text{w}}$ is not exactly close to U_{Tw} in figure 10.22, but still acts as the integral of U_{Tw}, as expected. Adding the proportional control term $P_{\text{c,T}}$ to the torque error T_e, will reveal if this is able to overcome that difference between U_{Tw} and $\dot{\tilde{T}}_{\text{w}}$, and control the torque towards the reference $T_{\text{w,ref}}$.

Some wheel torque responses with only the TDS enabled are shown in figure 10.23, with the remote control torque reference $T_{\text{w,rem,ref}}$ and the resulting wheel torque reference $T_{\text{w,ref}}$ from vehicle velocity.

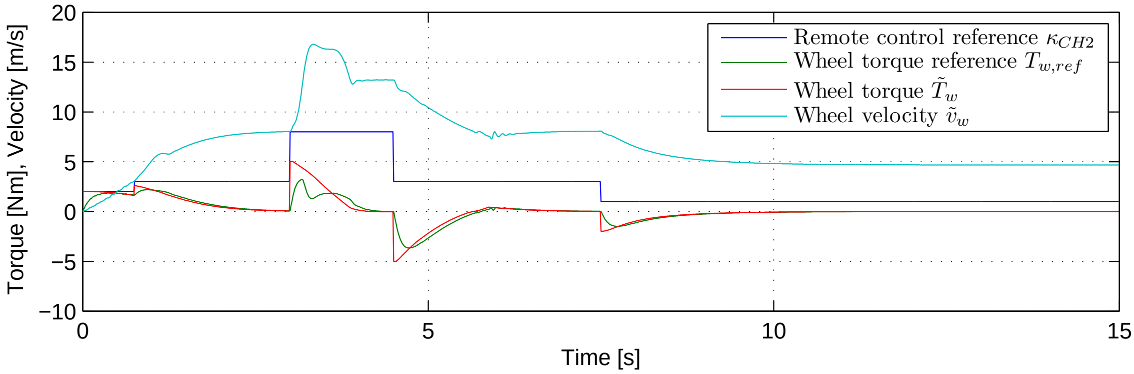

(a) Left front wheel torque and velocity response.

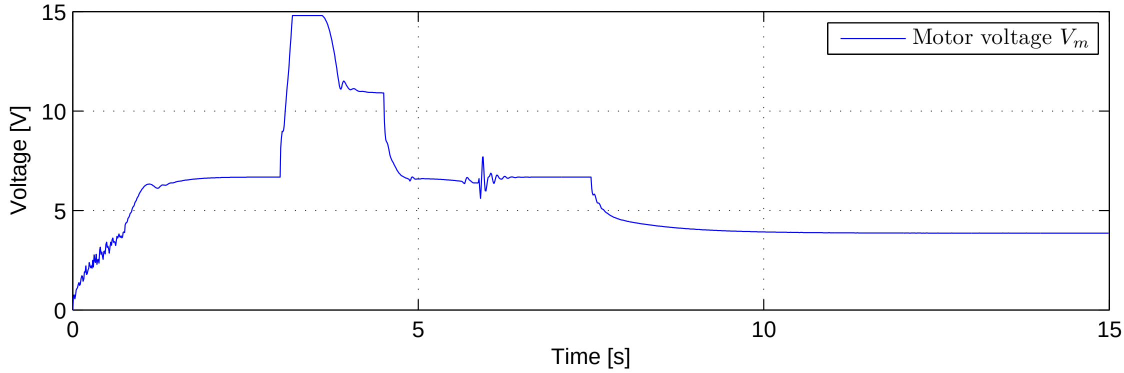

(b) Applied motor voltage from TDS on left front wheel.

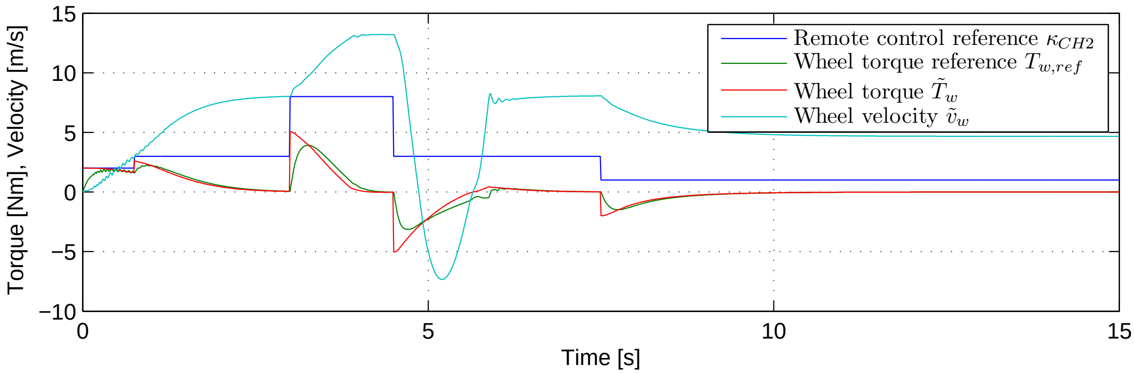

(c) Right rear wheel torque and velocity response.

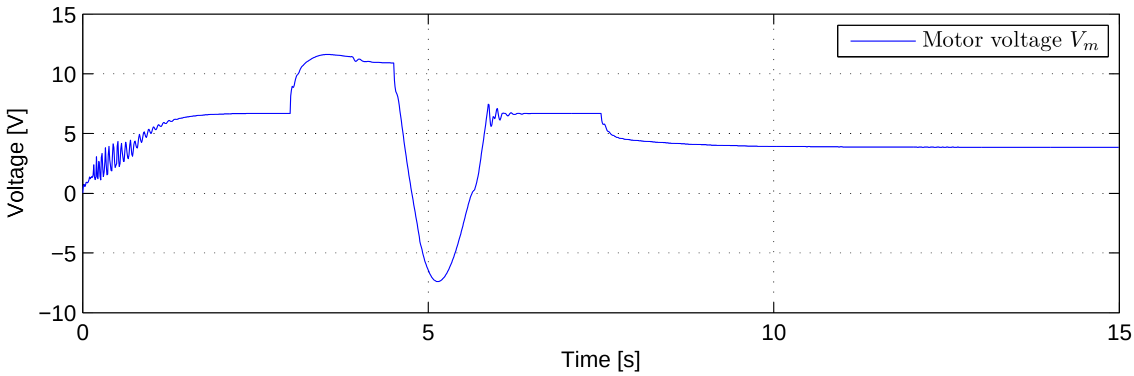

(d) Applied motor voltage from TDS on right rear wheel.

Figure 10.23. Performance of TDS.

Notice that the velocity of both wheel and vehicle decreases, when the remote control torque reference κ_{CH2} is zero, due to the velocity term, as expected. The simulation are performed with $P_{c,T} = 10$.

The wheel torque produced will decrease, when the vehicle and wheels accelerates and obtains velocity. To overcome this, the controller increases the motor driver signal and voltage, as shown in figure 10.23(b) and thereby also the torque. Though due to the limited supply of 14,8 V to the motors and motor drivers, the reachability of the wheel torque is constrained. The road conditions will determine the reachability of F_d. Thus up to a certain wheel velocity, it would be possible for the controller to obtain the reference torque $T_{w,ref}$. When the wheel velocity exceeds this point and the controller is already applying 14,8 V, the wheel torque has reached its limit, and will only decrease at increasing wheel velocity, as shown for the left front wheel in figure 10.23(a). In figure 10.23(c) and 10.23(d), the same is shown for the right rear wheel, which is able to reach the torque reference, since this has more traction, when the vehicle weight is distributed to the rear wheels when accelerating forward. The actual reachability of the wheel torque is determined by F_d, and thereby the road conditions, along with the motor driver supply limit and maximum angular velocity of the motor.

From the simulation responses, the TDS is found approved for controlling the torque towards its reference. The evaluation will now consider the TCS, and how this will perform together with the TDS.

TCS

As the TDS, the TCS is using feedback linearization, which is also evaluated separately, without the derivative and double derivative control activated. An illustration of a wheel slip response $\tilde{\lambda}$, where a sine function is asserted at U_λ is shown in figure 10.24. As described in section 8 of the controller design, TCS is only derived for positive wheel and vehicle velocities.

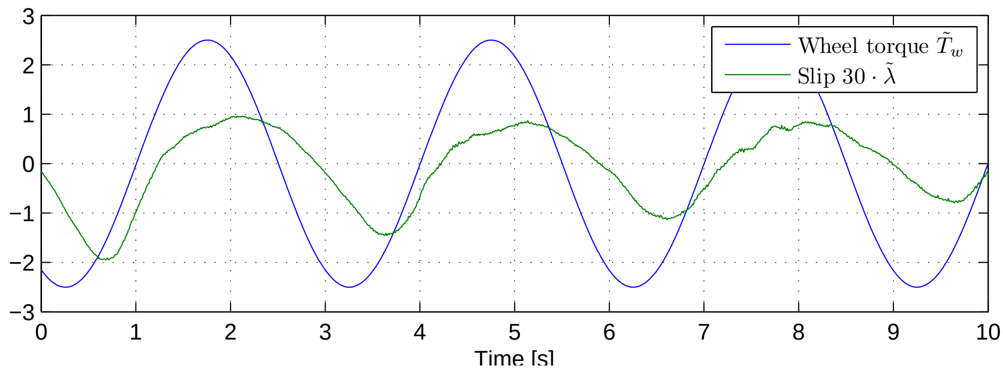

Figure 10.24. Left rear wheel slip feedback linearization.

In figure 10.24, $\tilde{\lambda}$ is multiplied by 30, since only the tendency of the curve is close to the double integral of U_λ. It is possible that this is again due to the reachability and estimation performance, which has influence on the feedback linearization. No solution has been found to enhance the performance of the feedback linearization, other than using the control U_λ to overcome this by trying to scale the error between U_λ and $\ddot{\lambda}$.

A slip ratio response of the TCS for one wheel is shown in figure 10.25. The performance of the TCS also depends on the estimation performance of χ_{dt} of the drive train, F_{d} and others, as for the TDS.

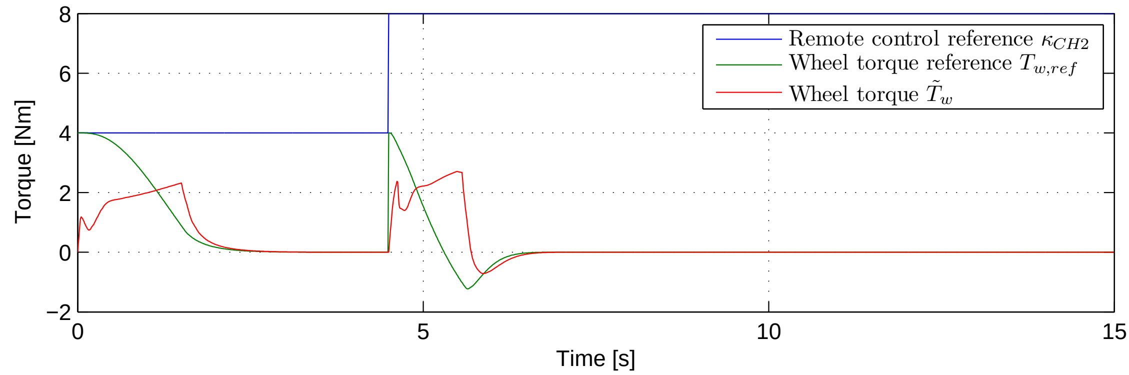

(a) Left front wheel user remote control reference and motor voltage.

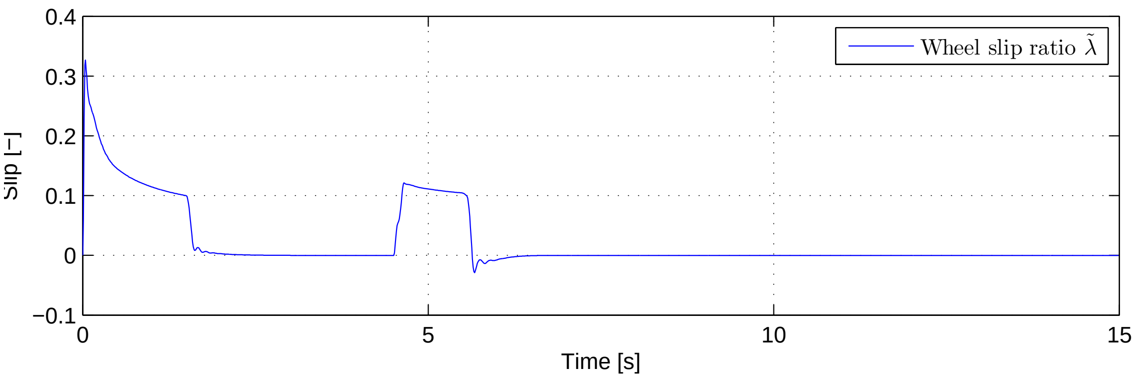

(b) Left front wheel torque slip ratio.

Figure 10.25. Performance of TDS.

The TCS is then able with this to limit slip ratio to a range of $[-0,1;0,1]$. The simulation are performed with control terms $P_{\text{c,T}} = 10$, $D_{\text{c},\lambda} = 80$ and $DD_{\text{c},\lambda} = 0.01$.

The derivative and double derivative control is activated, and the TDS, TCS and selector are to act together, controlling both wheel torque and slip, shown in in figure 10.25. As expected, the motor voltage and wheel torque is limited, when the slip exceeds 0,1. The selector then choces between the TDS and TCS, until a point where the slip is below 0,1. Hereafter only the TDS will act, since the wheels have reached a velocity where no more torque can be applied to increase wheel slip.

Summary

A supervisory control has been designed and evaluated. The TDS is found approved, when this is applied at each wheel and able to distribute torque evenly between the wheels using feedback linearization and proportional control. Using the same procedure adding feedback linearization, derivative and double derivative control on wheel slip, the TCS is also found approved for forward drive.

It was noticed for both TDS and TCS, that the performance is dependent on the extended Kalman filter estimation performance.

Chapter 11

Conclusion

The purpose of this project was to design supervisory control of a 4WD vehicle. The implications of this task was investigated in the introduction in chapter 1 and the subject was narrowed down, by defining demands and requirements in the scope in chapter 2. At this point it was decided to design an RC model car with individual 4WD electric wheel drive, by converting it from internal combustion engine and removing gearings and differentials. The project focus was chosen to concern implementation of a new wheel torque distribution and traction control system in a supervisory control.

This basis, resulted in a set of system requirements and demands, for the vehicle to be successfully modified. According to the these, an overall design was created in chapter 4, where relevant hardware was analyzed and investigated, before making a final design choice of motor and gearing, for the modification. The overall design and chosen hardware was then implemented in a hardware design phase in chapter 5.

Relevant dynamics of the modified vehicle was modeled in chapter 6. The model developed here was used to simulate the vehicle in simulations through out this project. Also the model was used as basis in the design of an observer in chapter 7. Choosing an extended Kalman filter for observer was necessary to handle nonlinearities in the vehicle model.

With a description of the vehicle dynamics, a supervisory control including TDS and TCS was developed in chapter 8. This using feedback linearization combined with proportional, derivative and double derivative control on the wheel torque and slip ratio.

The parameters of the vehicle have not been determined, since the equipment for this have not been available. However, sensor outputs from the vehicle have been recorded, and used for comparison of the vehicle model. The comparison showed, that the model principally is acceptable. Evaluating the Kalman filter by introducing a disturbance to the surface in a simulation setup, showed that the kalman filter is also acceptable, even though a parameter identification on the vehicle is essential for the performance. The evaluation also showed an unexpected high amount of sensor noise on the accelerometers which must be reduced to ensure proper state estimates.

CHAPTER 12

NOMENCLATURE

Variable	Description
A	Left wheel joint
acc_{dif}	Acceleration difference between wheel and vehicle
a_L	G_{LFW} approximation constant
a_{srm}	Steering servo motor position relation term
a_{dc}	The motor driver gain
$a_{\mathrm{T,ref}}$	Remote control term for torque reference $T_{\mathrm{w,ref}}$
$a_{\mathrm{v}} = \ddot{y}_{\mathrm{v}}$	Vehicle acceleration
$\mathbf{A}_{\mathrm{dt}}$	Drive train model system matrix
$\widetilde{\mathbf{A}}_{\mathrm{c}}$	Suspension Kalman filter system Jacobian matrix
A_{mag}	Constant in magic formula [1]
a_R	G_{RFW} approximation constant
B	Left wheel steering arm joint
b_L	G_{LFW} approximation constant
b_R	G_{RFW} approximation constant
BC	Left wheel toe rod length
$\mathrm{AB}_{\mathrm{LFW}}$	Left wheel steering arm
b_{s}	Suspension parameters - Viscosity constants
b_{m}	Motor viscous friction
b_{srm}	Servo motor viscous friction
$b_{\mathrm{T,ref}}$	Velocity dependent term for wheel torque reference $T_{\mathrm{w,ref}}$
$\mathbf{B}_{\mathrm{dt}}$	Drive train model input matrix
B_{mag}	Constant in magic formula [1]
CD	Steering idler arm length
$\mathbf{C}_{\mathrm{dt}}$	Drive train model output matrix
c_L	G_{LFW} approximation constant
C_{m}	Coulomb friction of motor
c_R	G_{RFW} approximation constant
C_{mag}	Constant in magic formula [1]

Table 12.1. Nomenclature table 1

Variable	Description
$\mathscr{C}_{\mathrm{T}}$	TDS output controllability matrix
D_{srm}	Steering servo signal κ_{CH1} duty cycle
$D_{\mathrm{c},\lambda}$	TCS derivative control term
$DD_{\mathrm{c},\lambda}$	TCS double derivative control term
d_{x}	x-coordinates of chassis corners relative to center of mass
d_{x}	x-coordinates of chassis corners relative to center of mass
$d_{\mathrm{x,zs}}$	x-coordinates of z-axis accelerometers relative to center of mass
d_{y}	y-coordinates of chassis corners relative to center of mass
$d_{\mathrm{y,zs}}$	y-coordinates of z-axis accelerometers relative to center of mass
d_{z}	z-coordinates of chassis corners relative to center of mass
$d_{\mathrm{x,p}}$	Chassis mass position factor for the x-coordinates of the wheels
$d_{\mathrm{y,p}}$	Chassis mass position factor for the y-coordinates of the wheels
$\mathbf{D}_{\mathrm{dt}}$	Drive train model feed forward matrix
D_{mag}	Constant in magic formula [1]
$F_{0,\mathrm{s}}$	Suspension parameters - Constant force offsets
F_{d}	Drive forces
$F_{\mathrm{N,w}}$	Normal force on wheels
$F_{\mathrm{N,w,worst}}$	Worst case of normal force on a wheels
F_{s}	Vertical forces from suspension
H	Right wheel steering arm joint
g	Gravitational acceleration of the Earth
G	Pitman arm joint
GH	Right wheel toe rod length
$\mathrm{G}_{\mathrm{LFW}}$	Approximated left front wheel steering angle
$\mathrm{G}_{\mathrm{RFW}}$	Approximated right front wheel steering angle
$\mathrm{G}_{\mathrm{srm}}$	Approximated steering servo motor response
$\mathrm{G}_{\mathrm{srm,a}}$	Approximated steering servo motor response with limited supply
$\widetilde{\mathbf{H}}_{\mathrm{c}}$	Suspension Kalman filter sensor output Jacobian matrix
$\widetilde{\mathbf{H}}_{\mathrm{dt}}$	Drive train Kalman filter sensor output matrix
I_{m}	Motor current
I_{srm}	Servo motor current
J	Right wheel joint
$J_{\mathrm{c},\theta}$	Inertia of chassis around x (pitch)
$J_{\mathrm{c},\phi}$	Inertia of chassis around y (roll)
$\mathrm{JH}_{\mathrm{RFW}}$	Right wheel steering arm
J_{m}	Inertia of motor

Table 12.2. Nomenclature table 2

Variable	**Description**
J_{srm}	Inertia of steering system
J_{w}	Inertia of wheel around x
K_{a}	Motor constant
$K_{\mathrm{a,srm}}$	Servo motor constant
K_{s}	Suspension parameters - Spring constants
K_{srm}	Steering servo proportional control term
$\widetilde{\mathbf{K}}_{\mathrm{c}}$	Suspension Kalman filter gain
$\widetilde{\mathbf{K}}_{\mathrm{dt}}$	Drive train Kalman filter gain
L_{m}	Inductance of motor
L_{srm}	Inductance of servo motor
m_{c}	Mass of the vehicle chassis
m_{v}	Mass of the vehicle
m_{w}	Mass of wheels
n	Discrete time variable
n_{w}	Number of wheels
N_{dt}	Drive train gear ratio
N_{tasks}	Total amount of real time system tasks
$\mathcal{N}\left(\mu,\sigma^2\right)$	Normal distribution with μ mean and σ standard deviation
$P_{\mathrm{c,T}}$	TDS proportional control term
p_{dc}	Motor driver control signal period
P_{m}	Motor output power
$\widetilde{\mathbf{P}}_{\mathrm{c}}^{\pm}$	Suspension Kalman filter covariance propagation matrix
$\widetilde{\mathbf{P}}_{\mathrm{dt}}^{\pm}$	Drive train Kalman filter covariance propagation matrix
$\widetilde{\mathbf{Q}}_{\mathrm{c}}$	Suspension Kalman filter process noise covariance matrix
$\widetilde{\mathbf{Q}}_{\mathrm{dt}}$	Drive train Kalman filter process noise covariance matrix
R	Servo motor position relation
r_{w}	Wheel radius
$r_{\mathrm{t,c\text{-}m}}$	Turn radius of center of mass
R_{m}	Electrical resistance in motor
R_{md}	Electrical resistance in motor driver
$\widetilde{\mathbf{R}}_{\mathrm{c}}$	Suspension Kalman filter sensor noise covariance matrix
$\widetilde{\mathbf{R}}_{\mathrm{dt}}$	Drive train Kalman filter sensor noise covariance matrix
R_{srm}	Electrical resistance in servo motor
t	Continuous time variable
t_{e}	Real time system task completion time

Table 12.3. Nomenclature table 3

Variable	Description
T_e	Wheel torque error
$t_{I_B=I_{B,max}}$	Battery current duration
T_m	Torque on motor shaft
t_s	Sample time for discrete time system
t_{slip}	Slip time with TCS
t_{stp}	Real time system task scheduling time period
$T_{w,ref}$	Wheel torque reference tor TDS control
T_w	Wheel torque. The torque coming from the drive train axle
$T_{w,err}$	Wheel torque control error
$T_{w,rip}$	Wheel torque variation due to TCS action
$T_{w,worst}$	Worst case wheel torque
U	Utilization of real time system task
$\mathcal{U}(a,b)$	Uniform distribution from a to b
U_{total}	Total utilization of real time system
U_{Tw}	TDS torque feedback linearization control term
U_λ	TCS wheel slip feedback linearization control term
$V_{Lyap,T}$	Wheel torque Lyapunov function
$V_{m,T}$	TDS motor driver signal
$V_{m,\lambda}$	TCS motor driver signal
V_{srm}	Servo motor voltage
$v_w = \omega_w \cdot r_w \neq \dot{y}_w$	Peripheral wheel velocity
$v_v = \dot{y}_v$	Vehicle velocity
$v_{w,max}$	Maximum available wheel velocity (see v_w)
$v_{w,min}$	Minimum available wheel velocity (see v_w)
V_m	Motor voltage
x	x-coordinate
y	y-coordinate $\left(\dot{y} = v\right)$
z	z-coordinate
z_c, $\dot{z}_c$, $\ddot{z}_c$	Chassis mass center position, velocity and acceleration along the z-axis
$z_{kf,o}$, $\dot{z}_{kf,o}$, $\ddot{z}_{kf,o}$	Kalman filter chassis corner position, velocity and acceleration along the z-axis
z_o, $\dot{z}_o$, $\ddot{z}_o$	Chassis corner position, velocity and acceleration along the z-axis

Table 12.4. Nomenclature table 4

Variable	Description
z_{w}, $\dot{z}_{\mathrm{w}}$, $\ddot{z}_{\mathrm{w}}$	Wheel position, velocity and acceleration along the z-axis
$\alpha_{\mathrm{Tw}}(\chi)$	TDS feedback linearization term
$\beta_{\mathrm{Tw}}(\chi)$	TDS feedback linearization term
γ_{dt}	Drive train model output vector
$\gamma_{\mathrm{kf,o}}^{\pm}$	Kalman filter suspension model intermediate result vector, a priori $(-)$ and a posteriori $(+)$ (Chassis corner position and velocity along z-axis)
γ_{o}	Suspension model intermediate result vector (Chassis corner position and velocity along z-axis)
$\delta_{\mathrm{max,dx}}$	Maximum model chassis mass position deviation in x direction
$\delta_{\mathrm{max,dy}}$	Maximum model chassis mass position deviation in y direction
$\Delta_{\mathrm{x,w}}$	x distance between wheels
$\Delta_{\mathrm{y,w}}$	y distance between wheels
ϵ_{λ}	Minimum denominator when calculating λ
$\zeta_{\mathrm{kf,o}}$	Kalman filter suspension model sensor estimate (Measured acceleration at chassis corners along z-axis)
ζ_{m}	Drive train model sensor output (Measured motor angular velocity)

Table 12.5. Nomenclature table 5

Variable	Description
ζ_{z}	Suspension model sensor output (Measured acceleration at chassis corners along z-axis)
ζ_{y}	Horizontal vehicle model sensor output (Measured acceleration along y-axis)
θ	Pitch of chassis
κ_{CH1}	RC-standard signal from remote control receiver channel 1
κ_{CH2}	RC-standard signal from remote control receiver channel 2
κ_{md}	RC-standard input signal to motor driver
κ_{srv}	RC-standard input signal to steering servo motor
λ	Slip ratio
λ_{e}	Wheel slip error
λ_{max}	Maximum available slip ratio
λ_{min}	Minimum available slip ratio
λ_{ref}	Wheel slip ratio reference
μ	Friction coefficient
$\mu_{\mathrm{worst}} = 1$	Worst case friction coefficient
ξ	Vector containing spring constants K_{s} and b_{s}
ξ_{x}	ξ weighted with the x-position of each wheel
ξ_{y}	ξ weighted with the y-position of each wheel
σ_{m}	Standard deviation of noise on ζ_{m}
σ_{y}	Standard deviation of noise on ζ_{y}
σ_{z}	Standard deviation of noise on ζ_{z}
ϕ	Roll of chassis
χ_{c}	Suspension model state vector
χ_{dt}	Drive train model state vector
$\chi_{\mathrm{kf,c}}^{\pm}$	Kalman filter suspension model a priori (−) and a posteriori (+) state vector
χ_{v}	Horizontal vehicle model state vector
ψ_{L}	Left front wheel steering angle
ψ_{r}	Steering servo motor reference angle
ψ_{R}	Right front wheel steering angle
ψ_{srm}	Steering servo motor angle
ψ_{e}	Steering servo motor angle error
$\psi_{\mathrm{srm,a}}$	Approximated steering servo response with constant rate turning
ψ_{srmv}	Actual turning response of steering servo
$\omega_{\mathrm{m}}, \dot{\omega}_{\mathrm{m}}$	Angular motor velocity and acceleration
ω_{srm}	Angular servo motor velocity
$\omega_{\mathrm{turn,srm}}$	Maximum steering servo turning rate of $\psi_{\mathrm{srm,a}}$

Table 12.6. Nomenclature table 6

Abbreviation	Description
AWD	All wheel drive
CAD	Computer aided design
EKF	Extended Kalman filter
IWD	Individual wheel drive
TCS	Traction control system
TDS	Torque distribution system
4WD	Four wheel drive

Table 12.7. Nomenclature table 7

Bibliography

[1] A. Alleyne. Improved vehicle performance using combined suspension and braking forces. *Vehicle System Dynamics*, 27:235–265, 1997.

[2] D. Crolla. *Automotive Engineering, Powertrain, Chassis System and Vehicle Body*, chapter 5.1 Transmission and driveline. Buttorworth-Heinemann, 2009.

[3] D. Crolla. *Automotive Engineering, Powertrain, Chassis System and Vehicle Body*, chapter 4.1.10.6 Traction control. Buttorworth-Heinemann, 2009.

[4] L. M. Giancarlo Genta. *The Automotive Chassis, System Design*, chapter 27.3.3 Traction control systems. Springer, 2009.

[5] L. M. Giancarlo Genta. *The Automotive Chassis, System Design*, chapter 27.4.3 VDS systems. Springer, 2009.

[6] HPC Gears Ltd. Hpc gears ltd. Catalogue.

[7] A. D. inc. *Low-Cost 2 g Dual-Axis Accelerometer with Duty Cycle Output*. Analog Devices inc., One Technology Way ,P.O. Box 9106, Norwood, MA 02062-9106, U.S.A., 2000.

[8] T. Instruments. *TMS320F28335, TMS320F28334, TMS320F28332, TMS320F28235, TMS320F28234, TMS320F28232 Digital Signal Controllers (DSCs)*. Texas Instruments, reviced march 2010 edition, June 2007.

[9] H. K. Khalil. *Nonlinear Systems*, chapter 13.2 Feedback Linearization. Prentice Hall, 2002.

[10] R. Rajamani. *Vehicle Dynamics and Control*, chapter 8.4.1 Independent four wheel drive systems. Springer, 2006.

[11] S. Srinivasan. *Automotive Mechanics*, chapter 4.3 The differential. Tata McGraw-Hill, 2003.

[12] www.mrslotcar.com. URL: http://www.mrslotcar.com/images/smartech_titan_01.jpg.

[13] www.teamnovak.com. www.teamnovak.com. Homepage.

[14] www.teamorion.com. www.teamorion.com. Homepage.

[15] D. Y. Yoichi Hori. Traction control for ev based on maximum transmissible torque estimation. *Springer Science*, Jan:9, Jan 2010.

List of Figures

Appendix

APPENDIX A

Journal of Measurements

A.1 Suspension

In order to model the vehicle in chapter 6, the suspension is modeled as a separate block *SUSPENSION* in section 6.4. The model provides information on the vertical force $F_{\mathrm{N,w},k}$ on each wheel. This is dependent on the parameters of the suspension spring and damper parameters, along with those parameters of the tire. Therefore three parameters are investigated for the front and rear suspension respectively. These are the constant force offset, spring coefficient and viscous damping factor. The constant force offset $F_{0,\mathrm{s}}$ is the force that would be measured from the suspension at a height of zero at zero vertical velocity. The spring coefficient K_s determines the spring force when the spring and tire are compressed or expanded. The force from the damper is determined by the viscous damping factor b_s, dependent on the velocity of the compression and expansion of suspension damper.

First the spring coefficient K_s is found for one front and rear suspension springs. The vehicle is fixed, and a scales is placed under the wheel of the spring being analyzed. The suspension is then compressed, by raising the scales under the wheel. Thereby the spring force is being measured as a weight on the scales and compression displacement of the wheel. An illustration of this is given in figure A.1.

It is then expected that the weight measures will be proportional to the suspension compression displacement, such that the spring coefficient K_s is found constant. Thus linear regressions are used on the measures for each spring, deriving the two spring coefficients. Notice that the spring coefficient are the combined of the suspension and tire. The front spring results of the measure and regressions are given in figure A.2, and the ones from the rear spring in figure A.3. Both the spring and damper has a limited range of compression and expansion. Therefore the displacement of the wheel is chosen within a range, so that the spring and damper are not fully compressed or expanded.

A.1.1 Experimental setup

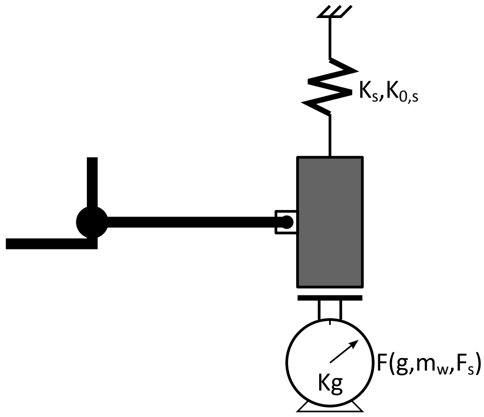

Figure A.1. Illustration of principal of measuring the spring constants.

A.1.2 Equipment

Equipment used for the experiment.

Item	Manufacturer	Model	Registration number
Scales	Kern	FCB12K1	AAU86759

Table A.1. Items used in measurement.

A.1.3 Results

Results from experiment.

Item	Mass [kg]
Vehicle	15,2
Wheel	0,729
Front wheel mounted on suspension	0,950
Rear wheel mounted on suspension	0,820

Table A.2. Part masses.

Chassis height [m]	Measured weight [Kg]
0,087	2,070
0,087	2,070
0,087	2,070
0,082	2,580
0,082	2,580
0,047	4,550
0,047	4,550
0,042	4,750

Table A.3. Front suspension measurements.

Chassis height [m]	Measured weight [Kg]
0,085	3,950
0,085	3,950
0.080	4,080
0.080	4,080
0,047	5,360
0,047	5,360
0,042	5,570
0,042	5,570

Table A.4. Rear suspension measurements.

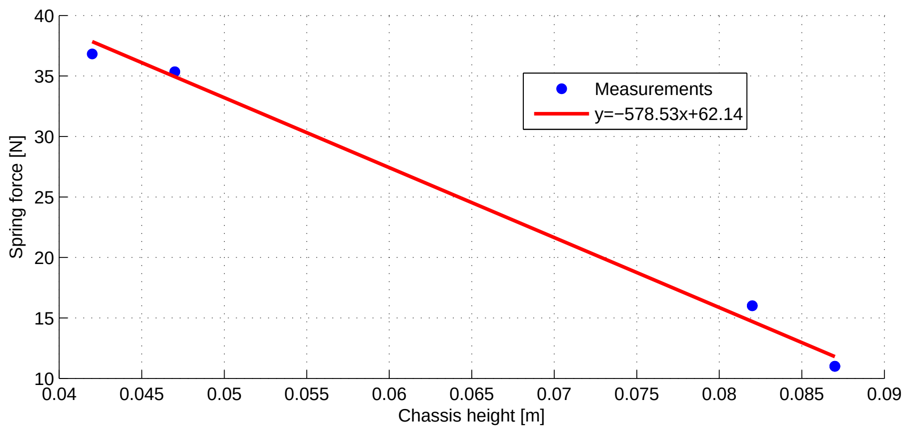

Figure A.2. Regression on front spring measurements.

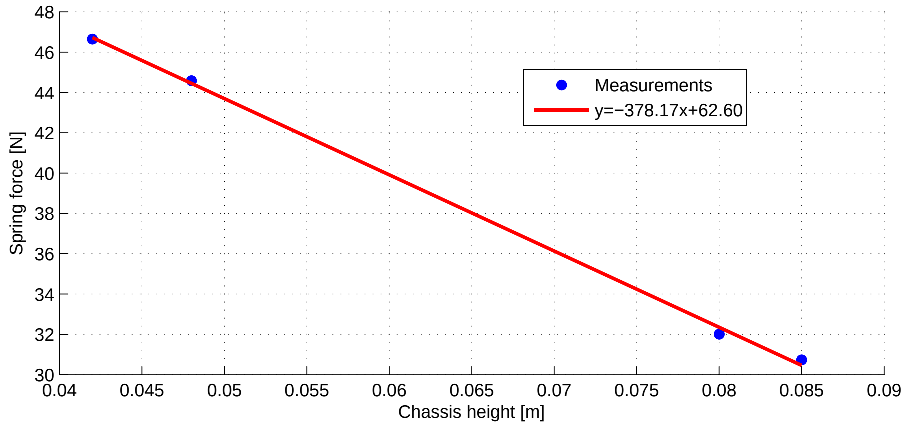

Figure A.3. Regression on rear spring measurements.

A.1.4 Analysis

As indicated in the result, the measurements and regressions are close, and thus the derived spring coefficient are found approved for use in the vehicle model. Notice that there is a difference between the front and rear suspension. Sources of error when determining these, are those of the precision of the scale and when measuring the displacement of the wheel, when the suspension is compressed. Thereby at each displacement, two results are measured.

With the spring coefficient found, the viscous damping factor b_s of the one front and rear suspension damper are to be found. It is expected that the damper force is proportional to the velocity of the compression and expansion of the suspension. The vehicle is fixed and the springs removed. A video recording is made, where the wheel is released from a raised position. An illustration of this setup is shown in figure A.4.

With the springs removed and gravitational force, this will result in expansion of the damper. The position of the wheel is then pointed out and analyzed in each frame of the video recording. To determine the scale of the video image, two outer position of the wheel rim is pointed out in the first frame. The first frame is shown in figure A.5. The velocity of the wheel, and thereby also the expansion of the damper, is then found from the difference in vertical position of the wheel between each frame and the video recording frame rate of 15 fps. Some of the wheel positions are illustrated in figure A.10.

As for the spring coefficients, both the front and rear viscous damping factors b_s are using regressions on the measurements of the positions. As for the springs, one viscous damping factor is found for the front dampers and one for the rear dampers. The front damper results of these are shown in figure A.11, and the ones of the rear damper is shown in figure A.12.

A.1.5 Experimental setup

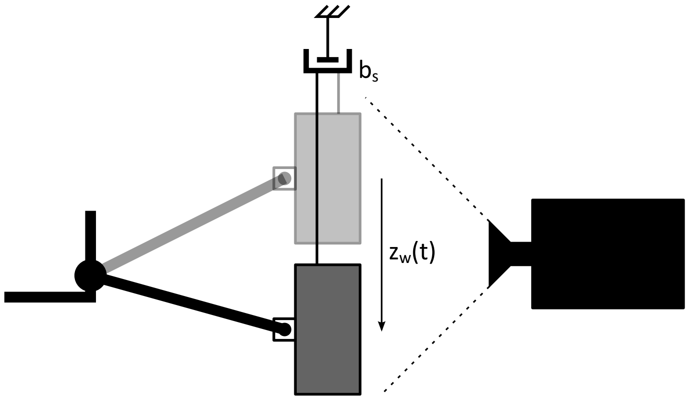

Figure A.4. Illustration of principal of measuring the viscous damping factor.

Figure A.5. Picture size calibration.

A.1.6 Equipment

Equipment used for the experiment.

Item	Manufacturer	Model	Registration number
Video camera	Canon	Powershot G9	6731409811

Table A.5. Items used in measurement.

A.1.7 Results

Results from experiment.

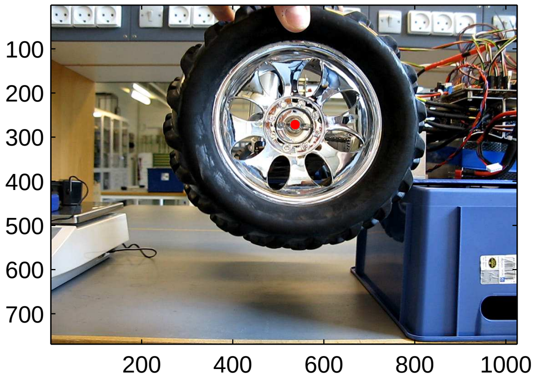

Figure A.6. Frame 1

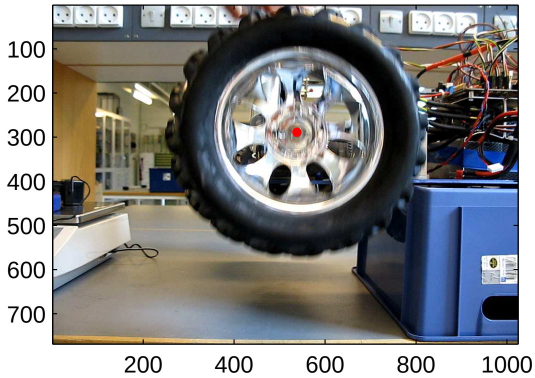

Figure A.7. Frame 2

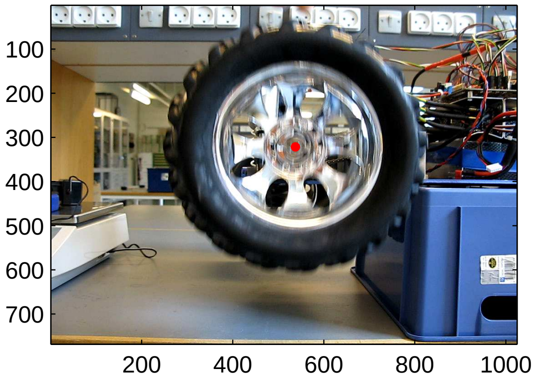

Figure A.8. Frame 3

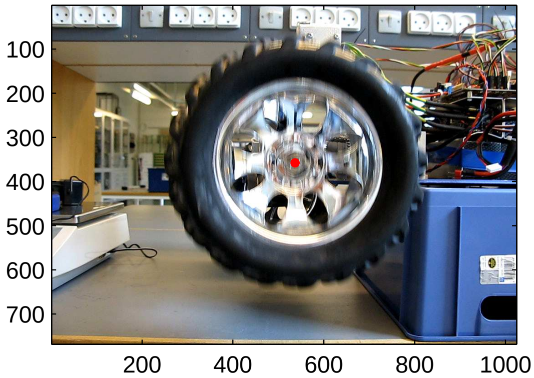

Figure A.9. Frame 4

Figure A.10. Illustration of wheel position in frames of a video recording.

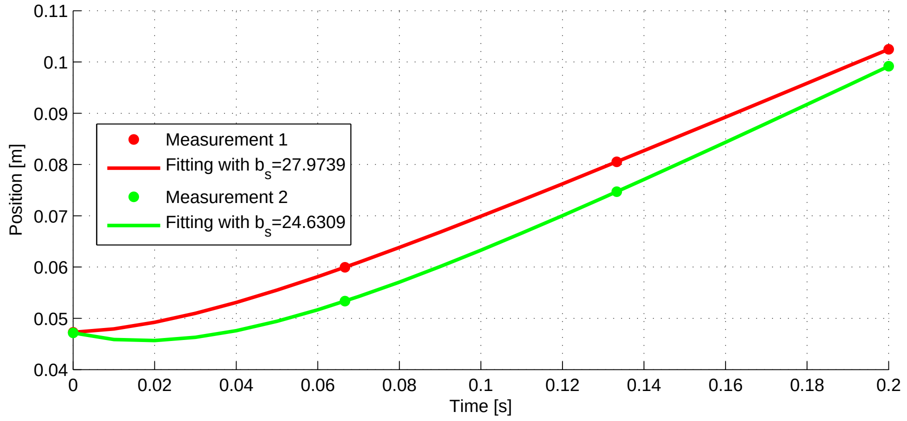

Figure A.11. Position function fitting to front damper measurements.

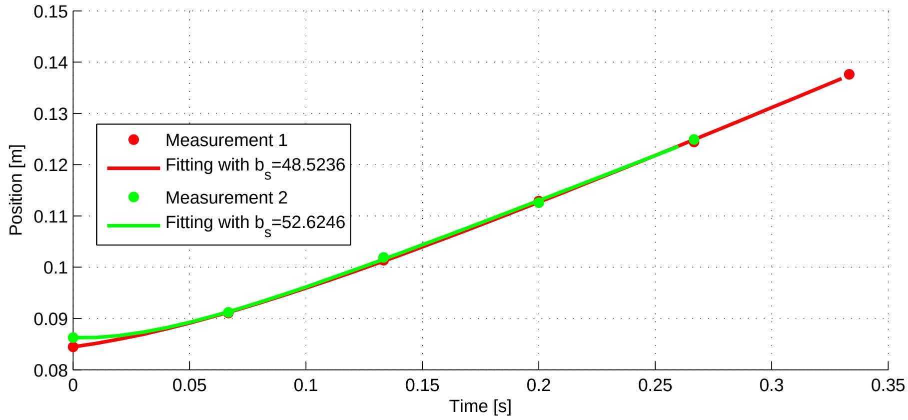

Figure A.12. Position function fitting to rear damper measurements.

A.1.8 Analysis

The regression results of the viscous damping factors are not linear as expected. Though this is due to that it is possible to use video frames in the regressions, where the damper is fully expanded or the wheel has not been released. To remove these regressions errors, the video frames used for analysis could be chosen such that the are only from after the wheel release and before fully expansion of the damper. This is illustrated in figure A.13.

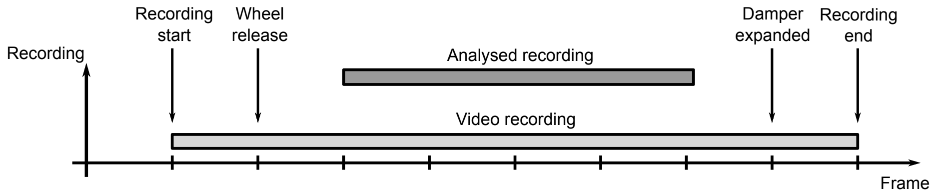

Figure A.13. Frame to be used for analysis of damping factors.

The resolution, frame rate and other parameters of the recording are also sources of error. The frame rate of 15 fps limits the regression resolution, since there is more than 60 ms between each frame. Also the image resolution limits the precision, when pointing out the position of the wheels. Though even with these, the derived viscous damping factors b_s of both the front and rear suspension dampers are found approved for use in the vehicle model.

A.2 Center of mass

The chassis mass position is to be found for the model of the vehicle suspension described in section 6.4. The wheel displacements $\overline{d}_x$ and $\overline{d}_y$ from the chassis mass center, will influence how the vehicle weight is distributed, thereby also the vertical force on each wheel and traction of this. Only $\overline{d}_y$ and the vertical distance of the chassis mass center over the chassis $\overline{d}_{z,c}$ are found, since the chassis mass center is considered in the middle of the vehicle in the x direction.

$\overline{d}_y$ and $\overline{d}_{z,c}$ are found by analyzing two images, where the vehicle is mounted from a camera stand with strings to the wheel shafts as shown in figure A.14. The strings are fitted, so that the vehicle is able to rotate in both the ϕ and θ direction. Above the vehicle a shaft is suspended from the camera stand, which will point directly towards the chassis mass position. The two images are taken with two different rotations of the vehicle and thus the point between the images where the suspended shaft will intersect, will be the chassis mass position.

To find the intersection of the suspended shaft between the two images, several recognition marks of some motor housing corners and there position are located in both images. The position and distance between the recognition marks are measured on the vehicle, and it is then possible to derive the the perspective and scale between images and vehicle.

From the image shown in figure A.15, the image perspective and scale is found using the motor housing recognition marks (red lines and dots). From this, the middle of vehicle is found (green lines), and then the intersection points between these and the line of the suspended shaft (blue line). These points are then applied in figure A.16. Again the intersection points between the line of the suspended shaft and lines between the motor housing corners are found. With the intersection points of the suspended shaft transfered from the first image, the chassis mass position is found by the intersection between the lines for the suspended shaft (yellow dot).

Since the vehicle front is applied with the steering system, it is expected that the weight from this will make the chassis mass position be closer to the front than the rear.

A.2.1 Experimental setup

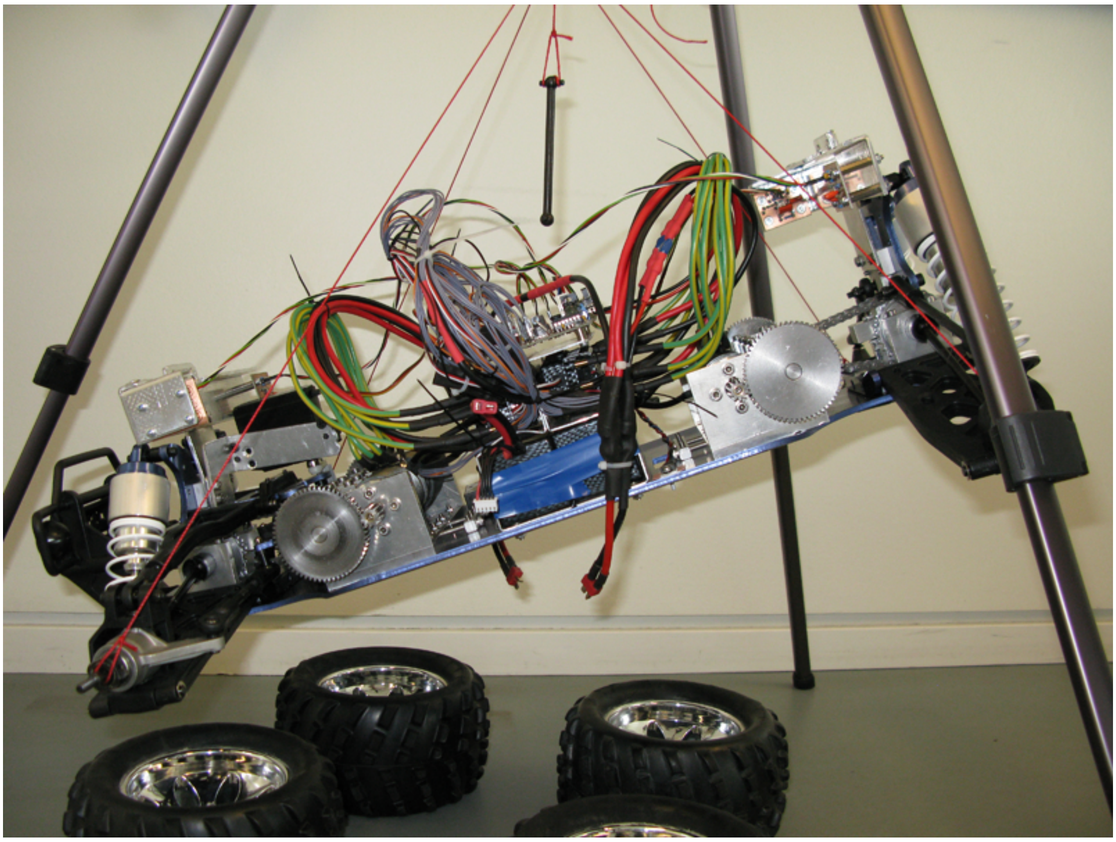

Figure A.14. Illustration of camera stand mounting when measuring chassis mass position

A.2.2 Equipment

Equipment used for the experiment.

Item	Manufacturer	Model	Registration number
Video camera	Canon	Powershot G9	6731409811

Table A.6. Items used in measurement

A.2.3 Results

Results from experiment.

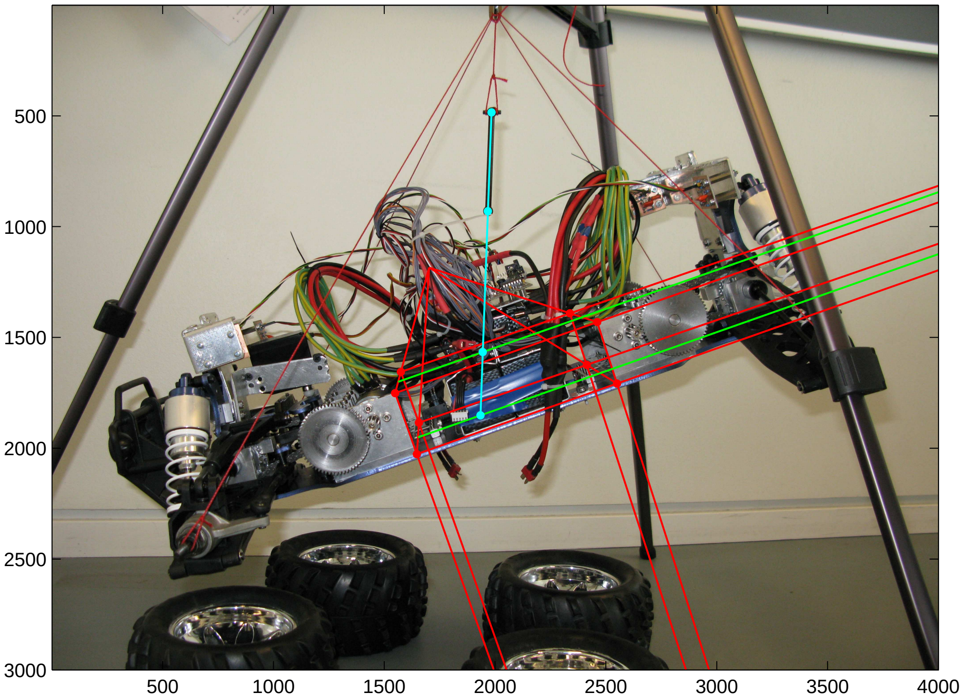

Figure A.15. Picture one in determining the center of mass of the chassis

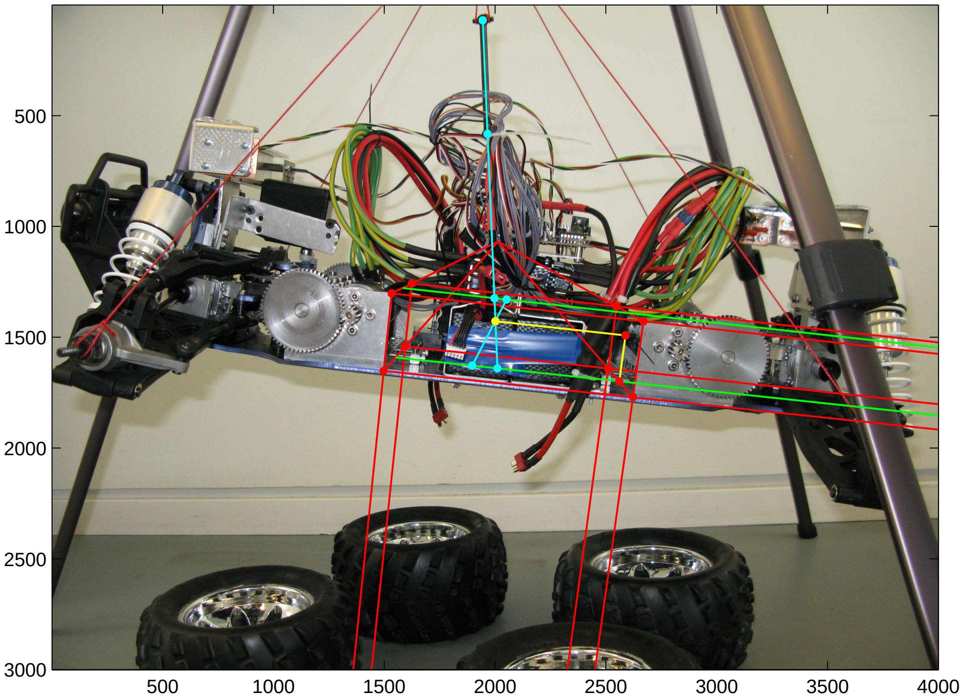

Figure A.16. Picture two in determining the center of mass of the chassis

A.2.4 Analysis

From the results the displacement $\overline{d}_\mathrm{y}$ and $\overline{d}_\mathrm{z,c}$, is determined from the distances (yellow lines) between chassis mass center and recognition marks of the motor housings, and the measured distances the recognition marks and wheels. $\overline{d}_\mathrm{y}$ for the front is found to be 100 mm, while 120 mm for the rear. As expected the is chassis mass center to the front wheels. Along with $\overline{d}_\mathrm{z,c}$ found to be 8 mm, the chassis mass center also above the chassis as expected, when this is where the drive trains and other are mounted.

Sources of error, when determining the chassis mass position are those from the camera resolution and selecting the same recognition marks in both images. If the motor housing corners are not pointed out at the same point, the image perspective and scale will be influenced, along the position of the transfered intersection points of the suspended shaft from the first image. Though the position found is approved without considered these errors, since the vehicle mass position is also affected by the wheel and suspension positions, which has not been included within the vehicle model.

A.3 Drive Train Parameter Estimation

In chapter 6 a model of the drive train, called the *DRIVETRAIN*, has been developed. The model is based on the parameters of the drive train on the vehicle, and the viscous friction is to be found. This will also indicate if the coulomb friction negligible, as assumed. The parameters are assumed to be the same for all drive trains, hence only one drive train will be investigated.

The parameters are found be applying several voltage signal to the vehicle, while measuring the wheel velocities from the motor drivers. These measures are transmitted over a wireless communication from the vehicle to a computer and stored. The parameters b_m and C_m are the found by using parameter fitting on the vehicle deacceleration. Parameter fitting of a differential equation is used both to describing the deacceleration with only the viscous friction b_m, and hereafter including the coulomb friction C_m. This will reveal if the coulomb friction is negligible or not.

The parameters to be determined is:

- Viscous friction of the motor b_m.
- Coulomb friction of the motor C_m.

A.3.1 Results

Results from experiment.

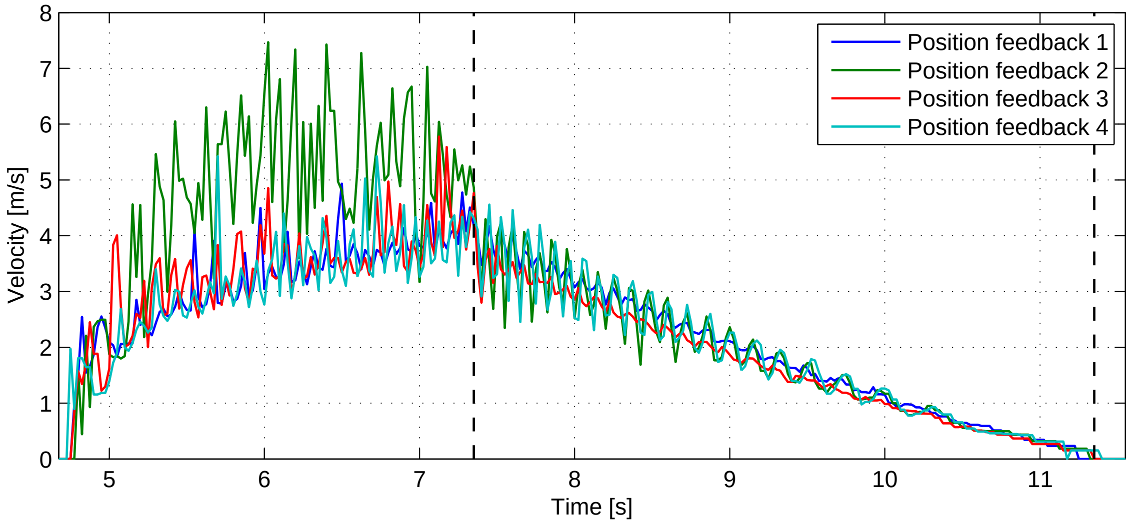

Figure A.17. Wheel velocity given step on motor driver input from $D_{\mathrm{md}} = 1541\ \mu S$.

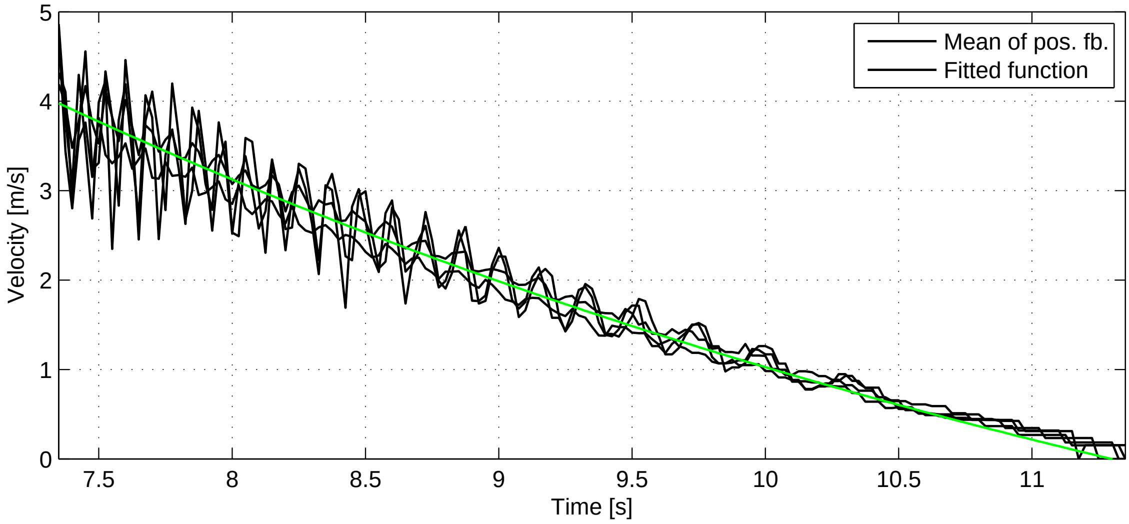

Figure A.18. Wheel velocity from 1 volt on drive trains to free running.

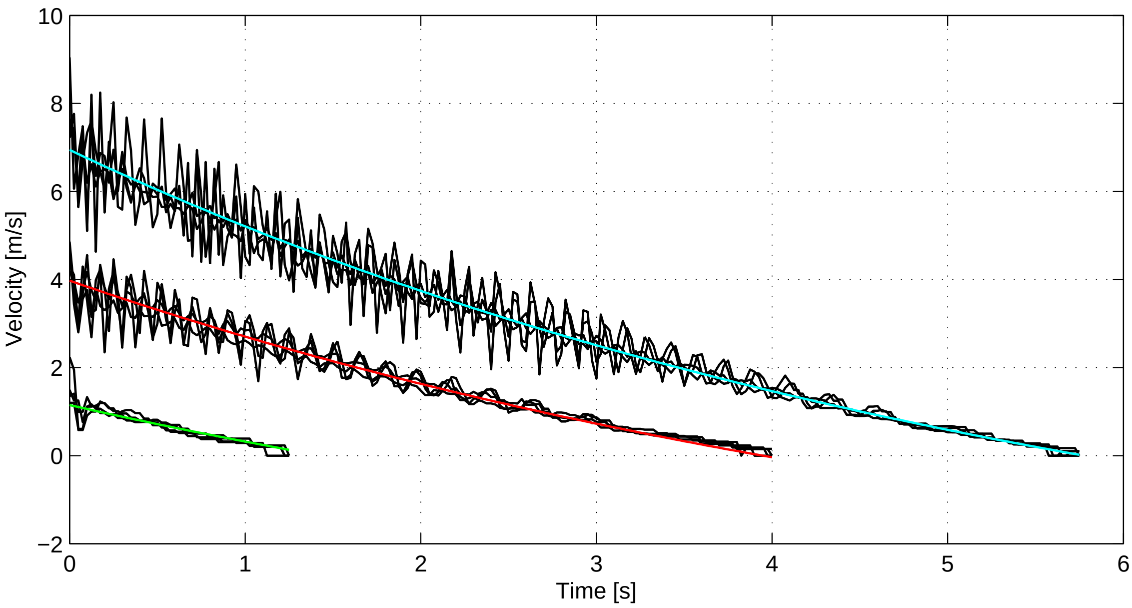

Figure A.19. Wheel velocity from 1, 2 and 4 volts respectively on drive trains to free running.

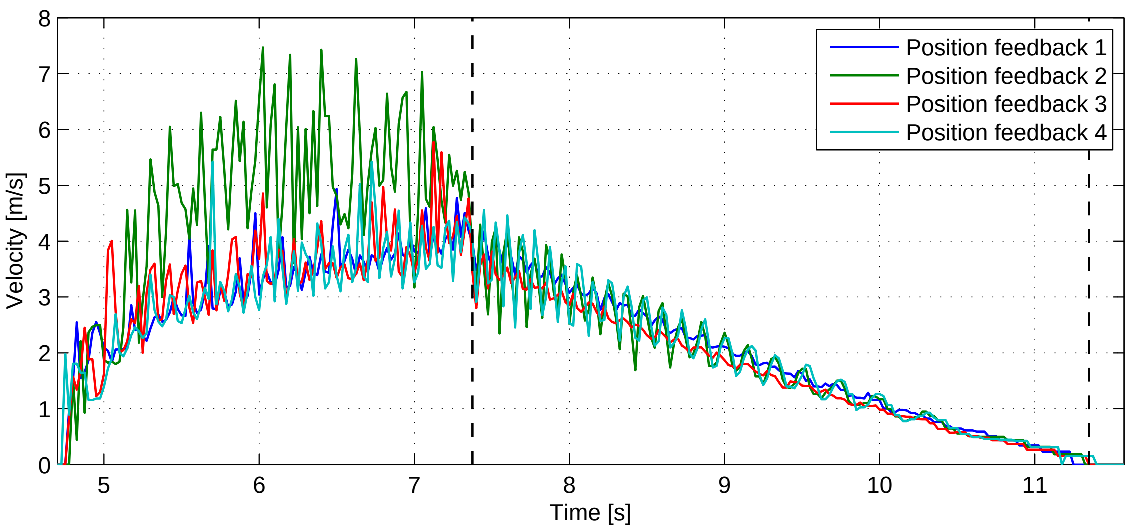

Figure A.20. Wheel velocity from 1 volt on drive trains to free running.

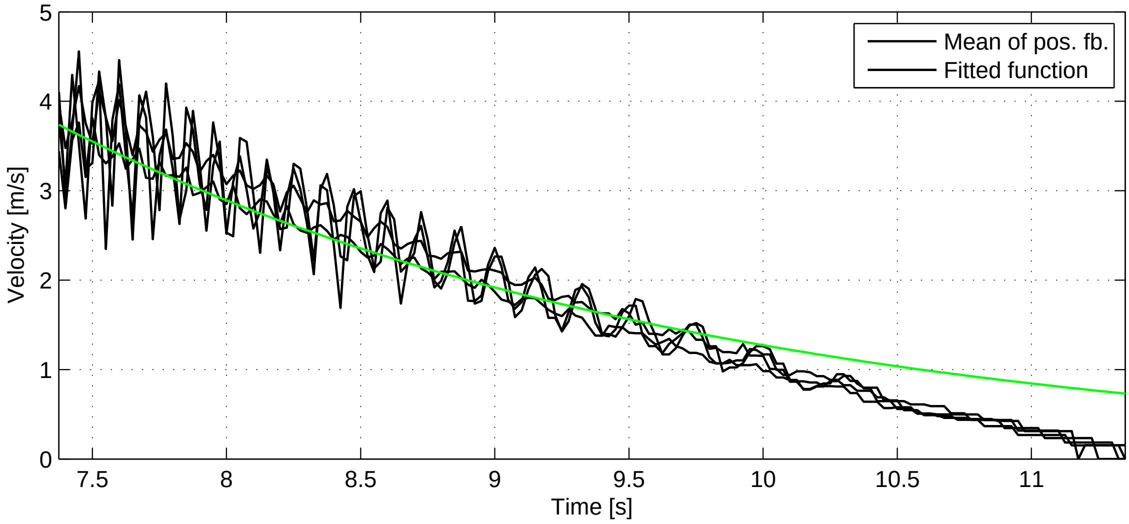

Figure A.21. Wheel velocity from 1 volt on drive trains to free running.

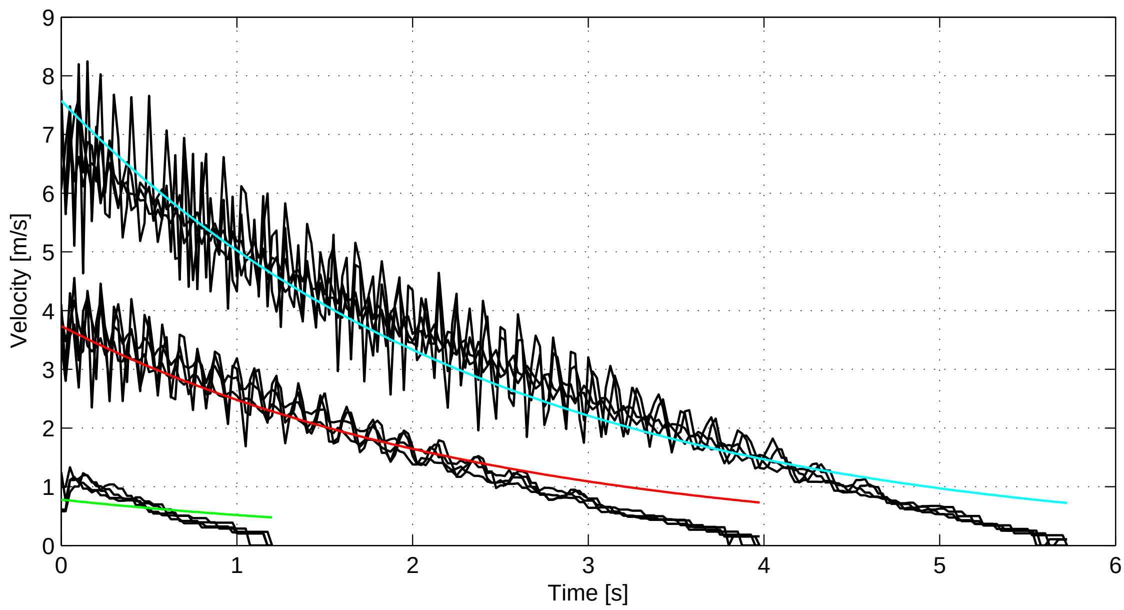

Figure A.22. Wheel velocity from 1, 2 and 4 volts respectively on drive trains to free running.

A.3.2 Analysis

The results indicate that the coulomb friction is not as negligible as assumed. The difference with including C_m is seen in figure A.17 and figure A.18. When C_m are removed from the differential equation, the parameter estimation performance is decreased as shown in figure A.20 and figure A.21. Including the coulomb friction in the model, will induce this to be hybrid.

A.4 Sensor Noise Standard Deviation

The following measures are used to determine the sensor noise standard deviation.

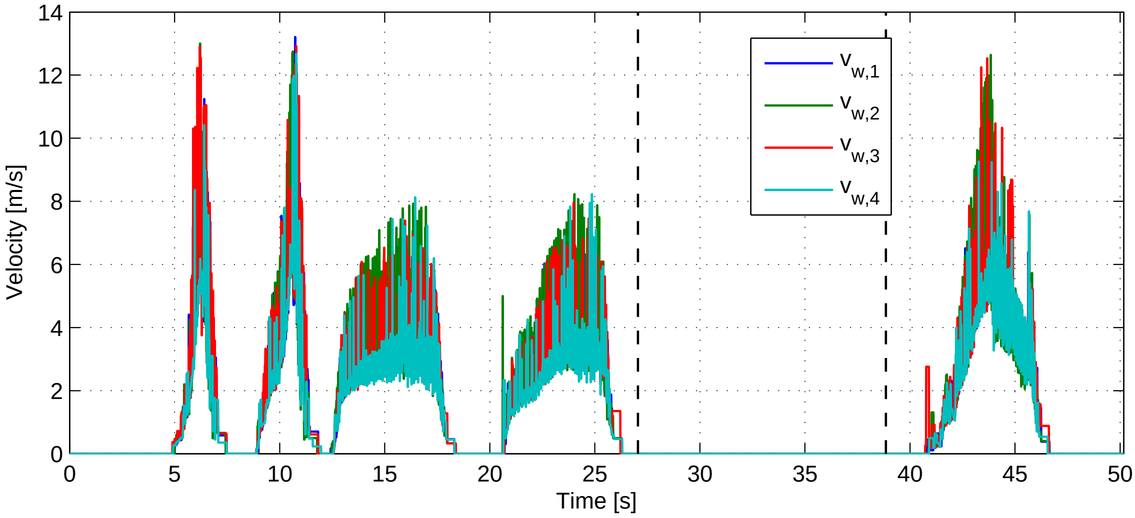

Figure A.23. Vehicle velocity used to choose the time series for accelerometer noise investigation given zero vehicle velocity.

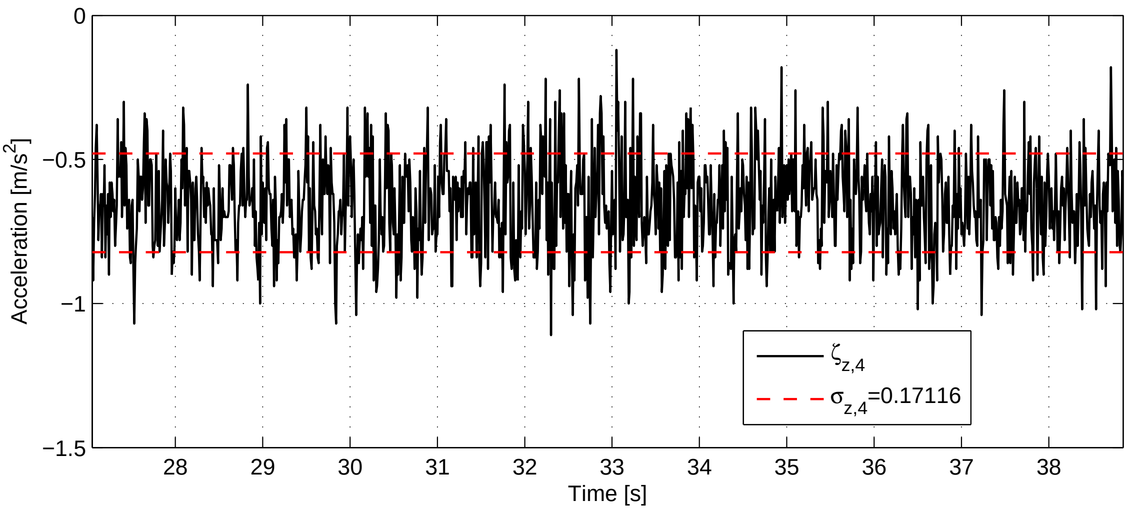

Figure A.24. Accelerometer noise standard deviation given zero vehicle velocity.

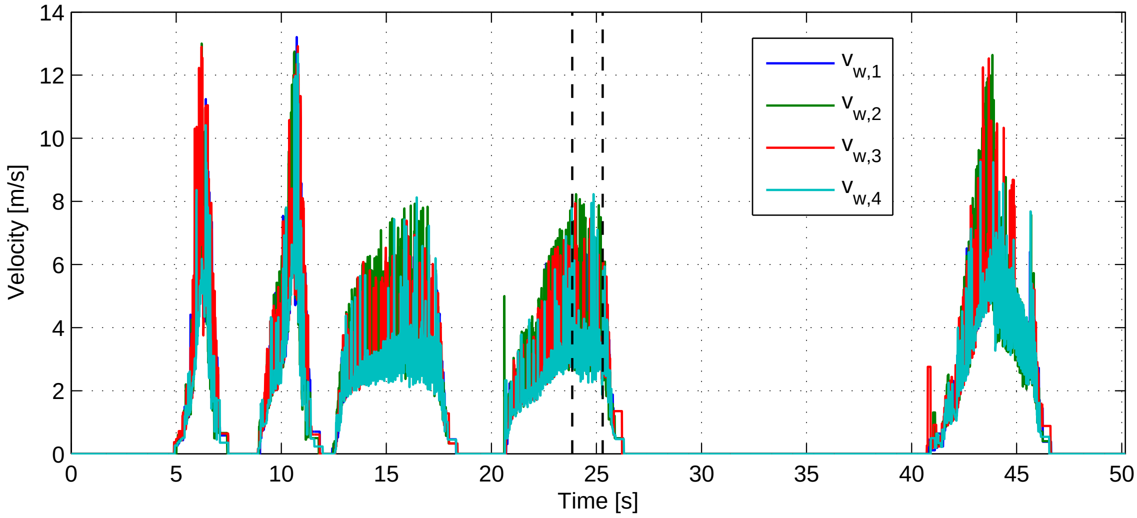

Figure A.25. Vehicle velocity data used to choose the time series for accelerometer noise investigation given vehicle drive noise.

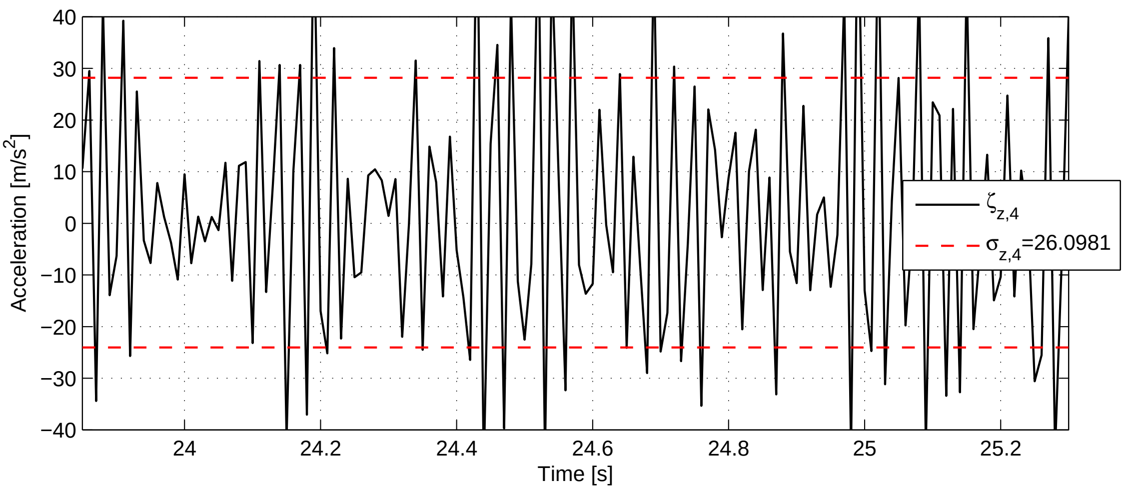

Figure A.26. Accelerometer noise standard deviation given vehicle drive noise.

APPENDIX B

Model Validation Plots

In chapter 10 the model is evaluated by comparing sensor outputs from the vehicle and sensor outputs from the *VEHICLE MODEL*. The sensor data from the vehicle is obtained by applying a user input via the remote control. The input signal is seen in figure B.1 to B.4. The sensor outputs are shown in figure B.5 to B.18. In this investigation the sensor noise in the *VEHICLE MODEL* is disabled, since only the actual movements are relevant.

Motor Input Voltage

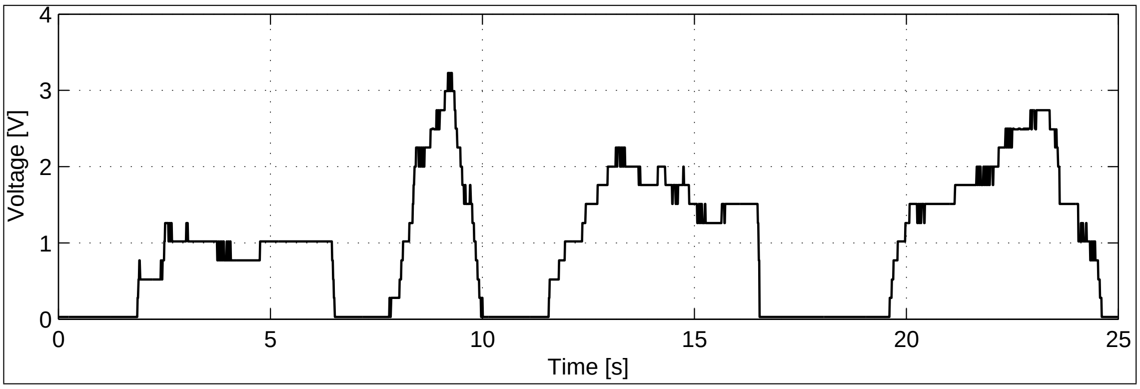

Figure B.1. Motor input voltage signal #1.

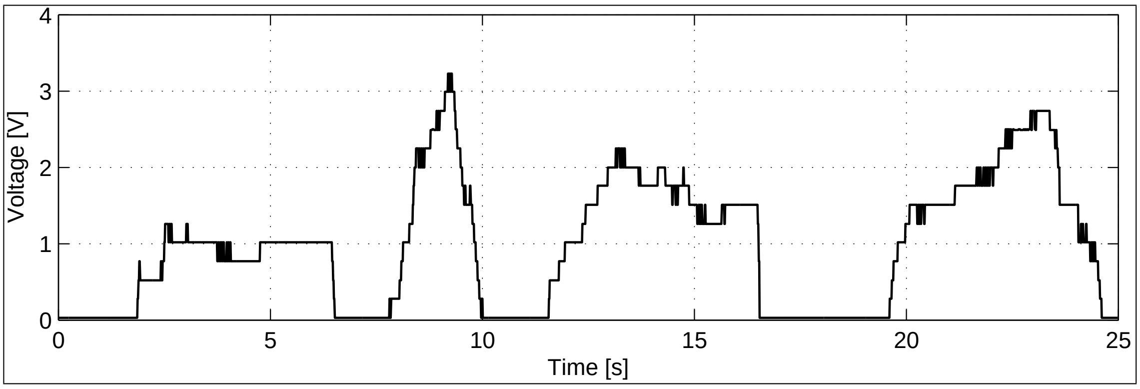

Figure B.2. Motor input voltage signal #2.

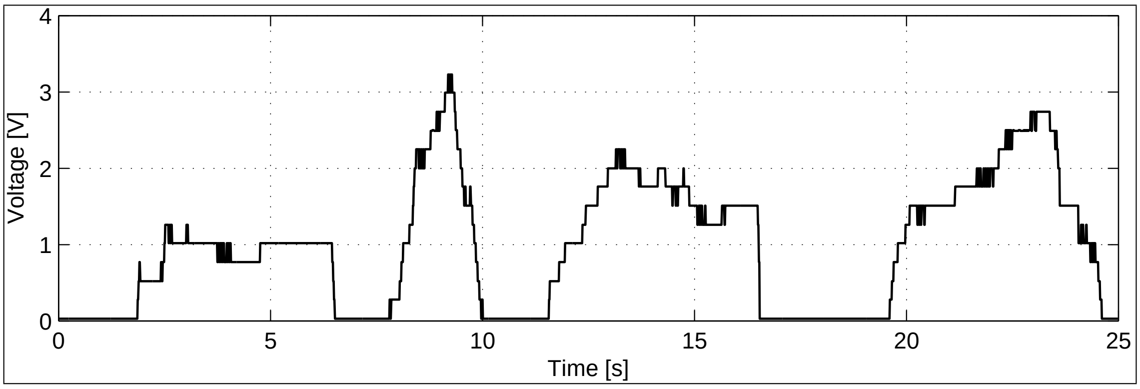

Figure B.3. Motor input voltage signal #3.

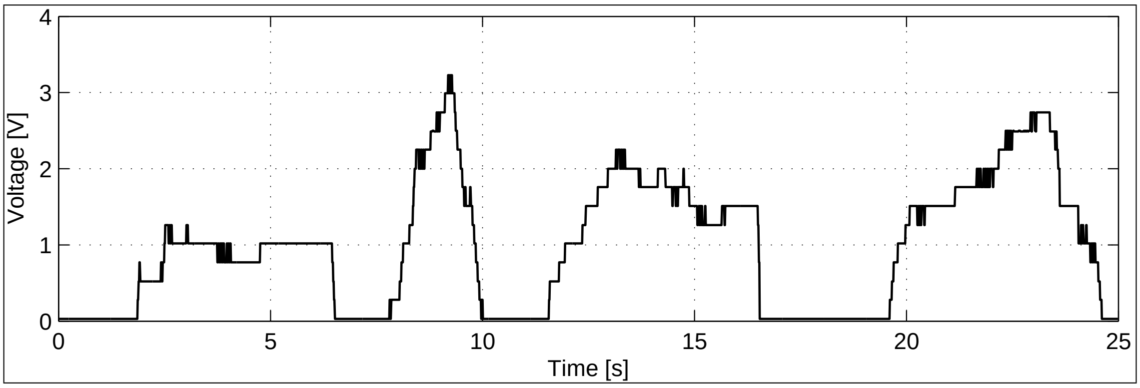

Figure B.4. Motor input voltage signal #4.

Motor Velocity Measurement

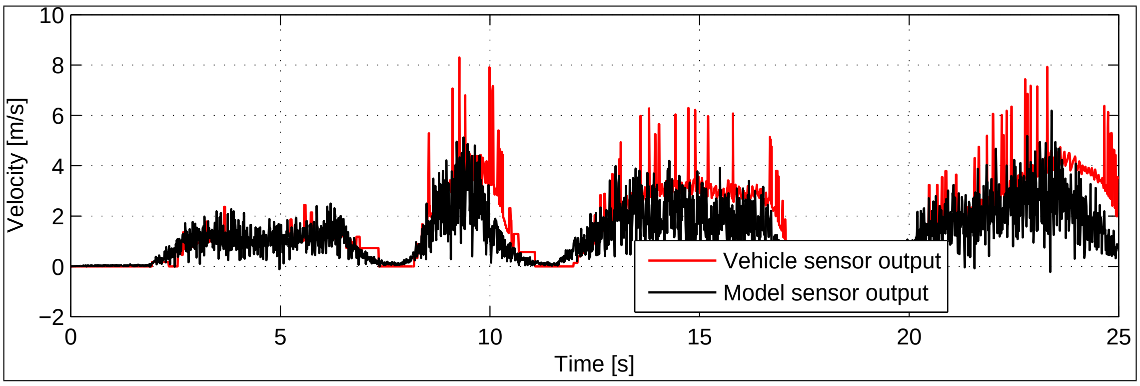

Figure B.5. Motor 1 sensor output signal.

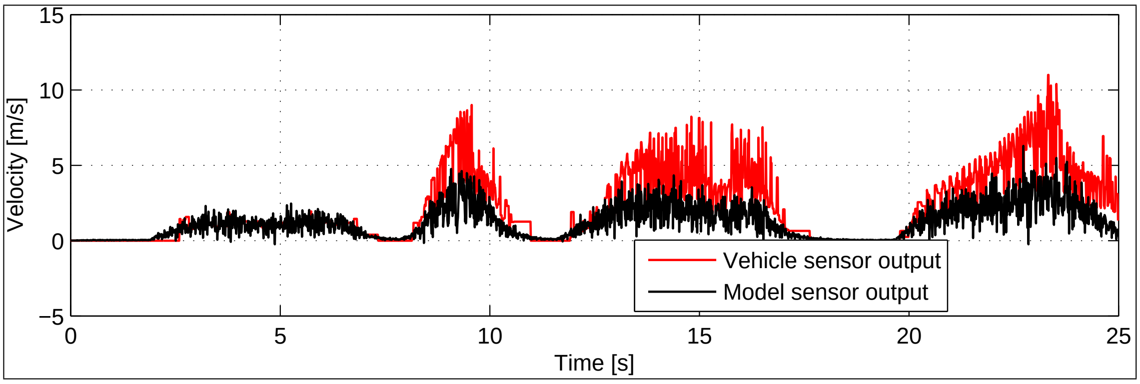

Figure B.6. Motor 2 sensor output signal.

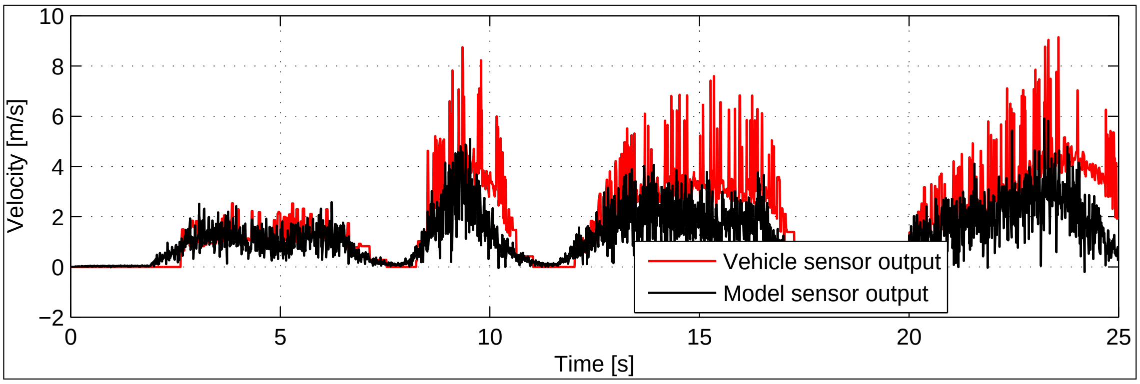

Figure B.7. Motor 3 sensor output signal.

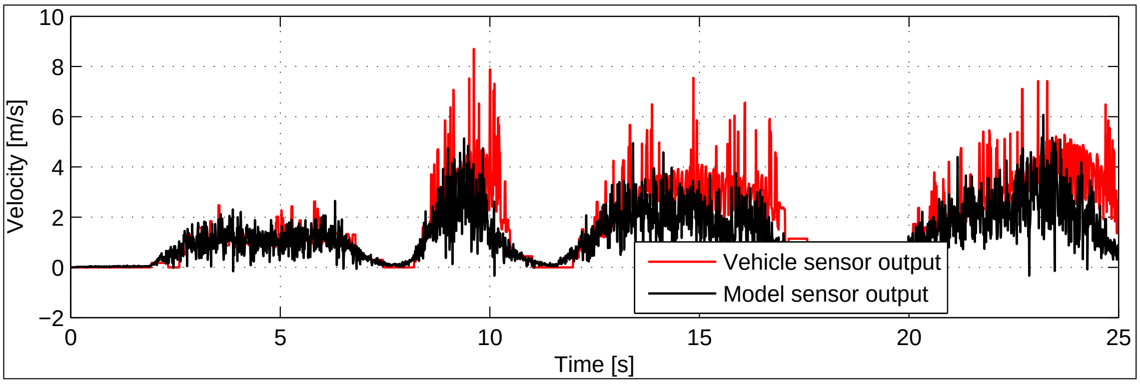

Figure B.8. Motor 4 sensor output signal.

Vertical Acceleration

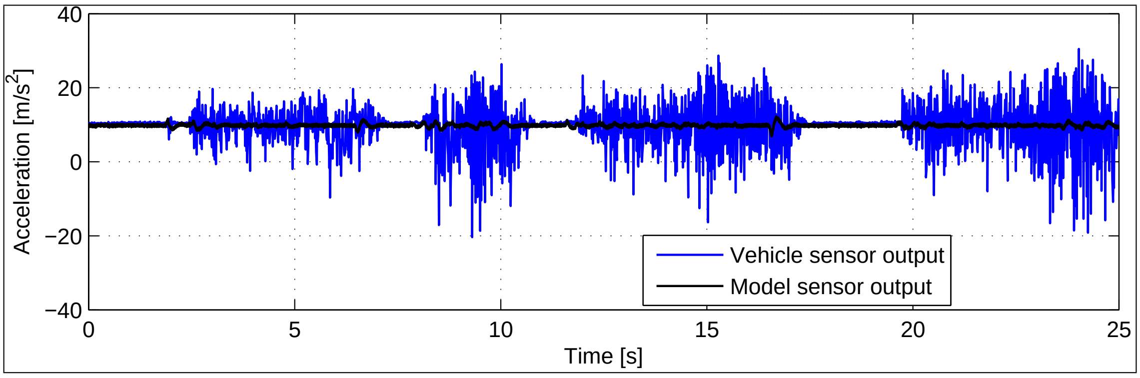

Figure B.9. Vertical acceleration sensor #1.

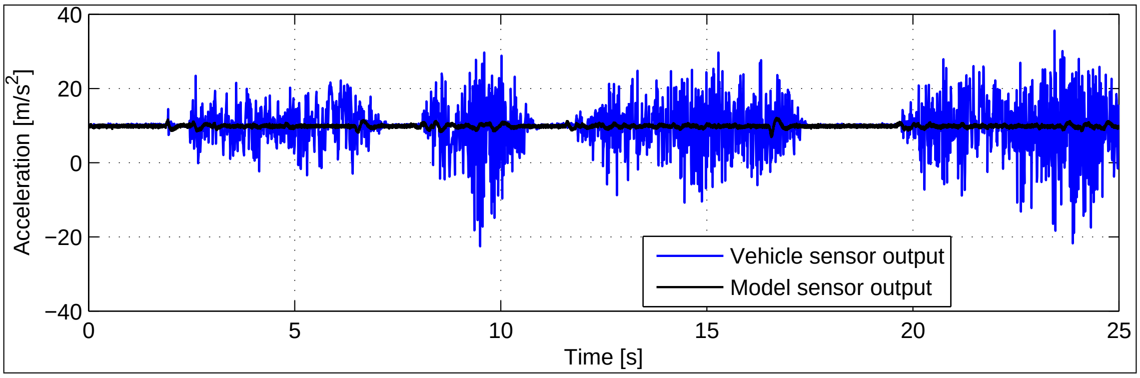

Figure B.10. Vertical acceleration sensor #2.

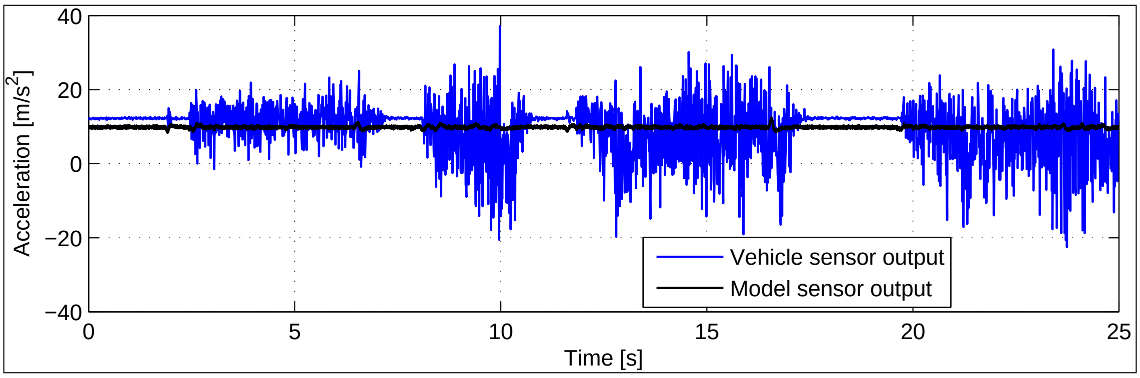

Figure B.11. Vertical acceleration sensor #3.

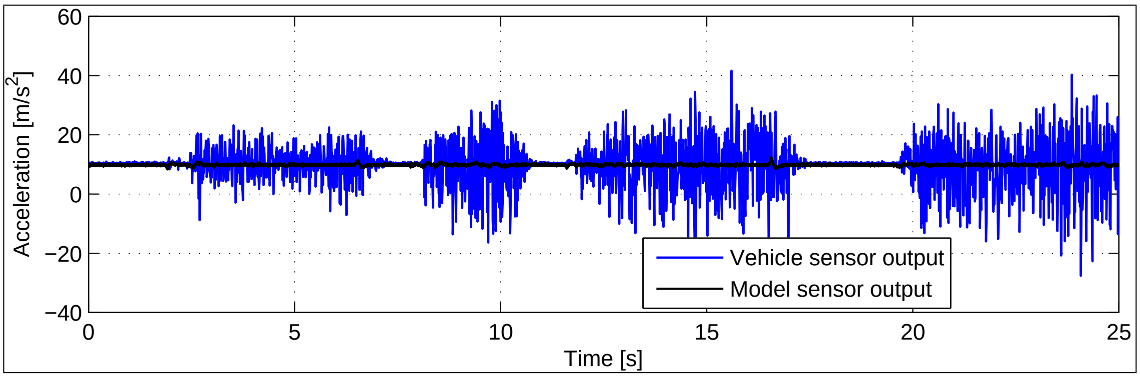

Figure B.12. Vertical acceleration sensor #4.

Vertical Acceleration Filtered

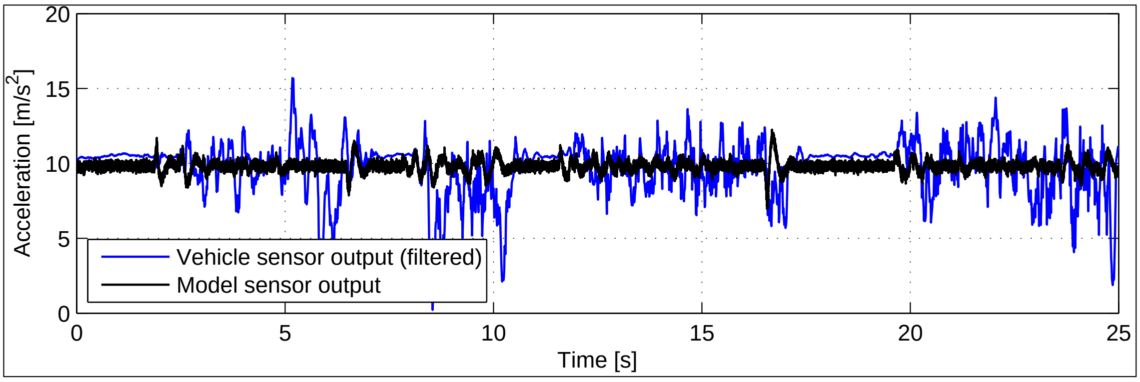

Figure B.13. Vertical acceleration sensor #1 filtered.

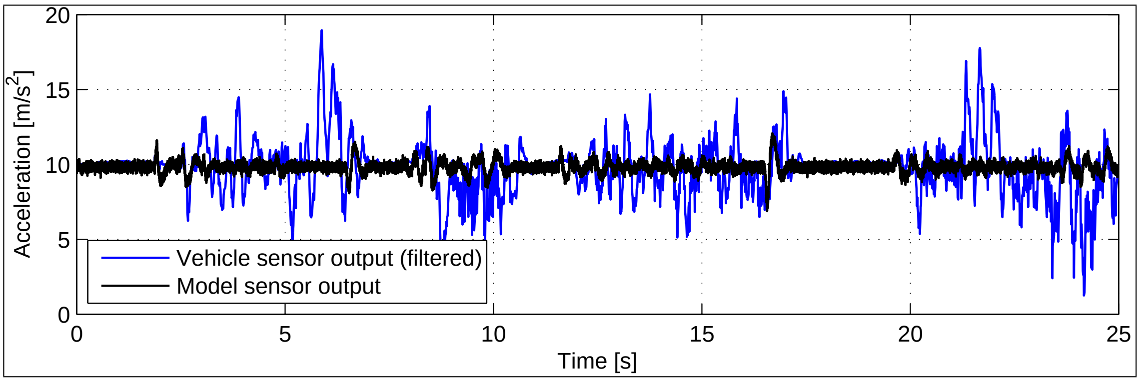

Figure B.14. Vertical acceleration sensor #2 filtered.

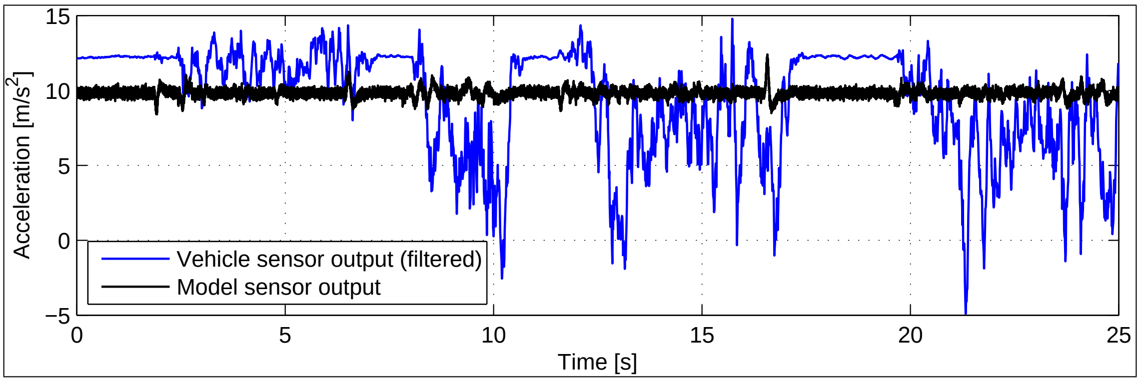

Figure B.15. Vertical acceleration sensor #3 filtered.

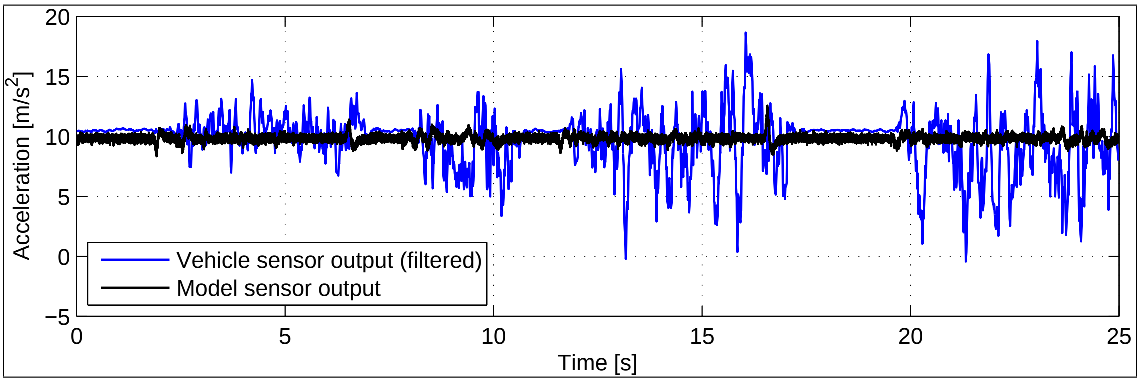

Figure B.16. Vertical acceleration sensor #4 filtered.

Horizontal Acceleration

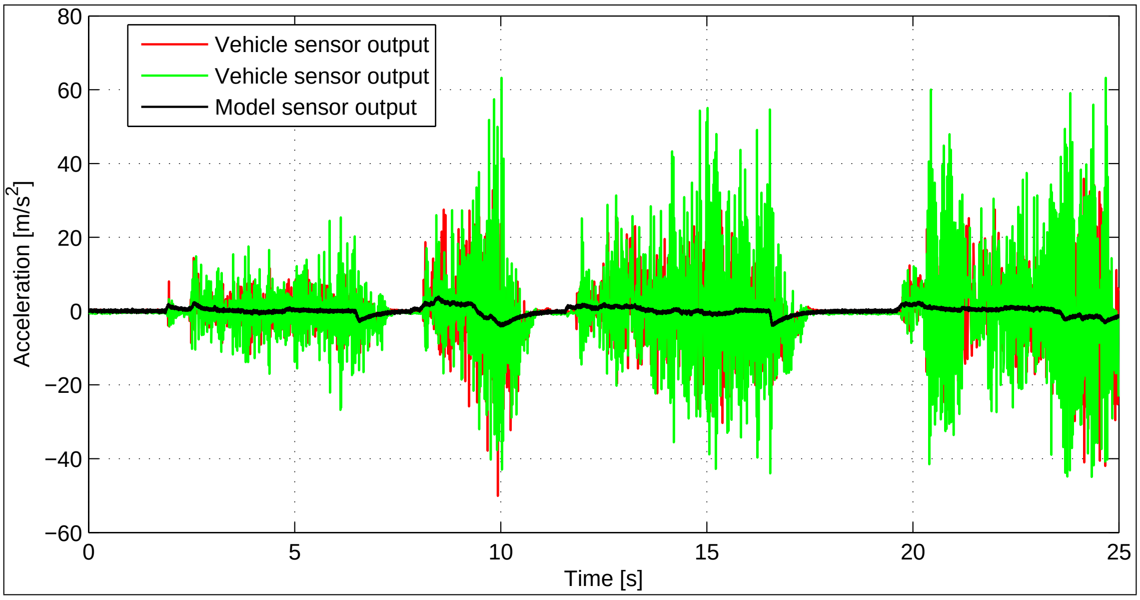

Figure B.17. Horizontal acceleration sensors.

Horizontal Acceleration Filtered

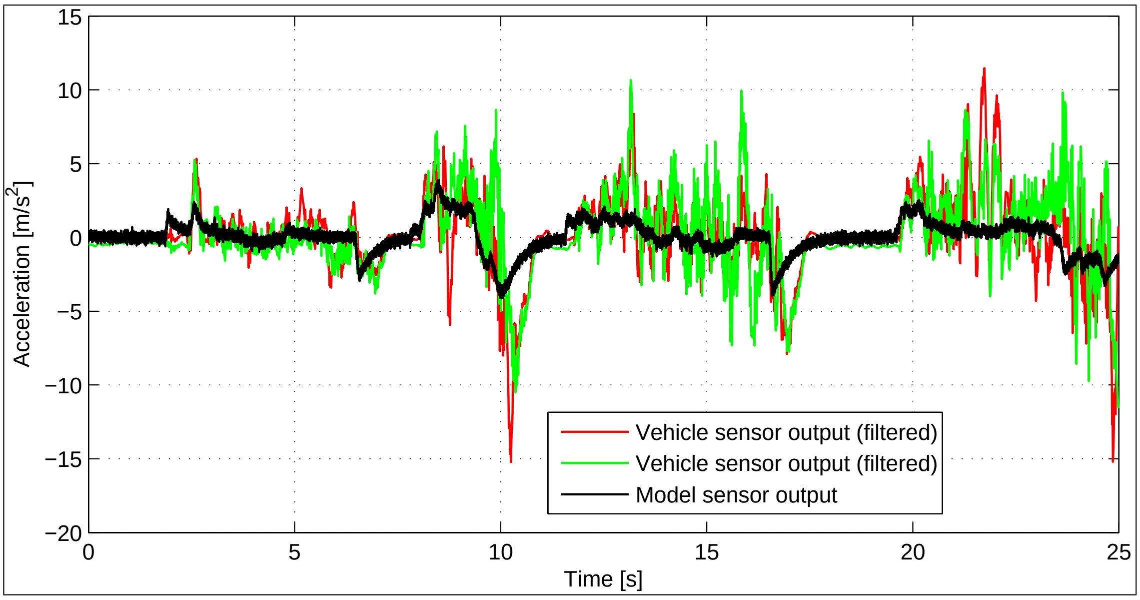

Figure B.18. Horizontal acceleration sensors filtered.

APPENDIX C

KALMAN FILTER VALIDATION PLOTS

In chapter 10 the Kalman filter, developed in chapter 7, is evaluated based on two sets of data. The data shown in figure C.5 to C.27 shows the states of the *VEHICLE MODEL* and the *VEHICLE KALMAN FILTER* given the input signal shown in figure C.1 to C.4. During this simulation, the coefficients in μ [1] have been altered.

Figure C.28 to C.50 shows the *VEHICLE KALMAN FILTER* state estimates when the vehicle sensor outputs from chapter B are given as inputs.

C.1 Model following

Motor Input Voltage

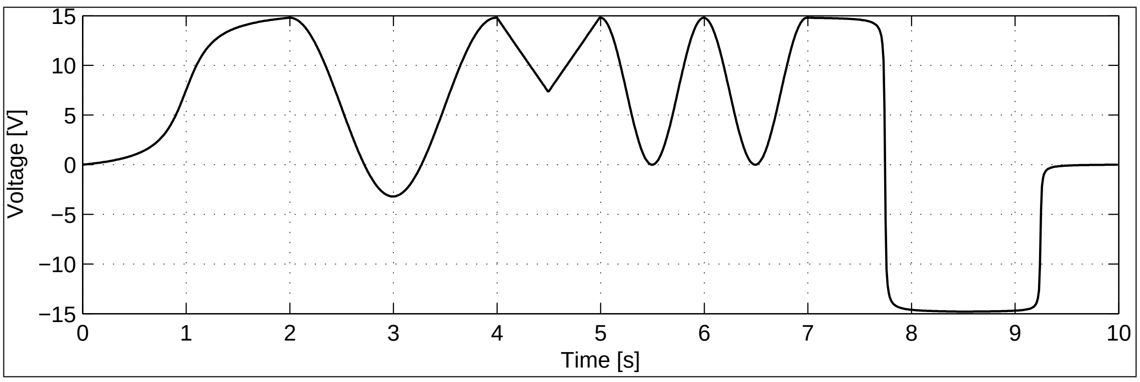

Figure C.1. Motor input voltage #1.

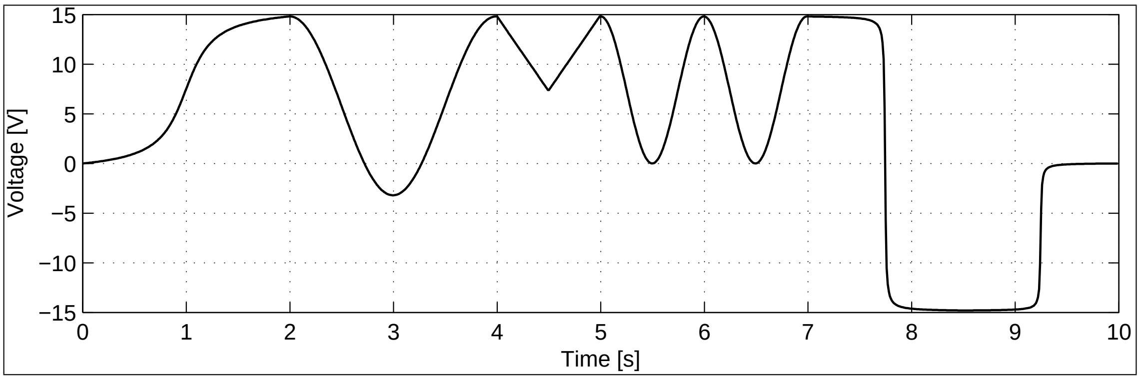

Figure C.2. Motor input voltage #2.

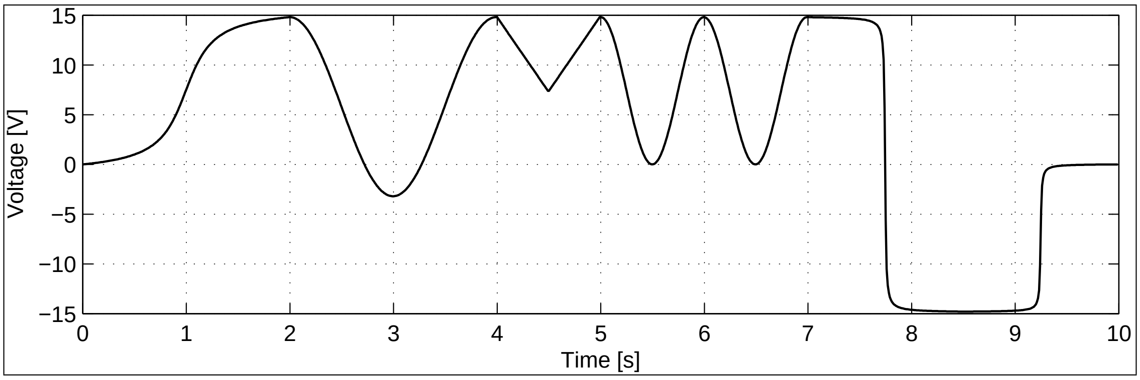

Figure C.3. Motor input voltage #3.

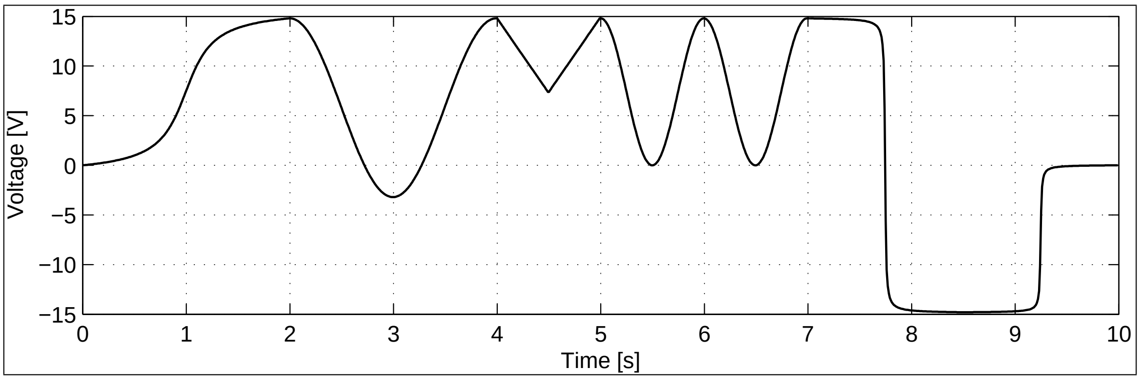

Figure C.4. Motor input voltage #4.

Motor Current

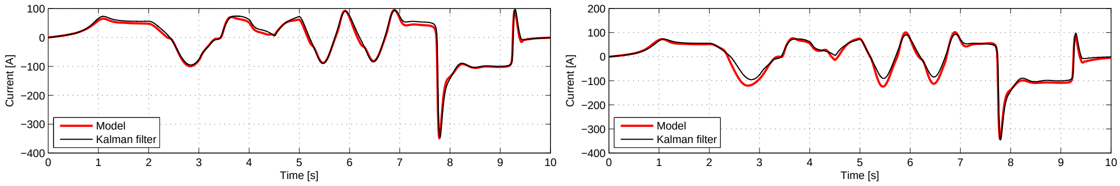

(a) With sensor update. (b) With sensor update disabled.

Figure C.5. Current in Motor #1.

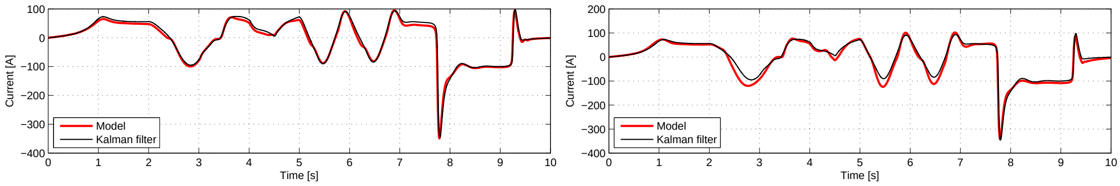

(a) With sensor update. (b) With sensor update disabled.

Figure C.6. Current in Motor #2.

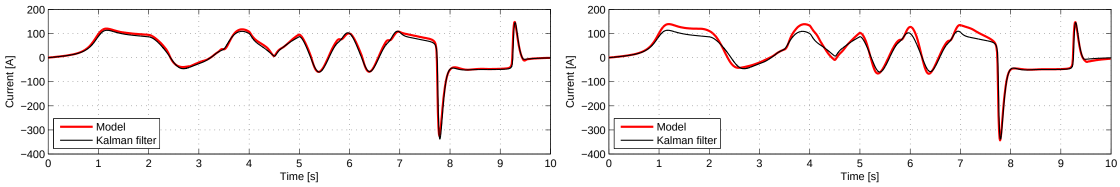

(a) With sensor update. (b) With sensor update disabled.

Figure C.7. Current in Motor #3.

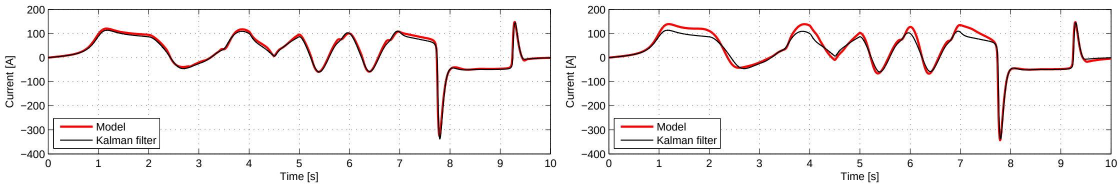

(a) With sensor update. (b) With sensor update disabled.

Figure C.8. Current in Motor #4.

Wheel Torque

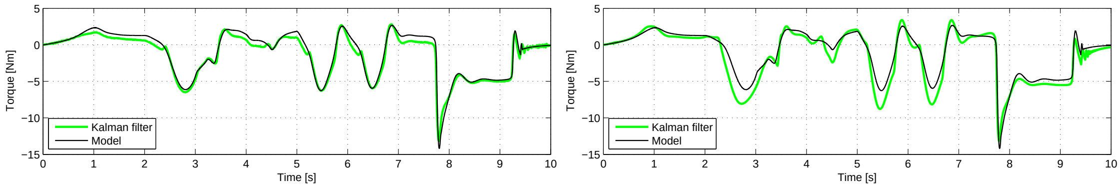

(a) With sensor update. (b) With sensor update disabled.

Figure C.9. Torque transfered to wheel #1.

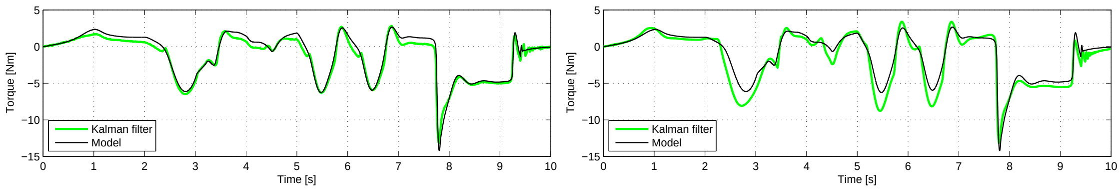

(a) With sensor update. (b) With sensor update disabled.

Figure C.10. Torque transfered to wheel #2.

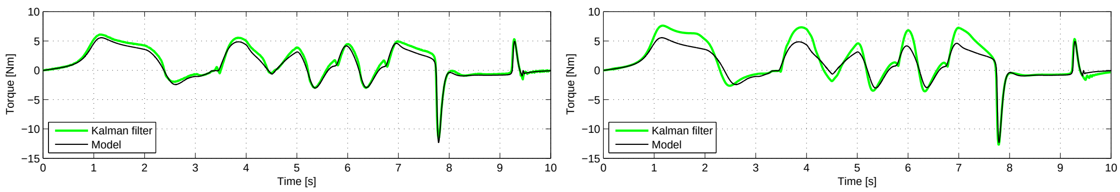

(a) With sensor update. (b) With sensor update disabled.

Figure C.11. Torque transfered to wheel #3.

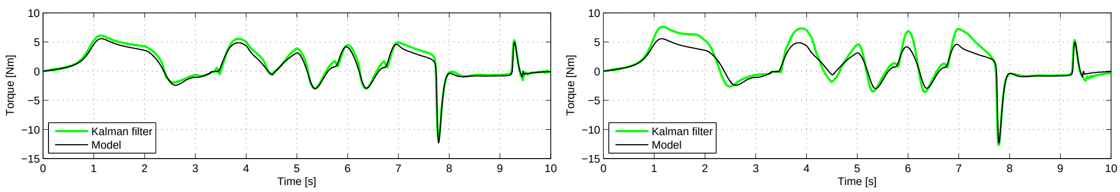

(a) With sensor update. (b) With sensor update disabled.

Figure C.12. Torque transfered to wheel #4.

Wheel and Vehicle Velocity

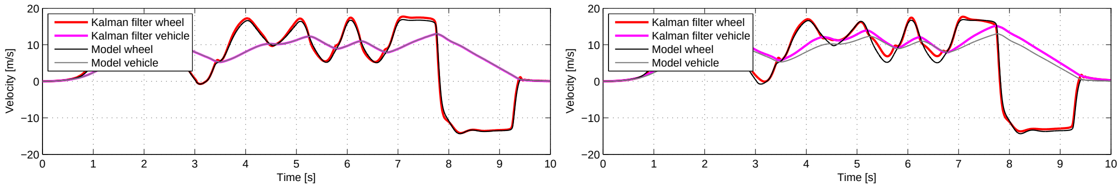

(a) With sensor update. (b) With sensor update disabled.

Figure C.13. Velocity on wheel #1 and vehicle.

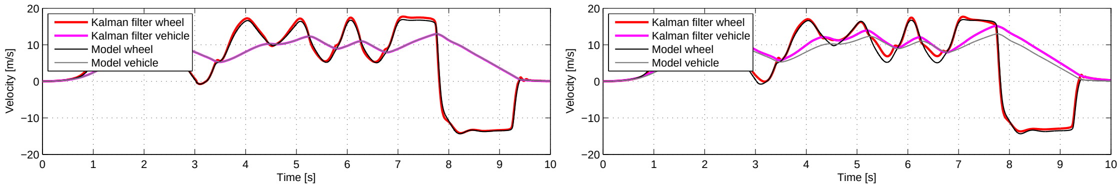

(a) With sensor update. (b) With sensor update disabled.

Figure C.14. Velocity on wheel #2 and vehicle.

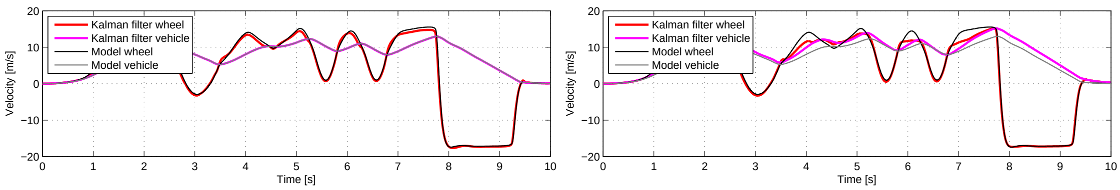

(a) With sensor update. (b) With sensor update disabled.

Figure C.15. Velocity on wheel #3 and vehicle.

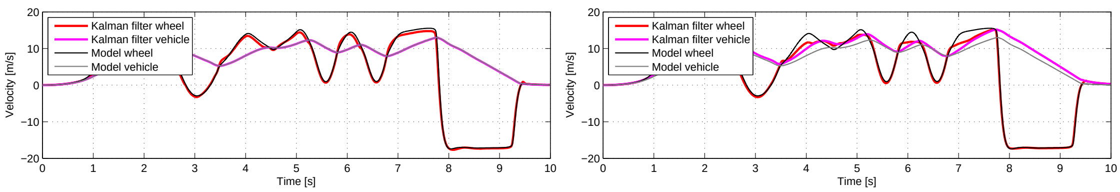

(a) With sensor update. (b) With sensor update disabled.

Figure C.16. Velocity on wheel #4 and vehicle.

Drive Force

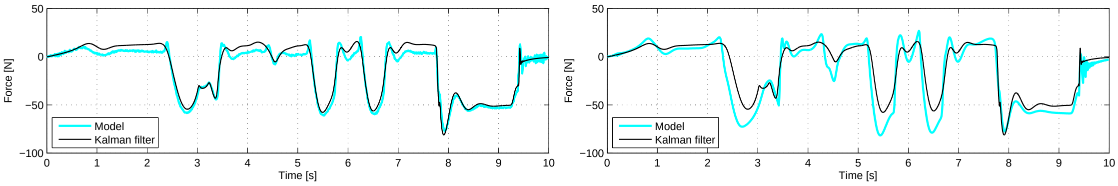

(a) With sensor update. (b) With sensor update disabled.

Figure C.17. Drive force from wheel #1.

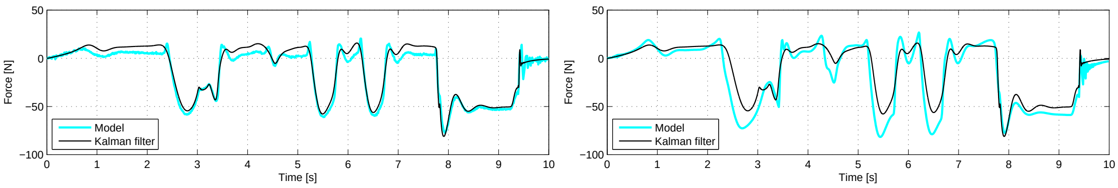

(a) With sensor update. (b) With sensor update disabled.

Figure C.18. Drive force from wheel #2.

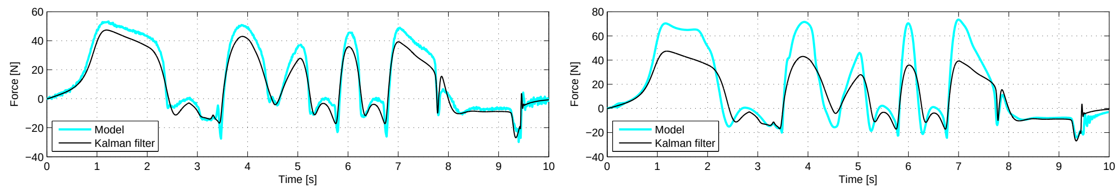

(a) With sensor update. (b) With sensor update disabled.

Figure C.19. Drive force from wheel #3.

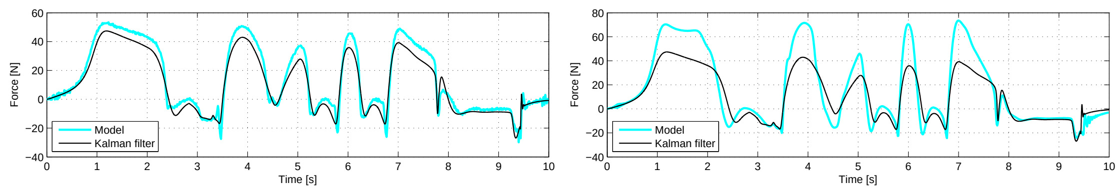

(a) With sensor update. (b) With sensor update disabled.

Figure C.20. Drive force from wheel #4.

Wheel Normal Force

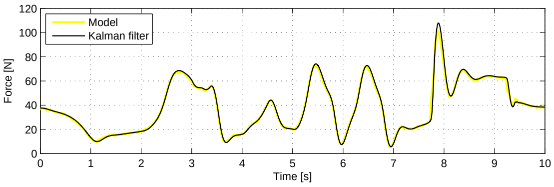

(a) With sensor update.

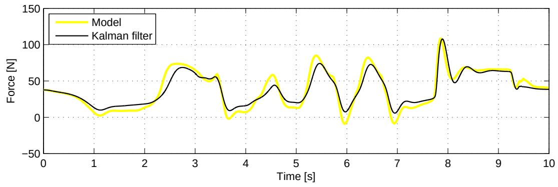

(b) With sensor update disabled.

Figure C.21. Normal force on wheel #1.

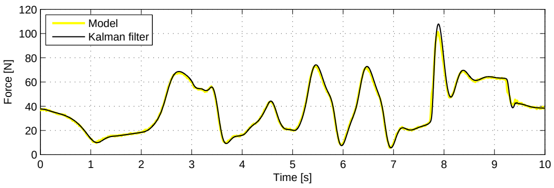

(a) With sensor update.

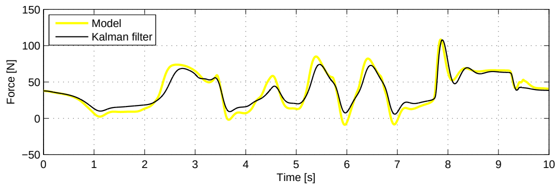

(b) With sensor update disabled.

Figure C.22. Normal force on wheel #2.

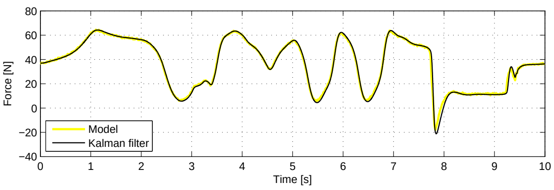

(a) With sensor update.

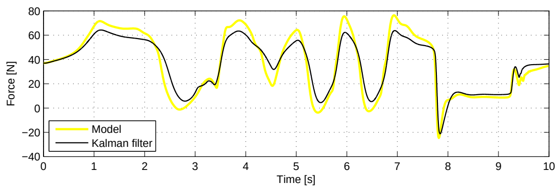

(b) With sensor update disabled.

Figure C.23. Normal force on wheel #3.

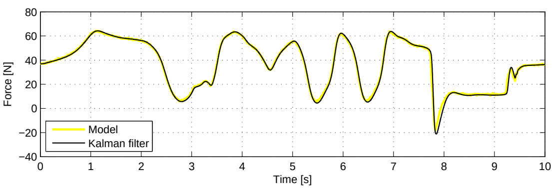

(a) With sensor update.

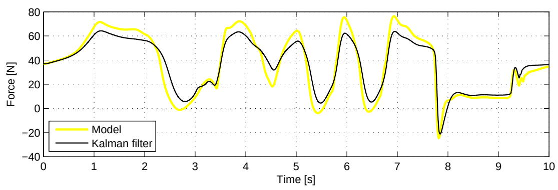

(b) With sensor update disabled.

Figure C.24. Normal force on wheel #4.

Chassis States

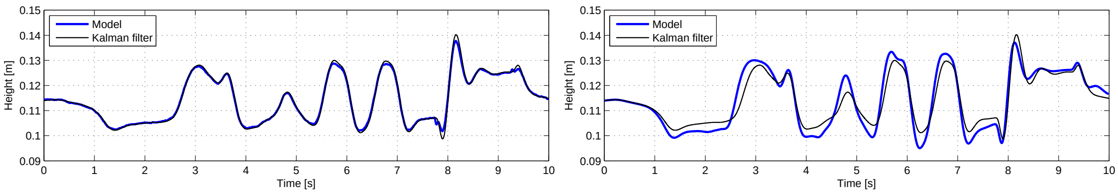

(a) With sensor update. (b) With sensor update disabled.

Figure C.25. Height of chassis mass center.

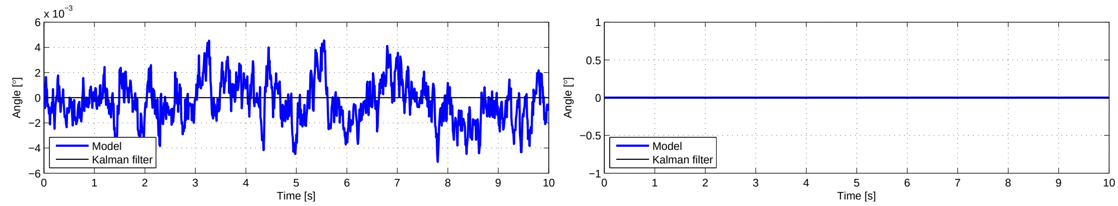

(a) With sensor update. (b) With sensor update disabled.

Figure C.26. Chassis roll.

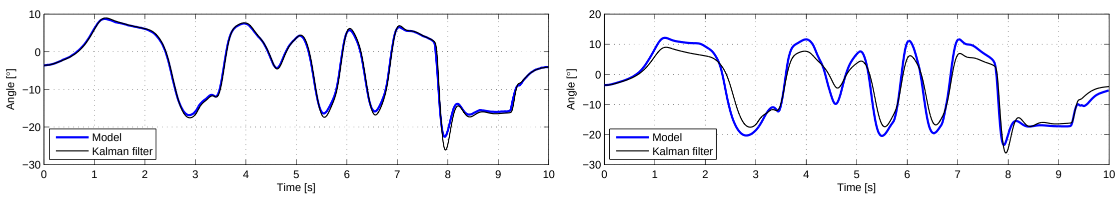

(a) With sensor update. (b) With sensor update disabled.

Figure C.27. Chassis pitch.

C.2 Noise reduction

Motor Input Voltage

Motor Current

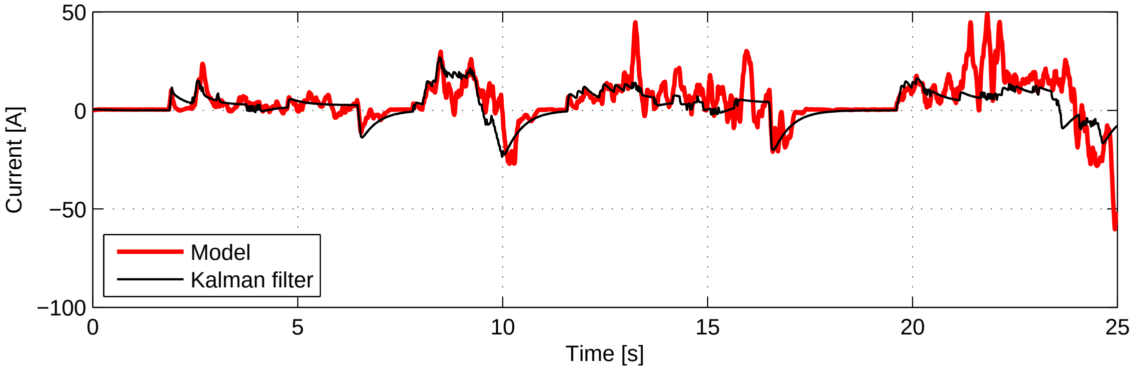

Figure C.28. Current in Motor #1.

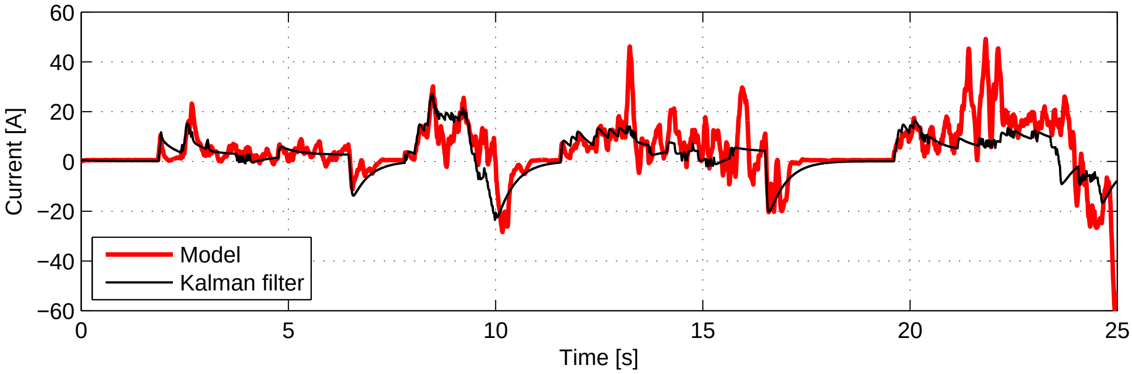

Figure C.29. Current in Motor #2.

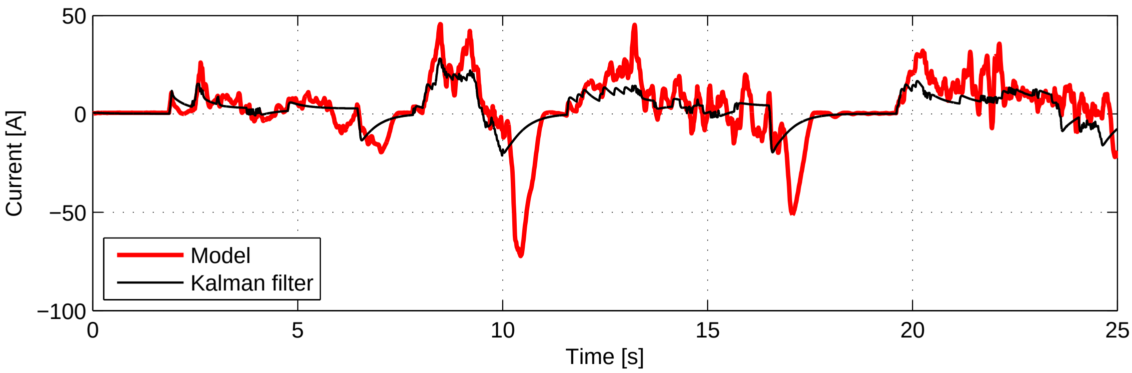

Figure C.30. Current in Motor #3.

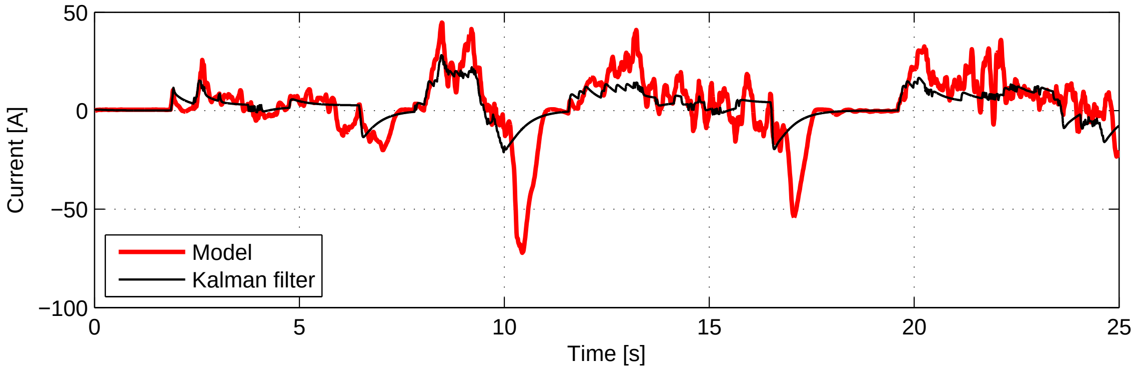

Figure C.31. Current in Motor #4.

Wheel Torque

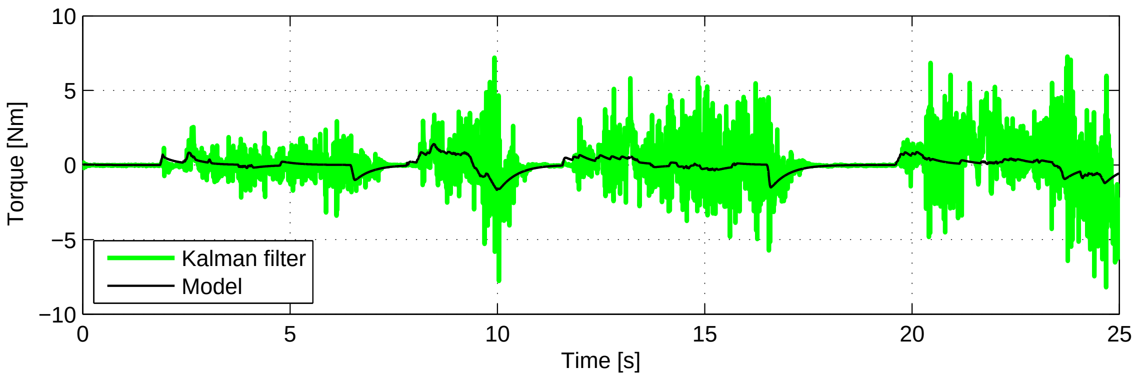

Figure C.32. Torque transfered to wheel #1.

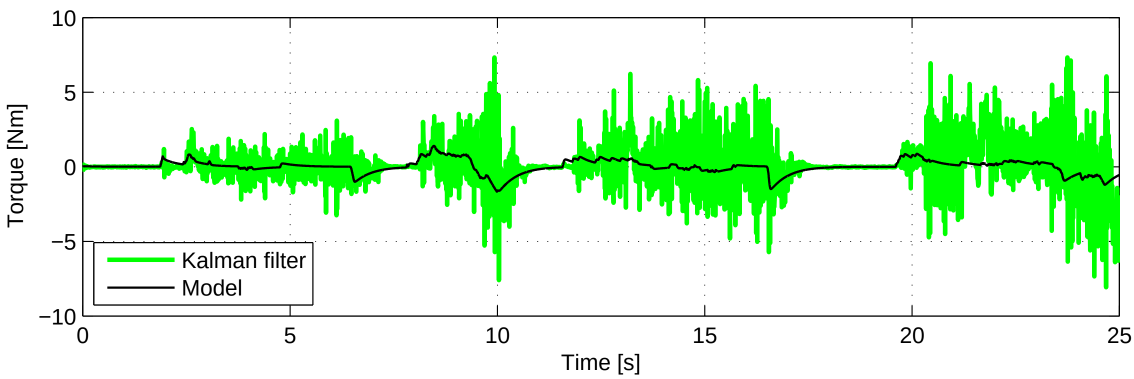

Figure C.33. Torque transfered to wheel #2.

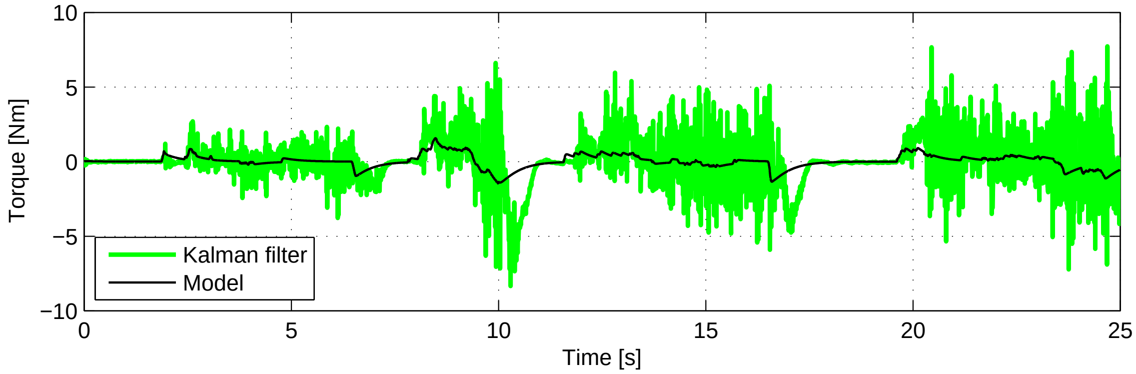

Figure C.34. Torque transfered to wheel #3.

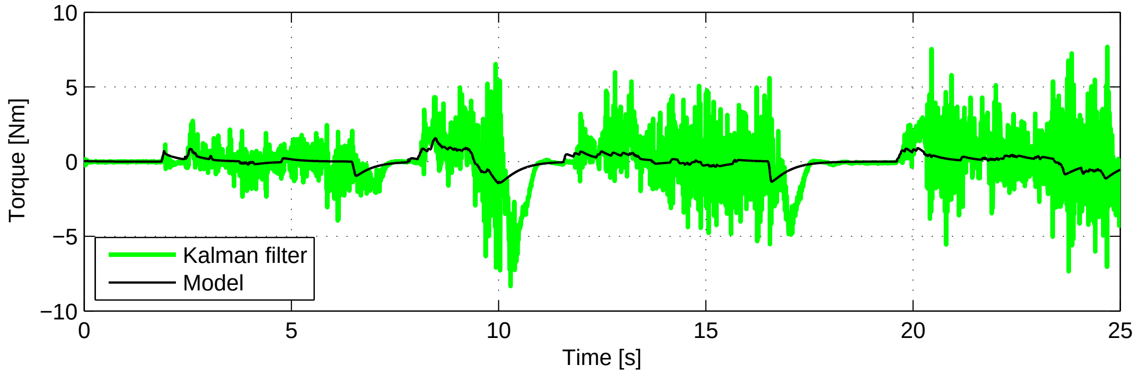

Figure C.35. Torque transfered to wheel #4.

Wheel and Vehicle Velocity

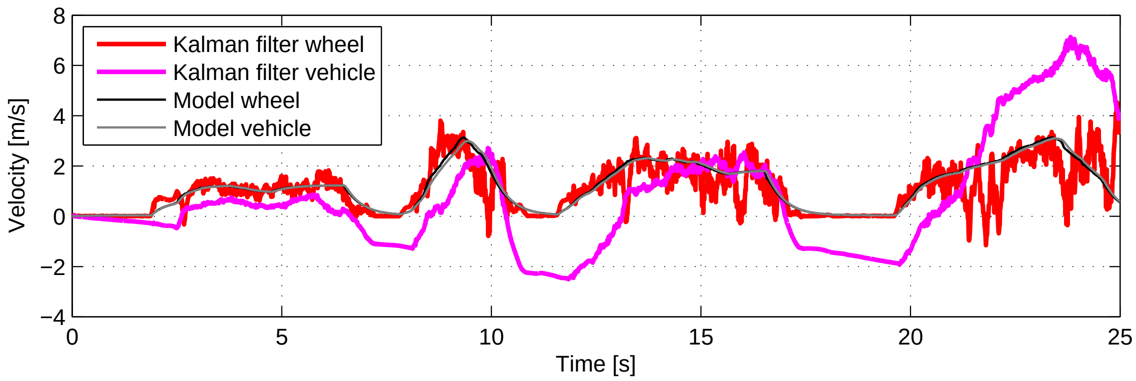

Figure C.36. Velocity on wheel #1 and vehicle velocity.

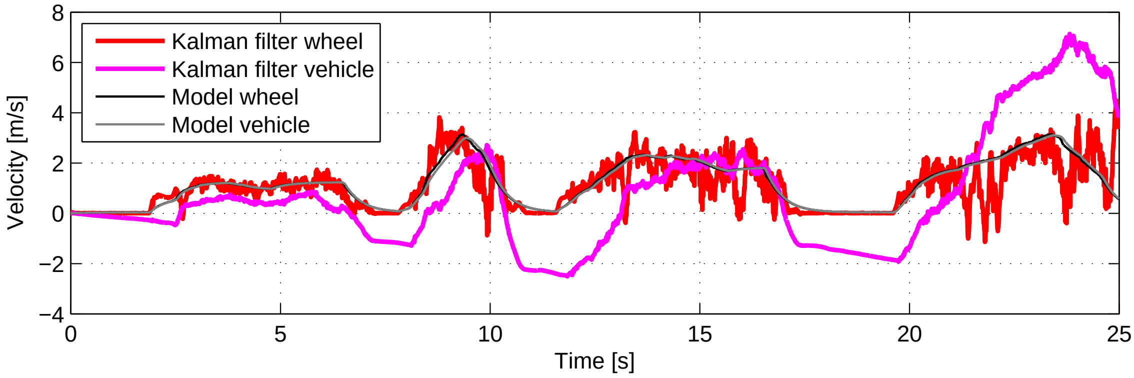

Figure C.37. Velocity on wheel #2 and vehicle velocity.

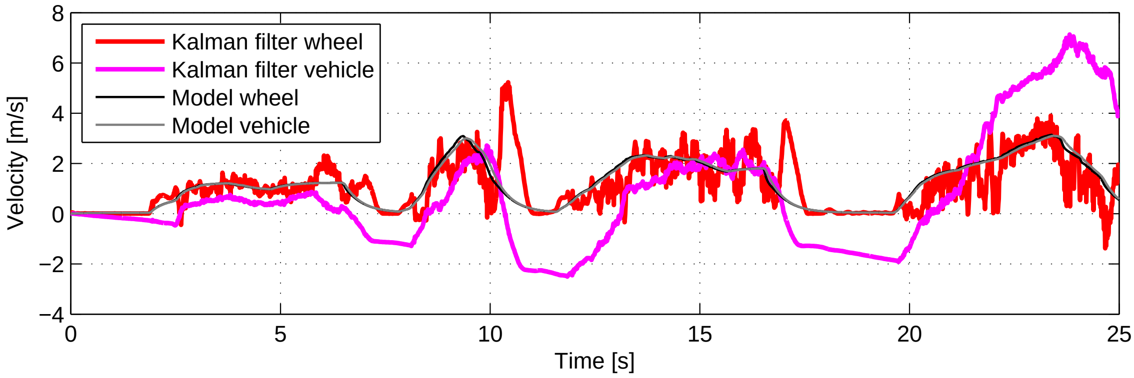

Figure C.38. Velocity on wheel #3 and vehicle velocity.

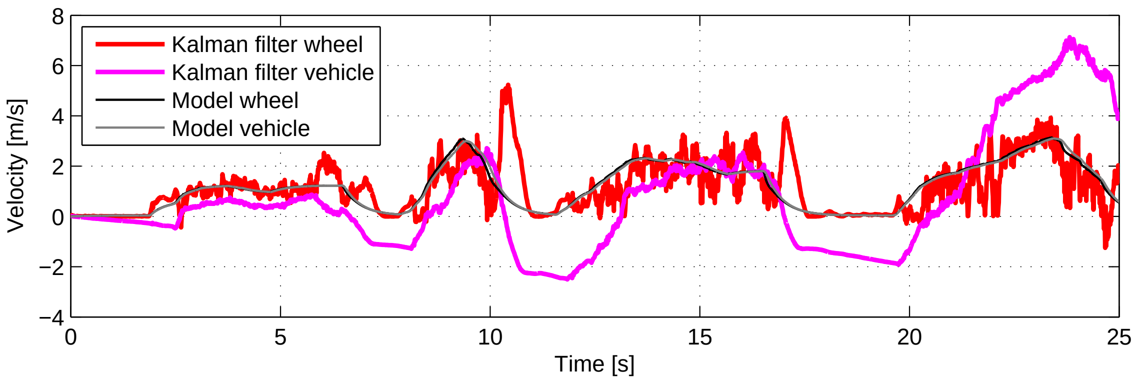

Figure C.39. Velocity on wheel #4 and vehicle velocity.

Drive Force

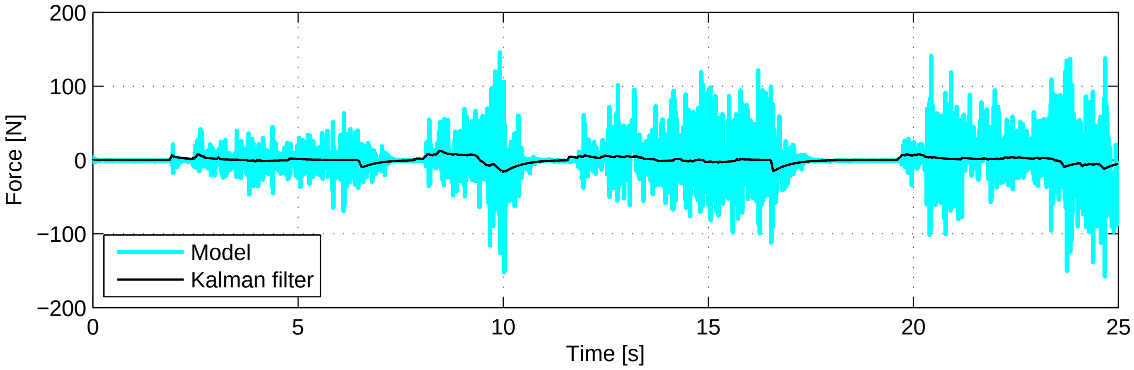

Figure C.40. Drive force from wheel #1.

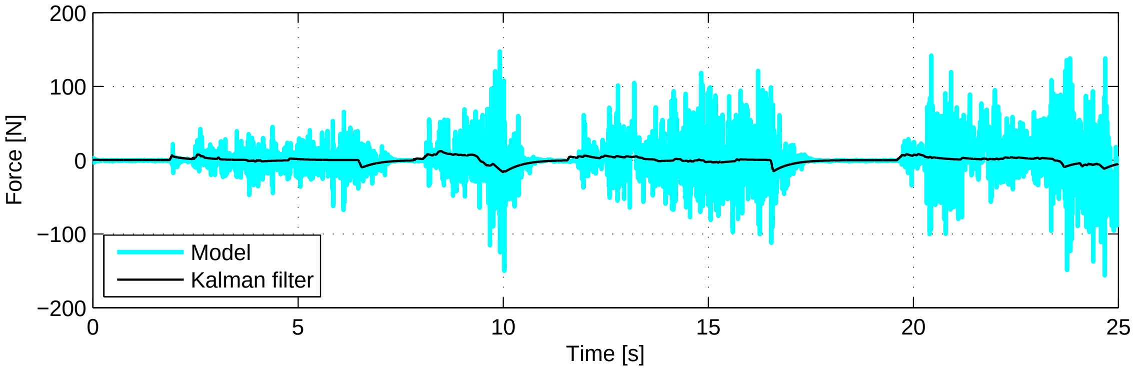

Figure C.41. Drive force from wheel #2.

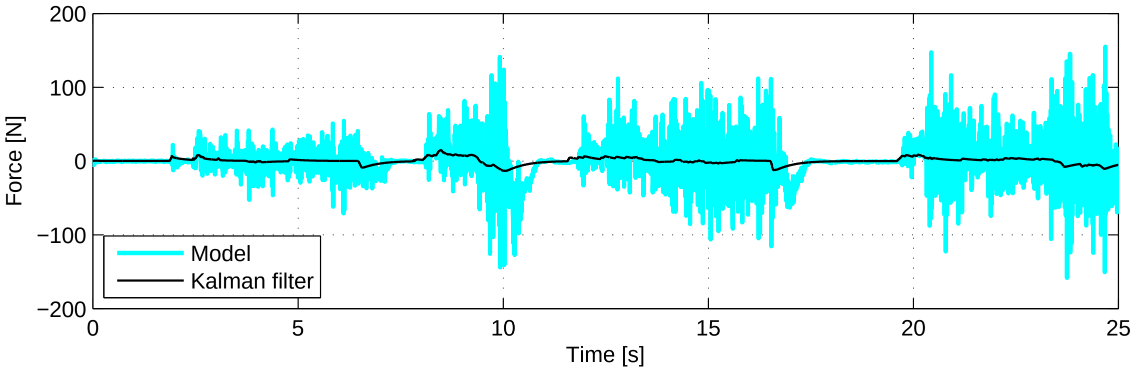

Figure C.42. Drive force from wheel #3.

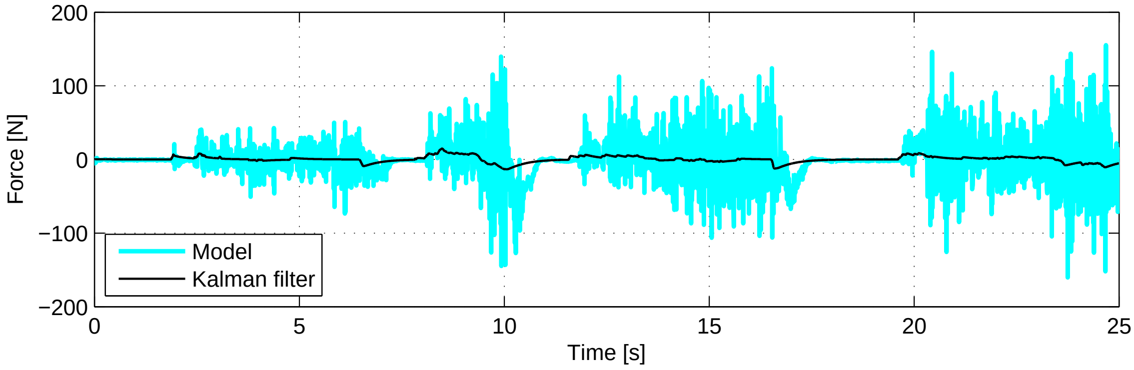

Figure C.43. Drive force from wheel #4.

Wheel Normal Force

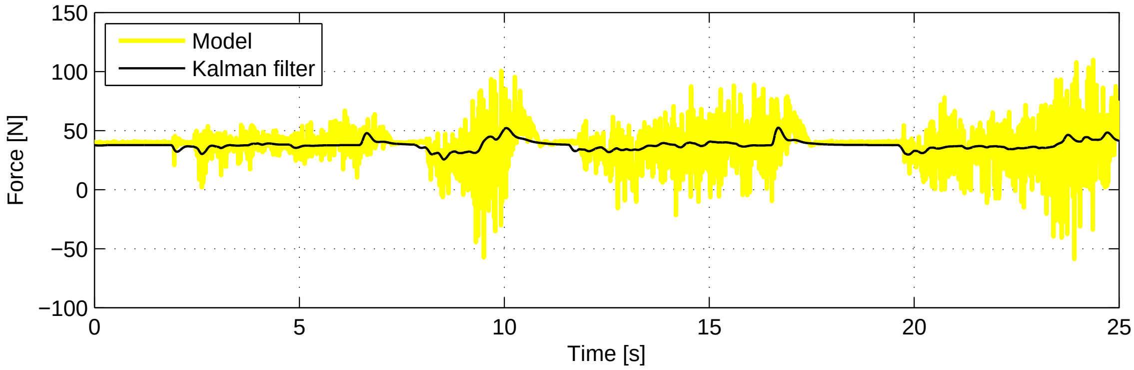

Figure C.44. Normal force on wheel #1.

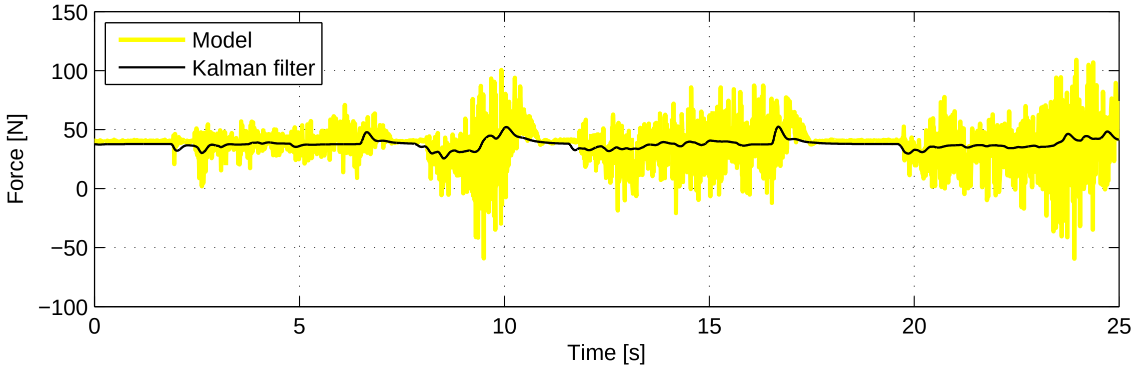

Figure C.45. Normal force on wheel #2.

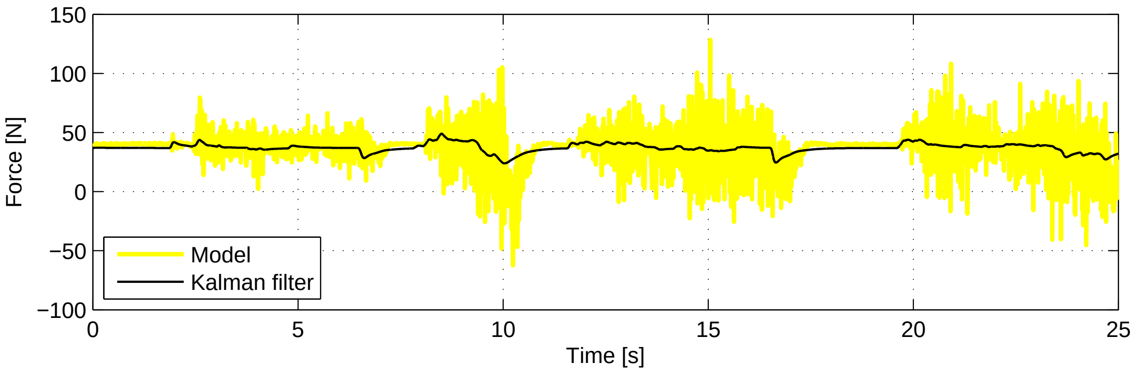

Figure C.46. Normal force on wheel #3.

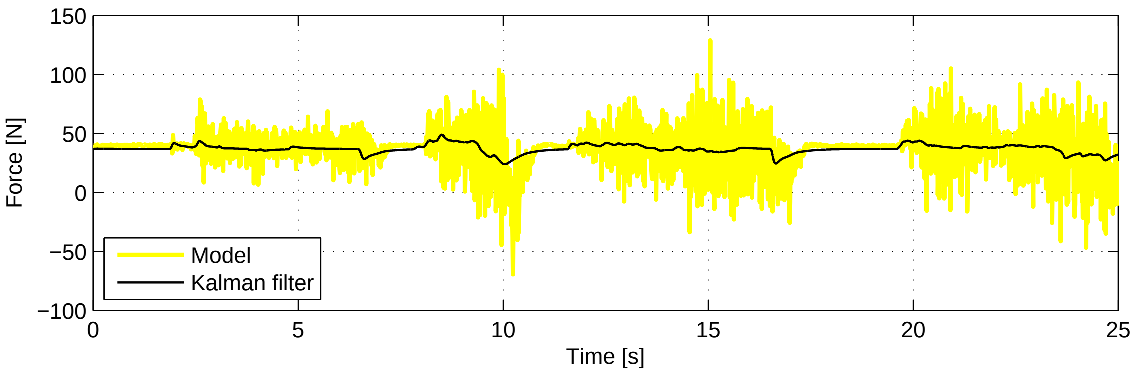

Figure C.47. Normal force on wheel #4.

Chassis States

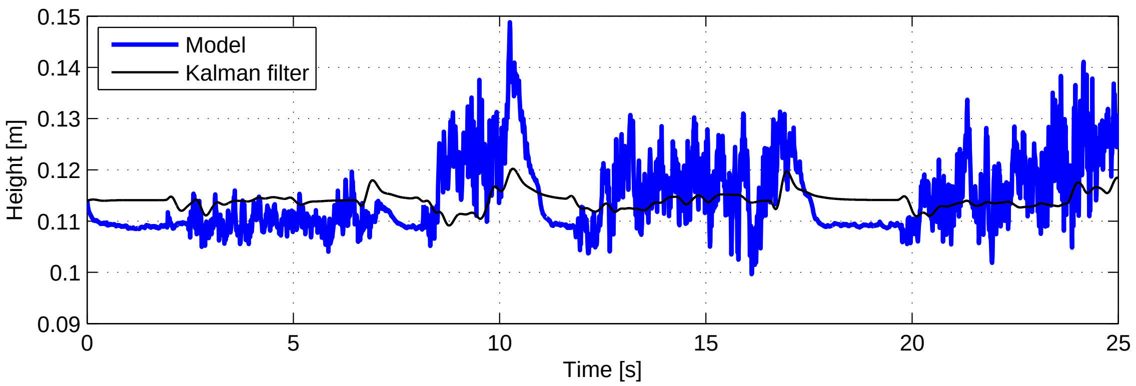

Figure C.48. Height of chassis mass center.

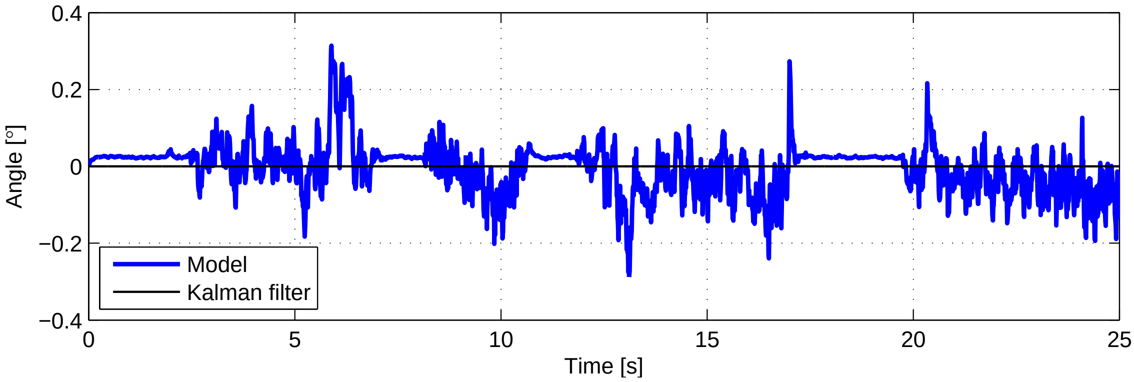

Figure C.49. Chassis roll.

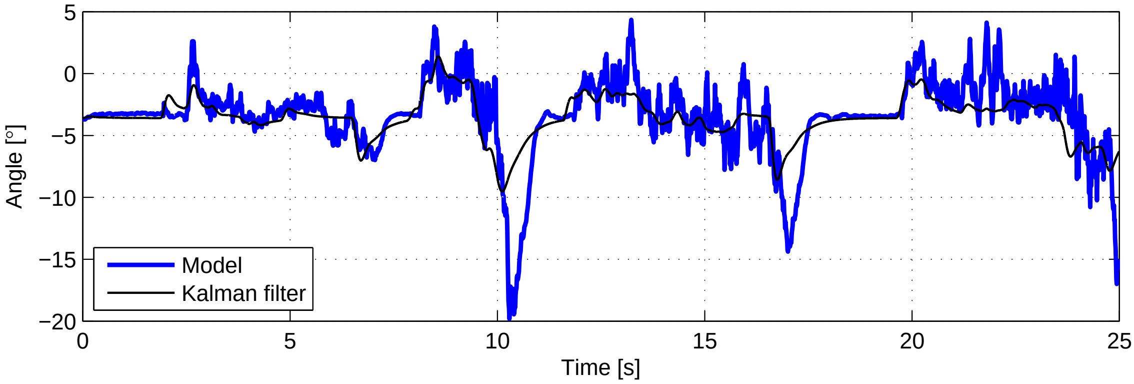

Figure C.50. Chassis pitch.

APPENDIX D

SUPERVISORY CONTROLLER VALIDATION PLOTS

In chapter 10 the supervisory control, developed in chapter 8, is evaluated based on estimates from the extended Kalman filter.

D.1 TDS

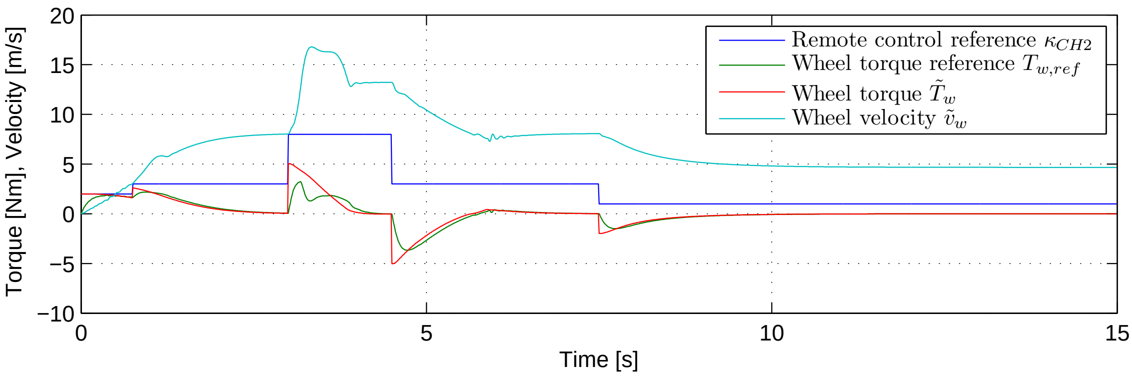

Figure D.1. Wheel #1 torque and velocity.

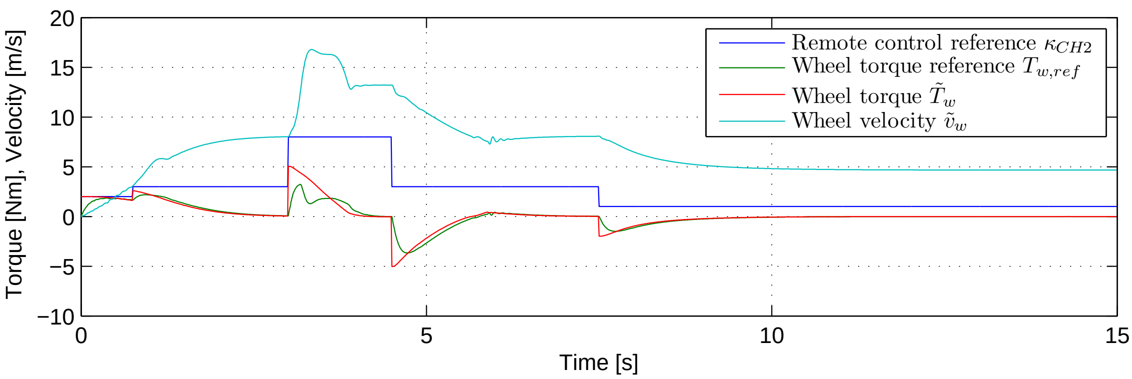

Figure D.2. Wheel #2 torque and velocity.

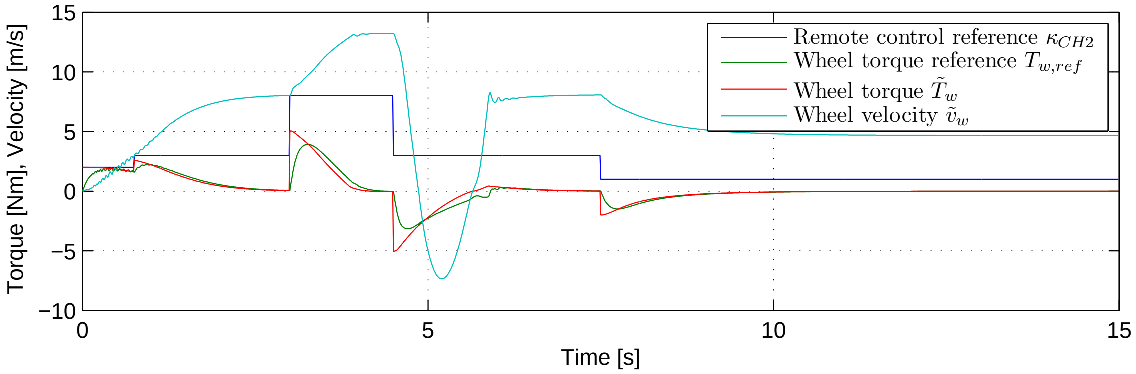

Figure D.3. Wheel #3 torque and velocity.

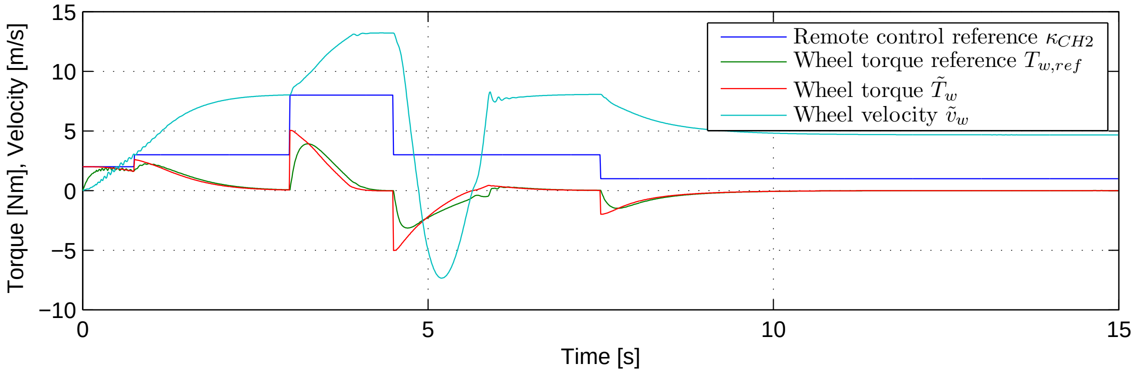

Figure D.4. Wheel #4 torque and voltage.

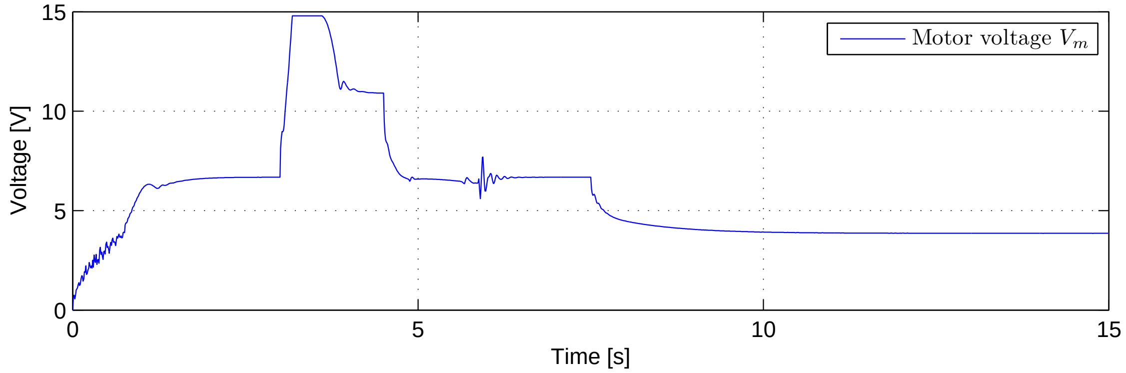

Figure D.5. Motor #1 voltage.

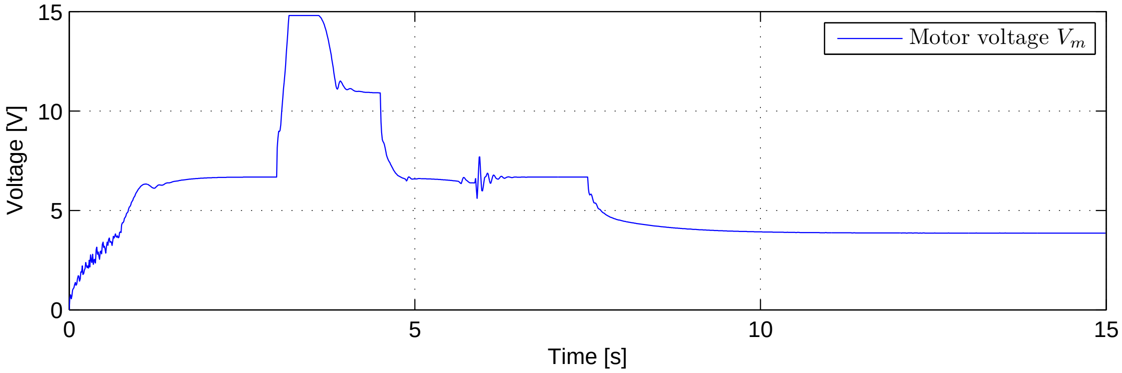

Figure D.6. Motor #2 voltage.

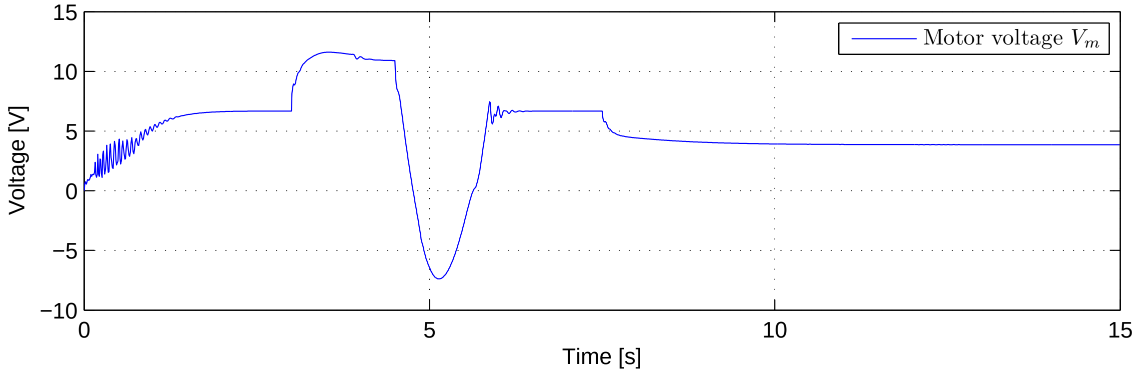

Figure D.7. Motor #3 voltage.

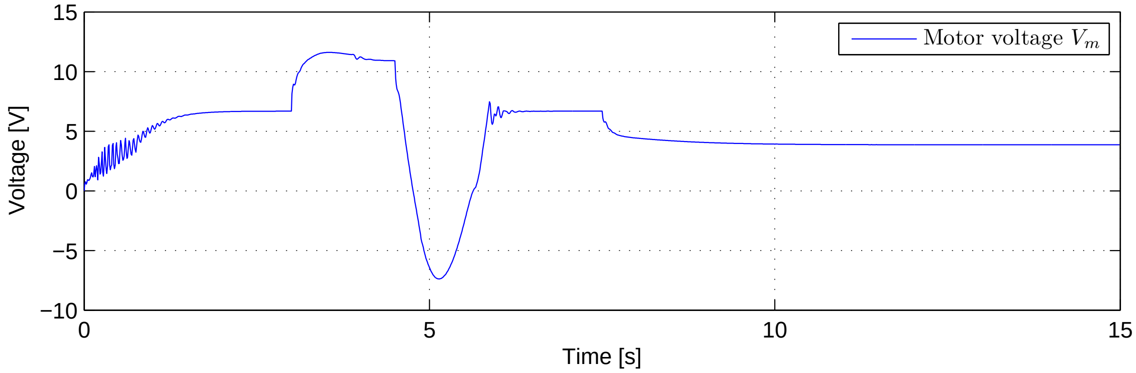

Figure D.8. Motor #4 voltage.

D.2 TDS, TCS and selector

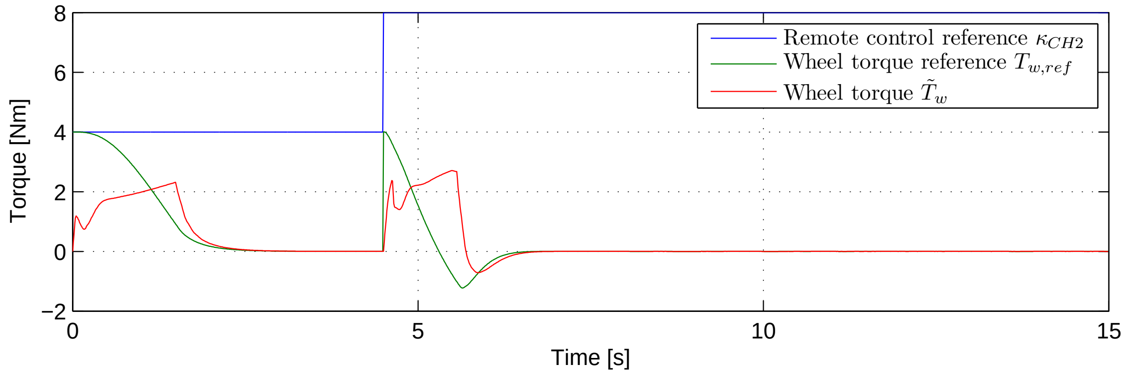

Figure D.9. Wheel #1 torque and motor voltage.

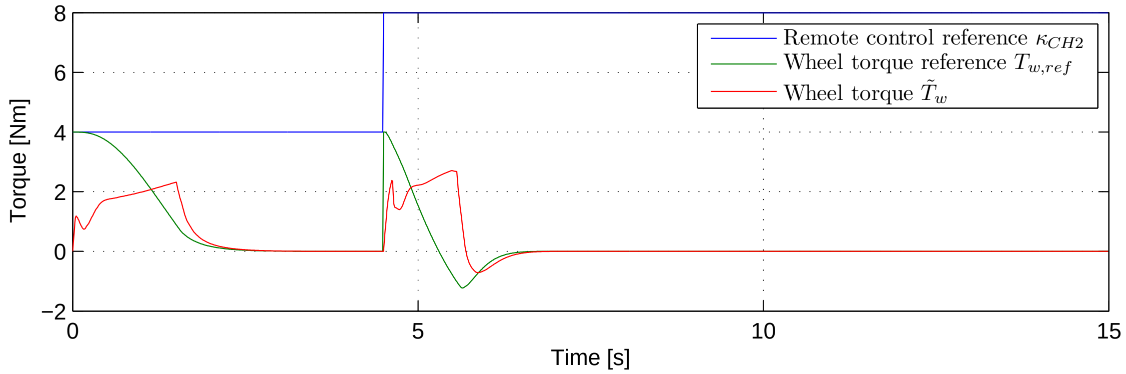

Figure D.10. Wheel #2 torque and motor voltage.

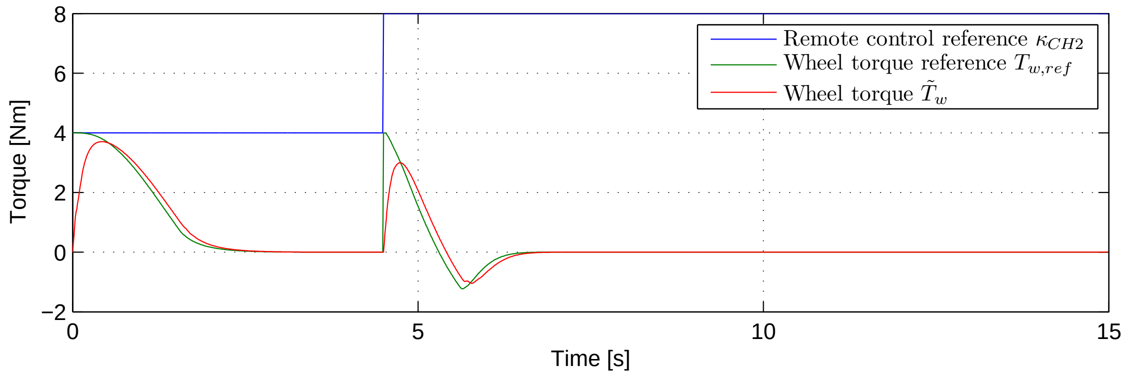

Figure D.11. Wheel #3 torque and motor voltage.

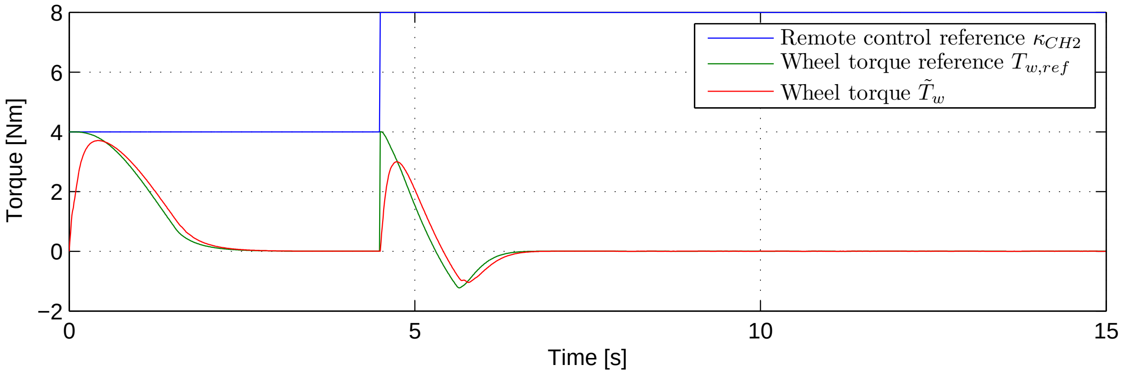

Figure D.12. Wheel #4 torque and motor voltage.

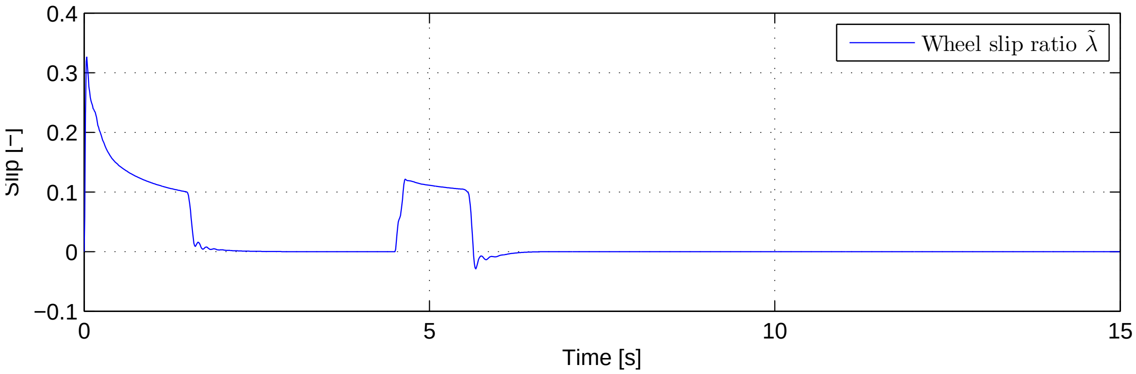

Figure D.13. Wheel #1 slip.

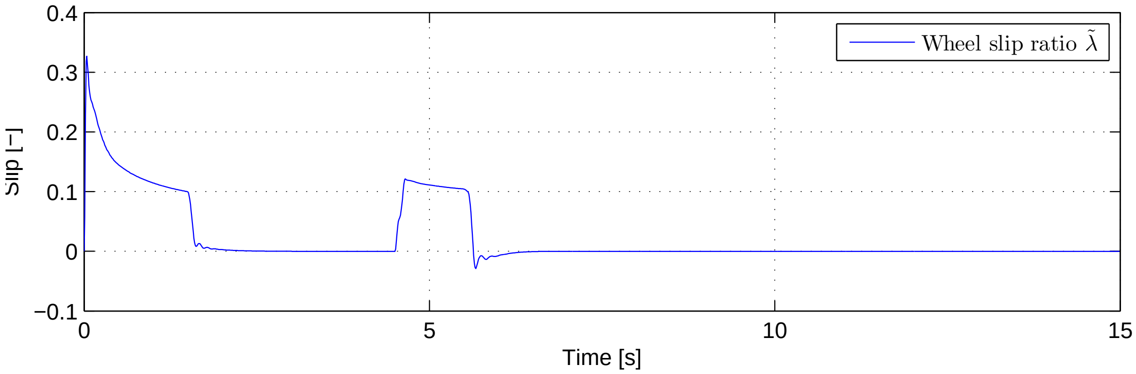

Figure D.14. Wheel #2 slip.

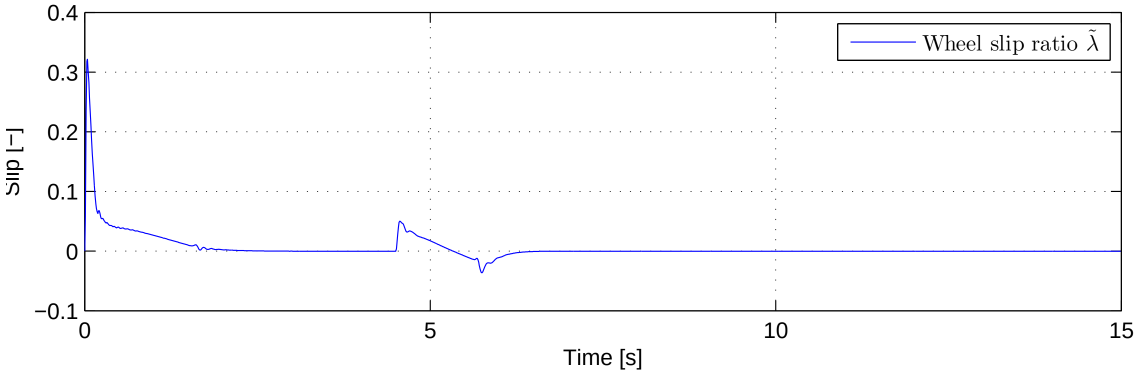

Figure D.15. Wheel #3 slip.

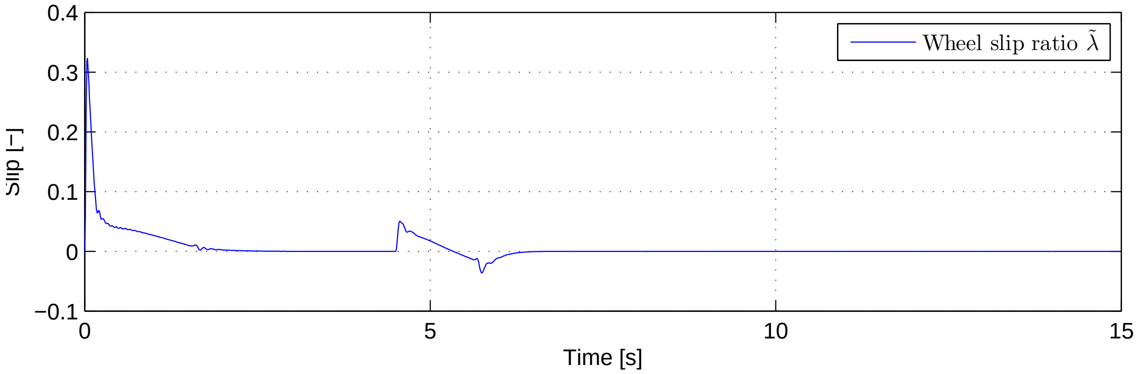

Figure D.16. Wheel #4 slip.

APPENDIX E

LIST OF ITEMS

Reference	Item	Manufacturer
Vehicle	#053410 1/5 "TITAN" MONSTER TRUCK 28cc 4WD 2.4Ghz	SMARTECH
DSP	TMS320F28335	Texas Instruments
F28335	F28335 Delfino Family control card from development kit C2000	Texas Instruments
XBEE	XB24-Z7WIT-004, XBEE ZB, 1 mW, W/WIRED	DIGI
XBEE explorer	WRL-08687, XBee Explorer USB	Sparkfun
ORI28813	Vortex MR8 2100 KV, code: ORI28813	Team Orion [14]
ORI65107	Vortex R8 S Brushless ESC (130A, 2-4S), code: ORI65107	Team Orion [14]
30 A-XL 050F	Teeth: 30, Diameter: 48,01 mm	HPC Gears Ltd [6]
10 A-XL 050F	Teeth: 10, Diameter: 15,67 mm	HPC Gears Ltd [6]
130XL	Teeth: 65, length: 330.2 mm, width: 12.7 mm	HPC Gears Ltd [6]
160XL	Teeth: 80, length: 406.4 mm, width: 12.7 mm	HPC Gears Ltd [6]
G1-10	Teeth: 10, diameter: 11 mm, width: 8 mm	HPC Gears Ltd [6]
G1-60	Teeth: 60, diameter: 60 mm, width: 8 mm	HPC Gears Ltd [6]

Table E.1. List of items applied in the project

APPENDIX F

CIRCUIT DIAGRAMS

F.1 Main board

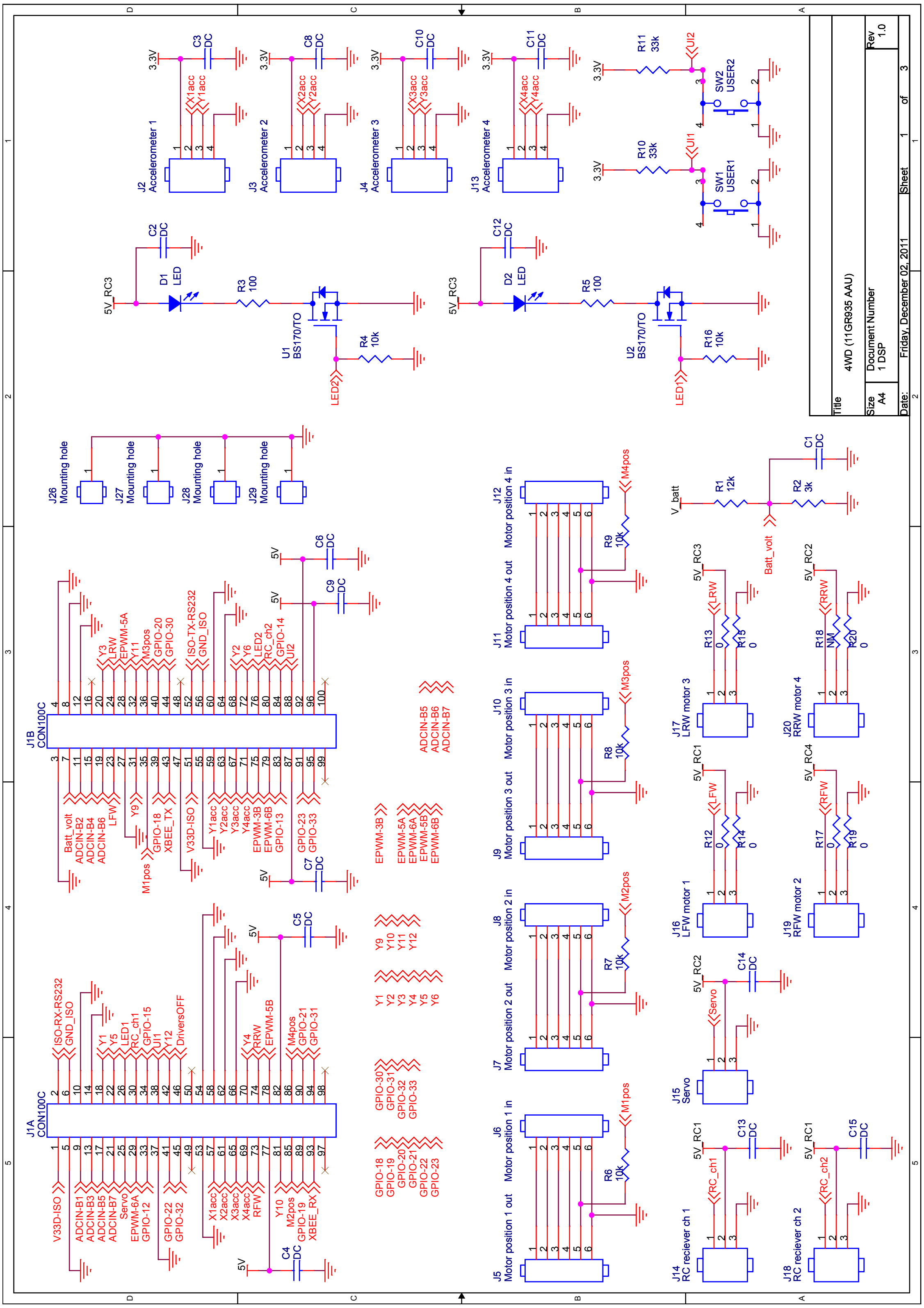

Figure F.1. Circuit diagram of main board page 1

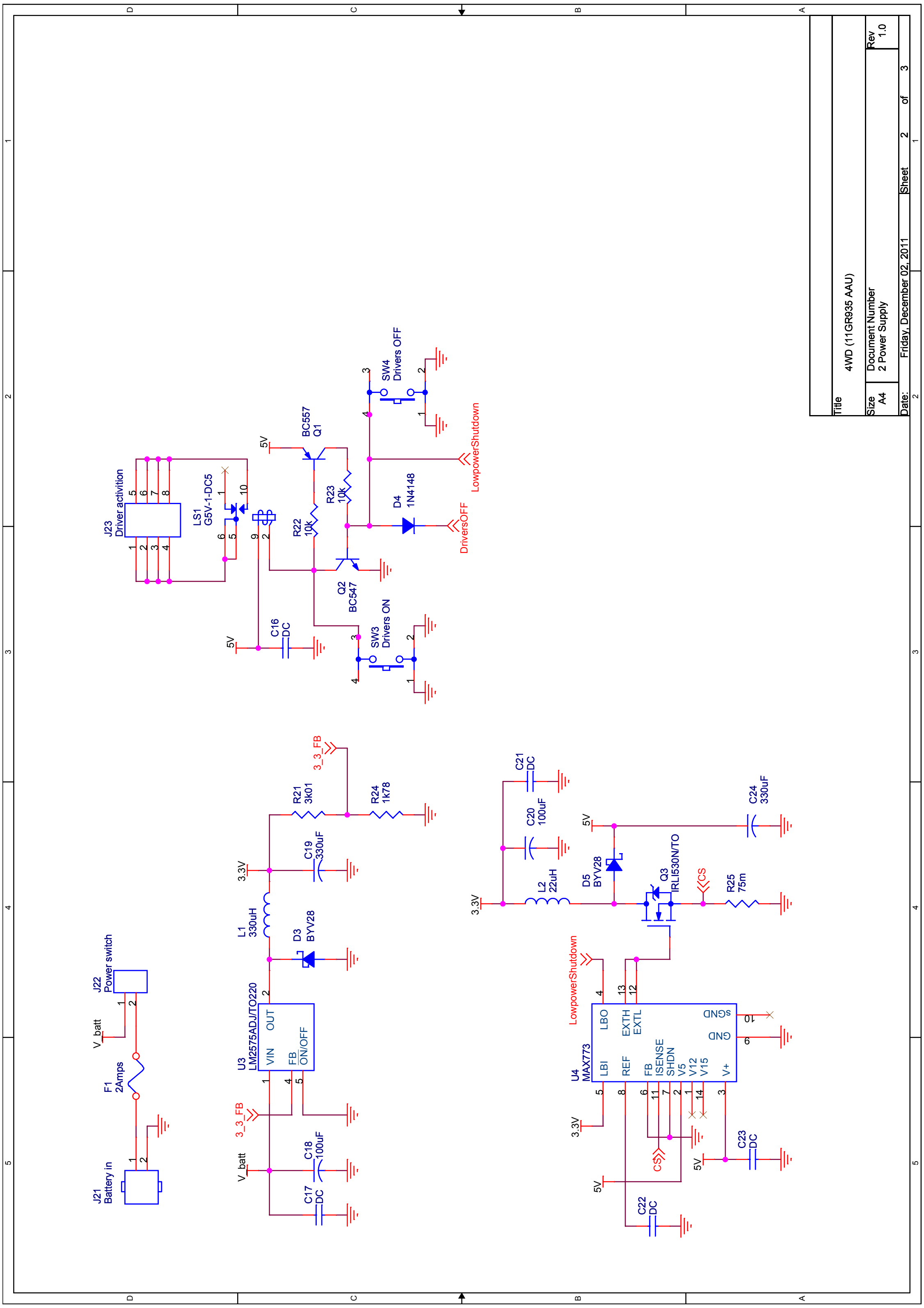

Figure F.2. Circuit diagram of main board page 2

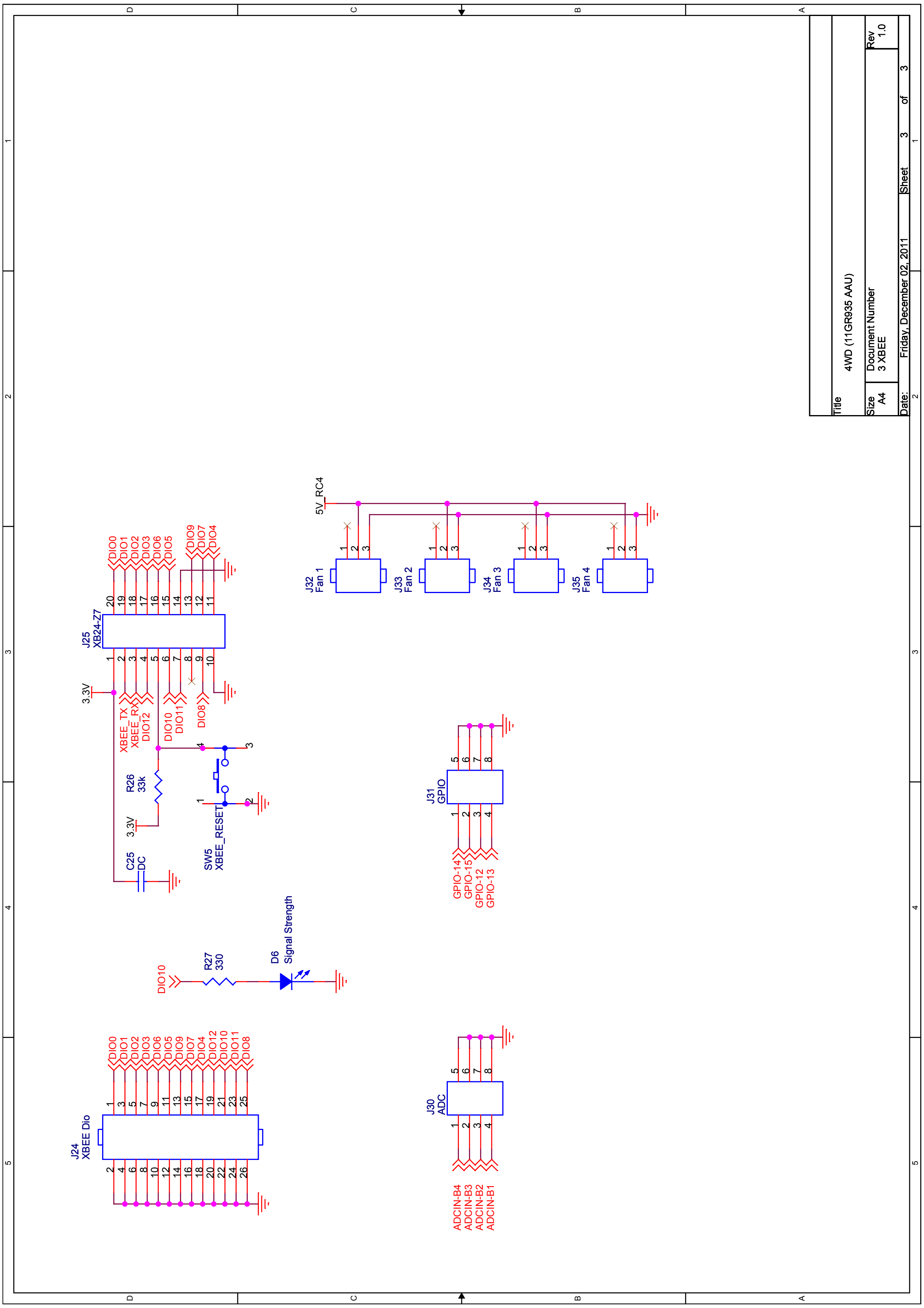

Figure F.3. Circuit diagram of main board page 3

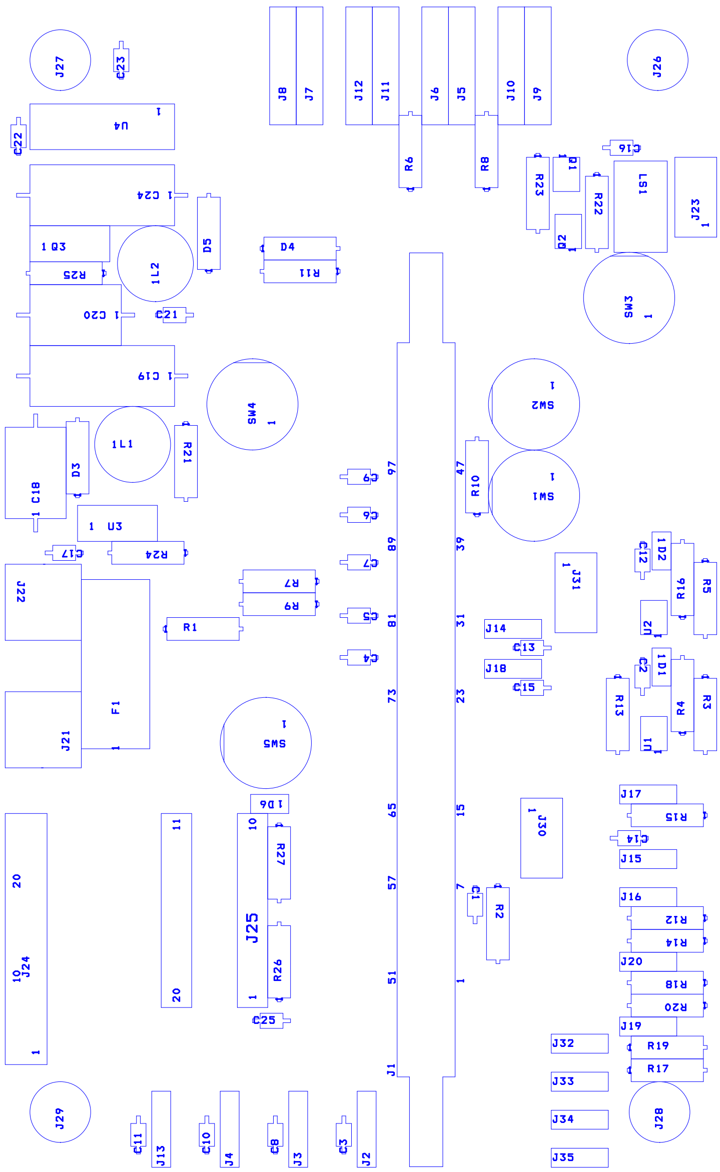

Figure F.4. Silk screen top of main board.

F.2 Accelerometer Board

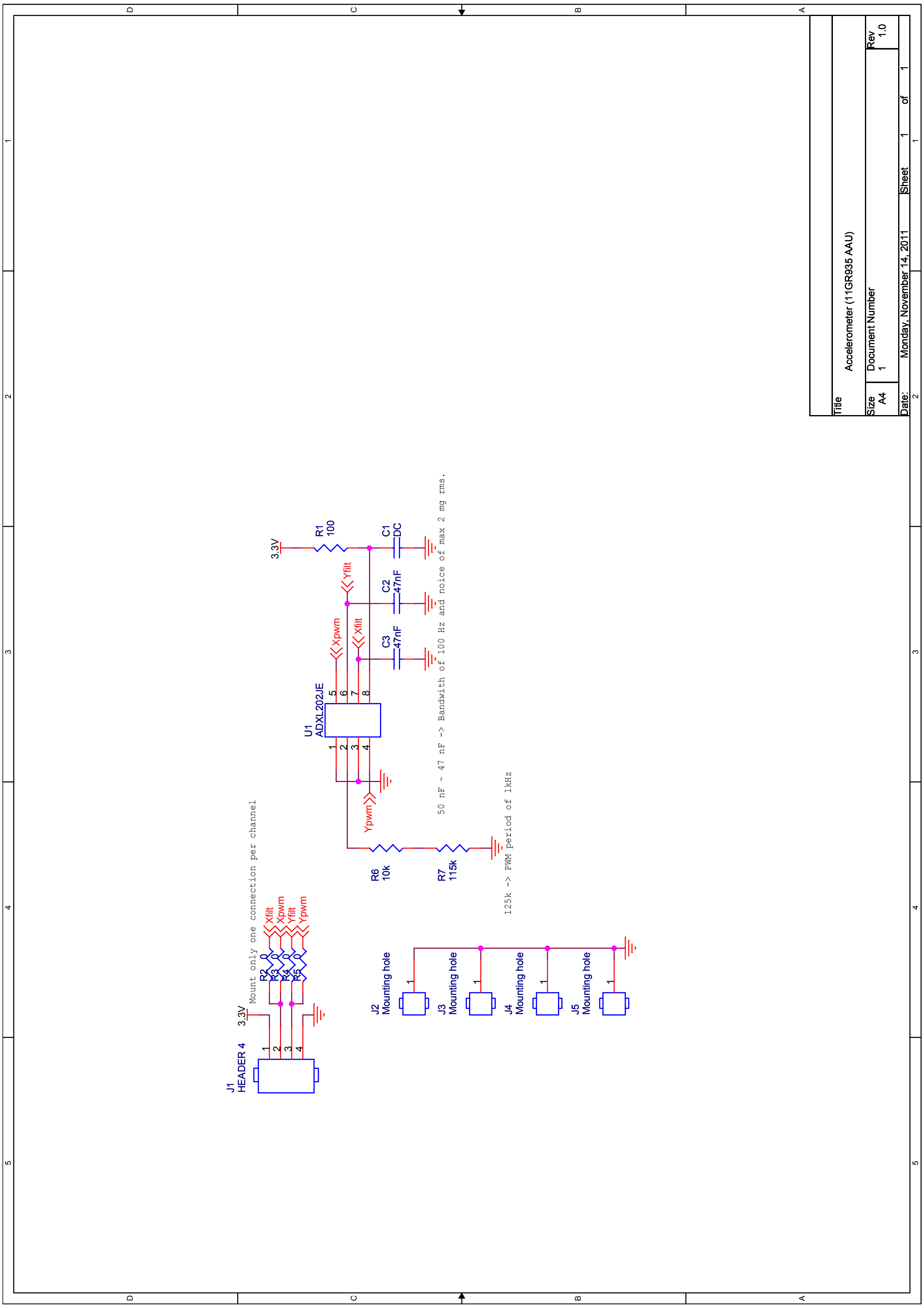

Figure F.5. Circuit diagram of accelerometer board

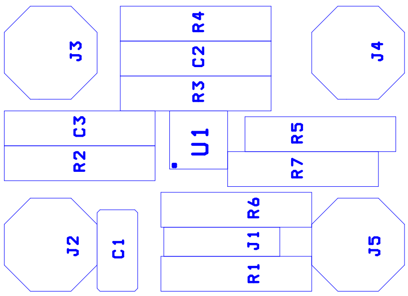

Figure F.6. Circuit diagram of accelerometer board

APPENDIX G

DIMENSIONS

APPENDIX H

REAL TIME SYSTEM WITH THREADING

In section a description of the real time system implemented on the DSC is included. The system would execute one task at a time according to a scheduling queue, with some specific routines handled at the same time. The following will describe how threading between the tasks in the scheduling queue could be implemented to the real time system.

When more than one task is located in a queue, a timer could every t_{thread} seconds change the execution of the current task to the next in the queue. Thus the execution will be divided evenly between the tasks. When the last task in the queue has been executed for t_{thread}, the execution could return to the first task in the queue again. Also if a task is done executing before the t_{thread} seconds are up, the execution should change to the next task.

Before the execution changes from a task to a new, the system must save the point where it was inside the task. When the execution return to a task is must continue from the point saved. If more than one task used the same parameters, scope protection must be used. One solution of scope protection is to prevent two tasks using the same parameters, by preventing the task with less priority from being executed until the other task in done executing and removed from the queue.

If some tasks require to be completed in one step without changing the execution to other tasks, these could be executed completely before changing as shown in figure H.1.

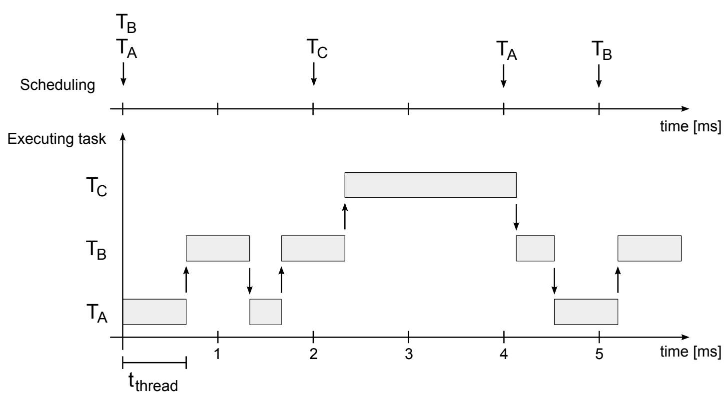

Figure H.1. Real time system with threading

Here task T_A and T_B is from 0 ms scheduled, and the execution is divided evenly between them by t_{thread} ms at a time. Task T_C must be executed is one step, and the execution is thereby not changing while handling this. When task T_C is done executing, the execution changes to task T_B, when this is the only one left in the queue. Before task T_B is done, task T_A is scheduled, and the two task is dividing the execution between them again.

Notice that around 1,6 ms and 4,4 ms the tasks are done executing before they have used t_{thread} ms of execution time, and the execution is just changed to the next task in the queue.

When execution is divided evenly between the task, the priority task priority does not have any influence. Implementing priority for executing some tasks more than other could be made by giving different t_{thread} to the tasks according to their priority. The tasks which are prioritized the most could e.g. have two t_{thread} cycles of execution before changing to another task.

With the threading, several tasks can be handled at the same time, instead of just one. Threading could be used when a task in a system prevents other tasks to be scheduled and executed at the same time, and thereby utilizes the system.

APPENDIX I

SUPPLEMENTS

Various documentation, simulations, graphs, images, scripts, videos etc. and a digital version of the report is located on the attached DVD, in the listed folders as in the following.

- `Circuit Diagrams` - Circuit diagrams files for vehicle hardware
- `Literature` - Cited literature
- `Pictures of Vehicle` - Pictures of vehicle
- `Program Code` - Program code for DSP and universal data interface
- `Report` - Digital version of report
- `Simulation Code` - Object oriented model files for vehicle simulation